Validation of popular nonsinusoidal power theories for the analysis and management of modern power systems

By

Abraham Paul Johannes Rens
M-Ing (E/E)., B-Ing (E/E)

THESIS

Submitted for the degree Doctor of Philosophy in Electrical Engineering at the Potchefstroom Campus of the North-West University

SUPERVISOR: PROF. PH Swart

November 2005

Potchefstroom

Preface

The focus of the research was on practical aspects pertaining to nonsinusoidal conditions in electrical power systems. Two aspects were specifically investigated, firstly practical power definitions and secondly, fundamental principles and techniques in localising a source of distortion in an interconnected power system. The research undertaken and the compilation of this document were carried out over a period in which a rapid advance in various aspects relating to nonsinusoidal conditions in electrical power system was experienced. The document reflects some of these developments. A noteworthy source of inspiration to the author, during the time of writing of this document, were the three-yearly held International Workshops on Power Definitions and Measurements under Nonsinusoidal Conditions organised by Prof. Alessandro Ferrero of the Politecnico di Milano in Milan. Research results for this thesis were presented at two of these workshops and it was possible to brush shoulders with the top workers in this field and to keep abreast with the work done by others.

Acknowledgements

To enable the financial requirements of this research, special recognition is given to the Tertiary Education Support Program of Eskom, the South African electrical utility and specifically in the person of Mr John Gossling who has allocated research grants. The Directors of the School of Electrical and Electronic Engineering at the Potchefstroom Campus of the North-West University, Proff Alwyn Hoffman and Albert Helberg, allocated additional support in finances and facilities.

The support to technical aspects of the study was done by Professor Piet Swart, the supervisor of this PhD study. Other academics that strongly influenced this work were Professor Alessandro Ferrero of the Politecnico di Milano in Milan, Italy, Professor Alexander Emanuel of the Worcester Polytechnic in Massachusetts, USA.

Additional Impedograph™ instrumentation and support were obtained from Mr Willie van Wyk of CT Lab[1] Stellenbosch.

The moral support to the study was carried out in excellence by my wife, Julialet and daughters, Adél and Sané, whilst God made the impossible practical.

[1] http://www.impedograph.com

Summary

Nonsinusoidal conditions are characteristic of modern electrical power systems. Technological advances such as that of the rapidly developing solid-state technology has accelerated the nonlinear loading of power systems. The thesis firstly reformulates and demonstrates multi-frequency power system analysis techniques.

Of special importance is the definition of energy under nonsinusoidal conditions. Popular nonsinusoidal power theories are evaluated and the approach of Czarnecki is shown to have an important deficiency in practical power system applications. The Czarnecki three-phase power components are shown to be questionable as to their physical significance. It is proposed that energy formulation should be carried out in a transformed domain and it is demonstrated that the well-known Park current and voltage vectors enable valid descriptions for energy phenomena in three wire three-phase power systems. A new transform that transforms four wire three-phase quantities to three-dimensional space vectors of voltage and current is shown to deserve further investigation towards implementation in compensation techniques and tariff systems.

Knowledge on the relative contribution to the overall distortion of a specific source of distortion in a power system requires the localisation thereof and a measurement technique. It is shown through time-domain modelling that it is not possible to localise distortion sources through single-point measurements in power systems in the presence of multiple harmonic distortion sources. This principle renders all attempts to quantify power system distortion through single-point measurements invalid. The implication is that penalisation of distorting customers by measuring their emission, will not be possible if all nodes over the power system is not measured synchronously. Therefore, final proof to this principle is given through the results obtained by measurements taken in a real-life power system.

The novel combination of a new power quality index and a distributed measurement system that does not require accurate synchronisation in time is proposed as a practical approach in quantifying distortion contribution of specific distortion sources and should be investigated further. It can aid towards managing nonsinusoidal conditions in a power system through the implementation thereof in a self-regulating tariff structure.

Opsomming

Moderne elektriese kragstelsels word gekenmerk deur nie-sinusvormige kondisies. Hierdie kondisies word veroorsaak deur die nie-lineêre belading van die kragstelsel wat weer die gevolg is van moderne ontwikkeling in vaste toestand silikontegnologie. Synde die nie-sinusvormige kondisies te bestudeer, herformuleer en demonstreer hierdie proefskrif eerstens multi-frekwensie analitiese tegnieke wat gebruik word in kragstelsels.

Spesiale aandag moet gegee word aan die definisie van energie wanneer golfvorme nie-sinusvormig is. Bekende drywingsteorieë word daarom geëvalueer. 'n Belangrike terkortkoming in die drywingsteorie van Czarnecki, wanneer dit toegepas word in praktiese kragstelsels, word hierdeur uitgewys. Die driefase drywingskomponente wat in die Czarnecki se drywingsteorie gedefinieër word, se fisiese betekenis word bevraagteken. 'n Alternatiewe benadering tot die definisie van driefase energie in 'n getransformeerde domein word dan ondersoek. Die Park spanning- en stroomvektore word toegepas in die beskryf van energie in drie draad driefase kragstelsels en gedemonstreer 'n geldige benadering te wees. Die addisioneel energie verskynsels wat in vier draad driefase kragstelsels voorkom, kan met 'n nuwe transform ondersoek word deurdat dit fase groothede volledig na driedimensionele ruimte-vektore transformeer. Hierdie benadering word as verdienstelik voorgehou tot verdere ondersoek in die toepassing van kompensasie tegnieke en tariefstelsels.

Kennis oor die relatiewe bydrae wat 'n spesifieke bron van distorsie in 'n kragstelsels lewer tot die totale distorsie, vereis weer kennis oor die geografiese ligging van die bron asook 'n meettegniek om dan die bydrae te meet. Tydvlak modellering word gedoen om aan te toon dat dit nie moontlik is om met enkelpuntmetings bronne van distorsie in 'n elektriese kragnetwerk te lokaliseer as hierdie bronne oral deur die netwerk versprei is nie. Omdat dit nie moontlik sal wees om kliënte wat distorsie veroorsaak te penaliseer sonder om al die nodes van die kragstelsel gelyktydig te meet nie, word hierdie beginsel dan finaal bevestig deur metings te verwerk wat geneem is in 'n werklike kragstelsel.

Die kreatiewe kombinasie van 'n nuwe kragkwaliteitindeks en 'n verspreide meetstelsel wat nie akkurate tyd-gesinkronisasie nodig het nie, word voorgestel as praktiese benadering tot die kwantifisering van die distorsiebydrae van 'n enkele distorsiebron in 'n kragnetwerk en behoort verder nagevors te word. Dit kan 'n belangrike hulpmiddel wees in die bestuur van nie-sinusvormige kondisies in 'n kragstelsel deur dit te implementeer in 'n selfregulerende tariefstelsel.

1 LIST OF SYMBOLS

General remarks: *Italic* font styles are used to indicate variables, regular font styles indicate constants. **Bold** font styles are used to indicate complex numbers, phasor, vector and matrix quantities. Lower case font styles are associated to time-dependent quantities, whilst capital letters are used to indicate RMS quantities

f_1: Fundamental frequency (subscript "1")

f_h: A harmonic frequency, $f_h=hf_1$

ω_1: Fundamental angular frequency, $\omega_1=2\pi f_1$

ω_h: Harmonic angular frequency, $\omega_h=h\omega_1$

h: Harmonic number

1.1 SINGLE-PHASE SYMBOLS

$v(t)_{1\phi}$: Single-phase time-dependent voltage

1ϕ Signifies "single-phase"

$\left|v(t)_{1\phi}\right|$: RMS value of a single-phase time-dependent voltage $v(t)_{1\phi}$

$v_h(t)_{1\phi}$: Single-phase time-dependent voltage as a function of harmonic number h

h: Harmonic number,

N Symbol N, typically used to indicate the highest harmonic order considered

$\boldsymbol{V}_{h,1\phi}$: Single -phase voltage harmonic phasor of harmonic order h

$\boldsymbol{V}^*_{h,1\phi}$: Complex conjugate of $\boldsymbol{V}_{h,1\phi}$

$V_{h,1\phi}$: RMS value of $\boldsymbol{V}_{h,1\phi}$

$V_{H,1\phi}$ RMS value of $v_H(t)_{1\phi}$

α_h: Phase angle of voltage harmonic phasor $\boldsymbol{V}_{h,1\phi}$

V_{DC}: Time-independent DC voltage value (average value)

$v_1(t)_{1\phi}$: Time-dependent single-phase fundamental frequency component of $v(t)_{1\phi}$

$\boldsymbol{V}_{1,1\phi}$: Single-phase fundamental frequency voltage phasor

$V_{1,1\phi}$ RMS value of $\boldsymbol{V}_{1,1\phi}$

$i(t)_{1\phi}$: Single-phase time-dependent current

$I_{1\phi}$: RMS value of a single phase current $i(t)_{1\phi}$

$\left|i(t)_{1\phi}\right|$: RMS value of a single-phase time-dependent current $i(t)_{1\phi}$, also written as $I_{1\phi}$

$\boldsymbol{I}_{h,1\phi}$: Single -phase current harmonic phasor of harmonic order h.

$\boldsymbol{I}^{*}_{h,1\phi}$: Complex conjugate of $\boldsymbol{I}_{h,1\phi}$

$I_{h,1\phi}$: RMS value of $\boldsymbol{I}_{h,1\phi}$

β_h: Phase angle of current harmonic phasor $\boldsymbol{I}_{h,1\phi}$

I_{DC}: Time-independent average current value

$i_1(t)_{1\phi}$: Time-dependent single-phase fundamental frequency component of $v(t)_{1\phi}$

$\boldsymbol{I}_{1,1\phi}$: Single-phase fundamental frequency current phasor.

$I_{1,1\phi}$ RMS value of $\boldsymbol{I}_{1,1\phi}$

$i_h(t)_{1\phi}$: Time-dependent single-phase perfectly sinusoidal current waveform written as a function of harmonic number

$I_{h,1\phi}$: RMS value of $i_h(t)_{1\phi}$

$I_{H,1\phi}$: RMS value of $i_H(t)_{1\phi}$, the distortion component of $i(t)_{1\phi}$

θ_h: Phase-angle difference between voltage harmonic phasor angle α_h and current harmonic phasor angle β_h

$\boldsymbol{S}_{h,1\phi}$: Single-phase complex power at harmonic number h

$S_{h,1\phi}$: Single-phase apparent power at harmonic number h

$\boldsymbol{S}_{1,1\phi}$: Single phase complex power in fundamental frequency

$S_{1,1\phi}$: Single phase apparent power in fundamental frequency

$S_{\Sigma,1\phi}$: *Joint (Total) Single Phase Apparent Power*

$P_{h,1\phi}$: Single-phase active power at a harmonic number h

$P_{1,1\phi}$: Single-phase active power at the fundamental frequency

$P_{\Sigma,1\phi}$: *Single phase Joint (Total) active power*

$P_{H,1\phi}$: *Single-phase Joint (Total) harmonic active power*, excluding the fundamental frequency

$Q_{1,1\phi}$: Single-phase reactive power in fundamental frequency

$\boldsymbol{Z}_{h,1\phi}$: A single-phase frequency dependent complex impedance, h the harmonic number

$R_{h,1\phi}$: Single-phase resistance at harmonic number h

$X_{h,1\phi}$: Single-phase the reactance at harmonic number h

$\boldsymbol{Y}_{h,1\phi}$: A single-phase frequency dependent complex admittance, h the harmonic number

$G_{h,1\phi}$: Single-phase conductance at harmonic number h

$B_{h,1\phi}$: Single-phase the susceptance at harmonic number h

$G_{e,1\phi}$: The equivalent conductance of a single-phase load element definable in terms of the total active power absorbed

$G_{h,1\phi}$: If the single-phase load equivalent conductance is dependent on harmonic number h, the subscript h are used to indicate an equivalent single-phase load conductance at that harmonic number

G_0: The DC load conductance value

$B_{e,1\phi}$: The equivalent susceptance of a single-phase load element definable in terms of the total imaginary power absorbed at a harmonic frequency

1.2 THREE-PHASE SYMBOLS

3ϕ: Signifies "three-phase"

$v_a(t)$: Phase a time-dependent voltage (referenced to earth plane)

$v_a(t)_1$: Phase a time-dependent fundamental frequency voltage (referenced to earth plane)

α_{a1}: Phase angle of $v_a(t)_1$

$v_a(t)_h$: Phase a time-dependent voltage at a harmonic frequency $h\omega_1$ (referenced to earth plane)

$\alpha_{a,h}$: Phase angle of $v_a(t)_h$

$|v_a(t)|$: RMS value of $v_a(t)$

$V_{a,h}$: Voltage harmonic phasor in phase a at a harmonic number h

$V_{a,h}$: RMS value of V_{ah}

V_{a0}: Average value of $v_a(t)$

V_a RMS value

$v_b(t)$: Phase b time-dependent voltage (referenced to earth plane)

$v_b(t)_1$: Phase b time-dependent fundamental frequency voltage (referenced to earth plane)

α_{b1}: Phase angle of $v_b(t)_1$

$v_b(t)_h$: Phase b time-dependent voltage at a harmonic frequency $h\omega_1$ (referenced to earth plane)

$\alpha_{b,h}$: Phase angle of $v_b(t)_h$

$|v_b(t)|$: RMS value of $v_b(t)$

$V_{b,h}$: Voltage harmonic phasor in phase b at a harmonic number h

$V_{b,h}$: RMS value of $V_{b,h}$

V_b RMS value

$v_c(t)$: Phase c time-dependent voltage (referenced to earth plane)

$v_c(t)_1$: Phase c time-dependent fundamental frequency voltage (referenced to earth plane)

α_{c1}: Phase angle of $v_c(t)_1$

$v_c(t)_h$: Phase c time-dependent voltage at a harmonic frequency $h\omega_1$ (referenced to earth plane)

$\alpha_{c,h}$: Phase angle of $v_c(t)_h$.

$|v_c(t)|$: RMS value of $v_c(t)$

$V_{c,h}$: Voltage harmonic phasor in phase c at a harmonic number h

$V_{c,h}$: RMS value of $V_{c,h}$

V_c RMS value $|v_c(t)|$

$v_n(t)$: Neutral conductor time-dependent voltage (referenced to earth plane)

$|v_n(t)|$: RMS value of $v_n(t)$

$V_{n,h}$: Voltage harmonic phasor of neutral conductor at a harmonic number h

$V_{n,h}$: RMS value of $V_{n,h}$

V_n RMS value

$v(t)_{3\phi}$: General vector of time-dependent three-phase voltages at a measuring terminal in a three-phase power system. Symbol $v(t)_{3\phi}$ is used interchangeably for either a three wire or a four wire three-phase power system and indicated in the text (where required) when $v(t)_{3\phi}$ is a three element vector (then written as $v(t)_{abc}$) and when $v(t)_{3\phi}$ is a four element vector it is written as $v(t)_{abcn}$

$\|v(t)_{3\phi}\|$: Norm of $v(t)_{3\phi}$, $\left\|v(t)_{3\phi}\right\| = \sqrt{\left(v(t)_{3\phi}.v(t)_{3\phi}\right)}$

$V_{3\phi}$: Generalised RMS value of nonsinusoidal three-phase voltages as used by Czarnecki [5],

V_e *Effective Voltage* (IEEE) of three-phase power system [20], three wire system, , four wire system

V_{e1}: Fundamental frequency component of V_e

V_{eH} Non-fundamental component of V_e

$V_a(h)$: Vector of phase *a* voltage harmonic phasors listed as a function of harmonic number *h*

$V_b(h)$: Vector of phase *b* voltage harmonic phasors listed as a function of harmonic number *h*

$V_c(h)$: Vector of phase *c* voltage harmonic phasors listed as a function of harmonic number *h*

$V_n(h)$: Vector of neutral voltage harmonic phasors listed as a function of harmonic number *h*

$V(h)_{abc}$: Three-phase voltage vector containing the *abc* three-phase voltage harmonic phasors in one vector and listed as a function of the harmonic number *h*: $V(h)_{abc} = \begin{bmatrix} V_a(h) \\ V_b(h) \\ V_c(h) \end{bmatrix}$

$V(h)_{abcn}$: Three-phase voltage vector containing the *abc* three-phase voltage harmonic phasors and the neutral conductor voltage harmonic phasor in one vector and listed as a function of the harmonic number *h*: $V(h)_{abcn} = \begin{bmatrix} V_a(h) \\ V_b(h) \\ V_c(h) \\ V_n(h) \end{bmatrix}$

$i_a(t)$: Phase *a* time-dependent current

$|i_a(t)|$: RMS value of $i_a(t)$

$I_{a,h}$: Current harmonic phasor in phase *a* at a harmonic number *h*

$I_{a,h}$: RMS value of $I_{a,h}$

I_a RMS value $|i_a(t)|$

I_{a0}: Average/DC value of $i_a(t)$

$i_b(t)$: Phase *b* time-dependent current

$|i_b(t)|$: RMS value of $i_b(t)$

$I_{b,h}$: Current harmonic phasor in phase *b* at a harmonic number *h*

$I_{b,h}$: RMS value of $I_{b,h}$

I_b RMS value $|i_b(t)|$

$i_c(t)$: Phase c time-dependent current

$|i_c(t)|$: RMS value of $i_c(t)$

$\boldsymbol{I}_{c,h}$: Current harmonic phasor in phase c at a harmonic number h

$I_{c,h}$: RMS value of $\boldsymbol{I}_{c,h}$

I_c RMS value $|i_c(t)|$

$i_n(t)$: Neutral conductor time-dependent current

$|i_n(t)|$: RMS value of $i_n(t)$

$\boldsymbol{I}_{n,h}$: Current harmonic phasor of neutral conductor at a harmonic number h

$I_{n,h}$: RMS value of $\boldsymbol{I}_{n,h}$

I_n RMS value $|i_n(t)|$

$\boldsymbol{i}(t)_{3\phi}$: Vector of time-dependent three-phase currents through a measuring terminal in a three-phase power system. Subscript "3ϕ" is used to indicate in general a three-phase power system. Symbol $\boldsymbol{i}(t)_{3\phi}$ is used interchangeably for either a three wire or a four wire three-phase power system and indicated in the text (where required) when $\boldsymbol{i}(t)_{3\phi}$ is a three element vector (then written as $\boldsymbol{i}(t)_{abc}$) and when $\boldsymbol{i}(t)_{3\phi}$ is a four element vector it is written as $\boldsymbol{i}(t)_{abcn}$

$||\boldsymbol{i}(t)_{3\phi}||$: Norm of $\boldsymbol{i}(t)_{3\phi}$

$I_{3\phi}$: *Generalised RMS value* of a nonsinusoidal three-phase current as used by Czarnecki [5] listed against symbol I_e to indicate the difference in definition

I_e *Effective Current* (IEEE) of three-phase power system [20]

$I_{e,1}$: Fundamental frequency component of I_e

I_{eH} Non-fundamental component of I_e

$\boldsymbol{I}_a(h)$: Vector of phase a current harmonic phasors listed as a function of harmonic number h

$\boldsymbol{I}_b(h)$: Vector of phase b current harmonic phasors listed as a function of harmonic number h

$\boldsymbol{I}_c(h)$: Vector of phase c current harmonic phasors listed as a function of harmonic number h

$\boldsymbol{I}_n(h)$: Vector of neutral current harmonic phasors listed as a function of harmonic number h

$\boldsymbol{I}(h)_{abc}$: Three-phase current vector containing the *abc* three-phase current harmonic phasors in one vector and listed as a function of the harmonic number h: $\boldsymbol{I}(h)_{abc} = \begin{bmatrix} \boldsymbol{I}_a(h) \\ \boldsymbol{I}_b(h) \\ \boldsymbol{I}_c(h) \end{bmatrix}$

$\boldsymbol{I}(h)_{abcn}$: Three-phase current vector containing the *abcn* three-phase current harmonic phasors in one vector and listed as a function of the harmonic number h: $\boldsymbol{I}(h)_{abcn} = \begin{bmatrix} \boldsymbol{I}_a(h) \\ \boldsymbol{I}_b(h) \\ \boldsymbol{I}_c(h) \\ \boldsymbol{I}_n(h) \end{bmatrix}$

$\boldsymbol{S}_{h,a}$: Complex power at a harmonic number h in phase a, similar for phases b and c

$S_{h,1\phi}$: Apparent power at a harmonic number h in phase a, similar for phases b and c

$P_{h,a}$: Active power at a harmonic number h in phase a, similar for phases b and c

$Q_{h,a}$: Reactive power at a harmonic number h in phase a, similar for phases b and c

$\boldsymbol{S}_{1,a}$: Complex power in the fundamental frequency component of phase a, similar for phases b and c

$S_{1,a}$: Apparent power in the fundamental frequency component of phase a, similar for phases b and c

$P_{1,a}$: Active power at the fundamental frequency in phase a, similar for phases b and c

$Q_{1,a}$: Reactive power at the fundamental frequency in phase a, similar for phases b and c

$S_{\Sigma,3\phi}$: *Three-phase Total* (or *Joint*) *Apparent Power*, also termed the *Arithmetic Three-phase Apparent power* [69]

S_V: The vector apparent power [69]

S_e: *System Apparent Power*, $S_e=3V_eI_e$ also termed the *System Equivalent Apparent Power* [94]

$S_{3\phi}$: Czarnecki apparent power definition [19] based on "generalised" three-phase voltage and current values: $S_{3\phi}= V_{3\phi} I_{3\phi}$

$P_{h,3\phi}$: *Three-phase Harmonic Active Power* at a harmonic number h summated over all three phases

$P_{1,3\phi}$: Three-phase active power in the fundamental frequency

$P_{\Sigma,3\phi}$: *Three-phase Total* (or *Joint*) *Active Power*, including the fundamental frequency

$P_{H,3\phi}$: *Three-phase Total* (or *Joint*) *Harmonic Active Power*, excluding the fundamental frequency

$Q_{1,3\phi}$: Three-phase fundamental frequency reactive power

G_0: DC load conductance value

$\beta_{a,h}$: Phase angle of current harmonic component in phase a of order h, similar for phases b and c

$\boldsymbol{Z}_{h,a}$: Impedance in phase element a as function of harmonic number, similar for phases b and c

$R_{h,a}$: Resistance in phase element a as function of harmonic number, similar for phases b and c

$X_{h,a}$: Reactance in phase element a as function of harmonic number, similar for phases b and c

$Y_{h,a}$: Admittance in phase element a as function of harmonic number, similar for phases b and c

$G_{h,a}$: Conductance in phase element a as function of harmonic number, similar for phases b and c

$B_{h,a}$: Susceptance in phase element a as function of harmonic number, similar for phases b and c

$G_{e,3\phi}$: *Equivalent Conductance* of a three-phase load element

$G_{h,3\phi}$: *Equivalent Conductance* of a three-phase load element at harmonic frequency $h\omega_1$

$B_{e,3\phi}$: *Equivalent Susceptance* of a three-phase load element

$B_{h,3\phi}$: *Equivalent Susceptance* of a three-phase load at harmonic frequency $h\omega_1$

1.3 ELECTRO-MAGNETIC SYMBOLS

$\vec{S}$: Poynting vector

$\vec{E}$: Electric field

$\vec{H}$: Magnetic field

$\vec{E}_1$: Electric field at the fundamental frequency produced by $v_1(t)_{1\phi}$

$\vec{E}_h$: Electric fields produced by the individual harmonic components $v_h(t)_{1\phi}$

$\vec{E}_H$: Electric field produced by the total non-fundamental frequency component, $v_H(t)_{1\phi}$

$\vec{H}_1$: Magnetic field (intensity) at the fundamental frequency as produced by $i_1(t)_{1\phi}$

$\vec{H}_h$: Magnetic fields produced by the individual harmonic frequencies $i_h(t)_{1\phi}$

$\vec{H}_H$: Magnetic field produced by the total non-fundamental frequency component, $i_H(t)_{1\phi}$

1.4 SEQUENCE DOMAIN SYMBOLS

$a(h)$: Fortesque transform operator as a function of harmonic number h

$A(h)$: Fortesque transformation matrix as a function of harmonic number h

$V_0(h)$: Vector of zero-sequence voltage harmonic phasors listed as a function of the harmonic

number h, the subscript "0" indicate the zero-sequence components

$\boldsymbol{V}_1(h)$: Vector of positive-sequence voltage harmonic phasors listed as a function of the harmonic number h, the subscript "1" indicate the positive sequence components

$\boldsymbol{V}_2(h)$: A vector of negative-sequence voltage harmonic phasors listed as a function of the harmonic number h, the subscript "2" indicate the negative sequence components

$\boldsymbol{V}_S(h)$: A vector of sequence voltage harmonics defined as $\boldsymbol{V}_s(h)=\begin{bmatrix}\boldsymbol{V}_0(h)\\ \boldsymbol{V}_1(h)\\ \boldsymbol{V}_2(h)\end{bmatrix}$

V_0: RMS value of the negative sequence three-phase voltage phasors $V_0=\|\boldsymbol{V}_0(h)\|$

V_1: RMS value of the positive sequence three-phase voltage phasors $V_1=\|\boldsymbol{V}_1(h)\|$

$\boldsymbol{V}_{1,h}$: Positive sequence voltage harmonic phasor at harmonic number h

$V_{1,h}$: RMS value of $\boldsymbol{V}_{1,h}$

$V_{1,1}$: RMS value of the positive sequence fundamental frequency voltage phasor

$V_{1,H}$ RMS value of the harmonic components in the positive sequence three-phase voltage phasors excluding the fundamental frequency component

V_2: RMS value of the negative sequence three-phase voltage phasors $V_2=\|\boldsymbol{V}_2(h)\|$

$V_{2,1}$: RMS value of the negative sequence fundamental frequency voltage phasor

$\boldsymbol{V}_{2,h}$: Negative sequence voltage harmonic phasor at harmonic number h

$V_{2,h}$: RMS value of $\boldsymbol{V}_{2,h}$

$V_{2,H}$ RMS value of the harmonic components in the negative sequence three-phase voltage phasors excluding the fundamental frequency component

$\boldsymbol{S}_S(h)$: Vector of complex power in the sequence components as function of harmonic number h

$\boldsymbol{S}_1(h)$: Vector of complex power in the positive sequence components as function of harmonic number h, subscript "1" signifies positive sequence component, similar for the zero and negative sequence components

$\boldsymbol{P}_s(h)$: The vector of active power in the sequence components as function of harmonic number h

$\boldsymbol{P}_1(h)$: Vector of active power in the positive sequence components as function of harmonic number h, subscript "1" signifies positive sequence component, similar for the zero and negative sequence components

$Q_s(h)$: Vector of non-active power in the sequence components as function of harmonic number h,

$Q_1(h)$: Vector of non-active power in the positive sequence components as function of harmonic number h, subscript "1" signifies positive sequence component, similar for the zero and negative sequence components Park domain symbols

T_{Park}: Transformation matrix that transforms phase-domain voltage and current vectors to the Park voltage and current vectors thereof

$v(t)_{\text{Park}}$: Park voltage vector

$v(t)_d$: Direct axis Park voltage vector component

$v(t)_q$: Quadrature axis Park voltage vector component

$v(t)_0$: Zero sequence voltage component resulting from Park transformation if three-phase system is unbalanced

$V_{\text{Park},h}$ Harmonic phasor of $v(t)_{\text{Park}}$ at harmonic number h

V_{Park}: RMS value (norm) of the Park voltage vector, $V_{\text{Park}}=\left\|v(t)_{\text{Park}}\right\|$

$i(t)_{\text{Park}}$: Park current vector

$i(t)_d$: Direct axis Park current vector component

$i(t)_q$: Quadrature axis Park current vector component

$i(t)_0$: Zero sequence current component resulting from Park transformation

$I_{\text{Park},h}$ Harmonic phasor of $i(t)_{\text{Park}}$ at harmonic number h

I_{Park}: RMS value (norm) of the Park current vector, found by $\left\|i(t)_{\text{Park}}\right\|$

$B_{e,\text{Park}}$: Equivalent susceptance associated to the Park imaginary power Q_{Park}

$I_{\text{Park},a}$: RMS value of the Park current vector derived from the Czarnecki/Fryze three-phase active current vector $i_a(t)_{3\phi}$ in (122) with similar physical meaning

$I_{\text{Park},s}$: RMS value of the Park current vector of the Czarnecki three-phase "scattered" current vector $i_s(t)_{3\phi}$ in (132) with similar physical meaning

$I_{\text{Park},r}$: RMS value of the Park current vector derived from the Czarnecki three-phase reactive current $i_r(t)_{3\phi}$ in (125) with similar physical meaning

$I_{\text{Park},rs}$: RMS value of the Park current vector $i_{r,s}(t)_{\text{Park}}$ which is an additional definition by Ferrero and Superti-Furga [26] termed the "scattered reactive" current

$B_{e,\text{Park}}$ Equivalent susceptance associated to the Park imaginary power Q_{Park}

$I_{\text{Park},f}$: RMS value of the Park current vector $i_f(t)_{\text{Park}}$ derived from the "generated" current vector of Czarnecki, $i_g(t)$ (127) with similar physical meaning

1.5 FGW DOMAIN SYMBOLS

T_{FGW}: Transformation matrix required to transform four wire phase-domain voltage and current vectors to three-dimensional voltage and current space vectors

$v(t)_{dqz}$: Voltage space vector

$v(t)_d$: Voltage space vector component of the d-axis

$v(t)_q$: Voltage space vector component of the q-axis

$v(t)_z$: Voltage space vector component of the z-axis

$v(t)_0$: Voltage space vector component of the 0-axis

$\bar{v}(t)_{dqz}$: Hypercomplex quantity to represent $\bar{v}(t)_{dqz} = v(t)_d \bar{v}_x + v(t)_q \bar{v}_y + v(t)_z \bar{v}_z$

$\bar{v}_x$, $\bar{v}_y$, $\bar{v}_z$: Hypercomplex units

V_d: RMS value of space-vector voltage component $v_d(t)$

V_q: RMS value of space-vector voltage component $v_q(t)$

V_z: RMS value of space-vector voltage component $v_z(t)$

V_{dqz}: RMS value of voltage space-vector, $V_{dqz}=\| v(t)_{dqz}\|$

$i(t)_{dqz}$: Current space vector

$i(t)_d$: Voltage space current component of the d-axis

$i(t)_q$: Voltage space current component of the q-axis

$i(t)_z$: Voltage space current component of the z-axis

$i(t)_0$: Voltage space current component of the 0-axis, similar to Fortesque zero sequence component

$\bar{i}(t)_{dqz}$: Hypercomplex quantity to represent $i(t)_{dqz}$: $\bar{i}(t)_{dqz} = i(t)_d \bar{v}_x + i(t)_q \bar{v}_y + i(t)_z \bar{v}_z$

I_d: RMS value of space-vector voltage component $v_d(t)$

I_q: RMS value of space-vector voltage component $v_q(t)$

I_z: RMS value of space-vector voltage component $v_z(t)$

I_{dqz} : RMS value of voltage space-vector, $I_{dqz}=\| \boldsymbol{i}(t)_{dqz} \|$

$\bar{a}(t)$ Hypercomplex power defined by $\bar{a}(t)=\bar{v}(t)_{dqz}\cdot\bar{i}(t)^{*}_{dqz}=a_s(t)+a_x(t)\bar{v}_x+a_y(t)\bar{v}_y+a_z(t)\bar{v}_z$

$a_s(t)$: Scalar component of the hypercomplex power $\bar{a}(t)$

$a_d(t)$: d-axis component of the hypercomplex power $\bar{a}(t)$

$a_q(t)$: q-axis component of the hypercomplex power $\bar{a}(t)$

$a_z(t)$: z-axis component of the hypercomplex power $\bar{a}(t)$

1.6 OTHER SYMBOLS

VTHD: Total Harmonic Voltage Distortion

ITHD: Total Harmonic Current Distortion

Q_r: Fryze and Czarnecki definition of reactive power, can be defined for both a single-phase and a three-phase load

Q_B: Budeanu's reactive power

D_B: Budeanu's "distortion" power

D_s: Czarnecki's "scattered" power

D_g: Czarnecki's "generated" current, can be defined for both a single-phase and a three-phase load

D_u: Czarnecki's "unbalance" power

C: Capacitor

R: Resistor

2 TABLE OF FIGURES

3 TABLE OF CONTENTS

1 THE NATURE, SOURCES, AND EFFECTS OF NON-SINUSOIDAL VOLTAGE AND CURRENT WAVEFORMS IN ELECTRICAL NETWORKS

1.1 INTRODUCTION

The main thrust in the work presented in this thesis lies in the critique of the methodologies proposed for the localisation of distortion sources in three-phase electrical power networks[2].

In a power system, distortion sources are distributed at random over the network. It was shown by Swart *et al.* [57] that it is not possible to geographically localise a source of distortion in an interconnected power system with distributed loads, through single-point measurements. Normally, power system measurements only employ single-point measurements. The measurements that are carried out at different metering points are typically not correlated or synchronised with each other and to synchronise them to a high enough accuracy for multipoint synchronised measurement calls for unusual measures and equipment. The fact that single point measurements cannot be used for distortion point localisation contains important practical implications. The validity of the above finding is therefore again investigated in this thesis and of the original frequency-domain modelling, on which the original findings were based, is now also extended to time-domain modelling [58].

A fundamental underlying principle that is used in the localisation of distortion in power networks is the definition of electrical power under conditions of non-sinusoidal currents and/or voltages. Where it is a relatively simple matter to define power unambiguously in electrical systems with sinusoidal voltages and currents, many alternative definitions are possible in equivalent systems in the presence of distorted waveforms. Even though different proposed theories may be mathematically sound, their definitions range from those in which the defined subcomponents have physically relatable quantities to those in which they merely consist of mathematically defined quantities that have little or no bearing on physically relatable components. A systematic study is therefore first required to compare the existing alternative power theories with regard to their utility in the localisation of distortion sources motivation for the research.

Energy phenomena associated with non-sinusoidal power systems were brought to the fore by advances in silicon semiconductor technology and their use in sophisticated non-linear energy-conversion for

---

[2] The initial research goal of the thesis rested on the hypothesis that it is not possible to use harmonic active power analysis in the localisation of multiple distortion sources by single-point measurements when these distortion sources are randomly distributed over the electrical power network.

specialised applications. Power theory formulations that cater for the analysis of these systems are even now widely debated because researchers in the field continually develop new insights. Because these power theories and accompanying power definitions are at the root of the electrical engineering concepts that structures the design and rating of a power system, these theories must be comprehensive, mathematically correct and physically relatable.

The drawing of non-sinusoidal currents by a customer will invariably bring about distortion in the voltages delivered by the utility, through voltage drops and resonances in the impedances of the network. As soon as a new and advanced energy conversion process is therefore commissioned and functional in the power system, monetary aspects need to be taken care of. In the main, a customer must be billed in accordance with the quantity of energy ("useful" energy) received from the utility. In addition utilities, who are the ultimately responsible parties, have to incur costs to mitigate deleterious side-effects brought about by harmonics injected by consumers, or to devise and implement deterrents in the tariff for consumers who do so. This scenario is a complex one in practical power systems, where multiple customers are supplied from the same point of common coupling (PCC) and in which the relative contributions to distortion have to be assigned to the guilty parties. A number of questions arise here with regard to multi-frequency power system operation:

- How to apportion the aggregate cost brought about by the distortion injected by consumers between the responsible parties: This cost includes that of energy losses by the supply authority, mitigation of the distortion by the utility, risk of damage to utility equipment, losses from sale of power to other consumers because of the presence of distortion, imbalance etc.
- Quantitative definitions for all the components of real and distortion power are necessary in order to calculate and apportion distortion in the network.

Power factor correction now has an additional component to the conventional displacement factor that engineers had to content with in single frequency systems. Passive power factor correction produces negative effects in the presence of harmonics and can no longer be implemented in the conventional manner. When used, tuned harmonic filters must be incorporated with the required capacitors and changes in circuit topology or loading elsewhere can introduce system resonances with disastrous consequences. Alternative remedies exist, such as the use of Static VAR systems and dynamic filters (active compensators), but are expensive and can only be optimally implemented in hybrid systems in which passive (harmonic filters), dynamic (pulse width modulated) and line frequency switched (static VAR) systems are used. The best allocation of the duty between these components can only be attained through complex control.

All in all, distortion power theory plays a major role. The definitions for real, imaginary and loading power requires to be physically meaningful and relatable and require the least complexity and difficulty in measurement. Classical power theory is comprehensive with regard to single-frequency systems and is

capable of addressing the whole spectrum of applications. Different sets of definitions have been proposed for multi-frequency systems, but are each directed at specific tasks, such as dynamic compensator control, power measurement for billing purposes, distortion source measurement and many more. The proponents of each of these theories claim unique as well as universal advantages for their definitions, but none of these are truly able to cover the whole spectrum of requirements. The search for a single power theory for distortion power in electrical power systems is a continuing one.

1.2 DOCUMENT LAYOUT

Chapter 1 sets the perspective and spells out the rationale behind the research that is undertaken generally and in the thesis. It presents the structure of the thesis and puts the rationale of the research undertaken and reported on into perspective.

Chapter 2 begins with a revisional discussion of mathematical techniques for analysing non-sinusoidal power system behaviour. Among other, the following approaches are introduced:

- The Classical Fortesque transform and the Park Transform is adapted for multi-frequency application.
- The Ferrero/Guilliani/Willems approach in which three-phase four-wire quantities can be transformed into four-dimensional "quaternal-like" domains that assigns physical insight to these quantities.

Chapter 2 then concludes with an examination of the fundamental mechanisms of energy transport in electrical systems through a field theory approach

Chapter 3 presents the experimental and historical background against which definitions and localisation techniques are developed in this thesis. It lays down the basis by means of which the data is obtained and explains the time-domain computer simulations and real-life measurements that are used. In the case of the latter it emphasises the difficulties and precautions that have to be taken with regard to the use of voltage and current transducers, anti-aliasing filters and analogue-digital converters. It discusses spectral leakage and the phase errors introduced by the asynchronous sampling of different input channels.

Chapter 4 focuses on non-sinusoidal power theories. The differences and relative features of time-domain and frequency-domain power definitions are discussed. The power theories chosen for comparative evaluation in this thesis are motivated, analysed and applied to simulated data. The inadequacy of the Budeanu power theory (according to Czarnecki [2]) is verified. This exercise shows how easily shortcomings can be overlooked unless a new power theory is evaluated extensively against a practical background.

The Czarnecki power theories are also subjected to scrutiny in Chapter 4. Czarnecki did not develop a

complete theory but began by defining distortion power in a single-phase power system first, with parameters defined only in that regime. That theory had to be extended to incorporate three-phase distortion power theory, for which additional definitions were required. Czarnecki's three-phase power theory is tested in this chapter against simulation and practically generated data, bringing certain inadequacies to the fore, which will be of great importance when these definitions were to be adopted in practice.

The Fryze-Bucholz-Depenbrock (FBD) power definitions and the power definitions based on the Park transform by Ferrero and Superti-Furga [26] represents alternative approaches to non-sinusoidal power analysis and is presented in order to furnish background to the power theory formulated by Ferrero, Giulliani and Willems [29]. (This power theory will be referred to in this thesis as the *FGW power theory*).

Chapter 5 employs time-domain modelling and real-life measurements to verify that the hypothesis on the localisation of distortion sources in a power system as formulated in section 1.1 is indeed valid. Chapter 5 additionally evaluates a number of different localisation principles proposed in literature. It is concluded with a tentative[3] solution [55] of the distortion localisation problem, based on a distributed measurement system that uses a new global power quality index.

1.3 THE SIGNIFICANCE OF ELECTRICAL POLLUTION

Electrical "pollution" is injected into a power system when non-sinusoidal voltages and currents are induced by load or supply system non-linear behaviour. Harmonic pollution is an unavoidable manifestation that has been accelerated in recent times by the introduction of larger quantities and higher power rated power electronic equipment using line frequency- and pulse width modulated switching techniques. The increase in the overall power rating of this type of equipment in power networks finds its cause in the continued development of solid-state state of the art development that introduces non-linear and time-invariant behaviour not present in single-frequency networks. "Electrical pollution" is analogous to industrial pollution, which is in turn brought about by the technologically based subsistence of humankind. In the latter case the mediums in which the pollution is propagated are air and water and in the former it is the power networks.

Electricity was the major driving force behind the technological revolution of the modern world (which is only about 100 years old). Efficient transmission of energy in this form is dependent on the linear behaviour of generating, distribution and consumption systems. Optimal system operation could be

[3] This technique was not investigated in sufficient detail to finalise possible practical application on general power systems and could be an interesting topic of another Ph.D. research topic.

maintained with conventional equipment. Normally, the worst condition that had to be artificially rectified was that of poor fundamental power factor (sometimes referred to as *displacement power factor*). With the introduction of power-electronic drives and converters harmonic distortion began to be brought about that were orders higher in magnitude than those that had formerly to be contended with and that called for much more sophisticated mitigation techniques than that of pure fundamental frequency phenomena. The simple calculations that were required with traditional systems were now no longer possible and new insights and new definitions had to be sought. Because electrical power is such an important commodity for commercial operations, maintenance of its quality was and is equally important to that in any of the other products or of any other raw material or product.

"Pollution" of the electrical energy source has financial implications that impact on both the supplier and the consumer. A "polluted" voltage source will bring about additional expenses to both domestic and industrial users whether they be in the form of derating of equipment, additional system energy losses or damage to equipment. The injection of new power components by non-sinusoidal behaviour also brings about inaccuracies in the readings of standard measuring instrumentation and will influence tariffs and system transmission capabilities. Metering errors in the presence of distorted voltages and currents are reported on comprehensively in the literature and a selection of references is listed in the bibliography.

Non-sinusoidal operation often has deleterious effects on the operation of power electronic systems. Examples are the synchronising errors that are experienced by thyristor control circuits as the result of multiple zero crossings in supply voltage signals, overheating and shortened life span of transformers and electro-mechanical machinery and the often fatal harmonically induced resonance in power factor correction capacitors.

A power system is typically an enormous electrical grid of interconnected generation, transmission, distribution and reticulation functions. Electrical neighbours have a mutual interaction because the method of utilisation of electricity by a given user can influence the effectiveness of connected processes by the others. The dominant component of pollution in electrical power networks is surely that of steady-state harmonic pollution, even though transient behaviour and dips also require consideration. Because the nature of waveform distortion can best be described by a summation of integer harmonic components with reference to the fundamental frequency, it is customary to refer to the concept of "steady state electrical pollution" as "harmonic pollution".

There are two other categories of steady state pollution that bear mentioning, namely that of the so-called inter-harmonics and subharmonics. The former is principally brought about by asynchronous switching frequencies in power electronic and the latter by stochastic conduction processes such as that taking place in arc furnaces. The magnitudes of the distortion of the first that are normally encountered in power networks puts it into the background as far as this study is concerned and the second one requires completely separate study. Both therefore fall beyond the scope of the study in this thesis and will not be

discussed. This thesis deals with the measurement and definition of the magnitude of steady state harmonic distortion and with the establishment of its locality in the power system.

1.4 THE IMPORTANCE FOR SPECIAL POWER DEFINITIONS FOR NON-SINUSOIDAL POWER SYSTEMS AND THE MOST APROPIATE POWER THEORY

1.4.1 Background

The need for special definitions for three-phase non-sinusoidal power systems is illustrated in this section against the ineffectiveness of the classical power definitions in the same environment. The history of development of alternative power theories is also briefly discussed.

Budeanu [1] began to develop the subject of power definition in 1927 when he attempted to explain why the relation of $S^2=P^2+Q^2$ is not valid for a network in the presence of non-sinusoidally shaped voltage and current waveforms. A different number of researchers have since contributed towards the development of a power theory that will overcome that anomaly and that can be used in practical non-sinusoidal situations. Although Budeanu first described this phenomenon through a frequency domain approach, it had already been observed by Steinmetz [19] in 1892. He realised that the ratio of active to apparent power decreases when a waveform becomes more distorted in the case of an electric arc. It was a very important discovery because at that time, it was generally accepted that the ratio of active power to apparent power was only influenced by the phase shift between the voltage and current of the fundamental frequency.

The most desirable features of a universal multi-frequency power theory are:

- It must, as far as possible consist of a generalisation of the classic single-frequency power theory that has by now been universally accepted.
- It must be as amenable to conventional measurement techniques as possible and require the minimum of sophistication in instrumentation.
- Its different defined components must be relatable to physically observable or ascribable phenomena and not to hypothetical or abstract mathematical definition.
- It must present a suitable basis for quantifiable measurement, control, tariff systems and design.
- It must cater for every conceivable practical situation and never violate circuit laws, regardless of which domain it is transformed into.

Unfortunately, even now, more than a century after Steinmetz and Budeanu, there is still a lack of agreement between engineers as to which multi-frequency power definitions are to be adopted universally and the search is still hot for a single theory that will conform to the requirements bulleted above.

1.4.2 The History of Non-Sinusoidal Power Theory

Those researchers who have contributed most significantly to power theory development during the 1900's are listed below. The names in bold list those who are most cited in the literature studied by the author.

Table 1: History of Distortion Power Theories

Lyon	1920	**Depenbrock**	1977-2003
Bucholz	1922	**Kusters and Moore**	1980
Budeanu	1927	Page	1980
Fryze	1932	**Nomowiesjki**	1981
Goodhue	1933	**Akagi-Nabae**	1983
Quade	1937	**Filipski**	1984
Nudelcu	1963	Sawicki	1986
Sharon	1972	**Czarnecki**	1987-1998
Shepherd-Zakikhani	1972	Enslin	1988
Emanuel	1974	**Tenti**	1990
Harashima	1976	**Ferrero**	1991-2003
		Willems	1992-2003
		IEEE, Emanuel	1996-2003

Either *time-domain* or *frequency-domain* approaches are adopted in a power theory. Time-domain contributions have mainly been made by Fryze [75], Kusters and Moore [34], Page [25] Akagi-Nabae [74], Ferrero, Superti-Furga [26] and Willems [33].

The following developments were in the frequency domain. Budeanu [1] published the first notable frequency-domain power theory that is still employed almost universally by engineers. Nomowiesjki's [66] work also resorts to those of the pioneers and more recently there were Bucholz and Goodhue [68] and Czarnecki. Last named contributed to the knowledge on non-sinusoidal power phenomena with a large number of publications [3], [5], [7], [8], [3], [10], [11], [17], [16]. Czarnecki also demonstrated a number of deficiencies in the Budeanu theory. The Bucholz and Goodhue definitions[4] were recently shown by Emanuel to be of practical value in modern power systems.

The theories developed by Depenbrock [78], Ferrero [26], [29], [28] and Emanuel [68] are most noticeable for their practical value to the engineer dealing with non-linear power systems. (Emanuel has contributed both individually and as Chairman of the IEEE Working Group on Non-sinusoidal Situations [69], [68], [67].) A more comprehensive list can be found in the bibliography.

[4] The author could not obtain a copy of their original work published in 1922 and 1933 respectively, but Emanuel [68] interprets their work comprehensively.

Final consensus has not yet been reached as to which power definitions best suits which applications, or better still on a universally applicable set of definitions. New contributions are still being published in the literature on an on-going basis. There is more agreement however on the validity of a number of concepts among those definitions, by a growing number of engineers, than before. A number of prominent non-sinusoidal power theories are critically analysed and evaluated in Chapter 4 and for one, has isolated an important deficiency of the Czarnecki three-phase power theory

An essential feature of a power theory is that it has to relate the defined components to physically definable or observable quantities without violating any of the established circuit laws. Various attempts have been made in the past to build all the above requirements into a single power theory.

It has then demonstrated that the generality and physically relatable components of the Ferrero, Guilliani and Willems [29] power theory furnish it with all the features necessary in this type of work. A further very essential feature of such a power theory is that it will relate the defined components to physically definable or observable quantities without violating any of the established circuit laws. Various attempts have been made in the past to build all the above requirements into a single power theory. Very recently a new theory/formulation was developed by Ferrero, Giuliani and Willems [29] that appears to accomplish all of this.

1.4.3 The generation of non-sinusoidal waveforms

It follows fundamentally that the ideal case for the transmission of energy in an alternating current system will take place when the voltage and current waveforms are in-phase replicas of each other. That ideal was initially realised when the major use of electricity was to supply power for heat and lighting. Under those conditions, a linear relation existed between the load current and its driving voltage. However, when transformers, rotating magnetic machinery and gas-discharge lamps began to be used, the load current profile lost its resemblance to that of the voltage and the non-linear relationship, which is so pronounced in modern power systems first began to manifest itself.

Technological advances in power conversion caused non-linear load currents to be drawn from the voltage source. Inevitable non-zero impedances in the system, between sources and loads, brought about non-sinusoidal voltage drops and brought about distortion in the voltages at other nodes in the network. Equipment of consumers who are connected to these nodes will experience these non-sinusoidal voltages and will, in turn, draw non-sinusoidal currents even though their loads are linear and non-distorting. This implies that any modern power system will experience a larger or smaller degree of non-sinusoidal waveform behaviour.

Ideal AC generators exhibit zero internal impedance and produce perfectly sinusoidal waveforms under any load condition. Practical alternators exhibit unavoidable synchronous impedance. Non-sinusoidal currents will therefore also cause the generator terminal voltage to become non-sinusoidal, although

only marginally so because of the relatively low value of that synchronous impedance. Greater distortion is brought about in the networks, however, because of their larger impedances, which are predominantly inductive with resultant delivery point harmonic distortion. To investigate the phenomena outlined above, refer to the single-line diagram below.

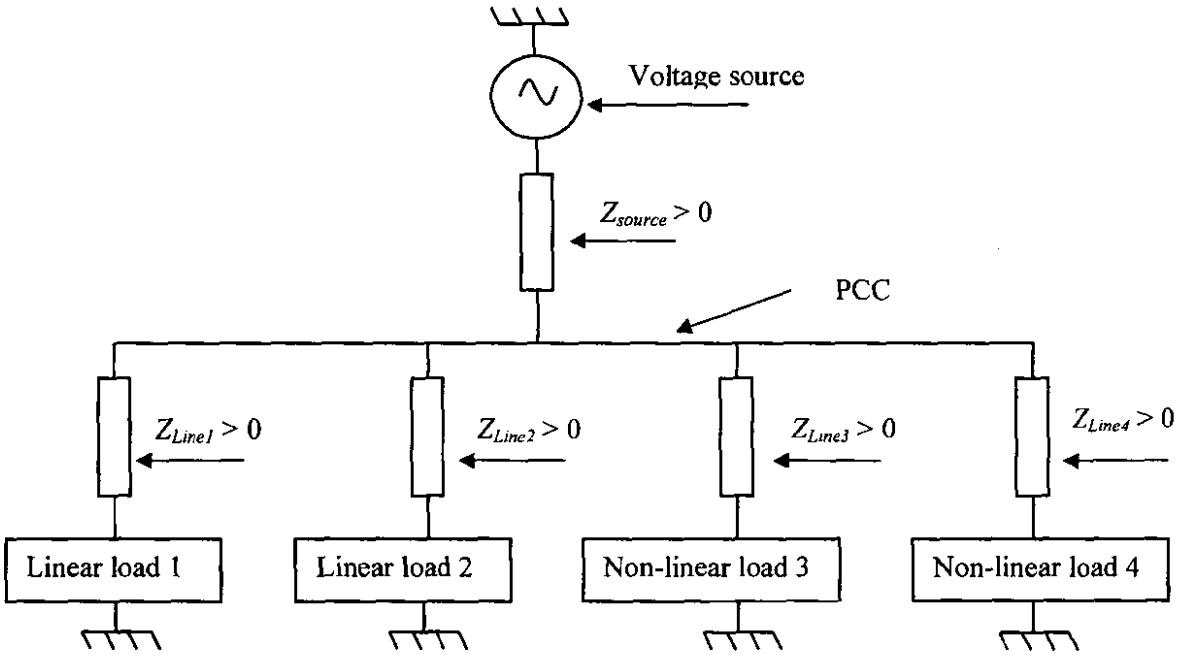

Figure 1: Sinusoidal voltage source feeding a combination of linear and non-linear loads

An electric utility (Voltage source in Figure 1) will supply a near-sinusoidally-shaped voltage waveform at the generator terminals. This generated voltage waveform is transmitted through a transmission network (with a relatively low impedance) to a *point of common coupling* (PCC).

Separate lines connect the generator to the four loads in Figure 1. Loads 3 and 4 are non-linear. The resulting load currents from these non-linear loads contain harmonic currents that are superimposed onto the fundamental source current. The lines that connect the PCC with the non-linear loads have frequency-dependent impedances. These bring about frequency-dependent voltage drops over these lines. Similar voltage drops will occur over the frequency dependent transmission line that connects the power station and the PCC. As a result of the superposition of the voltage drops at these harmonic frequencies onto the fundamental voltage signal, distorted voltage waveforms will result at each PCC, including those drawing only sinusoidal currents. Supply terminal voltages at Loads 1 and 2 will now be distorted, resulting also in them drawing distorted currents.

Electrical equipment can only be designed to operate optimally under sinusoidal conditions. Various detrimental effects are manifested in such equipment when operating under non-sinusoidal conditions. Inaccuracies are also brought about in conventional energy metering equipment that employs

mechanical integration. Customers that conform to the requirements of non-distortion will therefore be forced to operate their equipment under non-sinusoidal conditions. Their equipment will draw non-sinusoidal currents for which they may be doubly penalised; firstly because they are not the cause thereof and secondly because their metering equipment may malfunction and not show accurate readings.

The next section presents a brief overview of a number of non-linear loads that can bring about non-sinusoidal conditions in power systems.

1.4.4 Sources of Harmonic Distortion

It is possible to distinguish at least four categories of harmonic distortion sources:

1. **Non-linear components of small ratings**

A significant number of single-phase appliances convert energy obtained from low-voltage supplies through a solid-state converter. Examples of such converters are numerous. The most common types are the power supplies of computers and of television sets. When considered individually, each of these appliances has a very low power rating, but because of their large numbers, their aggregate contribution to distortion may be significant. Phase diversity may constitute an alleviating factor here, but the sheer total harmonic loading may still produce large levels of distortion on low-voltage systems.

Gas-discharge lighting in a building with considerable numbers of these devices connected to the same network is also a major contributor to harmonic distortion in a low-voltage power system. The diversity factors of different harmonic numbers, as typically used by reticulation engineers in low-voltage power systems, are listed in Table 2. Phase angle differences within given harmonics, means that the harmonic currents are not linearly additive and bring about diversity factors lower than unity.

Table 2: Harmonic current diversity

Current harmonic number	Diversity factor
3	1
5	0.9
7	0.9
9	0.6
11	0.6
13	0.6
15	0.5
17 and up	0.2
All even harmonics	0

The neutral conductor of a three-phase system that supplies three single-phase circuits in a star-connected configuration is normally not rated at the same current capacity than that of the phase conductors. Normally, neutral conductors only have to conduct the out of balance current. But, zero sequence third

harmonic currents in each of the three phases, due to unbalance, will add up in the neutral conductor. It is possible that a building in which the dominant load is composed of a large number of Personal Computers; the neutral RMS-current may be as large as 1.3 times that of a phase current. Good wiring practice in the presence of that type of loading requires that the neutral conductor must have twice the current rating of the phase conductors.

An awareness of the importance of energy-effective processes has led to regulations that assign importance to energy-efficiency in the design of new electrical equipment. About 90% of all motor loads in the USA [88] consist of "smaller" motors that are rated between a few hundred watt and 150 kW. The total motor load in the USA consumes 64% of all electrical power [88]. Energy-efficient control of these motors therefore presents an energy-saving opportunity. To achieve this, non-linear solid-state converters are the obvious choice between the utility and the motor but that leads to the introduction of even more non-linear harmonic-producing equipment than would normally apply.

Modern energy-efficient refrigeration equipment (e.g. refrigerators, air-conditioning) employs linear control over the cooling cycle. The conversion of single-phase power to controllable three-phase power is again made possible here through the use of power electronics. Three-phase induction machines are well suited for speed control applications and are now used in the construction of household refrigerators that employ single-phase input. Instead of using thermostatic on-off control, power electronics now make it possible to control the speed of the compressor to the level required to maintain the temperature at a specified level. This very nice feature is able to bring about a nett saving of energy, but again at the expense of additional non-linear, harmonic generating equipment.

2. **Large non-linear loads such as arc-furnaces**

Large loads range randomly in magnitude and relates specifically to the industrial plant used within. Power ratings of several megawatt are common and these loads are typically connected directly to the transmission network. The harmonic currents injected by equipment of this type vary randomly and are extremely asymmetrical. These harmonic currents that are injected into the network not only cause voltage distortion, but arc furnaces also cause flicker, although at a lower frequency than the fundamental.

3. **Three-phase static power converters and high-voltage transmission power electronics**

Line frequency controlled rectification is possible with 6-, 12- or even 24-pulse converters. These systems may be high-powered, as in the case of direct-current transmission systems, or medium-powered as in the case of railway traction applications. Large thyristor-controlled inverters are required to convert DC-transmitted energy to AC energy. The significant advance in silicon solid-state technology resulted in elegant solutions for the direct control of AC motors at a wide range of power levels.

Effective power factor correction is possible only when linear control is exercised over the magnitude and

sign of fundamental reactive power. A static VAR controller, (SVC) may be another significant contributor of harmonics when reactors are used in the line commutation mode to control the fundamental reactive power.

4. Classic iron-core sources of distortion

A transformer draws part of the current flowing into it to set up a magnetic flux inside the core. This magnetising/exciting current is characterised by a dominant third harmonic [96] component. The non-linear B-H curve of the magnetic materials that are used in the construction of the magnetic path in the core is the cause of this nonlinear exciting current. It has a frequency spectrum of uneven harmonics. The third harmonic current is typically 40% of the total RMS (root-mean-square) value of the exciting current. The exciting current itself is only about 5% of the rated current of a transformer. By using a delta winding on a transformer, the so-called triplen harmonic components can be minimised in the transformer internal windings, because they are zero sequence components. I^2R energy losses are caused by circulating harmonic currents in the transformer. It is interesting to observe that when the triplen harmonics are removed for example, the remaining 5^{th}, 7^{th}, 11^{th} and 13^{th} harmonic are of the same order as those produced by a 6-pulse rectifier with harmonic spectrum of $6k \pm 1$ ($k = 1,2, ...$). Because the fifth harmonic can be as high as 10% of the exciting current, it can have a perceptible effect on the load current of a transformer during light loading conditions.

When a transformer saturates as the result of an applied over-voltage, a significant rise can take place in the magnitudes of the magnetising harmonics. To minimise transformer core volume, high flux densities are used in core designs. A normal operating condition requires that the maximum flux magnitude should approach the saturation "knee" of the *B-H* curve. An increase in RMS voltage may drive the core just that much higher into saturation.

A rotating machine generates odd harmonics (without the triplens) due to a specific MMF distribution in the AC windings. Slot winding harmonics [96] are caused by the variation of permeance in the air-gap slots that has to be spaced at finite distances apart to accommodate windings.

Modern iron-core devices, in fact, contribute relatively more to harmonic distortion than the older iron-core devices did. Due to the competitiveness of the electrical equipment market, optimum utilisation of magnetic technologies such as those used in the telephone industry is less sensitive to non-sinusoidal conditions. Modern telephone lines are subjected to a lesser extent to interference caused by inductive coupling with power lines because analogue telephone links are being replaced by digital technology such as satellite links and digital optical fibre lines.

1.4.5 Parallel and Series Resonance

Power factor correction becomes unavoidable if the utility charges for apparent power drawn and

penalises the consumer for reactive power. Power factor correction capacitors furnish the negative reactive power that is required to improve a lagging power factor to acceptable levels. This extra capacitance in the power system can cause a localised resonant effect in the power system.

1.4.5.1 Parallel Resonance

Parallel resonance occurs when the impedance of a capacitor ($X_{C_{PF}}$) is equal in absolute value to the impedance ($X_{L_{series}}$) of the supply inductance. At the node in Figure 2 where the power factor correction capacitor is installed, the capacitor C_{PF} and the line inductance L_{series} forms a parallel circuit.

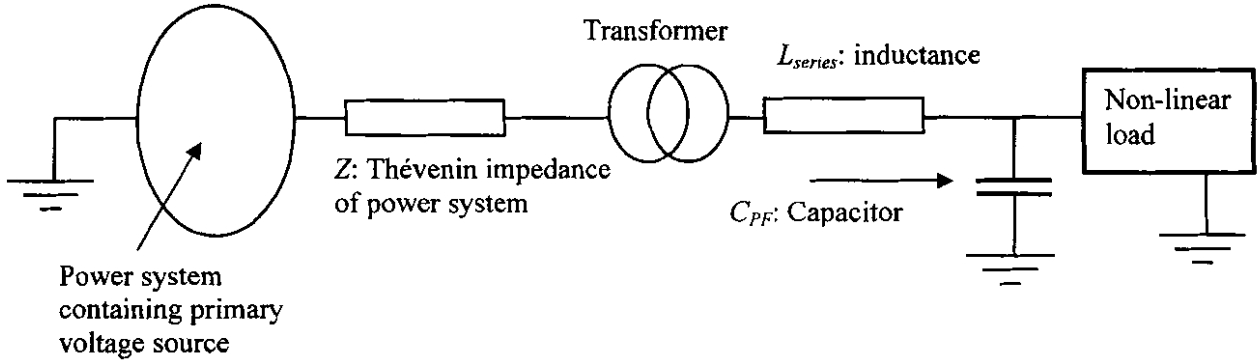

Figure 2: Parallel resonance

In a circuit such as Figure 2, parallel resonance may occur at angular frequency $\omega_{resonantP}$ according to:

$$\omega_{resonantP} = \frac{1}{\sqrt{L_{series} C_{PF}}} \tag{1}$$

There are other possible causes of parallel resonance. If the voltage source, in Figure 3, contains harmonic voltage components, parallel resonance may occur between the feeder line inductance (L_{series}) and the system capacitance (C_{system}), or between the feeder line inductance (L_{series}) and the power factor correction capacitors C_{PF} as the circuit below demonstrates:

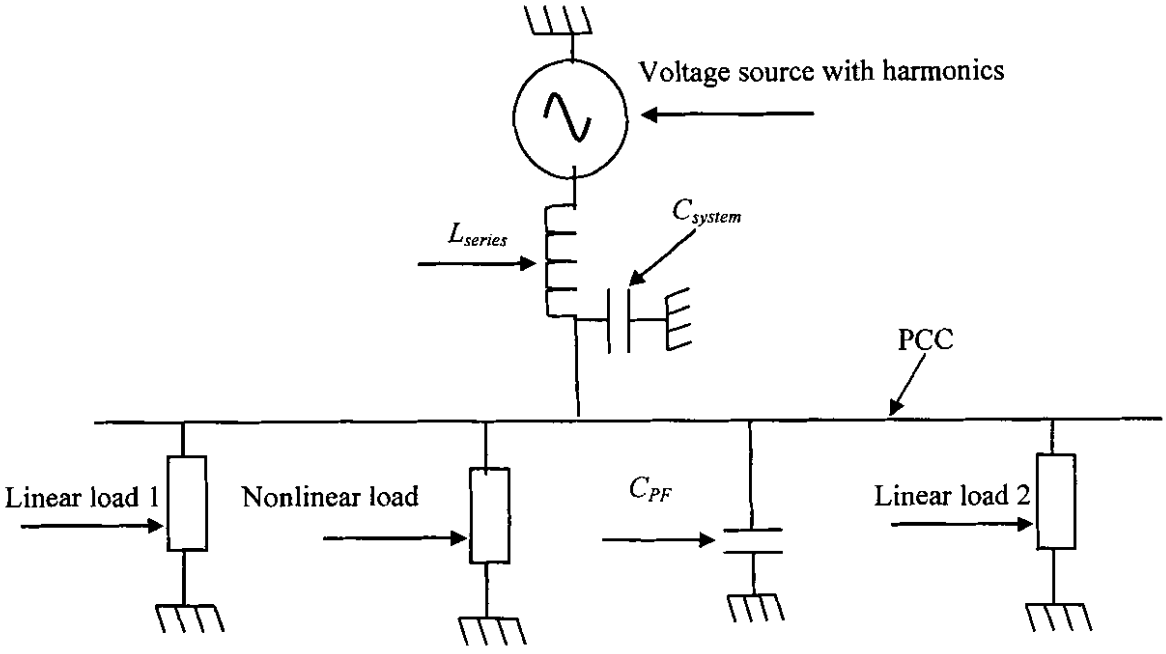

Figure 3: A PCC feeding both linear and non-linear loads, parallel resonance

Assume that a high value of a harmonic voltage is observed at the PCC. Inspection of the power system in Figure 3 shows that the voltage source feeds two possible parallel combinations of inductance and capacitance. The first parallel path is presented by the system inductance L_{series} and the system capacitance C_{system}. The second parallel path is presented by the system inductance L_{series} and the power factor correction capacitors C_{PF}. Because the non-linear load can also cause resonance and is in parallel with both the capacitors shown above, the cause of the resonance has to be found.

The cause of the resonance can be established by correlating the harmonic voltage at the PCC with the currents flowing in and out of the PCC. If the magnitude of the harmonic current flowing towards the PCC from the non-linear load is very small, the cause of the high harmonic voltage could be caused by the parallel combination of the supply line inductance, L_{series} and the system capacitance, C_{system}. If a large harmonic current is flowing into the non-linear load with a leading phase angle compared to the harmonic voltage observed at the PCC, the cause of the high harmonic voltage is the parallel resonance between the supply line inductance, L_{series} and the power factor correction capacitors, C_{PF}.

Before installing power factor correction capacitors, it must be verified that the resonant frequency does not coincide with known voltage harmonics. With the supply line from the voltage source to the PCC dominantly inductive, the parallel resonant frequency ($f_{resonantP}$) is generally formulated to be:

$$f_{resonantP} = f_1 \sqrt{\frac{S_{source}}{S_{capacitor}}} \tag{2}$$

1.4.5.2 Series Resonance

While parallel resonance is associated with a maximum impedance value for the parallel *LC* circuit, series resonance occurs when a series *LC* circuit has a minimum value of impedance. An example of series resonance is when a capacitor is connected in parallel with a linear load (such as for power factor correction) and in which the applied voltage signal has a non-sinusoidal component. This circuit, also, is supplied through a dominantly inductive transformer as shown below:

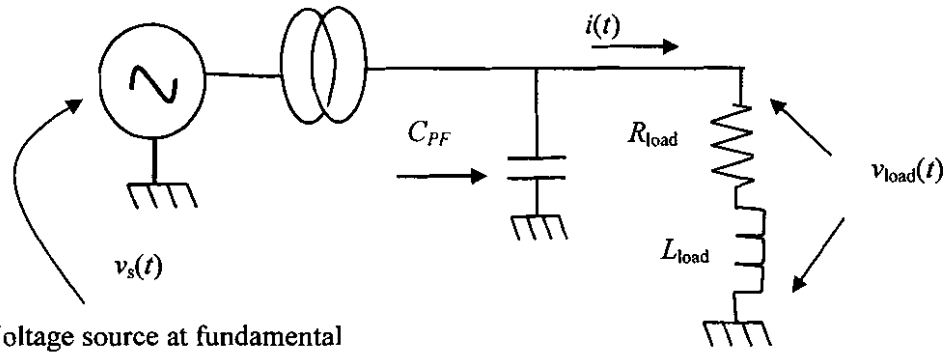

Figure 4: Series resonance

The voltage source $v_s(t)$, containing the harmonics is in series with the power factor correction capacitor C_{PF} and resonance takes place by virtue of the transformer leakage inductance and C_{PF} . Series resonance can bring about large harmonic currents even with small harmonic voltages present. The series resonant frequency ($f_{resonantS}$) is specified [95] by the following equation:

$$f_{resonantS} = f_1 \sqrt{\frac{S_{load}}{S_{C_{PF}} Z_{transformer}} - \frac{S_{load}^2}{S_{C_{PF}}^2}} \tag{3}$$

In the above equation, $Z_{transformer}$ is the transformer per unit (p.u.) impedance.

In both parallel and series resonant situations, capacitors can fail through overloading caused by I^2R heating or by dielectric stresses brought about through harmonic over-voltages. Cable insulation that is subjected to these harmonically induced over-voltages may also experience dielectric breakdown.

1.4.6 Other effects in a power system under non-sinusoidal conditions

Non-sinusoidal voltage and current waveforms reduce energy transfer efficiencies, compared to that achievable with pure sinusoidal waveforms. Applied to a purely resistive circuit, all the harmonic

components will contribute to the heat gained in the resistance, but the situation changes dramatically when the circuit also contains iron-cored equipment. Under those conditions additional losses are brought about that would not be the case with pure sinusoidal driving voltages.

Power systems will be at their most economical state when unity power factor is measurable everywhere. Under nonsinusoidal conditions, it is necessary to indicate whether the *true power factor* (also referred to as *overall power factor*) or the *displacement power factor* was measured.

The general effect of harmonics in the power system is well documented:

- The effect on iron-core equipment such as the additional losses and torques in rotating machines, additional hysteresis and eddy current losses in transformers,
- The skin effect in conductors and additional stress on capacitor banks,
- The influence on protection equipment and consumer equipment.

Literature, such as [89], [90], [91], [92], [93], [95], [96], discusses energy metering and instrumentation aspects under non-sinusoidal conditions.

Non-sinusoidal conditions bring about a violation of the well-known classical relationship $S^2=P^2+Q^2$. This phenomenon of $S^2-P^2-Q^2\neq 0$ was first described by Budeanu [1] in 1927 and defined to be caused by the "Budeanu distortion power" (symbol "D_B"), as described in the well-known non-sinusoidal Budeanu power theory. Budeanu's power theory is investigated in detail in chapter 4.

1.4.7 Requirements of a non-sinusoidal power theory

Assuming periodicity and steady-state operation, a power theory should be able to describe the additional power phenomena in both single-phase and three-phase power systems in a mathematically and physically sound manner. A three-phase power system could experience any combination of the following conditions:

- Non-linear or time-variant loading with reactive elements and non-zero commutation angles of controlled rectifiers;
- unbalanced loading between phases;
- a non-sinusoidal supply voltage;
- non-zero frequency-dependent supply source impedance; and

- asymmetrical three-phase supply voltage source.

Considering the above, important criteria for a three-phase power theory[5] are motivated next.

1.4.7.1 Conform to Electrical Network Laws

The formulation of power definitions must conform to accepted electrical network laws. If for example, certain current components are segregated from the total load current through mathematical definitions, these current components have to be auditable to account for the total current flowing through the node under investigation. The power definitions based on the different current components must then relate to the total apparent power observed at the cross-section.

1.4.7.2 Explain Physical Phenomena

Any power definition has to conform to the underlying electro-magnetic principles as described by Maxwell's laws and a power definition should as far as possible also support a physical interpretation. Mathematical manipulation of power definitions solely with the aim of overcoming mathematical/physical constraints retracts from its worth.

1.4.7.3 Be Measurable

A power theory has to be of value in practice. The quantities to be obtained and implemented in a power theory have to be measurable with instrumentation that is both practical and readily available. The subsequent signal processing of the measured data must not be unrealistic in terms of its demand on computing power and operator skill. The quantities must be extracted with sufficient certainty from measured voltage and current signals even in the presence of noise.

1.4.7.4 Economic Implications

Energy-effectiveness is a major issue in the economy of both the supplier and the consumer of electrical energy. The monetary implication of generating and transporting energy to a point of use in a non-sinusoidal power system must be accountable to the imposed tariff and the power definition must represent a fair quantitative measure of the costs incurred by the supply authority.

---

[5] It is not enough to regard a single-phase power theory as a special "one-phase" situation of a three-phase power theory. It is not a self-sufficient power theory because phenomena that are unique to only three-phase power systems, can not be adequately described in single-phase systems.

1.4.7.5 Enables Compensation

Compensation is used as a generic concept in this section to include both active filtering and reactive power compensation. Power definitions have to aid in interpreting unwanted power phenomena in sufficient detail to facilitate the design and rating of compensation equipment used for sinusoidal waveform restoration.

1.5 WHY IT IS IMPORTANT TO KNOW WHERE WAVEFORM DISTORTION ORIGINATES FROM

Distorted power system currents introduce voltage drops in system impedances that correspond to the frequency content of these currents. This introduces corresponding harmonic voltage components. The situation is aggravated where long transmission lines and distribution equipment of limited rating is the norm. A regulatory approach is therefore necessary to limit the number and magnitude of non-linear loads, penalising load current waveform distortion and low fundamental frequency power factor through the introduction of appropriate tariff structures.

The onus for mitigation of distortion rests with the consumer. Appropriate tariff structures that penalise distortion generation at its origin will be the most effective means of regulating the problem. The in-circuit location and identification (characterisation) of these loads are therefore required.

1.6 STANDARDS FOR HARMONIC LIMITS

The goal of harmonic standards is to control distortion of voltage and current waveforms to tolerable levels in order that customers can sustain production processes effectively. Different standards for limits on harmonics are used internationally. The approach is to either limit the distortion caused by non-linear load current, or by limiting voltage distortion. It therefore entails either a utility-based approach or a customer-based approach.

The following matters are typically addressed in such standards:

- Description of individual harmonic components allowed (voltage/current) in terms of amplitude.
- System voltage (transmission or distribution level) at which a quality of supply measurement is made.

The harmonic "capacity" of the system relates to the short-circuit impedance at the point of supply in per unit quantities. A "stiff" system, for example, will tolerate harmonics better than a "weak" system. The higher the system voltage, the lower the short-circuit rating in equivalent capacity systems. Harmonic currents therefore have less influence at a transmission voltage level than at a distribution voltage level.

- Definition of the harmonic limits

A mathematical formulation is required to quantitatively describe the different harmonic limits with respect to peak/RMS level, and the number of occurrences in a certain time interval. These limits must be able to be instrumented and verified.

- The method of measurement and characteristics of the instrumentation and data acquisition system

It is necessary to specify the measurement and analysis procedure applied, in order to ensure repeatability and reliability of the assessment of the power quality at a site under investigation. The maximum allowed uncertainty for each measurement should be specified.

- Description of the type of disturbing load

Different loads at different voltage levels and at different locations in the power system will affect power quality in different ways. A disturbing load has to be sufficiently characterised to be able to ascertain the possible effect that that load would have on the power system at a specific location.

More complex matters to be solved are issues such as distinguishing between the magnitudes of harmonic currents allocated to customers of different load ratings if the goal were to maintain the global *THVD* of the PCC at a certain level. According to the portion of the total load each customer will acquire at the PCC, the allowable harmonic current must be allocated (or apportioned) to each customer. Indeed, such allocation procedures form a typical section of a harmonic standard.

A customer, that is connected through relatively a low system impedance, with a non-linear load component, has a lesser influence on the *total harmonic voltage distortion* (*VTHD*) at the PCC and can be allocated a higher *total harmonic current distortion* (*ITHD*) than a customer that is connected through a higher system impedance. As the network expands, later customers will have to be allocated a more strict harmonic emission level to maintain the global *VTHD* to acceptable levels.

Managing harmonics in a power system is an interwoven and complex matter. It requires careful analysis of all the relevant factors. Although the goal of this thesis is not to compare and evaluate international harmonic standards, a brief overview is given to bring the non-sinusoidal scene into perspective. The South African, the American and the European approaches to harmonic standards are discussed consecutively in sections 1.6.1 to 1.6.3.

1.6.1 South Africa: NRS 048

The South African NRS048 document sets guidelines for the utility to ensure a voltage waveform of acceptable minimum quality at the point of supply to customers. It allows the utility to choose not to maintain that minimum standard at all busbars in its network. It covers not only harmonics but also other power quality aspects such as voltage dips, voltage regulation and flicker. Such standards necessarily require the utility to set up agreements with large customers to regulate their influence on the network. On the other hand, "electrically sensitive" customers may need quality of supply exceeding the typical minimum level. Special agreements are provided for in the South African harmonic standards and can be contracted between clients and utility.

Higher values of harmonic voltages are accommodated at lower voltage levels, as the system impedance is unavoidably higher. Matters such as how to apportion harmonic emission to new customers connected to a PCC, or guidelines on how to assess harmonic levels are discussed in detail in the NRS048 standard and can be found in the literature [103].material is required, bringing about the moving of operating points into the non-linear regions of the magnetic materials used in their design. Modern power systems can experience relatively higher levels of harmonics through iron-core equipment than their "older" counterparts did.

The limits on harmonics applicable to South Africa, is listed in appendix B.

1.6.2 American/IEEE 519-1992: IEEE Recommended Practices and Requirements for Harmonic Control in Electrical Power Systems

The IEEE 519 document is structured according to a current-based approach against the voltage-based approach of the NRS 048. It establishes limits on load current harmonics in recognition of voltage harmonic limits at user and utility buses. Consideration is given to short duration harmonics, background harmonics, interharmonics (harmonics that are not an integer multiple of the fundamental), even order harmonics, voltage notching and ringing. The standard applies to all types of static power converters used in industrial and commercial power systems. An application guide is also provided for harmonic control and reactive power compensation.

The IEEE 519 does not distinguish in detail between individual harmonics, while the NRS 048 considers each harmonic order up to the 25^{th} individually with different limits assigned to each. Harmonic limits applicable to the IEEE 519 standard, is listed in appendix A.

1.6.3 European: IEC/EN61000-3-*x*

The IEC standards are also current-based. The European IEC 61000-3-*x* indicates the various standards on harmonic control pertaining to Europe. For example, the IEC 61000-3-2 standards set limits for

harmonic current emissions below 16 A, which has been mandatory since 21st January 2001. Harmonic injection into the public distribution system is managed through these standards and therefore applies mainly to 230 V single-phase systems and 400 V three-phase systems. IEC 61000-3-12 describes harmonic control for low-voltage public power systems up to 75 A.

For three-phase systems of higher voltages, IEC 61000-3-6 is applicable. IEC 61000-3-6 is to be used as the basis for determining the requirements for connecting large distorting loads (producing harmonics and/or interharmonics) to public power systems. It serves as guidance for engineers to ensure the overall quality of supply in both MV and HV networks[6].

1.7 SUMMARY

Chapter 1 outlined the perspective and the rationale that supports the problem statements in this thesis. Non-sinusoidal operating conditions are unavoidable as the result of the introduction of modern semiconductor technology that has found widespread application in sophisticated energy conversion and control. New power definitions are needed to quantify non-sinusoidal operation in power systems. These alternative power definitions must be validated for application under these non-sinusoidal conditions.

The localisation of distortion sources in power systems will be required for effective mitigation thereof. Localisation techniques make use of power definitions that describe distortion. Present knowledge, based on a frequency domain modelling approach, rendered the application of harmonic active power useless for distortion source localisation when there are multiple distortion sources distributed throughout the network. Validation of the latter is required and it is possible to do similar investigations through time-domain modelling and real-life measurements.

[6] Details on the different guides are to be found at http://www.iec.ch/zone/emc/tables/lf_emission.htm.

2 ANALYSIS OF ELECTRICAL CIRCUITS UNDER NONSINUSOIDAL CONDITIONS

2.1 INTRODUCTION

Three-phase electrical power systems are the most effective solution towards achieving the generation, transmission and distribution of electrical energy. Three-phase power systems have additional requirements to those of single-phase power systems. For example, a three-phase power system should be balanced in terms of the loading between phases. Chapter 1 described in detail why waveform distortion occurs in a power system. To describe the various power phenomena associated with distorted waveforms in power systems require mathematical analysis. The first section of Chapter 2 therefore deals with the mathematical tools needed to carry out qualification and quantification of waveform distortion and to analyse the power system. Three mathematical analysis tools are presented in the first section of Chapter 2:

- The Fortesque transform for non-sinusoidal waveforms.
- The Park transform for non-sinusoidal waveforms.
- The analysis technique developed by Ferrero, Giuliani and Willems [29] to study the behaviour of four-wire three-phase power systems.

The second section of this chapter revises fundamental circuit theory. Electrical engineers employ circuit analysis techniques and rarely have to deal with field theory in their normal work. Much light, can however, be shed on electrical system behaviour through analyses through field theory. That is the case in multi-frequency steady state electrical system behaviour. Analysis of the operation of circuits through field theory in this chapter will further elucidate the fundamental concepts of steady-state multi-frequency power transportation phenomena. In this analysis, the propagation of power will be examined by the application of Maxwell's Equations and the Poynting-Vector.

2.2 THE FORTESQUE TRANSFORM AND NON-SINUSOIDAL WAVEFORMS

Fortesque formulated a mathematical transformation that enables the linear transformation of phase-domain components to a sequence-domain containing a set of symmetrical components. Analysis of a three-phase circuit with non-sinusoidal waveforms requires a modification of the conventional Fortesque transformation derived in 1918 [97]. Take note that it is only valid for periodic signals showing only harmonic distortion (h can only be an integer).

2.2.1 Fortesque Transform Redefined for Non-Sinusoidal Circuits

The complex operator $\boldsymbol{a}$ used in the classical Fortesque transform requires redefinition as voltage and

current signals to be transformed are no longer pure sinusoidal waveforms. It is accomplished by defining a harmonic-dependent complex operator $a(h)$:

$$a(h) = 1 \cdot e^{j\frac{2 \cdot \pi \cdot h}{3}} \tag{4}$$

The 3 x 3 Fortesque transformation matrix $A(h)$ is then defined as:

$$A(h) = \begin{bmatrix} 1 & 1 & 1 \\ 1 & a(h)^2 & a(h) \\ 1 & a(h) & a(h)^2 \end{bmatrix} \tag{5}$$

Transformation of the three-phase voltage harmonic vector $V(h)_{abc}$ to the sequence domain is defined as:

$$\begin{bmatrix} V_0(h) \\ V_1(h) \\ V_2(h) \end{bmatrix} = \frac{1}{3} \begin{bmatrix} 1 & 1 & 1 \\ 1 & a(h) & a(h)^2 \\ 1 & a(h)^2 & a(h) \end{bmatrix} \begin{bmatrix} V_a(h) \\ V_b(h) \\ V_c(h) \end{bmatrix} \tag{6}$$

The compact notation of the above is written as:

$$V_s(h) = A(h)^{-1} V(h)_{abc} \tag{7}$$

Transformation of the three-phase current harmonic vector $I(h)_{abc}$ to the sequence domain is defined as:

$$\begin{bmatrix} I_0(h) \\ I_1(h) \\ I_2(h) \end{bmatrix} = \frac{1}{3} \begin{bmatrix} 1 & 1 & 1 \\ 1 & a(h) & a(h)^2 \\ 1 & a(h)^2 & a(h) \end{bmatrix} \begin{bmatrix} I_a(h) \\ I_b(h) \\ I_c(h) \end{bmatrix} \tag{8}$$

The compact notation of the above is written as:

$$I_s(h) = A(h)^{-1} I(h)_{abc} \tag{9}$$

The inverse Fortesque transforms follows to be:

$$V(h)_{abc} = A(h) V_s(h); \;\; I(h)_{abc} = A(h) I_s(h) \tag{10}$$

2.3 THE PARK TRANSFORM AND NON-SINUSOIDAL WAVEFORMS[7]

The *d-q* theory is widely employed in analysing the transient behaviour of electrical machines. Park formulated this transformation of three-phase quantities to orthogonal *d-q* quantities in 1922. The transformation converts time-dependent three-phase three-wire voltage vector $v(t)_{abc}$ and the time-dependent three-phase line current vector $i(t)_{abc}$ to time-dependent Park voltage vector $v(t)_{\text{Park}}$ and Park current vectors $i(t)_{\text{Park}}$ respectively. It is a linear orthogonal transformation which makes use of an orthogonal matrix T_{Park}:

$$T_{\text{Park}} = \begin{bmatrix} \sqrt{2/3} & -\sqrt{1/6} & -\sqrt{1/6} \\ 0 & \sqrt{1/2} & -\sqrt{1/2} \\ \sqrt{1/3} & \sqrt{1/3} & \sqrt{1/3} \end{bmatrix}; \quad |T_{\text{Park}}| = 1 \tag{11}$$

The Park transformation of the voltage phase-domain vector is defined as:

$$\begin{bmatrix} v_d(t) \\ v_q(t) \\ v_0(t) \end{bmatrix} = \begin{bmatrix} \sqrt{2/3} & -\sqrt{1/6} & -\sqrt{1/6} \\ 0 & \sqrt{1/2} & -\sqrt{1/2} \\ \sqrt{1/3} & \sqrt{1/3} & \sqrt{1/3} \end{bmatrix} * \begin{bmatrix} v_a(t) \\ v_b(t) \\ v_c(t) \end{bmatrix} \tag{12}$$

The compact notation of the above is:

$$v(t)_{\text{Park}} = T_{\text{Park}} v(t)_{abc} \tag{13}$$

The Park transformation of the current phase-domain vector is defined as:

$$\begin{bmatrix} i_d(t) \\ i_q(t) \\ i_0(t) \end{bmatrix} = \begin{bmatrix} \sqrt{2/3} & -\sqrt{1/6} & -\sqrt{1/6} \\ 0 & \sqrt{1/2} & -\sqrt{1/2} \\ \sqrt{1/3} & \sqrt{1/3} & \sqrt{1/3} \end{bmatrix} * \begin{bmatrix} i_a(t) \\ i_b(t) \\ i_c(t) \end{bmatrix} \tag{14}$$

---

[7] Note that the Park transformation is a particular case of the Clarke transformation.

The compact notation of the above is:

$$\boldsymbol{i}(t)_{\text{Park}} = \boldsymbol{T}_{\text{Park}}\boldsymbol{i}(t)_{abc} \tag{15}$$

The time-dependent Park voltage $\boldsymbol{v}(t)_{\text{Park}}$ and current $\boldsymbol{i}(t)_{\text{Park}}$ vectors are complex and contain two orthogonal quantities:

$$\boldsymbol{v}(t)_{\text{Park}} = v(t)_d + \mathrm{j}v(t)_q \tag{16}$$

$$\boldsymbol{i}(t)_{\text{Park}} = i(t)_d + \mathrm{j}i(t)_q \tag{17}$$

The multi-frequency Park transformation also yields zero-sequence components $v_0(t)$ and $i_0(t)$ that are similar to the zero-sequence components yielded by its single-frequency counterpart. As in the single-frequency case, no zero-sequence components exist when the phase-domain voltage vectors have a common reference and current vectors do not have a common return (neutral).

The inverse multi-frequency Park transform for voltage is given by:

$$\begin{bmatrix} v_a(t) \\ v_b(t) \\ v_c(t) \end{bmatrix} = \begin{bmatrix} \sqrt{2/3} & -\sqrt{1/6} & -\sqrt{1/6} \\ 0 & \sqrt{1/2} & -\sqrt{1/2} \\ \sqrt{1/3} & \sqrt{1/3} & \sqrt{1/3} \end{bmatrix}^{-1} \begin{bmatrix} v_d(t) \\ v_q(t) \\ v_0(t) \end{bmatrix} \tag{18}$$

$$\begin{bmatrix} i_a(t) \\ i_b(t) \\ i_c(t) \end{bmatrix} = \begin{bmatrix} \sqrt{2/3} & -\sqrt{1/6} & -\sqrt{1/6} \\ 0 & \sqrt{1/2} & -\sqrt{1/2} \\ \sqrt{1/3} & \sqrt{1/3} & \sqrt{1/3} \end{bmatrix}^{-1} \begin{bmatrix} i_d(t) \\ i_q(t) \\ i_0(t) \end{bmatrix} \tag{19}$$

Because $\boldsymbol{T}_{\text{Park}}$ is an orthogonal matrix, $\boldsymbol{T}_{\text{Park}}^{-1} = \boldsymbol{T}_{\text{Park}}^{T}$.

The sequence powers yielded by the multi-frequency Park transform follows analogously from that of its original single frequency counterpart [44].

The relationship between the Fortesque sequence domain components and the Park components [26] written below for a single frequency, are as follows:

$$v(t)_{\text{Park}} = V_{1,1}e^{j\omega_1 t} + V_{2,1}^{*}e^{-j\omega_1 t}\ ^{8} \tag{20}$$

$$v_0(t) = \sqrt{2} * \text{Re}[V_{0,1}e^{j\omega_1 t}] \tag{21}$$

$$i(t)_{\text{Park}} = I_{1,1}e^{j\omega_1 t} + I_{2,1}^{*}e^{-j\omega_1 t} \tag{22}$$

$$i_0(t) = \sqrt{2} * \text{Re}[I_{0,1}e^{j\omega_1 t}] \tag{23}$$

The above equations show that the Park voltage and current vector can be obtained from only the positive sequence components in a balanced three-phase system with positive phase rotation as the negative and zero sequence components will not exist.

If the phase domain voltage and current waveforms are nonsinusoidal and is transformed to the Park domain, then the Park voltage and current vectors can be decomposed into Fourier series [26]:

$$v(t)_{\text{Park}} = \sum_{h=-\infty}^{\infty} V_{\text{Park},h}e^{jh\omega_1 t} \tag{24}$$

$$i(t)_{\text{Park}} = \sum_{h=-\infty}^{\infty} I_{\text{Park},h}e^{jh\omega_1 t} \tag{25}$$

The quantities $V_{\text{Park},h}$ and $I_{\text{Park},h}$ are Park harmonic phasors of voltage and current respectively. $V_{\text{Park},h}e^{jh\omega_1 t}$ and $I_{\text{Park},h}e^{jh\omega_1 t}$ are Park vectors with constant magnitude $V_{\text{Park},h}$ and $I_{\text{Park},h}$ that rotate in a positive or a negative direction as a function of the sign of the harmonic index h and with the rotational speed proportional to the index number h. The Park voltage and current vectors are related to positive and negative sequence components, Park harmonic components with positive harmonic frequencies (h>0) are related to positive sequence components and Park harmonic components at negative harmonic frequencies (h<0)) represents negative sequence symmetrical components:

$$\begin{aligned} V_{\text{Park},h} &= V_{1,h} \text{ and } I_{\text{Park},h} = I_{1,h} \text{ if } h > 0 \\ V_{\text{Park},h} &= V_{2,h}^{*} \text{ and } I_{\text{Park},h} = I_{2,h}^{*} \text{ if } h < 0 \end{aligned} \tag{26}$$

---

[8] The frequency component assumed in this example is the fundamental frequency components of positive sequence and negative sequence phasors, h =1 in $V_{1,h}$ and $V_{2,h}$. The superscript "*" indicate the complex conjugate.

The RMS value of the Park voltage vector (similar for the Park current vector) is expressed as:

$$V_{\text{Park}} = \sqrt{\sum_{h=-\infty}^{+\infty} V_{\text{Park},h}^2} \tag{27}$$

The special consideration of separate zero sequence quantities of the Park transform when applied to four-wire unbalanced three-phase power systems, is overcome by the transformation presented in section 2.4.

2.4 THE FERRERO, GUILIANI, WILLEMS (FGW) SPACE-VECTOR TRANSFORMATION OF FOUR-CONDUCTOR THREE-PHASE QUANTITIES

2.4.1 Introduction

A three-wire three-phase power system can be completely described by its Park voltage and current vectors. When a four-wire three-phase system is analysed, the zero-sequence components represent an "extra" system and has to be considered separately. A new transformation principle devised by Ferrero, Giuliani and Willems[9] [29] enabled analysis of transformed quantities in a single new domain. A space-vector transformation was formulated [29] that transforms both voltage and current vectors of both three-wire and four-wire power systems into a single domain. An important feature of the resulting FGW power definitions is that these new power definitions are not simply an extension of single-phase-based power definitions. This transform enables independent power definitions in a new domain. The mathematical principles of this transformation are presented in the following section.

2.4.2 FGW transformation principles and mathematical definitions

The FGW transformation transforms both three wire and four wire three-phase power system quantities to three-dimensional *hypercomplex quantities*. The concept of a space vector defined in the *d-q* domain is extended by means of a new mathematical principle to the concept of a space vector that is a hypercomplex quantity in a three-dimensional domain.

The transformation matrix as defined [29] possesses the following characteristics:

- It is orthogonal.
- A diagonal impedance matrix results if the phase impedance matrix is symmetrical with equal off-diagonal elements.

[9] This transform is abbreviated as the FGW transform in this thesis.

- Three linearly independent voltage and current components in the FGW domain represent the four linearly dependent voltage and current components of a four-conductor three-phase power system.

- The FGW transformation matrix transforms three-wire three-phase quantities to Park quantities just like the Park transformation matrix.

The FGW transformation matrix is defined[10] below:

$$\boldsymbol{T}_{FGW} = \sqrt{\frac{2}{3}} \begin{bmatrix} 1 & -\frac{1}{2} & -\frac{1}{2} & 0 \\ 0 & \frac{\sqrt{3}}{2} & -\frac{\sqrt{3}}{2} & 0 \\ \frac{1}{\sqrt{2}} & \frac{1}{\sqrt{2}} & \frac{1}{\sqrt{2}} & -\frac{3}{\sqrt{2}} \\ \frac{\sqrt{3}}{2\sqrt{2}} & \frac{\sqrt{3}}{2\sqrt{2}} & \frac{\sqrt{3}}{2\sqrt{2}} & -\frac{\sqrt{3}}{2\sqrt{2}} \end{bmatrix}; \quad |\boldsymbol{T}_{FGW}| = 1 \tag{28}$$

A four-wire three-phase power system is shown in Figure 5:

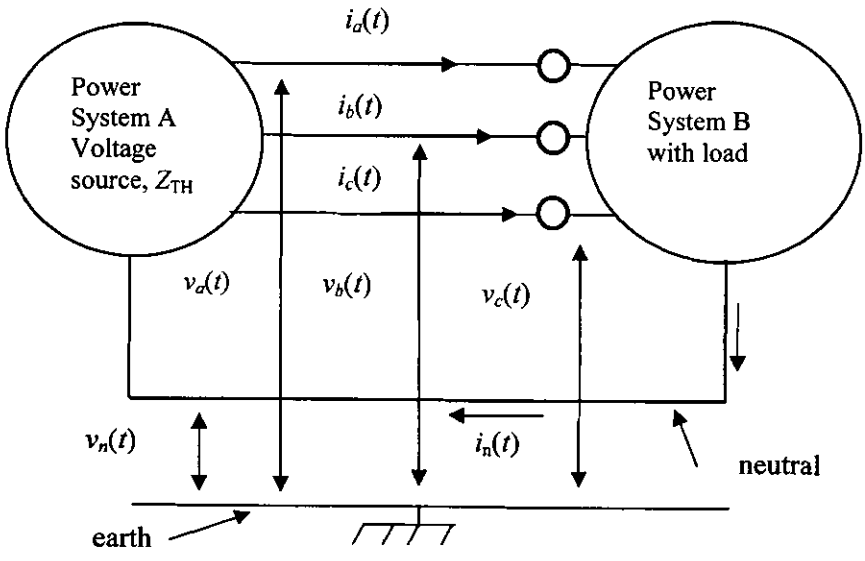

Figure 5: Three-phase four-wire power system

Transformation of the four-wire three-phase quantities to the three-dimensional space-vectors is defined as follows:

[10] Take note that the numerical error in the formulation of [*T*] in [29] is corrected in this thesis.

$$\begin{bmatrix} v_d(t) \\ v_q(t) \\ v_z(t) \\ v_0(t) \end{bmatrix} = \begin{bmatrix} 1 & -\frac{1}{2} & -\frac{1}{2} & 0 \\ 0 & \frac{\sqrt{3}}{2} & -\frac{\sqrt{3}}{2} & 0 \\ \frac{1}{2\sqrt{2}} & \frac{1}{2\sqrt{2}} & \frac{1}{2\sqrt{2}} & -\frac{3}{2\sqrt{2}} \\ \frac{3}{2\sqrt{2}} & \frac{3}{2\sqrt{2}} & \frac{3}{2\sqrt{2}} & -\frac{3}{2\sqrt{2}} \end{bmatrix} \begin{bmatrix} v_a(t) \\ v_b(t) \\ v_c(t) \\ v_n(t) \end{bmatrix} \tag{29}$$

$$\begin{bmatrix} i_d(t) \\ i_q(t) \\ i_z(t) \\ i_0(t) \end{bmatrix} = \begin{bmatrix} 1 & -\frac{1}{2} & -\frac{1}{2} & 0 \\ 0 & \frac{\sqrt{3}}{2} & -\frac{\sqrt{3}}{2} & 0 \\ \frac{1}{2\sqrt{2}} & \frac{1}{2\sqrt{2}} & \frac{1}{2\sqrt{2}} & -\frac{3}{2\sqrt{2}} \\ \frac{3}{2\sqrt{2}} & \frac{3}{2\sqrt{2}} & \frac{3}{2\sqrt{2}} & -\frac{3}{2\sqrt{2}} \end{bmatrix} \begin{bmatrix} i_a(t) \\ i_b(t) \\ i_c(t) \\ i_n(t) \end{bmatrix} \tag{30}$$

The compact notations for the space-vectors of voltage and current are:

$$v(t)_{dqz0} = \begin{bmatrix} v_d(t) \\ v_q(t) \\ v_z(t) \\ v_0(t) \end{bmatrix} \tag{31}$$

$$i(t)_{dqz0} = \begin{bmatrix} i_d(t) \\ i_q(t) \\ i_z(t) \\ i_0(t) \end{bmatrix} \tag{32}$$

The sum of the four line currents will always be zero [29], hence $i_0(t)=0$. If the line voltages are measured with respect to a virtual star connection, it would also summate to zero, hence $v_0(t)=0$. The space-vectors of voltage and current then reduce to three-dimensional [29] space vectors:

$$v(t)_{dqz} = \begin{bmatrix} v_d(t) \\ v_q(t) \\ v_z(t) \end{bmatrix} \tag{33}$$

$$i(t)_{dqz} = \begin{bmatrix} i_d(t) \\ i_q(t) \\ i_z(t) \end{bmatrix} \tag{34}$$

The four-wire three-phase system is fully presentable in a three-dimensional space by the three linearly-independently transformed voltages and currents defined in (33) and (34). The RMS values of the space-vectors relate to the RMS values of phase vectors as follows:

$$\begin{aligned} V_{dqz} &= \sqrt{V_d^2 + V_q^2 + V_z^2} \\ &= \sqrt{V_a^2 + V_b^2 + V_c^2 + V_n^2} \\ &= V_{3\Phi} \end{aligned} \tag{35}$$

$$\begin{aligned} I_{dqz} &= \sqrt{I_d^2 + I_q^2 + I_z^2} \\ &= \sqrt{I_a^2 + I_b^2 + I_c^2 + I_n^2} \\ &= I_{3\Phi} \end{aligned} \tag{36}$$

The space vectors can also be written in terms of hypercomplex quantities $\bar{\nu}_x$, $\bar{\nu}_y, \bar{\nu}_z$. The voltage space vector can be written as:

$$\bar{v}(t)_{dqz} = v(t)_d \bar{\nu}_x + v(t)_q \bar{\nu}_y + v(t)_z \bar{\nu}_z \tag{37}$$

The current space vector can be written as:

$$\bar{i}(t)_{dqz} = i(t)_d \bar{\nu}_x + i(t)_q \bar{\nu}_y + i(t)_z \bar{\nu}_z \tag{38}$$

The latter equations will allow the use of hypercomplex algebra to formulate power definitions to analyse a four wire three-phase power system under nonsinusoidal conditions as demonstrated later in Chapter 4.

2.5 THE PHYSICAL SIGNIFICANCE OF POWER AS EXPLAINED BY THE POYNTING VECTOR

The phenomenon of "power propagation" relates to the application of a power theory. Electrical power requires a valid description through proper definition of the phenomena that are associated with electrical power. This enables utilities and clients to agree on, amongst others, the monetary implication of energy sales. The physical mechanisms, by which electrical power is transported from a point of generation to a point of consumption, is best understood through application of electromagnetic principles. Poyntings's theorem state that "the work done on the charges by the electromagnetic force is equal to the decrease in energy stored in the field, less the energy which flowed out of through the surface" [102]. The Poynting vector $\vec{S}$ by definition furnishes an electromagnetic description of the energy propagated through a point:

$$\vec{S} = \overline{E} \times \overline{H} \text{ watts/m}^2 \tag{39}$$

The magnitude of the Poynting vector at a given point and at a given time represents the magnitude of surface power density as the symbols in (40) indicate. The *energy transported per unit time* across a certain surface (denoted ***da***) is then simply ***S.da***.

The radiated power is included in the Poynting vector flux. It is shown in [28] that the time-dependent energy that flows in or out of a dielectric or magnetic field does not give rise to irradiation energy. Practical power systems presents such a scenario as the diameter of the least spherical surface containing the power system will always be by much greater than any of the wavelengths associated to the magnetic and electric fields in practical power systems.

If the Poynting vector is calculated for sinusoidally varying electric and magnetic fields, then an *active* and a *non-active* Poynting vector can be distinguished respectively [30]:

$$\begin{aligned} p(t)_{\text{in}} &= -\oint_{CS} \left(\overline{E} \times \overline{H}\right) da \\ &= \int_{v} \vec{E} \cdot \vec{J} dv + \frac{\partial W_Q}{\partial t} \\ &= p(t)_P + p(t)_Q \end{aligned} \tag{41}$$

In the above equation, $p(t)_{\text{in}}$ represents the nett power flowing into a volume v through its enclosed surface, *CS*. Symbol ***da*** represents an element of the surface area for the purpose of calculating the

integral above. Note that the minus sign is required as energy is entering the volume v.

The $p(t)_P$ component of the above equation explains the transfer of energy by the fundamental frequency electric and magnetic fields into volume v and includes:

- dielectric losses,
- eddy current and hysteresis losses,
- Joule losses,
- useful power transferred to volume v,
- the rate at which energy flow is converted, for example, into mechanical energy.

The non-active component $p(t)_Q$ explains that at twice the fundamental frequency, energy oscillates between the load and the source. The non-active part causes energy to be stored in electric and magnetic fields inside the volume.

Although the Poynting vector $\vec{S} = \vec{E} \times \vec{H}$ can explain the energy entering or leaving a volume at a certain point on a surface, it is not clear how to assign a physical meaning to $\vec{S}$ when the magnetic and electric fields are static. No energy is entering or leaving the surface therefore, mathematically, $\vec{E} \times \vec{H} \neq 0$.

In a power system where the voltages and currents are time-dependent, the resultant fields and the Poynting vector are time-dependent. The solution to the static field paradox is that $\vec{S}$ represents [30] not only the density of energy flow but $\vec{S}$ simultaneously explains the momentum density of electromagnetic fields.

The Poynting vector can also explain physical principles pertaining to power when the waveforms in the electrical network are non-sinusoidal. The next section briefly presents the application of the Poynting vector under non-sinusoidal conditions.

2.6 THE POYNTING VECTOR AND NONSINUSOIDAL WAVEFORMS

If a voltage and/or current waveform is nonsinusoidal in time, a finite series of harmonic frequency components can represent the distorted time-domain waveform. Each harmonic voltage and current component will cause a respective electric and magnetic field resulting in different Poynting vectors. This is not a straightforward matter, as interaction between electric and magnetic fields at different harmonic frequencies requires careful consideration of the physical significance thereof. Čakareski and Emanuel [30] used the Poynting vector to study the physical processes associated with non-sinusoidal power system waveforms. A brief presentation thereof is given below.

Assume that a single-phase nonsinusoidal voltage and current waveform can be written as a sum of

harmonic frequency components consisting of a fundamental frequency component (fundamental angular frequency $2\pi f_1 = \omega_1$) and subsequent harmonic frequency components (at harmonic angular frequencies $h\omega_1$ with h the integer harmonic number):

$$\begin{aligned} v(t)_{1\phi} &= \sum_{h=1} \sqrt{2} V_{h,1\phi} \sin(h\omega_1 t + \alpha_h) \\ &= \sqrt{2} V_{1,1\phi} \sin(\omega_1 t + \alpha_1) + \sum_{h\neq 1} \sqrt{2} V_{h,1\phi} \sin(h\omega_1 t + \alpha_h) \\ &= v_{1,1\phi}(t) + v_{H,1\phi}(t) \end{aligned} \tag{42}$$

$$\begin{aligned} i(t)_{1\phi} &= \sum_{h=1} \sqrt{2} I_{h,1\phi} \sin(h\omega_1 t + \alpha_h - \beta_h) \\ &= \sqrt{2} I_{1,1\phi} \sin(\omega_1 t + \alpha_1 - \beta_1) + \sum_{h\neq 1} \sqrt{2} I_{h,1\phi} \sin(h\omega_1 t + \alpha_h - \beta_h) \\ &= i_{1,1\phi}(t) + i_{H,1\phi}(t) \end{aligned} \tag{43}$$

The calculation of the resulting electric fields is carried out in terms of the voltage harmonic components:

The resulting Poynting vectors are calculated from:

$$\vec{S} = \left(\vec{E}_1 + \vec{E}_H\right) \times \left(\vec{H}_1 + \vec{H}_H\right) \tag{44}$$

Čakareski and Emanuel [30] defined four different Poynting vectors applicable to a single-phase power system:

1. A Poynting vector at the fundamental frequency, $\vec{S}_1$. It transfers both *active* and *non-active* power at the fundamental frequency:

$$\vec{S}_1 = \vec{E}_1 \times \vec{H}_1 \tag{45}$$

Poynting vector $\vec{S}_1$ sustains the time-dependent *active* power $p_R(t)_1$ and the time-dependent *non-active* power $p_X(t)_1$ at the fundamental frequency:

$$\begin{aligned} p_R(t)_1 &= V_{1,1\phi} I_{1,1\phi} \cos(\alpha_1 - \beta_1)\{1 - \cos(2\omega_1 t + 2\alpha_1)\} \\ p_X(t)_1 &= V_{1,1\phi} I_{1,1\phi} \sin(\alpha_1 - \beta_1)\{\sin(2\omega_1 t + 2\alpha_1)\} \end{aligned} \tag{46}$$

2. A Poynting vector $\vec{S}_{DI}$ is associated [30] with the distortion in current, termed the *current distortion Poynting vector*:

$$\vec{S}_{DI} = \vec{E}_1 \times \vec{H}_H \tag{47}$$

$\vec{S}_{DI}$ sustains the time-dependent *current distortion power* $p_{DI}(t)$:

$$p_{DI}(t) = 2V_{1,1\phi} \sum_{h \neq 1} I_{h,1\phi} \sin\left[h\omega_1 t + \alpha_h - \beta_h\right] \sin\left(\omega_1 t + \alpha_1\right) \tag{48}$$

3. A Poynting vector $\vec{S}_{VI}$ is associated [30] with the distortion in voltage, termed the *voltage distortion Poynting vector*:

$$\vec{S}_{DV} = \vec{E}_H \times \vec{H}_1 \tag{49}$$

Poynting vector $\vec{S}_{VI}$ sustains the time-dependent *voltage distortion power* $p_{DV}(t)$:

$$p_{DV}(t) = 2I_{1,1\phi} \sum_{h \neq 1} V_{h,1\phi} \sin\left[h\omega t + \alpha_h\right] \sin\left(\omega_1 t + \alpha_1 - \beta_1\right) \tag{50}$$

4. The fourth Poynting vector defined [30] is *the harmonic Poynting vector*, $\vec{S}_H$ to represent the transfer of energy at all harmonic numbers. The fundamental frequency is excluded but the mutual interaction between harmonic numbers included:

$$\vec{S}_H = \vec{E}_H \times \vec{H}_H \tag{51}$$

The *harmonic Poynting vector* sustains both the time-dependent harmonic *active* power $p_H(t)$ and a time-dependent *non-active* harmonic power $p_{QH}(t)$ (not to be termed harmonic *reactive* power):

$$\begin{aligned} p_{RH}(t) &= \sum_{h \neq 1} V_{h,1\phi} I_{h,1\phi} \cos\left(\alpha_h - \beta_h\right)\left[1 - 2\cos\left(h\omega_1 t\right)\right] \\ p_{QH}(t) &= \sum_{h \neq 1} -V_{h,1\phi} I_{h,1\phi} \sin\left(\alpha_h - \beta_h\right) \sin\left(2h\omega_1 t + \alpha_h\right) \ldots \\ &\ldots + \sum_{m \neq n; n \neq 1} 2V_{m,1\phi} I_{n,1\phi} \sin\left(m\omega_1 t + \alpha_m\right) \sin\left(n\omega_1 t + \alpha_n - \beta_n\right) \end{aligned} \tag{52}$$

If the physical significance of the above Poynting vectors is considered, the following conclusions are drawn [30]:

- Only $\vec{S}_1$ transmits useful energy from the source to the load.
- Poynting vectors $\vec{S}_{DI}$, $\vec{S}_{VI}$ and $\vec{S}_H$ can be considered as supporting the "polluting" electro-magnetic energy.
- Both $\vec{S}_{DI}$ and $\vec{S}_{VI}$ are associated with the useless reciprocation of energy.
- $\vec{S}_H$ sustain both the energy losses in the transmission system and the useless reciprocations of energy.

Application of the Poynting vector in three-phase power systems is not easy. It becomes even more difficult when non-sinusoidal and unbalanced conditions are introduced.

As the Poynting vector presents a bridge between field and circuit theory, it was used by Ferrero [28] to find a physical explanation to the non-active part of the Park power. The Park transform is a proven three-phase circuit analysis tool to enable single-phase space vector representation of three-phase voltage and current vectors. These space vectors enabled calculation of the Poynting vector, hence the term "Poynting-Park" vector in [28].

The flux of the Poynting-Park vector was calculated for the conduction, electric displacement and magnetic fields by Ferrero [28]. (The results is discussed in chapter 5 and listed in Table 19.) It is shown to be scalar complex quantities.

The most important conclusion resulting from the study of the Park-Poynting vector is that the three-phase compensation technique developed by Akagi-Nabae, has a sound physical explanation. Energy for the compensator is not required from an "outside" source; it is taken from other phases to compensate energy variation in one phase. The Park-Poynting vector explains that the Park imaginary power is a physical phenomenon of energy variation ("bouncing") between phases.

2.7 SUMMARY

The Fortesque and Park transform was redefined to include analysis of multi-frequency circuits. A new transformation principle devised by Ferrero, Giuliani and Willems [29] is an innovative mathematical aid in the analysis of four wire three-phase power systems under non-sinusoidal conditions.

The physical phenomena observed in electrical power networks are best studied by the investigation of the interaction of electric and magnetic fields. The fundamental mathematical principles of the field theory are found in Maxwell's equations and the Poynting vector. The Poynting vector shows that energy is transported by the interaction of electric and magnetic fields. The application of the Poynting vector

under sinusoidal conditions is well known. The significance of the Poynting vector under non-sinusoidal conditions was investigated for a single-phase network in Chapter 2. Extension to a three-phase power system with non-sinusoidal waveforms seems to contain valuable insight towards the physical significance of power phenomena.

Čakareski and Emanuel [30] have shown that the non-active components of the Poynting vector under non-sinusoidal conditions in three-phase networks can physically explain the three causes of a deteriorating power factor:

(*a*) due to reactive elements,

(*b*) due to the current harmonics caused by non-linear loads, and

(*c*) due to the load unbalance between phases.

The non-active part of the Poynting vector was demonstrated [30] to be associated with the "unwanted/polluting" energy in non-sinusoidal power systems. Application of the Poynting vector in three-phase power systems is done through the Park transformation of voltage and current vectors. It is shown that the Poynting-Park vector explains the Park imaginary power.

3 DATA GENERATION

3.1 BACKGROUND

The three-phase power theory of Czarnecki [5] is reported in chapter 4 to lack practical application. This claim must be supported, amongst others, by the manner in which the data was obtained. Similarly, the findings that Chapter 5 make will show that it is not possible to apply harmonic active power in the localisation of multiple distortion sources by single-point measurements when these distortion sources are distributed over the electrical power network. That finding will have to be supported by reliable data. Data has to be obtained for the purpose of this research both through computer simulation and from measurements taken in a power system configured in a laboratory. The principles and correctness of generating this data are supported in this chapter under:

- The principles of the simulation and analysis software ,
- the design and specification of the hardware used to obtain real-life measurements,
- practical aspects of digital data analysis.

3.2 DIGITAL POWER SYSTEM SOFTWARE SIMULATION

The power system phenomena investigated in this thesis pertains to only steady state non-sinusoidal voltage and current waveforms. Two digital simulation approaches are possible:

1. A *frequency-domain* approach: A non-sinusoidal power system is presentable as a superposition of solutions obtained by analysing the power system response at the different discrete frequencies required to represent the original non-sinusoidal time waveform.
2. A *time-domain* approach: In the physical power system it is a non-sinusoidal voltage or current waveform that "exists" in the time domain (the frequency domain is a synthetic representation).

Either frequency-domain models or time-domain models can be used to represent the power system components. These simulation approaches are briefly compared below.

3.2.1 Frequency domain simulation

Frequency-domain simulation is a direct solution of the effects of individual harmonics that are injected into a power system. Non-linear loads can be modelled for most practical situations as Norton equivalent current sources in parallel with Norton equivalent admittances. The three-phase fundamental voltage supply at a PCC is well balanced under most conditions making it possible to use single-phase analysis in

the frequency domain.

The modelling of power system components in the frequency domain can be undertaken by writing custom developed routines in software such as MathCAD™ [11] or through a commercially available power system simulator such as PSS/E™[12].

Frequency domain modelling[13] was for example used in the research of Swart *et al* [57] to show that it is not possible to localise a source of waveform distortion in an interconnected power system through single-point measurements when these sources of distortion are distributed over the network. This is a very important result with far-reaching impact on other attempts to localise a source of distortion.

3.2.2 Time domain modelling

Commercial software-based power system simulators were not available for the research undertaken in this thesis. One of the research goals was to validate the findings of Swart *et al* [57] by means of both a comparative computer-based time-domain simulation and a hardware-based measurement. A time-domain power system simulator ATP[14], a royalty-free power system simulator powerful enough for the research goals envisaged, was therefore chosen.

The simulation approach use of ATP is to use time-domain models of power system components. It is possible to model the power system components through the solution of mathematical expressions that relates voltages and currents in the time-domain in difference equations through numerical integration. Power system components are described in the exact mathematical way they behave in the time domain, for example:

Resistor: $v(t) = Ri(t)$

Inductor: $v(t) = L\frac{di(t)}{dt}$

Detailed and accurate time domain models are possible. Time-domain mathematical equations can describe components such as non-linear resistors and inductors, switches, voltage and current sources, power electronics and dynamic rotating machines.

---

[11] http://www.mathcad.com

[12] http://www.pti-us.com/pti/software/psse/

[13] The modelling approach used by Swart *et al* is not reported in this thesis as it is reported in [57].

[14] ATP (Alternative Transients Program) has its roots in EMTP (Electro Magnetic Transients Program) but is the Royalty-Free version (after 1984) of which continuous development takes place and to which only licensed holders has access on a non-commercial basis. More information is available at http://www.ee.mtu.edu/atp/.

Trapezoidal integration of the second order is used in the solution of ordinary differential equations. The solution approach consists of a set of algebraic equations to be solved at every time step [80]. Non-zero initial conditions can be obtained by a steady state solution or the user can specify specific values. The simulation time step (time interval between the successive solutions of the network equations) is controllable. The solution of one timing instance is used as the initial condition to the successive solution of the simulation equations and a progressive time-domain solution results.

3.3 SIMULATION WITH ATP

ATP development was carried out in FORTRAN during the earlier years, before present-day computer technology reached sufficient sophistication and user-friendliness. Input to ATP was by "punch-card" type of programming of large mainframe computers. Row-by-row column-sensitive commands had to be generated in an exact fashion requiring high precision.

The Windows™ range of operating systems and accompanying software dominates the modern scene, however, making the task much faster and lending it to general analysis tasks that would formerly have been formidable in the light of the large amount of work and preparation needed. Prof. Hans Kristian Hoidalen of SINTEF Energy Research, Trondheim, Norway, revolutionised the ATP process by writing a graphical mouse-driven pre-processing package, ATPDRAW, for Windows[15]. ATPDRAW and ATP in combination with mathematical software such as Matlab™ and MathCad™ present a complete digital power system experimental[16] platform.

ATP and ATPDRAW were extensively used in the research reported in this thesis and the basic philosophy behind this "digital power system" is informative. The following flow-diagram representation describes the interaction between ATP, ATPDRAW and a data analysis package such as MathCAD™:

[15] http://www.ee.mtu/atp/ATPDraw/ATPDraw.html

[16] The flow-diagram conceptualise the ATP simulation process.

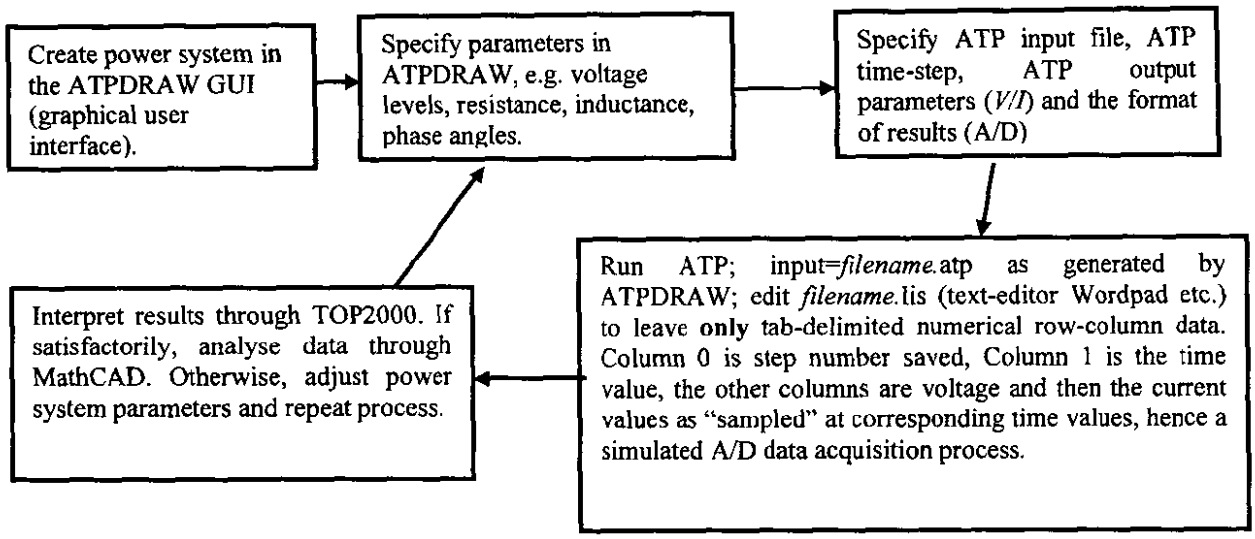

Figure 6: Visualisation of the process of ATP based power system studies

Figure 6 visualises the configuration and application of ATP to study a power system. The digital power system data simulates A/D samples that can be saved for mathematical analysis. It is similar to an A/D data acquisition process in a real analogue power system and affords a valuable comparison between the two main sources of data used in the analysis.

TOP2000[17] is a post-processing package that can immediately analyse and graph the ATP results. If these waveforms appeared to be valid, detail investigations were justified. MathCAD™ was used for the analysis in this thesis.

3.4 LABORATORY POWER SYSTEM

To obtain measurements from a high-voltage industrial power system pertaining to the power system phenomena investigated in this thesis, is neither practical nor easy. To install specialised instrumentation of sufficient accuracy in an industrial power system will be difficult and time consuming and very risky due to the risk of influencing the protection circuitry.

It is not a straightforward matter to measure harmonic components in terms of harmonic components phase and magnitude to a high degree of accuracy. Harmonic components can be very small in magnitude compared to the magnitude of the fundamental frequency components. Typical power system instrumentation (current transformers (CT's) and voltage transformers (VT's)) suffer from phase errors at higher frequencies and lower accuracies at the small amplitudes of the harmonic components to be measured.

[17] http://www.pqsoft.com/top/

Special consideration is required for the bandwidth and the accuracy of the instrumentation that is commercially available for measurements at high power levels. To buy/develop instrumentation of suitable accuracy is very expensive.

Further, it is impossible in an interconnected power system, with generation and loads distributed over the power system, to conduct experiments in a controlled manner. It will be difficult, and often impossible, to assign a unique cause to a specific phenomenon that is observed.

A solution in obtaining power system measured data was to scale the power system down but to keep parameters representative of an industrial power system. A laboratory power system with appropriate instrumentation was developed. The electrical parameters such as supply voltage waveform amplitude and shape and the size and nature of loads were designed to be individually controllable. A schematic representation of a section of this scaled-down system is shown in Figure 7:

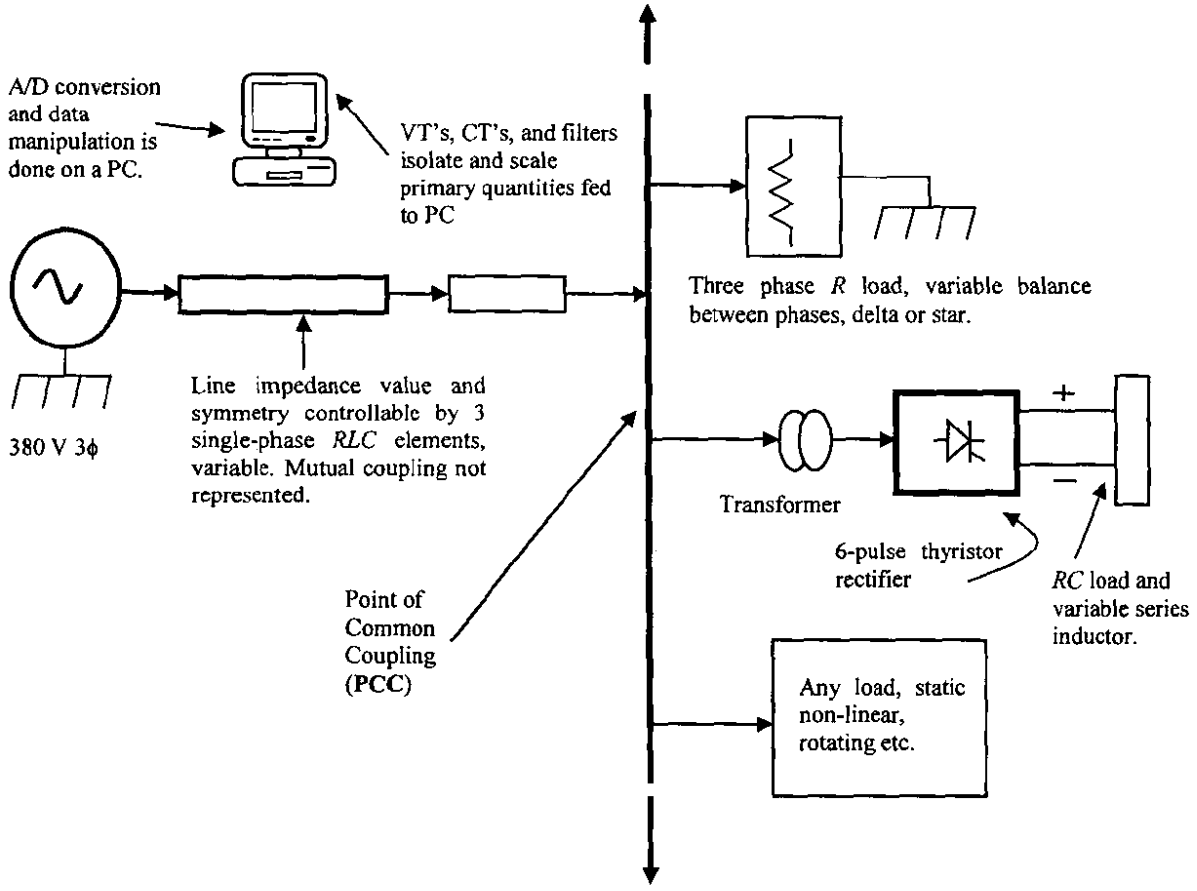

Figure 7: Schematic of a section of the laboratory power system

When taking measurements in an unbalanced nonsinusoidal four wire three-phase power system, four voltages and four currents have to be measured. To validate the hypothesis on the localisation of distortion sources [57], it is required that all nodes in the power system have to be measured simultaneously and to be time-synchronised. The power system configured to study the localisation of distortion sources had 3 nodes. A total of 24 input channels in the A/D card must then be used.

Wide-bandwidth high accuracy voltage and current transformers (VT's and CT's) based on the LEM[18] product range was used. The configuration of the VT's and CT's to obtain measurements at a node, is shown in Figure 8. Both the CT and VT are closed loop Hall-effect sensors with claimed nonlinearities of less then 0.2% and inaccuracies of less then 1%.

It is important to note that the output signal obtained from a CT and its signal conditioning electronics if compared to the output signal obtained from a VT and its signal conditioning electronics will introduce additional phase errors. Each CT and VT channel has unique phase characteristics; ideally it should have been equal. The phase errors that asynchronous analog-digital conversion (ADC) introduces, is a separate effect.

[18] http://www.lem.com; Accuracy summary on the VT (LV 25-P) and CT (LA 25-NP) to be found in Appendix 1.

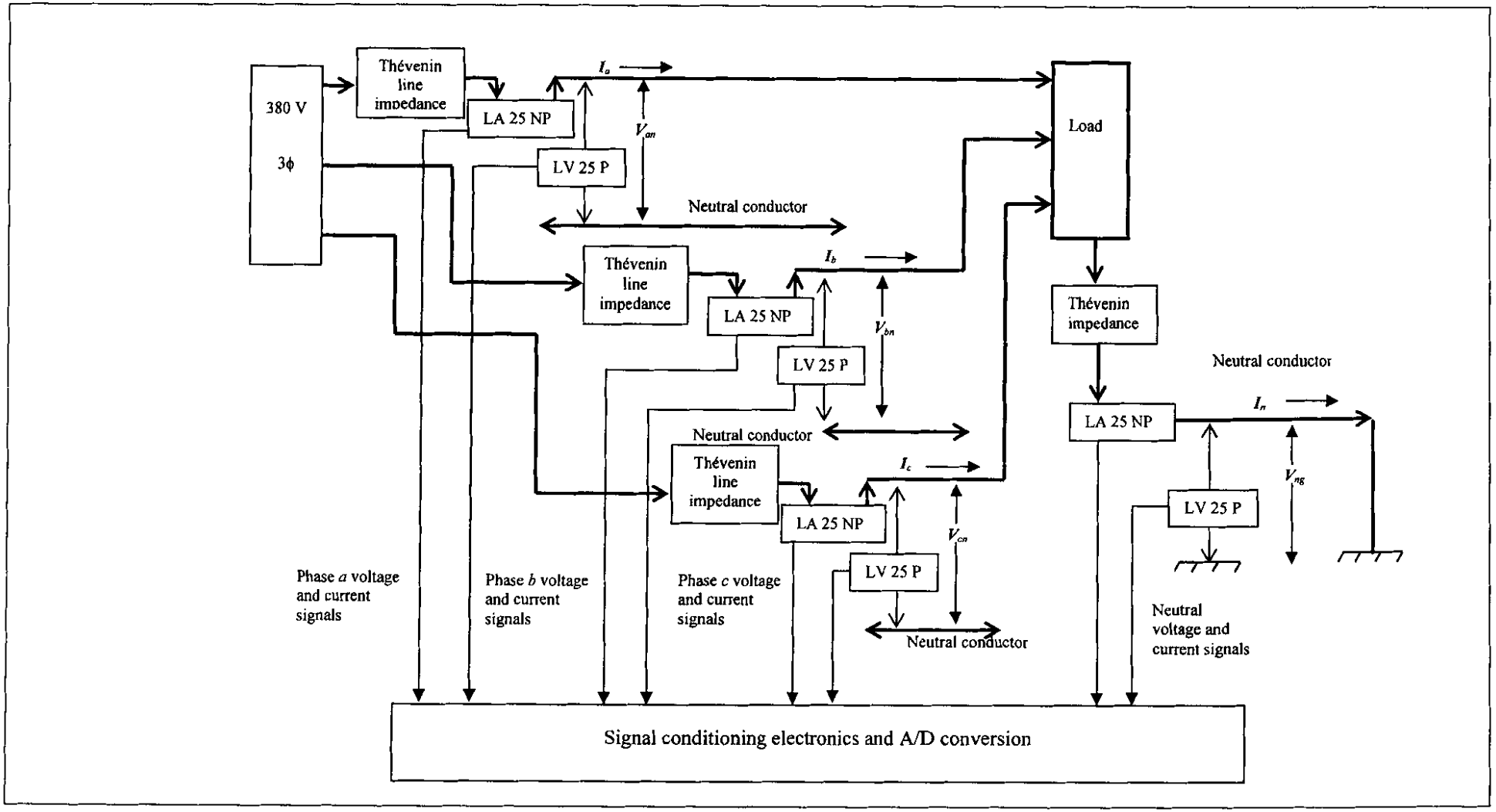

Figure 8: Instrumentation layout of one node

The signals obtained from the VT's and CT's had to be conditioned in terms of amplitude and frequency content. A block diagram of the conceptual signal conditioning design is shown in Figure 9.

A 10 pole low-pass filter restricted the frequency content of the acquired waveforms to user-selectable values. For example, when 24 waveforms had to be measured simultaneously, the highest rate at which 2^n data points could be obtained per channel on the PCI 6031E[19] A/D card, is 3200 Hz. In this example, to ensure that the Nyquist criterium on data sampling is respected, the signal to be digitised can be restricted at 1250 Hz (25^{th} harmonic component). For other cases, it is possible to select cut-off frequencies on the signals to be digitised at[20] 10 kHz, 5 kHz, 2.5 kHz, 1.25 kHz, 550 Hz, 250 Hz and 150 Hz.

An amplitude swing of ±5 V is to be expected from the VT's and CT's. The amplitude of the input signal to the signal condition section is scalable by a factor of 0.5 in order for the optimum performance of the switching filter. If the DC level of the signal is unacceptable, a high-pass 2 pole filter is adequate to remove the DC component of the signal. The last analog 2-pole elliptical low-pass filter has a gain of 2 which restore the original amplitude level of the measured signal that the VT and CT feed to the signal conditioning electronics.

---

[19] http://sine.ni.com/apps/we/nioc.vp?cid=1055&lang=US; Performance summary to be found in Appendix 1.

[20] The actual -3 dB point was set up a bit higher to ensure that for example, a 1250 Hz harmonic component was not attenuated at all. Frequency components lower, and at, in the example of 1250 Hz was ensured to be contained in the linear region of the filter.

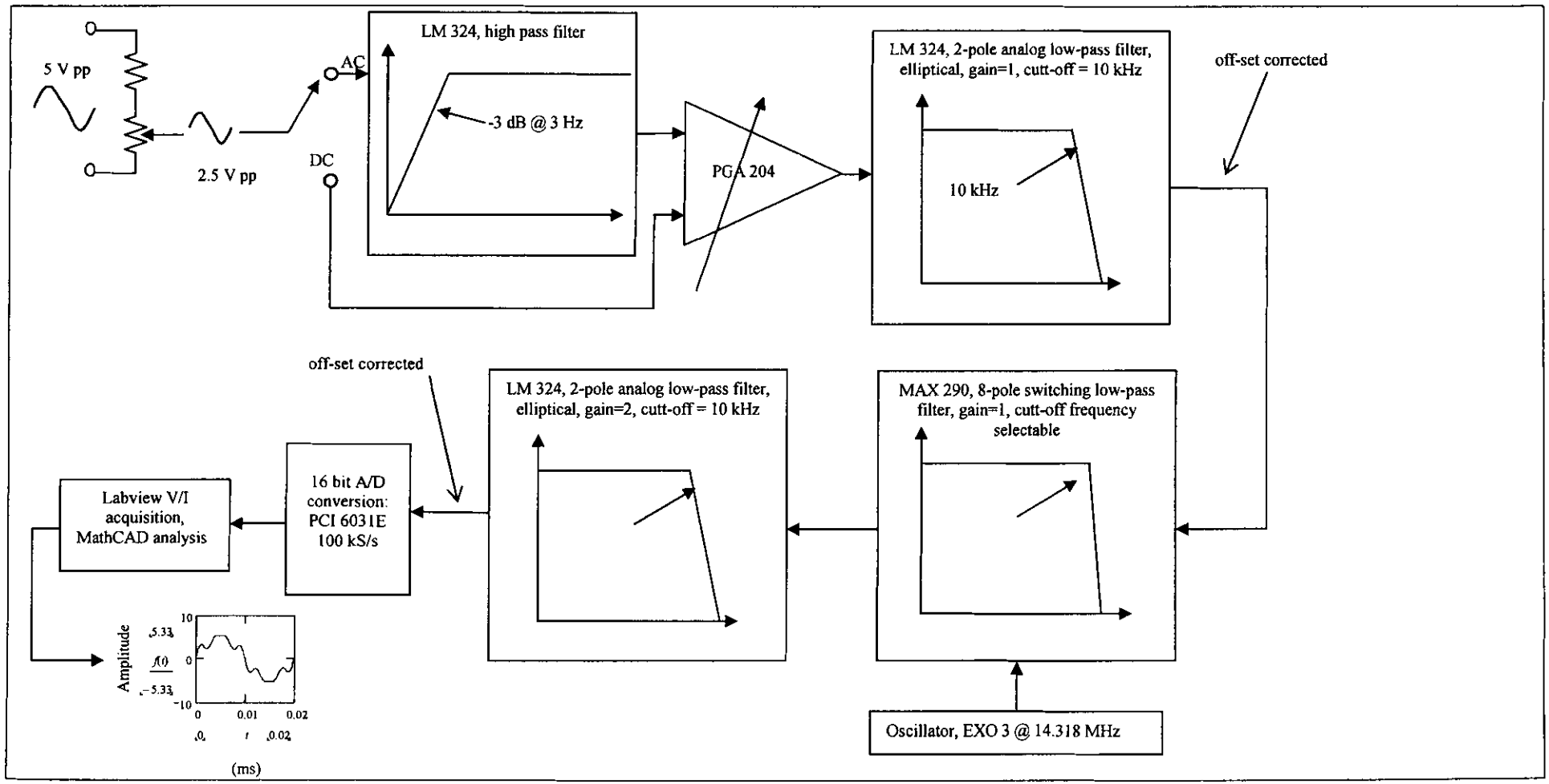

Figure 9: Signal condition and A/D conversion

Adjustable gain is possible with a programmable gain amplifier, the PGA 204. A gain factor of 10^0, 10^1, 10^2, and 10^3 is user-selectable. This linearity of this amplifier over the frequencies to be expected in power system signals is excellent. Amplification is necessary when small signals are acquired such as the neutral-earth voltage.

The smallest detectable voltage change measurable with the 16 bit A/D card used, (National Instruments PCI 6031E) is 152.6 μV (with a voltage input range of 0–10 V). The A/D deviation from linearity, or, the non-linearity of the A/D process of the PCI 6031E, is specified as ± 0.5 LSB (least significant bit). This number is an indication of how "sensitive" the analogue to digital conversion (ADC) process is. For example, if the input signal is slightly above 5000 μV, such as an increase to 5100 μV, it is not recognised. This increase is within the 0.5 LSB (0.5 x 152.6 μV) uncertainty range. However if the signal increases to 5200 μV, it will be recognised with certainty.

The effective resolution to be expected from any ADC is dictated by the signal-noise ratio (SNR) of the experimental setup and the specific A/D card. The resulting SNR was not scientifically evaluated. Hand calculations indicated that higher than 13 bits resolution was probably already into the noise band of information.

The sampling frequency setting of the A/D card is adjustable to select a frequency which will minimise aliasing. The maximum sampling rate is a 100 Ks/s. When only 3 voltage and 3 current channels were configured, 12.8 kHz per channel can be set which enable 256 data points (2^8 data points in a 50 Hz fundamental frequency cycle).

In the case of measuring 24 channels in a single-ended configuration, the maximum possible sampling frequency decrease to 4.16 kHz per channel. A data rate of 3200 Hz per channel setting relate to 2^6 (64) data points in a 50 Hz fundamental frequency cycle. The filter configuration is designed for effective 10 pole low-pass filtering at the 25^{th} harmonic component. The Nyquist requirement of 2500 Hz is therefore achieved.

It is not easy to estimate the overall metrological characteristics of the digital measurement process. The "error"/uncertainty that result influences the subsequent digital signal processing.

A standard instrument against which to evaluate the accuracy of the comprehensive measurement system is not readily obtainable. A very useful contribution to establish the overall accuracy of a digital measurement system is reported in [32]. A method to estimate the uncertainty associated with the signal conditioning elements (VT's, CT's, filters, amplification, isolation etc.) and the analogue to digital conversion process is also proposed in [32]. This method requires a practical investigation with specialised supporting instrumentation and it estimates the final uncertainty based on a Monte Carlo procedure. The results reported in [32] are very promising with respect to the validation of accuracy of a

digital measurement system. To repeat the similar calibration procedure with the limited resources available to the author was not possible.

This computer-based measuring system was used to obtain waveform data to study power theories as reported in chapter 4. Due to the acquisition of a meter with an accuracy of class 1 (Impedograph^{TM}) that could measure all eight data inputs channels simultaneously and with the feature of time-synchronisation between different meters, the measurements as used in chapter 5 was obtained with three of these meters. Application of the Impedograph^{TM} is therefore presented in section 3.5.

3.5 MEASUREMENTS: COMMERCIAL INSTRUMENTATION

The Impedograph^{TM} [21]measuring instrument is of class 1 accuracy and verified as such by the South African National Standards (SANS) body. This meter was used to obtain high accuracy measurements when investigating the research problem on the localisation on distortion sources reported in chapter 5.

A brief overview of the important features of Impedograph^{TM} is given below.

- Four differential voltage input channels at 0.1% accuracy from 50-460 V RMS and with a resolution of 15 mV RMS.
- Four current input channels with 0.1% accuracy from 0.2 A to 7.5 A RMS and a resolution of 250 μA RMS.
- All eight channels are simultaneously digitised at 16 bits per channel.
- Hardware synchronisation to the fundamental frequency is done and 512 samples per fundamental cycle taken.
- External GPS time synchronisation is possible whilst the internal clock is of a 100 PPM accuracy.
- Eight digital input channels are available to be used for example as a trigger input to commence sampling of voltage and current input channels.
- Remote data acquisition and setup is done through TCP/IP communication.

The results of a time-domain simulation reported in chapter 5 had to be validated by real life measurements. Swart *et al* [57] state the requirements of such an investigation to be the simultaneous measurement of three-phase voltages and currents in all nodes of the power system. For the purpose of

[21] http://www.impedograph.com

the study undertaken, synchronised measurements are required at 3 three-phase terminals, two which are connected to two different loads and one terminal to which the voltage supply source is connected. An illustration of such configuration is given below.

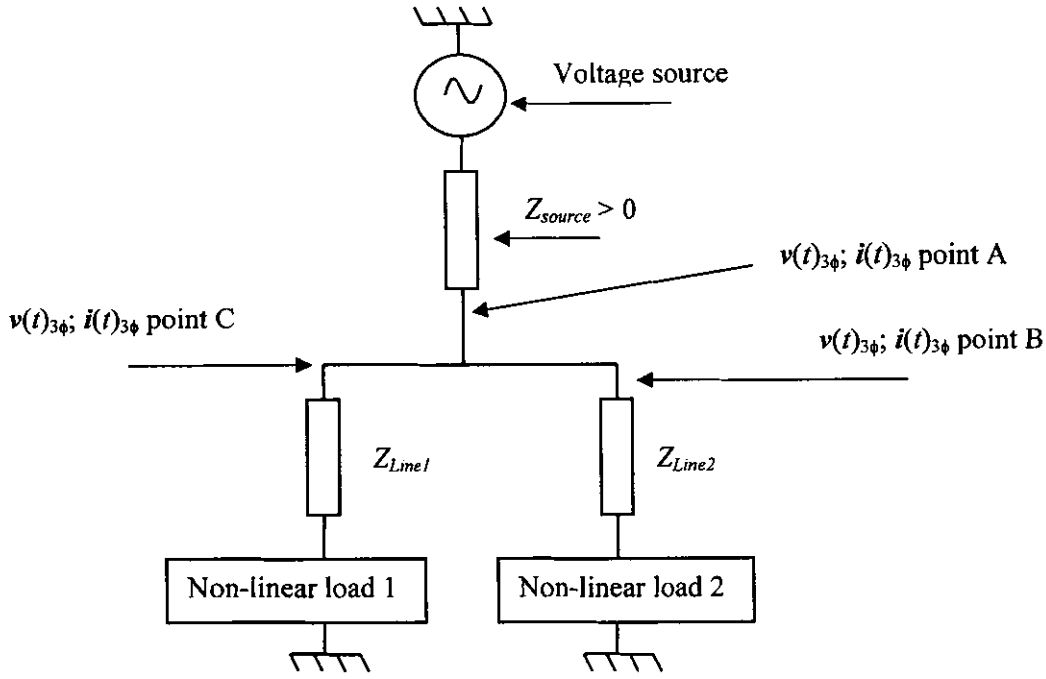

Figure 10: Measurement configuration for Impedograph™

Three Impedographs was installed, one each at point A, B and C in Figure 10. The meters are externally synchronised to obtain simultaneous sampling of 18 different input channels representing 3 voltages and 3 currents at each measuring point. Synchronisation of time between the Impedographs is achieved by generating an external trigger pulse to a digital input trigger of each. The distance between each unit was a few metres and wave propagation between digital inputs therefore negligible.

The meters were configured to acquire 3 fundamental waveform cycles on the 18 input channels before and after the trigger signal is detected. The trigger signal was also used to represent a change in the electrical condition of the power system depicted in Figure 10. For each change in condition, synchronised readings of 3 sets of three-phase voltage and current waveforms were studied in MathCAD.

The analysis and the interpretation of the results, is presented in Chapter 5.

3.6 SIMULTANEOUS SAMPLING

It is not possible to sample the different input channels simultaneously with the PCI 6031E A/D card. A small time-difference result between the time the data point of one waveform is obtained at a channel and the time the corresponding data point is obtained at another input channel. It is necessary to evaluate the effect of a multiplexed sampling process.

The PCI 6031E A/D card[22] has a time interval of 10 μs between successive samples taken at adjacent channels. Possible errors result in the calculation of average power, as the next section 3.6.1 demonstrates. "Off-line" compensation is presented in section 3.6.2.

3.6.1 Harmonic components and non-simultaneous sampling

3.6.1.1 Error in the phase angle

Assume that two adjacent channels are used as the input of a pure sinusoidal voltage and current signal. Further assume that the signals under consideration are harmonic frequency components at 1250 Hz[23], each with peak amplitude of 10 V (the full-scale value measurable by the A/D card in single-ended configuration). The phase difference between the voltage and current waveform in real time is 40^0 (current lagging voltage).

The percentage phase error due to non-simultaneous sampling is therefore:

$$Phase\ error = \frac{10*10^{-6}}{800*10^{-6}}*100 = 1.25\%$$

The waveforms $i_{actual}(t)$ and $i_{measured}(t)$ respectively represent a simulated "error-free" signal and a non-simultaneously measured signal, referenced to the voltage signal $v(t)$:

---

[22] The performance data of the PCI 6031E is listed in Appendix D.

[23] If a 50 Hz voltage signal was fed to a 6 pulse rectifier, then the current withdrawn will have harmonic frequencies which are an integer number $h = 6k \pm 1$. With $k = 4$, h = harmonic order of the fundamental frequency signal, 1250 Hz is the one harmonic obtained. The idea is to investigate the effect of the 10 μs mismatch between two adjacent A/D input channels on one of the higher frequency components in the "distorted" current and voltage digitised signals.

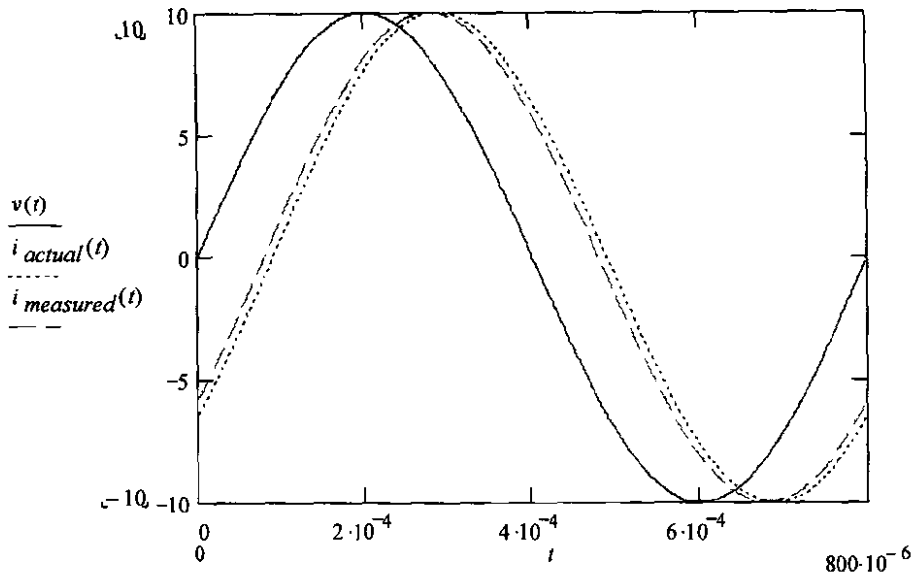

Figure 11: Voltage and current waveform to demonstrate non-simultaneous digitising, 10 μs (1 channel) between two channels

With $v(t)$ as the reference signal, the phase angle error in Figure 11 between $i_{actual}(t)$ and $i_{measured}(t)$ can be written as:

$$\begin{aligned} v(t) &= 10\sin(2*\pi*1250*t) \\ i_{actual}(t) &= 10\sin(2*\pi*1250*t-40^0) \\ i_{measured}(t) &= 10\sin(2*\pi*1250*t-35.5^0) \end{aligned} \tag{53}$$

The phase angle between the current and voltage, if measured simultaneously, should have been -40^0 (current lagging voltage). In terms of degrees, the measurement error is 4.5^0.The error caused by this multiplex time interval resulted in the erroneous phase angle, measured as -35.5^0.

3.6.1.2 Measurement error in active power measurement

The calculation of active power is also in error when based on the measured values:

$$\begin{aligned} P_{measured} &= V_{1\phi} I_{1\phi} \cos(\alpha-\beta) \\ &= \frac{10}{\sqrt{2}} * \frac{10}{\sqrt{2}} \cos\left[0-\left(-35.5^0\right)\right] \\ &= 40.706 \text{ Watt} \end{aligned}$$

Without a measurement error, the active power is:

$$P_{actual} = V_{1\phi} I_{1\phi} \cos(\alpha - \beta)$$
$$= \frac{10}{\sqrt{2}} * \frac{10}{\sqrt{2}} \cos\left[0 - (-40^{\circ})\right]$$
$$= 38.302 \text{ Watt}$$

The percentage error in the active power is:

$$\%\text{Error} = \frac{P_{measured} - P_{actual}}{P_{actual}} * 100$$
$$= +6.275\%$$

A significant error results at high harmonic frequencies but at the fundamental frequency, this error is very small. Take note that the assumption was made that the channels above are adjacent which represents the smallest possible error. Assume the channels are wired in the following sequence:

$v_{an}(t)$ to channel 1, $v_{bn}(t)$ to channel 2, $v_{cn}(t)$ to channel 3, $i_a(t)$ to channel 4, $i_b(t)$ to channel 5, $i_c(t)$ tochannel 6

The phase error between the voltage and current signal in a phase is 30 μs as demonstrated in Figure 12:

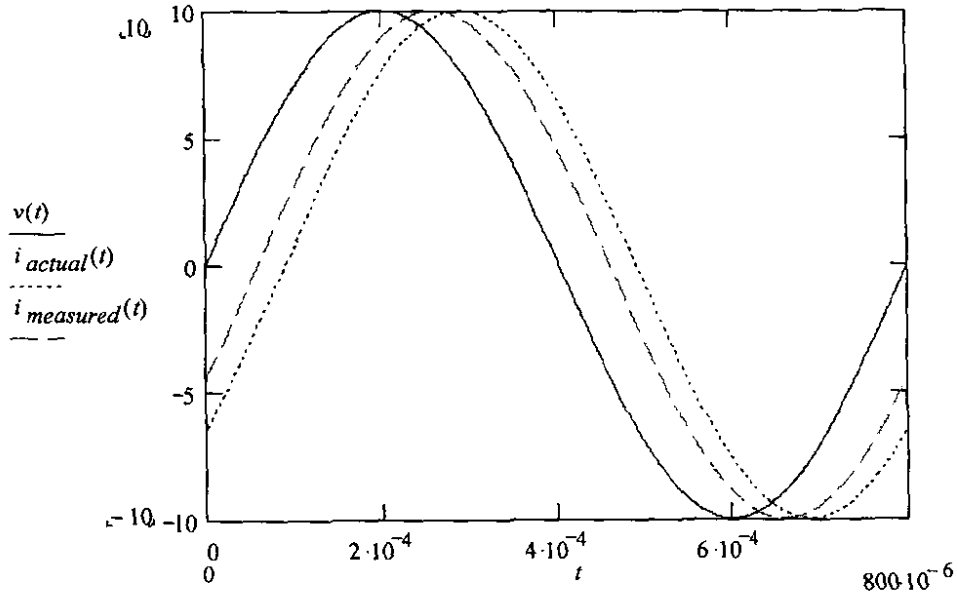

Figure 12: Voltage and current waveform, non-simultaneous digitising, 30 μs (3channels separation)

The phase error in Figure 12 is now 13.5^0 and the resultant active power error is 16.825%. The error is progressive as function of frequency and of channel number. It is not negligible, even when two adjacent channels are considered.

3.6.1.3 Error in the apparent power and the complex power

Frequency domain analysis of power theories in a three-phase power system is not influenced when the

concept of "effective values" [20] is used for current and voltage in the calculation of apparent power. The apparent power definitions used in these equations are not influenced by the phase angle error introduced by the non-simultaneous sampling. The same is not true, however, when the *complex power* ($S_{1\phi}$) is calculated per phase and per harmonic:

$$S_{1\phi} = V_{1\phi} \times I_{1\phi}^{*} = V_{1\phi}\angle\alpha\left(I_{1\phi}\angle-\beta\right)^{*} = V_{1\phi}\angle\alpha\left(I_{1\phi}\angle\beta\right) = P_{1\phi} + jQ_{1\phi} \tag{54}$$

In the above equation it can be seen that the phase angle error in (α - β) due to non-simultaneous sampling influences the active- ($P_{1\phi}$) and the imaginary- ($Q_{1\phi}$) power.

3.6.2 Compensation of non-simultaneous sampling

3.6.2.1 A frequency- domain phase compensation function

A simple solution does not exist to the non-simultaneous sampling problem by compensating the time-domain data for the multiplex time error. The error in phase measurement can be compensated by a frequency dependent (or harmonic dependent) phase adjustment function. Such a *phase compensation function* must have the following characteristics:

- The amplitude must be unity and independent of frequency.
- The phase correction must be a function of frequency.

The compensation function below satisfies the above requirements:

$$PhaseCorrectionFunction(h) = 1 * e^{-j\omega_1 h t_{error}} \tag{55}$$

In the above equation, $\omega_1=2\pi f_1$ with f_1 the fundamental frequency, whilst h is the harmonic order and t_{error} the digitising time-interval that causes the phase error. This phase correction function has the amplitude and phase dependency shown in Figure 13 on harmonic order:

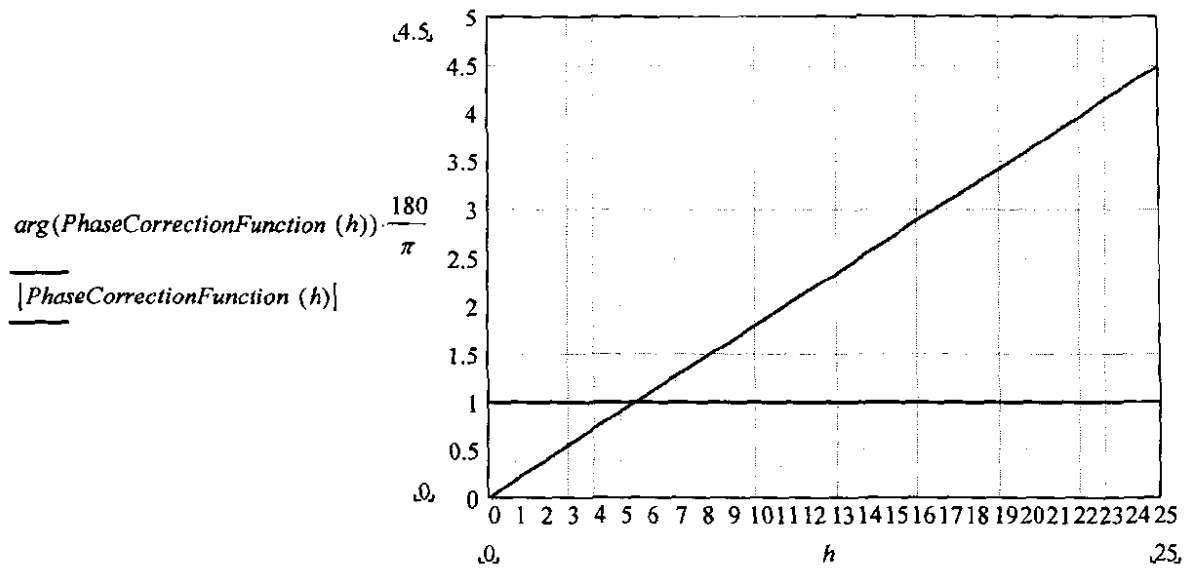

Figure 13: The phase and amplitude dependency on harmonic order of the phase compensation function

An additional requirement indicated in Figure 13 is that the channel number[24] should be included in the phase compensation function as redefined below:

$$PhaseCorrection(h,c) = 1 \cdot e^{j \cdot \varepsilon_{0_c} \cdot c \cdot 1_{error} \cdot h} \tag{56}$$

3.6.2.2 Application of phase compensation function

Assume the digitised data acquired by an A/D process to be in row-column format and arranged according to the following matrix:

$$Matrix_{time} = \begin{bmatrix} t_0 & v_a(t_0) & v_b(t_0) & v_c(t_0) & i_a(t_0) & i_b(t_0) & i_c(t_0) \\ t_1 & v_a(t_1) & v_b(t_1) & v_c(t_1) & i_a(t_1) & i_b(t_1) & i_c(t_1) \\ t_2 & v_a(t_2) & v_b(t_2) & v_c(t_2) & i_a(t_2) & i_b(t_2) & i_c(t_2) \\ \cdot & \cdot & \cdot & \cdot & \cdot & \cdot & \cdot \\ \cdot & \cdot & \cdot & \cdot & \cdot & \cdot & \cdot \\ t_{end} & v_a(t_{end}) & v_b(t_{end}) & v_c(t_{end}) & i_a(t_{end}) & i_b(t_{end}) & i_c(t_{end}) \end{bmatrix} \tag{57}$$

$Matrix_{time}$ is a matrix containing digitised time domain data. Timing instances t_0.....t_{end} represents the A/D timing value assigned to the data points. For instance, $v_a(t_0)$ in the second column (column number j = 2 and row number i = 1) is the amplitude of voltage in phase a at time t_0. Element $v_b(t_0)$ is the amplitude

[24] c: Channel number ε [0;1,2,....N-1], N = number of channels

of voltage in phase b taken at (t_0 + one multiplex time interval). Element $v_c(t_0)$ is the amplitude of voltage in phase c taken at (t_0 + two multiplex time intervals). Similarly, the amplitude of current in phase c, $i_c(t_0)$, is taken at real time (t_0 + 5 x multiplex time intervals). After another multiplex time interval, the data row is completed for t_0 and the process is repeated in the next row. The multiplex time interval for the PCI6031E card is 10 μs and in the example used above, timing instance t_1 will therefore be in real time 60 μs later than the time assigned to t_0.

The Fourier transformation of the time-domain data in $Matrix_{time}$ results in $Matrix_{FFT}$:

$$Matrix_{FFT} = \begin{bmatrix} V_{a1} & V_{b1} & V_{c1} & I_{a1} & I_{b1} & I_{c1} \\ V_{a2} & V_{b2} & V_{c2} & I_{a2} & I_{b2} & I_{c2} \\ V_{a3} & V_{b3} & V_{c3} & I_{a3} & I_{b3} & I_{c3} \\ & & & & & \\ V_{aN} & V_{bN} & V_{cN} & I_{aN} & I_{bN} & I_{cN} \end{bmatrix} \tag{58}$$

$Matrix_{FFT}$: This is a matrix containing the frequency domain data. For example, V_{a1} is the RMS fundamental harmonic phasor of the voltage in phase a, $V_{a1} = |V_{a1}|e^{j\alpha_{a1}}$. ($P$ = phase number a, b, c; h = harmonic number with N the highest harmonic order considered. The harmonic current phasors is $I_{Ph} = |I_{Ph}|e^{j\beta_{Ph}}$.

Phase compensation requires application of the *phase compensation function* onto the matrix of frequency data:

$$Matrix_{FFT}(h,c) = Matrix_{FFT}(h,c) \cdot PhaseCorrection(h,c) \tag{59}$$

Application of the *phase compensation function* per channel number (c = column number) and per harmonic order (h), demonstrates that both the channel number and the harmonic order have the required progressive influence on the phase compensation:

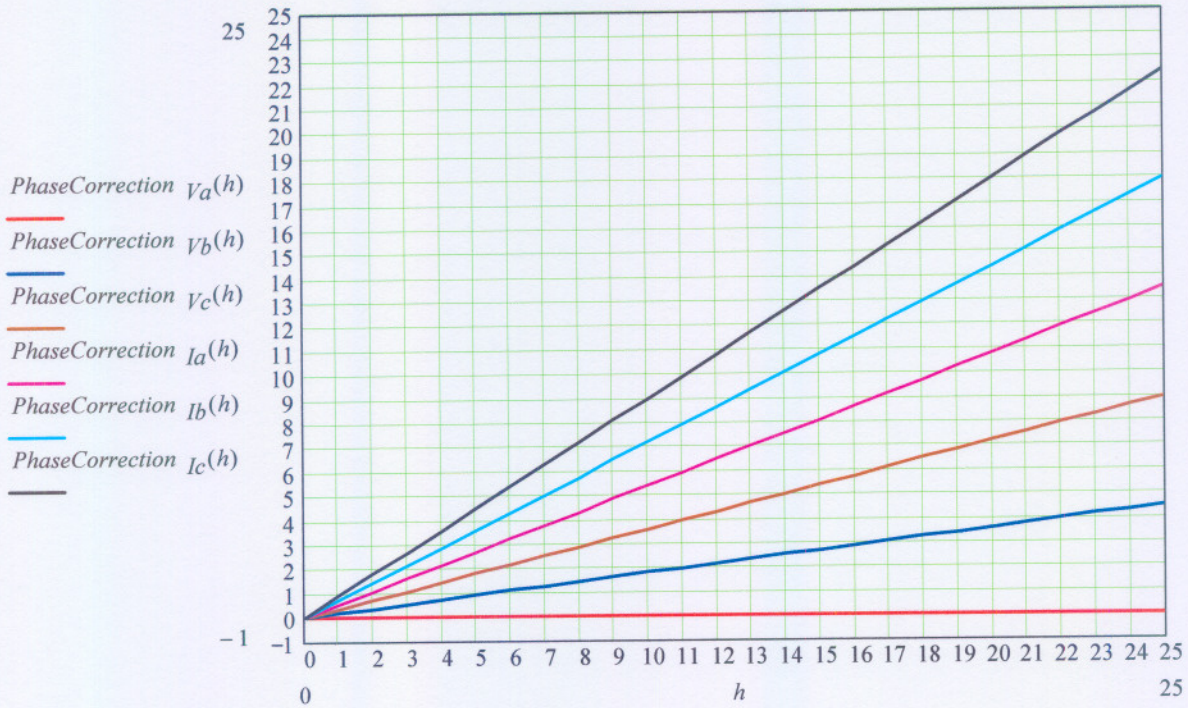

Figure 14: Phase correction applied per channel number and per harmonic order

Figure 14 show that the *phase correction function* simulates a simultaneous sampling process. It is important to realise that this compensation scheme is valid only when steady state conditions prevail. The laboratory power system enables control on electrical parameters to ensure such a stable steady state. In an industrial power system, it is not necessary valid to assume steady state conditions. The wavelet transform can be used to evaluate the time dependency of harmonic components and hence the assumption of a steady state.

The necessity of simultaneous sampling in a three-phase power system is demonstrated in the comparison of values in Table 3. The "uncorrected" and "corrected" values of *total active power* and *total harmonic active power* are respectively listed as measured in the laboratory power system under non-sinusoidal conditions:

Table 3: Comparison of simultaneous and non-simultaneous sampling

	$P_{3\phi}$ (Watts)	$P_{3\phi,H}$ (Watts)
Non-simultaneous Sampling	21580.52	-116.87
Simultaneous sampling	21722.51	-127.24
Difference in Watts:	142.00	10.37
Difference in %:	0.6 %	8.2 %

The error is very small for the *total active power* as the phase error at the fundamental frequency

components is very small. The error of 8.2 % in the *total harmonic active power* is significant.

When digital measurement instrumentation is used to study power quality issues, simultaneous sampling is important to avoid significant errors. Non-simultaneous sampling could cause erroneous interpretations of the measurements.

3.7 SYNCHRONOUS SAMPLING AND THE FFT

A sampling frequency that is not synchronised with the fundamental frequency component of the signal to be sampled is a cause of errors in the determination of the phase and amplitude of harmonic components. Such a sampling frequency can satisfy the Nyquist theorem but because of the non-synchronisation, spectral leakage can exist. Unavoidable truncation of a sampled signal to a finite length of samples is another cause of spectral leakage.

The literature in [81] - [86] proposes several mathematical solutions such as interpolation algorithms and windowing functions. These approaches can reduce the measurement errors, but cannot completely remove it [85]. A solution to spectral leakage is to synchronise the sampling frequency with the signal to be measured and to obtain an integer number of samples.

Ferrero and Ottoboni [84], [85] reported a hardware solution to the synchronisation problem. The hardware determines the fundamental frequency and multiplies it by an appropriate integer in order to generate a synchronised sampling frequency.

3.7.1 Spectral leakage correction through windowing

Certain windowing-techniques (such as that reported in [86], [82], [83]) deliver satisfactorily results in "moving" harmonic energy to the harmonic number were it should have been, in other words "correcting" the amplitude spectrum. Although the error in amplitude is reduced, the phase errors can be worse than it was before. Ferrero and Ottoboni [81] have shown that for the usual non-symmetrical sequences employed in DFT algorithms, the phase errors are the dominant error in "short-range" leakage and cannot be reduced by data windows. Complex interpolation algorithms, which are computing intensive, should be used provided the harmonic interference is negligible. Ferrero and Ottoboni further demonstrated the success of an alternative DFT algorithm, which reduce this phase error significantly without an increase in the computation burden.

Windowing functions are integrated in some mathematical packages and can be used with relative ease, but may be unsatisfactorily when used to study power phenomena in non-sinusoidal power systems. Power calculations require accurate phase information. If non-synchronised digitising measurement systems are used, an "alternative" DFT algorithm in [81] should be used in analysis of the data.

3.7.2 Considerations on the measurements obtained

The sampling frequency is controlled and the number of data points to be sampled in a fundamental cycle can be predetermined. The sampling frequency was chosen to be 12.8 kHz representing 1024 samples over 4 fundamental 50 Hz periods, or 80 ms. The minimum power system frequency was 49.7 Hz. Spectral leakage can result if only one 20 ms window of data is analysed. For example if it is assumed that the fundamental frequency is 50 Hz and not 49.7 Hz, then a data-window of 20 ms results in 256 samples. The "true" fundamental cycle is 20.120724 ms, however. A sampling time interval of 78.125 μs (12.8 kHz) results in 257.55 samples in this fundamental period. Rounding off this number to 258 or to 257 samples causes spectral leakage.

If 4 fundamental periods (50 Hz cycles) of this 49.7 Hz signal is sampled, the data window is 80 ms. The number of data points are now 1030 and cause less spectral leakage. The worst frequency condition was 49.91 Hz that resulted in 1026 samples (1024 samples are exactly 80 ms) in a four fundamental period data window.

3.7.2.1 MathCAD procedure to measure fundamental frequency

A MathCAD procedure was written to establish the fundamental frequency of the acquired signal in the time domain. An example of the practical nature of the problem is found in the following: Observe typical voltage waveforms in Figure 15 and the load current waveforms in Figure 16 measured in the laboratory at the terminals of a nonlinear load.

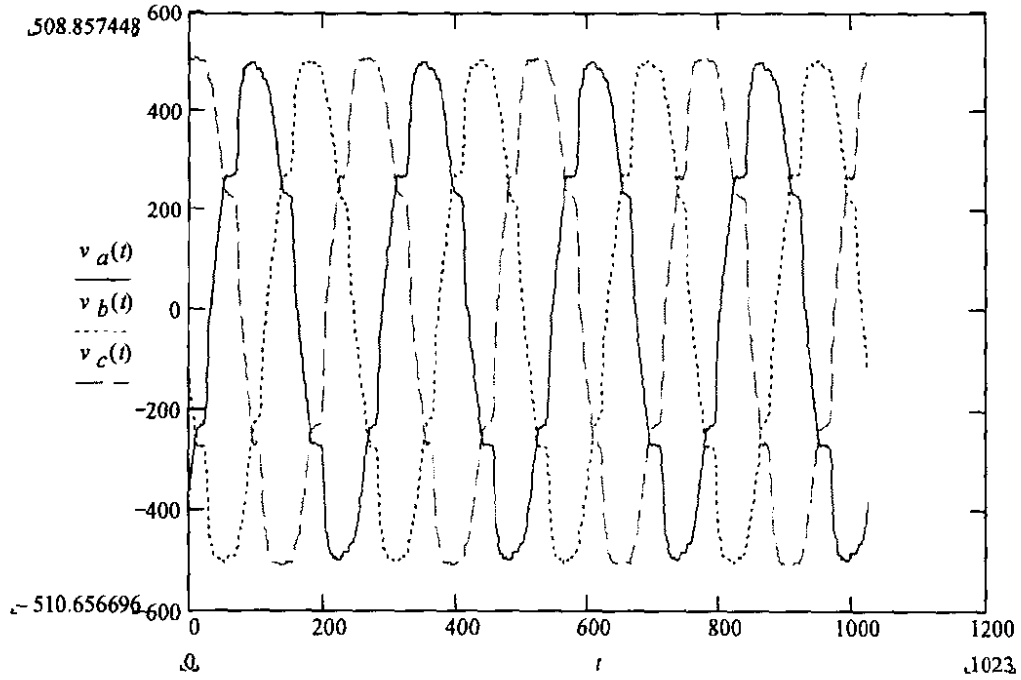

Figure 15: Three-phase load voltage waveforms corresponding to currents withdrawn in Figure 16

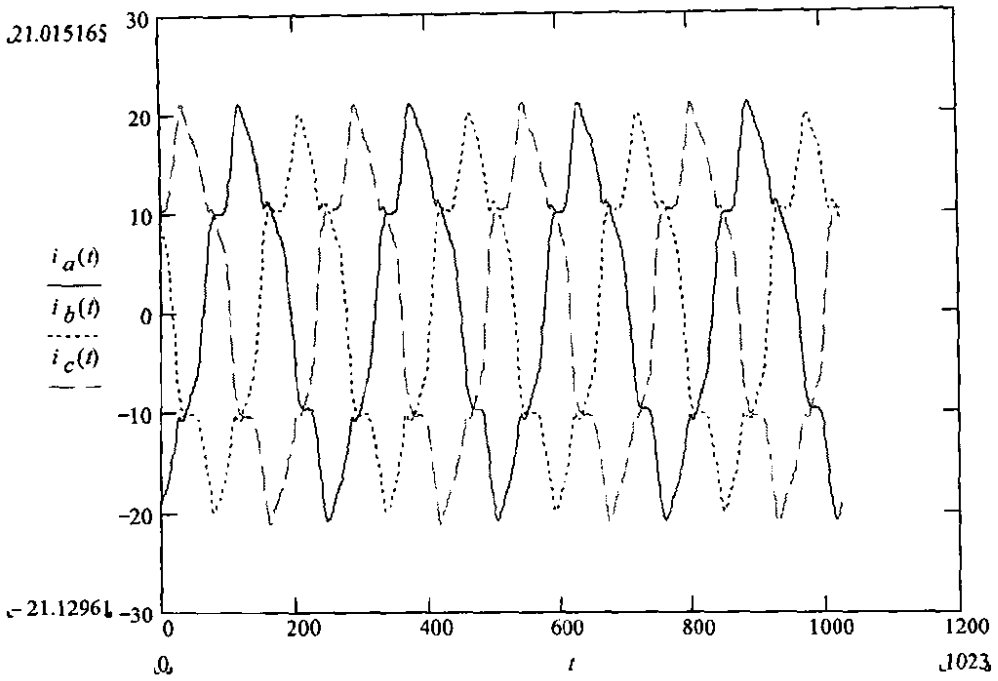

Figure 16: Load current waveforms corresponding to the voltage waveforms in Figure 15

The no-load voltage waveforms at the terminals of this nonlinear load are shown in Figure 17

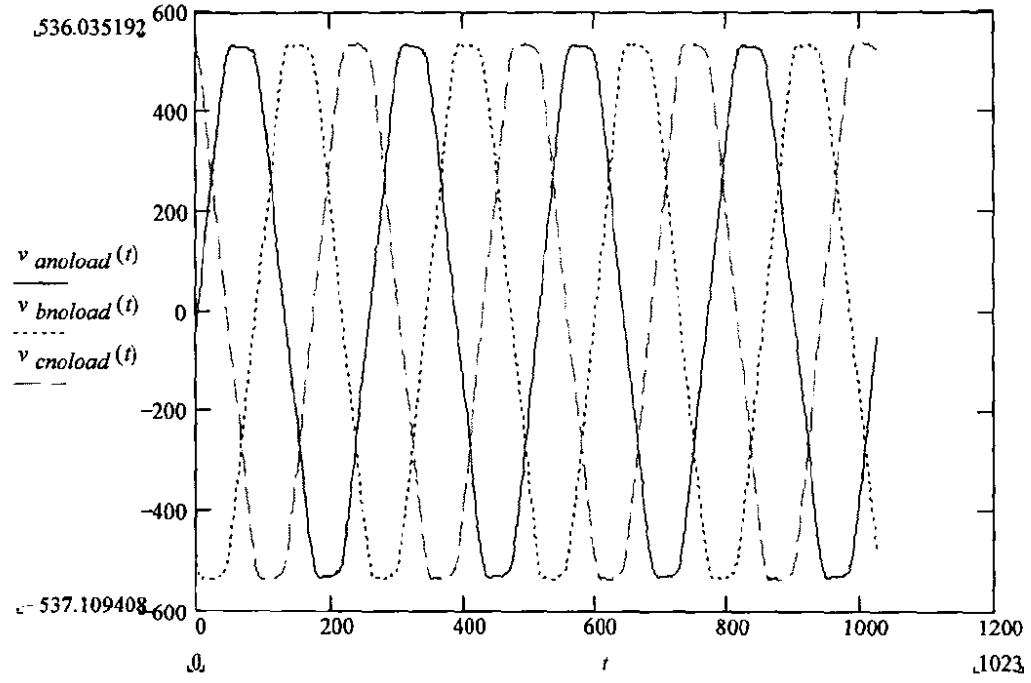

Figure 17: The no-load voltage waveforms corresponding to the voltage waveforms when connected to a load as in Figure 15

The minimum value of the voltage signal results from the following MathCAD function:

$$ClosestToZero := min\left(\overrightarrow{|V_{anoload}|}\right) \tag{60}$$

In the above equation, $V_{anoload}$ is the vector of phase voltage values of the time-dependent phase a voltage $v_{anoload}(t)$ digitised at discrete time intervals. The individual data points are represented by the row index t of the vector $V_{anoload}$:

$$v_{anoload}(t) := V_{anoload_t} \tag{61}$$

Equation (60) finds the absolute minimum value in the digitised voltage vector $V_{anoload}$. The "near zero-crossing" of the signal does not necessarily have an exact zero voltage value that can be used as an indicator of a zero-crossing of that signal.

The MathCAD subroutine to find the real time, at which the minimum voltage value has occurred in the signal under investigation, is given below:

$$v_{anoload}(t) := V_{anoload_t} \tag{62}$$

$$TimeOfMinValue := \left| \begin{array}{l} for \quad t \in 0..(NumberOfSamples - 1) \\ \quad (TimeOfMinValue_t \leftarrow SamplingTimes_t) \quad if \quad \left|V_{anoload_t}\right| = ClosestToZero \\ TimeOfMinValue \end{array} \right. \tag{63}$$

For example, the real time found at which the absolute minimum value occurs in the phase a voltage waveform of Figure 17 is:

$$|TimeOfMinValue| = 0.070335 \text{ Seconds}$$

This specific minimum amplitude value will not necessarily repeat in that time-window under consideration. A weighting factor was introduced to find the "other" zero-crossings. "Extra" zero crossings can also occur around zero in a distorted waveform. The MathCAD routine below detects the "other" minimum values in the voltage vector $V_{anoload}$:

$$ZeroValuesV_{anoload_t} := \left| \begin{array}{l} V_{anoload_t} \quad if \quad \left|V_{anoload_t}\right| \leq (7 \cdot ClosestToZero) \\ 0 \quad otherwise \end{array} \right. \tag{64}$$

The factor of 7 used above can be any integer; it depends on the specific waveform under investigation. A visual inspection on the results of the subroutine above, as a function of the waveform in which it occurs, is required to determine the correct weighting factor to be used. The zero-crossings marked in Figure 18

illustrate an example of the results obtained by the subroutine shown in equation (64):

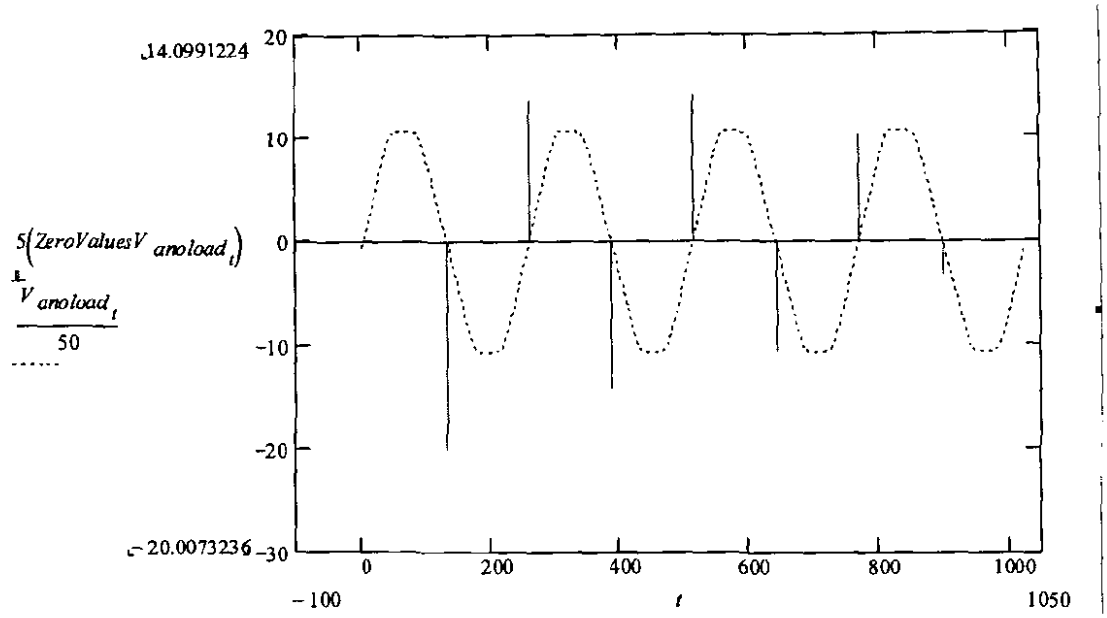

Figure 18: Zero-crossings in the phase *a* no load voltage of Figure 17

A minimum value is indeed located at time t = 70.335 milliseconds. Only one zero-crossing should be located at either a positive or a negative amplitude value. If both a positive and a negative zero-crossing marker results close to a given zero-crossing, it is because the factor in the subroutine in equation (64) was not chosen correctly. Careful adjustment thereof until the "unwanted" zero-crossing indicator disappears is then required. Although two "zero-crossings" are not marked in Figure 18, the marked "zero-crossings" furnish enough information to calculate the period of the waveform.

Three complete fundamental waveform cycles are marked in Figure 18. A vector containing the real time values of the zero-crossing markers is extracted from the original waveform data:

$$ZeroValuesV_{anoload_t} := \begin{cases} V_{anoload_t} & \text{if } \left|V_{anoload_t}\right| \le (7 \cdot ClosestToZero) \\ 0 & otherwise \end{cases} \tag{65}$$

$$t := 0\,,1\,..\,last(SamplingTimes)$$

$$ZeroPoints_t := \begin{cases} t & if\ ZeroValuesV_{anoload_t} \neq 0 \\ 0 & otherwise \end{cases}$$

$$c(x) := x > 0$$

$$Extract(V\,,c) := \left| \begin{array}{l} i \leftarrow 0 \\ U \leftarrow 0 \\ for\ \ j \in 0\,..\,rows(V) - 1 \\ \quad if\ \ c(V_j) = 1 \\ \quad\quad \left| \begin{array}{l} U_i \leftarrow V_j \\ i \leftarrow i + 1 \end{array} \right. \\ U \end{array} \right. \tag{66}$$

$$E := Extract(ZeroPoints\,,c)$$

The result of the routine in equation (66) as applied to Figure 18 is a vector [E] that contains the real time values:

$$E = \begin{pmatrix} 131 \\ 259 \\ 387 \\ 515 \\ 643 \\ 771 \\ 899 \end{pmatrix}.$$

The average period over the three periods contained in vector $\boldsymbol{E}$ is 0.0200064 ms or 49.9840051184 Hz. The sampling frequency of 12.8 kHz for the waveforms in Figure 15, Figure 16 and Figure 17 investigated above results in 1024.33 data points in 80.0256 ms. Analysis of only 1024 data points caused negligible spectral leakage.

3.8 SUMMARY

Both the process by which data is generated and the correctness of data is fundamental to this work. Results obtained by data analysis have to be repeatable to sustain any conclusion. Careful consideration of the manner in which power system data is analysed, is important. Significant errors can be the results of parameters over which little or no control exist, such as the variation in the fundamental power system frequency. Hardware synchronisation of the sampling frequency and the fundamental frequency as discussed in section 3.7 is a powerful counter measure. Compensation of the phase error introduced by the multiplex timing intervals of A/D conversion is possible through innovative software routines.

The experimental and measuring processes to generate appropriate data for the research undertaken in this thesis, was carefully designed. Data analysis methods were configured to be sensitive to possible errors such as spectral leakage. The validity of results was continuously verified. All possible measures that are practical were applied to ensure that the results obtained and the conclusions reported in this thesis, are reliable and valid.

4 NON-SINUSOIDAL ELECTRICAL POWER THEORY

4.1 INTRODUCTION

A practical power system contains non-sinusoidal voltage and current waveforms that require special consideration when defining power. The classical power theory can not satisfactorily describe power phenomena under non-sinusoidal waveform conditions. This chapter critically evaluates a number of non-sinusoidal power theories.

The importance of the inadequacies found in the classical power theory to describe the power phenomena of non-linear power system operation were highlighted in the early 1920's by Bucholz (1922). The well-known Budeanu formulation followed in 1927. Fryze reinterpreted [75] Budeanu's definitions in 1932. Thereafter many other attempts followed when it became increasingly important for a power theory to describe power under non-sinusoidal conditions. The need to reach a conclusion on power definitions was again emphasised from the middle 1980's [2], [11], [16], [22]. For example, Czarnecki communicated this deficiency unambiguously in an IEEE Transactions paper entitled "What is wrong with the Budeanu Concept of Reactive Power and Distortion Power and why it should be abandoned" [2]. Even today there is disagreement over several aspects and definitions in non-sinusoidal power theory. The need for universally accepted power definitions has come to the fore now, like never before, in order that designs and energy accounts can be defined and used unambiguously and through which distortion compensation can be specified.

Chapter 4 isolates and demonstrates a deficiency in the three-phase power theory of Czarnecki. One reason in the formulation of his power theory was to present an alternative to the Budeanu power theory (which he demonstrated to be flawed). The Budeanu power theory in section 4.2 and the single-phase power theory investigation of section 4.3 are not novel. The principles put forward by Czarnecki is repeated with realistic circuit values and then tested in ATP. This is to further a solid understanding to the three-phase power theory formulation of Czarnecki which is then shown to be flawed if used in practical power systems.

4.2 BUDEANU AND THE CONCEPT OF DISTORTION POWER

4.2.1 The Budeanu reactive power

The Budeanu [1] power definitions require decomposition of voltage and current time domain quantities into frequency domain quantities. Budeanu defined the total reactive power at a measurement cross section in a single-phase electrical network with non-sinusoidal voltage and current waveforms, as a quantity, Q_B:

$$Q_B = \sum_{h=1}^{\infty} V_{h,1\phi} I_{h,1\phi} \sin(\alpha_h - \beta_h) = \sum_{h=1}^{\infty} Q_{h,1\phi} \tag{67}$$

To investigate the physical significance to the formulation above, it is necessary to systematically review the fundamental concepts of power when waveforms in an electrical circuit are non-sinusoidal. Assume that a non-sinusoidal, single-phase, time-dependent voltage $v(t)_{1\phi}$ with fixed repetitive period T is applied to a load and that it can therefore be represented as a finite series of harmonic components:

$$v(t)_{1\phi} = \sum_{h=1}^{N} v_h(t)_{1\phi} = \sum_{h=1}^{N} \sqrt{2} V_{h,1\phi} \sin(h\omega_1 t + \alpha_h) \tag{68}$$

The single phase distortion component of $v(t)_{1\phi}$ can be isolated as $v_H(t)_{1\phi}$:

$$v_H(t)_{1\phi} = \sum_{h\neq 1}^{N} \sqrt{2} V_h \sin(h\omega t + \alpha_h) \tag{69}$$

If voltage $v(t)_{1\phi}$ is applied to a frequency dependent impedance load, the resulting time-dependent load current $i(t)_{1\phi}$ can be mathematically written as:

$$i(t)_{1\phi} = \sum_{h=1}^{N} i_h(t)_{1\phi} = \sum_{h=1}^{N} \sqrt{2} I_{h,1\phi} \sin(h\omega_1 t + \beta_h) \tag{70}$$

The distortion components of of $i(t)_{1\phi}$ can be isolated as $i_H(t)_{1\phi}$:

$$i_H(t)_{1\phi} = \sum_{h\neq 1}^{N} \sqrt{2} I_h \sin(h\omega_1 t + \beta_h) \tag{71}$$

The effect of voltage and current, termed the *effective* or *RMS* values, follows from the individual harmonic phasors:

$$V_{1\phi} = \sqrt{\sum_{h=1}^{N} \left| V_{h,1\phi}^2 \right|}, \quad I_{1\phi} = \sqrt{\sum_{h=1}^{N} \left| I_{h,1\phi}^2 \right|} \tag{72}$$

Voltage $v(t)_{1\phi}$ and current $i(t)_{1\phi}$ can additionally be written as complexors in terms of harmonic phasors:

$$v(t)_{1\phi} = \sum_{h=0}^{N} v_h(t)_{1\phi} \; ; \; v_h(t)_{1\phi} = V_{h,1\phi} e^{j(h\omega t)}$$

$$i(t)_{1\phi} = \sum_{h=0}^{N} i_h(t)_{1\phi} \; ; \; i_h(t)_{1\phi} = I_{h,1\phi} e^{j(h\omega t)} \tag{73}$$

Take note in the above definition of the voltage and current, the bold script indicate the complexor representation of $v(t)_{1\phi}$ and $i(t)_{1\phi}$. The complexor itself is not measurable by direct means, only $v(t)_{1\phi}$ and $i(t)_{1\phi}$ are. Classical power theory formulates time-dependent reactive power in a harmonic component to be:

$$q(t)_h = \mathrm{Re}\left[\sqrt{2}\boldsymbol{v}(t)_h\right]\mathrm{Im}\left[\sqrt{2}\boldsymbol{i}(t)_h\right] \tag{74}$$

In the equation above, the time-dependent reactive power is written in terms of a specific harmonic order, h. The time-dependent reactive power representative of a circuit under distorted conditions can then be written as:

$$q(t) = \sum_{h=1}^{N} q(t)_h \tag{75}$$

The average value of the above can then be written as:

$$Q_B = \frac{1}{T}\int_T q(t) = \frac{1}{T}\int_T \sum_{h=1}^{N} q(t)_h = \sum_{h=1}^{\infty} V_{h,1\phi} I_{h,1\phi} \sin(\alpha_h - \beta_h) \tag{76}$$

Equations (75) and (66) define the same quantity. It was formulate by Budeanu as the reactive power of a circuit under distorted waveform conditions. Some literature terms this quantity the *Joint Reactive Power* but it is better known as the *Budeanu Reactive Power*. The Budeanu reactive power employs an algebraic summation of all the reactive powers at each harmonic frequency.

The physical nature of reactive power was investigated through the application of field theory in Chapter 2 of this document. It was shown not to contribe to real energy transfer because the physical nature of reactive power represents an energy accumulation in the electric and magnetic fields of the reactance components of the load and the source that results in oscillatory exchange of energy between these elements. When the waveforms are non-sinusoidal, a similar explanation to that of reactive power can be assigned to the harmonic reactive power Q_h at each harmonic order h.

4.2.2 Active power in a nonsinusoidal single-phase circuit

The formulation of the Budeanu active power is through a similar approach. Classical power theory formulates *Time-dependent Active Power* to be, in terms of a harmonic component:

$$p_h(t)_{1\phi} = \mathrm{Re}\left[\sqrt{2}v_h(t)_{1\phi}\right]\mathrm{Re}\left[\sqrt{2}i_h(t)_{1\phi}\right] \tag{77}$$

The *Time-dependent Total Active Power* of a circuit under distorted waveform conditions is:

$$p(t)_{1\phi} = \sum_{h=1}^{N} p_h(t)_{1\phi} \tag{78}$$

The *Total* (or *Joint*) *Average Active Power* requires integration over a period T:

$$P_{1\phi} = \frac{1}{T}\int_T p(t)_{1\phi}\,dt = \sum_{h=1}^{N} V_{h,1\phi} I_{h,1\phi}\cos(\alpha_h - \beta_h) \tag{79}$$

4.2.3 Apparent and Complex power in a nonsinusoidal single-phase circuit

The classic power definition above is an accepted formulation with unambiguous physical explanation as defined for waveforms that are perfectly sinusoidal and repetitive. It can be written both in terms of harmonic components and average values of active and reactive power as:

$$\boldsymbol{S}_{h,1\phi} = \boldsymbol{V}_{h,1\phi}\boldsymbol{I}^*_{h,1\phi} = P_{h,1\phi} + jQ_{h,1\phi} \tag{80}$$

The *Total* or *Joint Complex Power* for a circuit is found by summing the complex power in all the harmonic components (including the fundamental):

$$\boldsymbol{S}_{1\phi} = \sum_{h=1}^{N} \boldsymbol{S}_{h,1\phi} \tag{81}$$

The *Total* (or *Joint*) *Single-phase Apparent Power* delivered to a circuit is defined as the product of the scalar values of the voltage and current at the terminals of that circuit:

$$S_{1\phi} = V_{1\phi} I_{1\phi} \tag{82}$$

It is important to note that equations (79) and (80) contain the Schwartz inequality [98] which, in terms of

the quantities defined in this document, can be written as:

$$S_{1\phi}^2 \geq P_{1\phi}^2 + Q_{1\phi}^2 \tag{83}$$

4.2.4 The Budeanu Distortion power

Budeanu introduced the concept of "distortion power", D_B to account for the anomaly between the measured *Total Apparent Power* (also referred to as *Loading Power*) and that predicted by the summation of the *orthogonal Real-* and *Reactive* components alone (Equation (82)):

$$D_B \equiv \sqrt{S_{1\phi}^2 - P_{1\phi}^2 - Q_B^{\,2}} \tag{84}$$

The apparent power definition in terms of Budeanu's formulation can be written as:

$$S_{1\phi} = \sqrt{P_{1\phi}^2 + Q_B^2 + D_B^2} \tag{85}$$

The cause to D_B can be found in a mathematical investigation on the formulation of apparent power:

$$S_{1\phi} = \sqrt{\sum_{h=1}^{N} \left|V_{h,1\phi}\right|^2 \sum_{h=1}^{N} \left|I_{h,1\phi}\right|^2} = \sqrt{\sum_{h=1}^{N} \left|V_{h,1\phi}^2\right|} \sqrt{\sum_{h=1}^{N} \left|I_{h,1\phi}^2\right|} \tag{86}$$

Multiplication of equal and unequal harmonic numbers is required in the above equation:

$$S_{1\phi}^2 = \sum_{h=1}^{N} \left|V_{h,1\phi}^2\right| \left|I_{h,1\phi}^2\right| + \sum_{h,k=1(h\neq k)}^{N} \left|V_{h,1\phi}^2\right| \left|I_{k,1\phi}^2\right| \tag{87}$$

The above equation contains the *Joint Active Power* ($P_{1\phi}$), the *Budeanu* (or *Joint*) *Reactive Power* (Q_B) and the *Budeanu Distortion Power* D_B:

$$S_{1\phi} = \sqrt{\left(\sum_{h=1}^{N} P_{h,1\phi}\right)^2 + \left(\sum_{h=1}^{N} Q_B\right)^2 + \left(\sum_{h,k=1(h\neq k)}^{N} \left|V_{h,1\phi}\right| \left|I_{k,1\phi}\right|\right)^2} \tag{88}$$

The Budeanu *Distortion Power* is caused by the interaction of unlike harmonic numbers; the physical significance thereof is investigated in the next sections.

4.2.5 Significance of Q_B and D_B

Shepherd and Zakikhani reported in 1972 that Q_B is not a quantity with physical significance [73]. Filipski [36] reported on practical aspects of the measuring of the "distortion" power in 1984.Pretorius *et al* [38] reported that Q_B measured under certain distorted waveform conditions gives erroneous results. Czarnecki [2] was the first to successfully design practical metering systems in the 1970's to measure Budeanu's powers.

Czarnecki [2] reported in 1987 that the quantities Q_B and D_B do not possess physical attributes in terms of the power phenomena in non-sinusoidal circuits and that it cannot be used in the design of compensating circuits. He has shown that D_B is not related to the magnitude of waveform distortion as was commonly accepted until then. The concept of a "distorting" power has no physical significance. However, even today the concept of "distortion" power is widely used amongst engineers. Furthermore, Budeanu's reactive power definition in (66) does not relate to the physical process of oscillatory energy exchange between load and source, as will be demonstrated in a subsequent section (4.2.6). It is therefore important to validate Czarnecki's findings on the errors in Budeanu's power theory and it is empirically investigated in the next section.

4.2.6 The error in the formulation of Budeanu's power definitions

A similar approach to the investigation done by Czarnecki on the significance of Budeanu's reactive and distortion power is used, but with the difference that realistic circuit values are used in a time-domain simulation. The results obtained are not novel but validates the conclusion by Czarnecki reported in [2] and [3]. It is an interesting demonstration to the possible pitfalls in formulating power definitions that seems mathematically sound, but which not necessarily explain physical phenomena.

In an electrical network with non-sinusoidal waveforms and frequency dependent impedances, the harmonic voltage and current phasors at each harmonic number h will have different phase angles. The harmonic reactive powers are summed over all the harmonic frequencies to obtain Budeanu's reactive power. Q_B can even sum to zero due to different signs in Q_h at different harmonic numbers, although the individual Q_h terms can be nonzero. The oscillatory nature of reactive power is therefore not reflected by Q_B. A $Q_B = 0$ can be interpreted as if the power factor of the load is unity, which is false as the individual Q_h are not zero. This aspect of Budeanu's reactive power is subsequently validated.

The square of the apparent power at a harmonic frequency can be written as:

$$S_{h,1\phi}^2 = \left|v_h(t)_{1\phi}\right|^2 \left|i_h(t)_{1\phi}\right|^2 \tag{89}$$

If the above equation is divided by $\left|v(t)_{1\phi}\right|^2$, the following results are obtained [2]:

$$\frac{S_{h,1\phi}^2}{\left|v_h(t)_{1\phi}\right|^2} = \frac{\left|v_h(t)_{1\phi}\right|^2 \left|i_h(t)_{1\phi}\right|^2}{\left|v_h(t)_{1\phi}\right|^2} = \left|i_h(t)_{1\phi}\right|^2 = \left|I_{h,1\phi}\right|^2 = \left|\frac{P_{h,1\phi}}{V_{h,1\phi}}\right|^2 + \left|\frac{Q_{h,1\phi}}{V_{h,1\phi}}\right|^2 \tag{90}$$

Two orthogonal current components are definable above. Further, harmonic current phasors are mutually orthogonal, therefore [2]:

$$\left|i(t)_{1\phi}\right|^2 = \sum_{h=1}^{\infty}\left|i_h(t)_{1\phi}\right|^2 = \sum_{h=1}^{\infty}\left|\frac{P_{h,1\phi}}{V_{h,1\phi}}\right|^2 + \sum_{h=1}^{\infty}\left|\frac{Q_{h,1\phi}}{V_{h,1\phi}}\right|^2 \tag{91}$$

The square of apparent power can now be rewritten as:

$$\begin{aligned} S_{1\phi}^2 &= V_{1\phi}^2 I_{1\phi}^2 \\ &= V_{1\phi}^2 \sum_{h=1}^{\infty}\left|\frac{P_{h,1\phi}}{V_{h,1\phi}}\right|^2 + V_{1\phi}^2 \sum_{h=1}^{\infty}\left|\frac{Q_{h,1\phi}}{V_{h,1\phi}}\right|^2 \end{aligned} \tag{92}$$

Czarnecki [2] used the latter equation to explain why apparent power will increase when the voltage and the current waveforms are non-sinusoidal. The term $\sum_{h=1}^{\infty}\left|\frac{Q_{h,1\phi}}{V_{h,1\phi}}\right|^2$ was isolated as the component causing such increase and not because of the Budeanu reactive power definition, $Q_B = \sum_{h=1}^{\infty} Q_{h,1\phi}$.

The apparent power will be a minimum when at each harmonic number h the value of Q_h is zero. The Budeanu reactive power Q_B can be zero even if the Q_h terms themselves are not zero.

The following conclusions on the Budeanu apparent power are now clear:

- Not only will Q_B be affected by reciprocating energy transmission, D_B will also be affected.
- Neither Q_B nor D_B is distinctively related to phenomena responsible for apparent power increase.

4.2.7 The use of Q_B to improve the power factor

To design power factor correction based on the aggregated total of reactive power (Budeanu's Q_B) is not a scientifically sound approach. Some engineers and metering equipment use this Budeanu definition of reactive power. A simple demonstration, similar to the approach used by Czarnecki [4] [15] is carried out to establish if the Budeanu reactive power enables power factor correction.

In the following circuit, a non-sinusoidal voltage $v(t)_{1\phi}$ that contains a 5th, 7th, and a 11th harmonic component feeds a linear load consisting of a series resistor and inductor. A parallel capacitor is used to improve the power factor to unity:

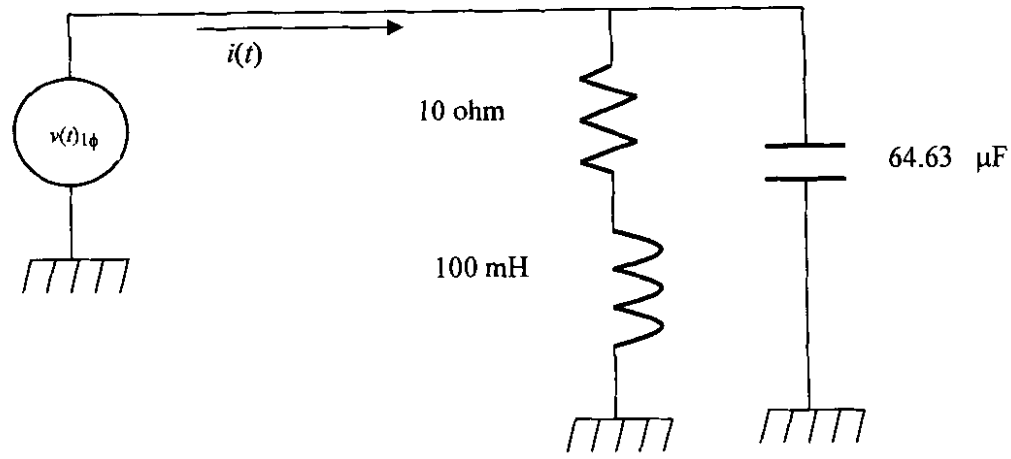

Figure 19: Investigating power factor improvement through utilization of Q_B

The voltage source signal $v(t)_{1\phi}$ is defined as:

$$v(t)_{1\phi} = \frac{100}{h}\sin(2\cdot\pi\cdot 50\cdot h\cdot t);\ h\in[1,5,7,11] \tag{93}$$

Without a capacitor based on the circuit values shown above, the resulting power factor (PF) is found to be 0.3 lagging. Assume that the Budeanu's reactive power definition of Q_B is used and a capacitor value calculated to compensate the PF to unity:

$$C = \frac{Q_B}{V_1^2\omega_1 + V_7^2\omega_7 + V_7^2\omega_7 + V_{11}^2\omega_{11}} \tag{94}$$

The compensated circuit was modelled in ATP and the results are listed in Table 4:

Table 4: Power factor correction results based on Budeanu's Q_B

Symbol	Without a capacitor	Compensated	Units
$S_{1\phi}$	602.445	412.374	VA
$P_{1\phi}$	180.906	181.031	Watt
Q_B	574.4	3.572	VAr
D_B	16.658	370.497	VAr
PF	0.3	0.439	
C	0	64.63	μF

The results listed in Table 4 indicate that:

- Although Q_B is completely compensated by the capacitor, the power factor of the compensated circuit did not change significantly.

- The apparent power is lower in the compensated circuit but significant unnecessary loading remains (difference between apparent power and real power is significant).

- Budeanu's reactive power definition (Q_B) is not useful for power factor compensation.

- Power factor correction results in the "distortion power" (D_B) to increase significantly due to increased interaction between uneven harmonic voltage and current components.

4.2.8 The relation between Budeanu's "distortion power" and waveform distortion

Budeanu's "distortion power" D_B cannot be used to quantify the degree of waveform distortion nor can it be used to quantify the degree of nonlinearity in an electrical circuit [3]. A similar circuit to the investigation of Czarnecki [3] is studied in ATP but with common circuit values:

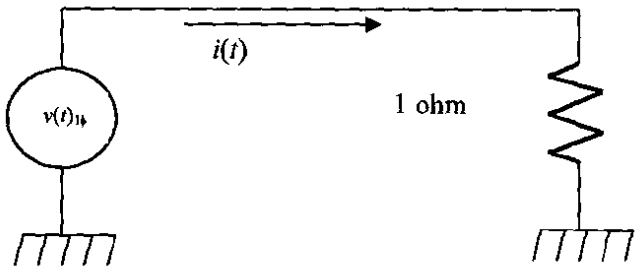

Figure 20: Non-sinusoidal voltage source feeding a resistive load

Assume that the single-phase voltage source contains a 3rd, 5th and a 7th harmonic component:

$$v(t)_{1\phi} = \frac{1}{h}\sin(2\cdot\pi\cdot 50\cdot h\cdot t);\ h\in[1,3,5,7] \tag{95}$$

The distorted voltage and current waveforms are shown in Figure 21:

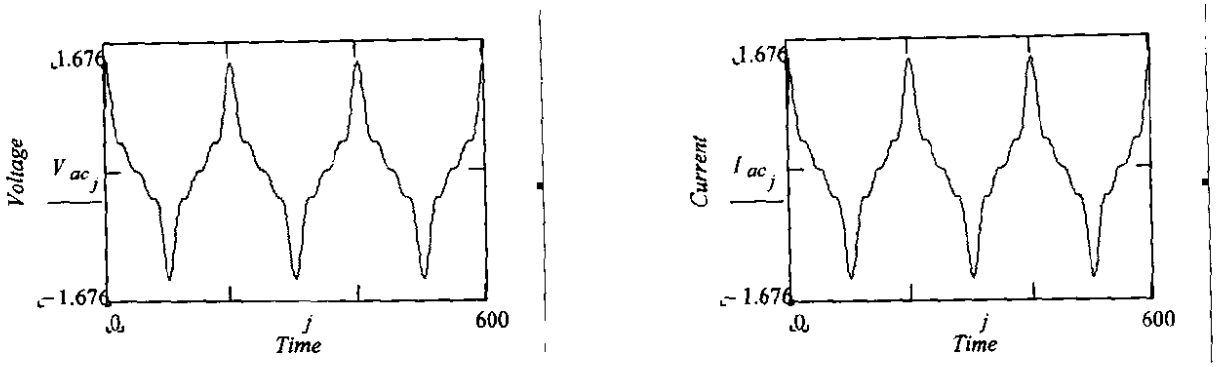

Figure 21: and Current waveform as measured in

The resulting Budeanu powers are:

Table 5: Budeanu's power components for the circuit in

$S_{1\phi}$	1.194 VA
$P_{1\phi}$	1.194 Watt
Q_B	0 VAr
D_B	0 VAr

The values listed in Table 5 enable the following conclusions to be made:

- D_B has a zero value and should have indicated that the waveforms are perfectly sinusoidal and not distorted but both voltage and current are in fact distorted.
- Therefore, D_B does not relate to the degree of waveform distortion.

Assume that a certain load is *frequency dependent*, but that this load appears under certain conditions to be *frequency independent*. An example is a load impedance that can be configured as a combination of reactive elements that have the same impedance value at two different frequencies. This load can also have the ability to change the load current waveform such that it is not an exact replica of the applied voltage waveform. Such a load is generally termed to be a "distorting" load. Consider the circuit of Figure 22:

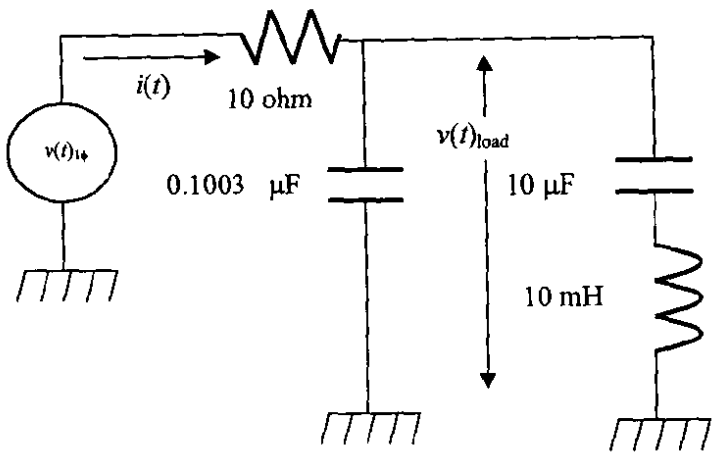

Figure 22: Investigating the relation between D_B and the nonlinearity of the load

Assume that the single-phase voltage source contains only a third harmonic component:

$$v(t)_{1\phi} = \frac{100}{h}\sin(2\cdot\pi\cdot 50\cdot h\cdot t);\ h\in[1,3] \tag{96}$$

This circuit was studied in ATP with the load elements of 10 ohm, 10 mH and 10 μF arbitrarily chosen. The following voltage and current waveforms result at the load terminals:

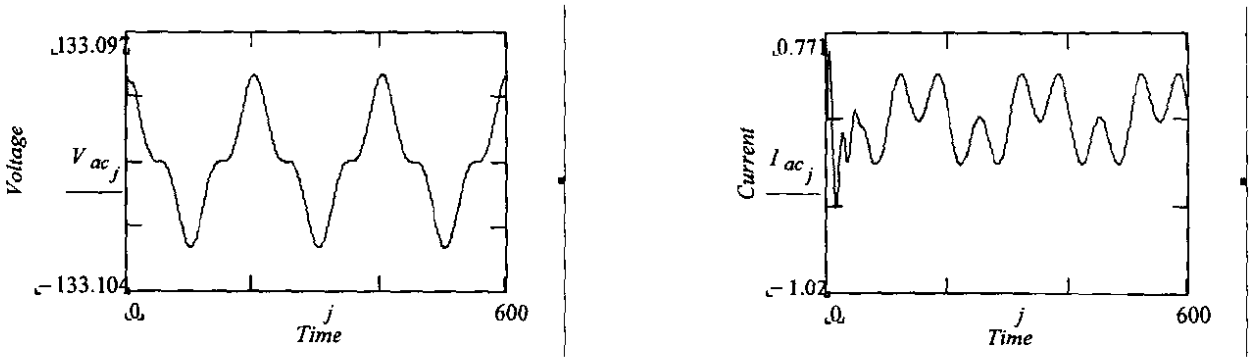

Figure 23: Voltage and current waveform at the load terminals of Figure 22

The resulting Budeanu powers are tabled below:

Table 6: Results of Budeanu's powers for the circuit in Figure 22

$S_{1\phi}$	43.484 VA
$P_{1\phi}$	0 Watt
Q_B	43.484 VAR
D_B	0 VAR

The following conclusion is based on the results listed in Table 6:

- Budeanu's distortion power (D_B=0) is not a measure of the degree of waveform distortion, the current and voltage waveform in Figure 22 is clearly distorted

4.3 THE POWER THEORY OF L.S. CZARNECKI

Different approaches to the definition of the non-active power components in steady-state non-sinusoidal power systems have been proposed in the literature, both in the time and frequency domain. The following three-phase conditions have to be considered when defining these non-active power components:

- Unbalanced load currents
- Non-sinusoidal load currents
- Non-sinusoidal supply voltage
- Asymmetrical supply voltage
- Nonzero supply impedance

A common goal with power definitions is to achieve mathematical formulations that will facilitate power factor maximisation to enable optimisation of active energy transfer. To achieve this, physical insight into the working of the power system, in the light of the different power phenomena and their physical interpretation is of paramount importance. Some power components of well-known non-sinusoidal power theories lack physical interpretation to a greater or lesser degree. Power definitions have not yet converged to general agreement on all aspects of non-sinusoidal three-phase power phenomena.

Prof. Czarnecki contributed[25] significantly to the development of knowledge on non-sinusoidal power theory. His contributions were recognised by, amongst others, the IEEE in granting him a fellowship. The Wiley Encyclopaedia on Electrical Engineering dedicated a supplement [19] to his description of harmonics and power phenomena. It summarises important aspects of non-sinusoidal power theory as

[25] Referenced literature [2]..[19] represents some popular publications by L.S. Czarnecki.

developed by Czarnecki. The Czarnecki power theory appears to be mathematically sound and is easy to apply to frequency domain data.

Czarnecki's power theory claims to be successful in defining all possible non-sinusoidal power phenomena, both for single- and three-phase electrical networks. It attempts to interpret all these power phenomena unambiguously with a physical explanation assigned to each. It is important for example, that the design of compensation schemes and tariff systems are based on sound scientific principles. The next section formulates the Czarnecki single-phase power theory and investigates compensation requirements based on these power definitions.

4.3.1 Czarnecki's Single-Phase Power Theory

Czarnecki's single-phase non-sinusoidal power theory is based on decomposing a single-phase, non-sinusoidal, load current into four orthogonal components. Each of the four load current components is associated with four different power components transferred to the load with each power and each current component assigned a unique physical explanation. Czarnecki's three-phase power theory is based on the single-phase power theory and expanded on by including a fifth component to describe the possible unbalance in a three-phase power system.

Although Czarnecki's power definitions claim to be suitable for analysing all possible three-phase power scenarios correctly, it remains controversial. If his theory can be proved to be indeed a valid approach to study three-phase non-sinusoidal power system phenomena, it will be a valuable contribution to knowledge. Engineers have to unambiguously measure non-sinusoidal quantities and apply appropriate compensation. The Czarnecki power theory is carefully studied with this in mind in the following sections.

4.3.1.1 Decomposition of the Non-sinusoidal Single-Phase Load Current

Consider a non-sinusoidal periodic single-phase voltage signal $v(t)_{1\phi}$ with a fundamental frequency of ω_1 that is applied to a load that is a linear frequency-dependent admittance $\boldsymbol{Y}_h=G_h+jB_h$:

$$v(t)_{1\phi} = V_0 + \sqrt{2}\,\mathrm{Re}\sum_{h\in N} V_{h,1\phi} e^{jh\omega_1 t} \tag{97}$$

If the voltage signal in above is applied to a single-phase frequency dependent admittance $\boldsymbol{Y}_{h,1\phi}=G_{h,1\phi}+jB_{h,1\phi}$, which is a function of harmonic number h, the load current can be written as:

$$i(t)_{1\phi} = G_0 V_0 + \sqrt{2}\,\mathrm{Re}\sum_{h\in N} (G_{h,1\phi} + \mathrm{j}B_{h,1\phi}) V_{h,1\phi} e^{jh\omega_1 t} \tag{98}$$

The single-phase total active power $P_{1\phi}$, transferred by the source to the load, is similar to the active power consumed by a load with the following "*effective*" conductance:

$$G_{e,1\phi} = \frac{P_{1\phi}}{\left|v(t)_{1\phi}\right|^2} \tag{99}$$

Fryze [75] first defined the component of the load current that exclusively transports the real power $P_{1\phi}$, termed the "active" current:

$$i_a(t)_{1\phi} = G_{e,1\phi} v(t)_{1\phi} = G_{e,1\phi} V_0 + \sqrt{2}\,\mathrm{Re}\sum_{h\in N} G_{e,1\phi} V_{h,1\phi} \mathrm{e}^{jh\omega_1 t} \tag{100}$$

The current component $i_a(t)_{1\phi}$ is the useful component in the load current as it is responsible for active power transfer to the load. The "rest" of the load current can be mathematically isolated:

$$\begin{aligned} i(t)_{1\phi} - i_a(t)_{1\phi} &= (G_0 - G_{e,1\phi})V_0 + \sqrt{2}\,\mathrm{Re}\sum_{h\in N}(G_{h,1\phi} + \mathrm{j}B_{h,1\phi} - G_{e,1\phi})V_{h,1\phi} e^{jh\omega_1 t} \\ &= \sqrt{2}\,\mathrm{Re}\sum_{h\in N}\mathrm{j}B_{h,1\phi} V_{h,1\phi} e^{jh\omega_1 t} + i_s(t)_{1\phi} \\ &= \sqrt{2}\,\mathrm{Re}\sum_{h\in N}\mathrm{j}B_{h,1\phi} V_{h,1\phi} e^{jh\omega_1 t} + (G_0 - G_{e,1\phi})V_0 + \sqrt{2}\,\mathrm{Re}\sum_{h\in N}(G_{h,1\phi} - G_{e,1\phi})V_{h,1\phi}\mathrm{e}^{jhw_1 t} \\ &= i_r(t)_{1\phi} + i_s(t)_{1\phi} \end{aligned} \tag{101}$$

with

$$\begin{aligned} i_r(t)_{1\phi} &= \sqrt{2}\,\mathrm{Re}\sum_{h\in N}\mathrm{j}B_{h,1\phi} V_{h,1\phi} e^{jh\omega_1 t} \\ i_s(t)_{1\phi} &= (G_0 - G_{e,1\phi})V_0 + \sqrt{2}\,\mathrm{Re}\sum_{h\in N}(G_{h,1\phi} - G_{e,1\phi})V_{h,1\phi}\mathrm{e}^{jhw_1 t} \end{aligned} \tag{102}$$

The above two equations isolate the "unnecessary" components of the load current mathematically. Physical significance is to be found in that the Czarnecki reactive current $i_r(t)_{1\phi}$ is defined as the load current component only associated with the susceptance component of the load impedance. It is the same reactive current definition formulated by Shepherd and Zakikhani [73] for a single-phase non-sinusoidal current. Take note that it is not the Budeanu reactive power definition. Czarnecki's reactive current is mathematically different.

The physical explanation of the Czarnecki reactive current is the same as for a sinusoidal single-phase reactive current in that it supports the oscillatory exchange of energy between the reactive elements in the load and the source. The $i_r(t)_{1\phi}$ component is unwanted and has to be compensated to improve the power

factor of the load as will be shown.

The second "extra" load current component $i_s(t)_{1\phi}$ is termed by Czarnecki as the "*scattered*" current. It is associated with current components resulting from the "scattering" of conductances around an effective conductance value, $G_{e,1\phi}$.

The load current resulting from a non-sinusoidal single-phase voltage applied to a linear frequency-dependent load is therefore defined by Czarnecki to consist of three components:

$$i(t)_{1\phi} = i_a(t)_{1\phi} + i_r(t)_{1\phi} + i_s(t)_{1\phi} \tag{103}$$

These three current components are mutually orthogonal [5]:

$$|i(t)|^2 = |i_a(t)|^2 + |i_r(t)|^2 + |i_s(t)|^2 \tag{104}$$

The magnitudes of the active, scattered and reactive current are defined as follows:

$$\begin{aligned} |i_a(t)|_{1\phi} &= \frac{P_{1\phi}}{|v(t)_{1\phi}|^2} \\ |i_r(t)_{1\phi}| &= \sqrt{\sum_{h\in N} B_{h,1\phi}^2 V_{h,1\phi}^2} = \sqrt{\sum_{h\in N}\left(\frac{Q_{h,1\phi}}{V_{h,1\phi}}\right)^2} \\ |i_s(t)_{1\phi}| &= \sqrt{\sum_{n\in N}[(G_0 - G_{e,1\phi})^2 V_0^2 + (G_{h,1\phi} - G_0)^2 V_{h,1\phi}^2]} \end{aligned} \tag{105}$$

The single-phase apparent power $S_{1\phi}$ in term of the above current decompositon relates to three different power components:

$$\begin{aligned} S_{1\phi}^2 &= |i(t)_{1\phi}|^2 |v(t)_{1\phi}|^2 \\ &= |i_a(t)_{1\phi}|^2 |v(t)_{1\phi}|^2 + |i_r(t)_{1\phi}|^2 |v(t)_{1\phi}|^2 + |i_s(t)_{1\phi}|^2 |v(t)_{1\phi}|^2 \\ &= P_{1\phi}^2 + Q_{r,1\phi}^2 + D_{s,1\phi}^2 \end{aligned} \tag{106}$$

The above decomposition of apperent power contains the *active power* $P_{1\phi}$, the *Czarnecki reactive power* Q_r and the *Czarnecki distortion power* D_s. These single-phase power equations, by the nature of their definition, adapt very easily into frequency domain calculations.

A nonlinear load or a time-variant load can increase the RMS value of the load current. This phenomenon was isolated as a fourth current component by Czarnecki [5]. It is termed "*generated current*" and is

investigated when the three-phase power theory of Czarnecki is studied in section 4.3.2.

The next section briefly investigates the application and physical significance of the *active current*, the *reactive current* and the *scattered current*.

4.3.1.2 Power factor and the Czarnecki single-phase current components

The power factor (*PF*) of a single-phase load can be written in terms of the Czarnecki single-phase current and power components:

$$PF = \frac{P_{1\phi}}{S_{1\phi}} = \frac{\left|i_a(t)_{1\phi}\right|}{\sqrt{\left|i_a(t)_{1\phi}\right|^2 + \left|i_r(t)_{1\phi}\right|^2 + \left|i_s(t)_{1\phi}\right|^2}} = \frac{P_{1\phi}}{P_{1\phi} + Q_{r,1\phi} + D_{s,1\phi}} \tag{107}$$

The following conclusions are based on the above *PF* formulation:

- To achieve maximum utilisation of the energy source, the *active current* $i_a(t)_{1\phi}$ should be the only current component in the load current.

- If load resistance (conductance) is frequency-dependent ($G_{h,1\phi} \neq G_{e,1\phi}$), the *scattered current* $i_s(t)_{1\phi}$ is an unwanted component of the load current. It causes an increase in the load current due to the "scattering" of conductances $G_{h,1\phi}$ around the equivalent conductance $G_{e,1\phi}$. The difference value ($G_{h,1\phi} - G_{e,1\phi}$) can be positive or negative. A passive network will not be able to compensate the *PF* to unity.

- The Czarnecki total single-phase reactive current $i_r(t)_{1\phi}$ is the result of the aggregated effect of reactive currents $i_{rh}(t)_{1\phi}$ at each harmonic number h. This reactive current $i_{rh}(t)_{1\phi}$ is an extra component in the total harmonic load current $i_h(t)_{1\phi}$ (due to each $\frac{Q_{h,1\phi}}{V_{h,1\phi}}$ term as isolated by Czarnecki). It is the physical reason for the increase in the load current drawn. Budeanu's reactive power definition cannot do the same. Compensation of these unwanted harmonic reactive currents is possible by means of a passive network as demonstrated in the next section.

4.3.1.3 Compensation of the single-phase reactive current

The single-phase reactive power $Q_{r,1\phi}$ of Czarnecki (similar to that of Shephard and Zakikhani [73]) can be compensated by a passive reactive network. Consider the circuit in Figure 24. It is similar to the configuration Czarnecki used [6] but with more general circuit values:

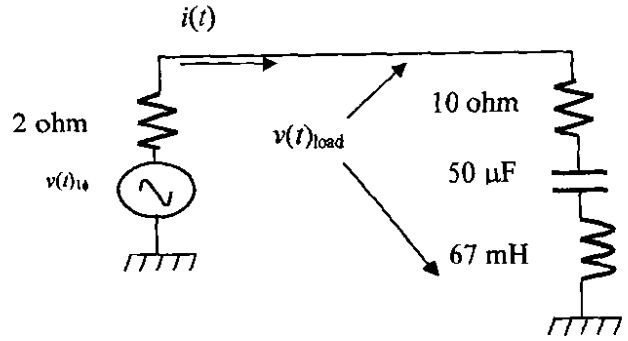

Figure 24: *RLC* load with equal conductances at the 1st and 3rd harmonic

The single-phase voltage source $v(t)_{1\phi}$ contains a fundamental and a 3rd harmonic component. The load voltage $v(t)_{load}$ and the load current $i(t)_{1\phi}$ obtained from an ATP simulation is shown in Figure 25.

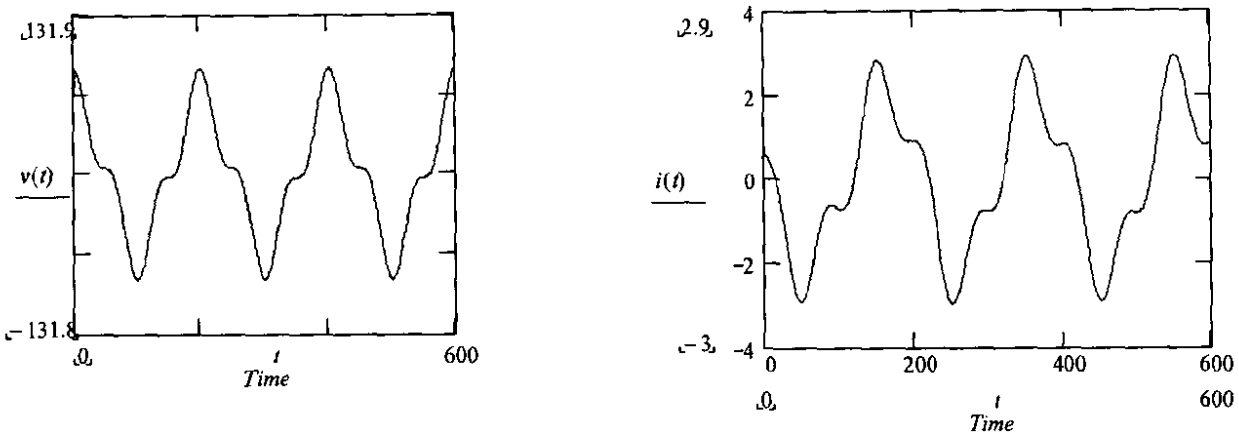

Figure 25: Voltage and current waveform measured in Figure 24

Application of the required formulations to obtain the Czarnecki *active power, reactive power, scattered power* and *PF*, results in the values in Table 7:

Table 7: Czarnecki single-phase power components for Figure 25

Symbol	Value	Unit
ω_1 (= 2π50)	314.16	rad/sec
$G_{1,1\phi}$	5.25E-3	S
$B_{1,1\phi}$	j0.02	S
$G_{e,1\phi}$	5.25E-3	S
ω_3 (= 3x2π50)	942.48	rad/sec
$G_{3,1\phi}$	5.26E-3	S
$B_{3,1\phi}$	-j0.02	S
$G_{e,1\phi}$	5.25E-3	S
$P_{1\phi}$	57.06	watt
PF	0.23 lagging	
$Q_{r,1\phi}$	242.41	VAr
$D_{s,1\phi}$	0.11	VAr

The sign of the values obtained for the susceptances $B_{1,1\phi}$ and $B_{3,1\phi}$ in Table 7 indicate that the Czarnecki *reactive power* has to be delivered at the fundamental frequency component and consumed at the third harmonic component by the compensating circuit. Such compensation is possible with a parallel *LC* compensating circuit.

Minimizing the reactive current $i_r(t)_{1\phi}$ in Figure 24 requires that susceptances have to chosen such that compensating susceptance at the fundamental harmonic must be equal to the load susceptance at the fundamental harmonic ($-B_{C1}=B_{1,1\phi}$) and similar for the third harmonic ($-B_{C3}=B_{3,1\phi}$). In general, minimisation of the Czarnecki single-phase reactive current will require that:

$$\left|i_r(t)_{1\phi}\right| = \sqrt{\sum_{h\in N}(B_{h,1\phi}+B_{Ch})^2 V_{h,1\phi}^2} \tag{108}$$

The compensated circuit is shown in Figure 26:

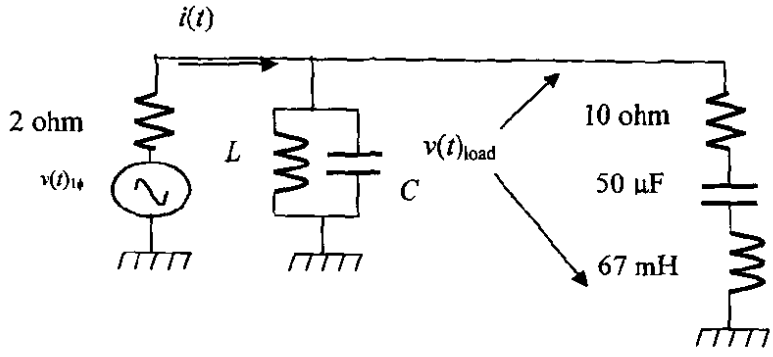

Figure 26: Parallel *LC* compensating circuit integrated into Figure 24

Empirical algebraic manipulation of the equations representative of the circuit in Figure 25 results in the design equations for the parallel *LC* compensating circuit. Firstly, the susceptance of the compensating circuit inductance and capacitance is:

$$B_h = \frac{-\omega_h L + \dfrac{1}{\omega_h C}}{\dfrac{L}{C}} \tag{109}$$

Secondly, the inductance is related to the capacitance:

$$L = \frac{1}{\omega_h(\omega_h C + B_h)} \tag{110}$$

Lastly, it is required that G_1=G_3, therefore the value of compensating capacitance is:

$$C = \frac{\omega_3 B_3 - \omega_1 B_1}{\omega_1^2 - \omega_3^2} \tag{111}$$

The resulting load voltage and current waveforms for the compensated circuit are shown in Figure 27

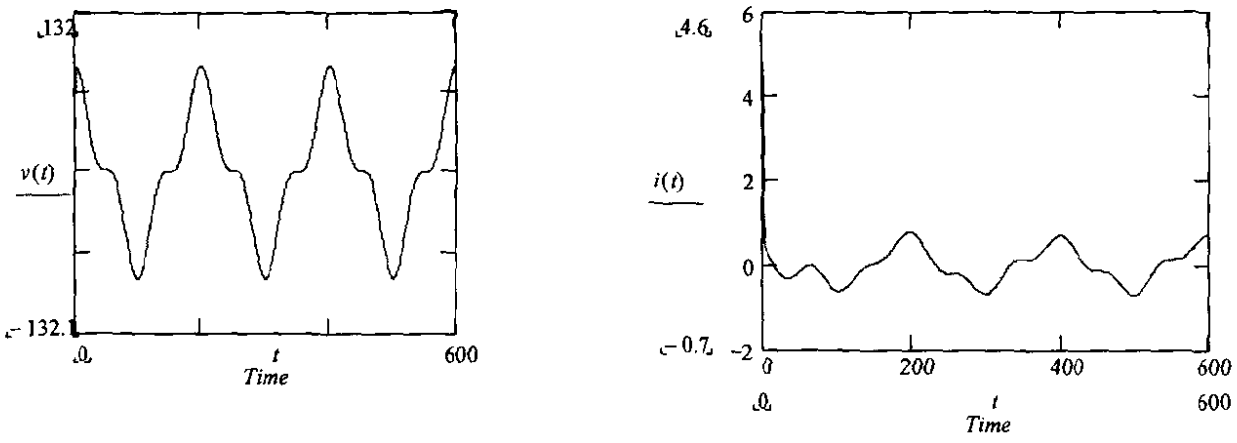

Figure 27 Voltage and current waveforms for the compensated circuit in Figure 26

The concept of "lesser loading" due to the decrease in the current drawn from the source is illustrated by the comparison of Figure 27 and Figure 25. Results on the analysis of the compensated waveforms are tabled below.

Table 8: Results of waveform analysis for compensated circuit in Figure 27

Symbol	Value	Unit
$G_{1,1\phi}$	5.26E-3	S
$B_{1,1\phi}$	-j5.59E-5	S
$G_{e,1\phi}$	5.26E-3	S
$G_{3,1\phi}$	5.27E-3	S
$B_{3,1\phi}$	-j4.81E-5	S
$G_{e,\phi}$	5.26E-3	S
$P_{1\phi}$	57.23	watt
PF	0.99	
$Q_{r,1\phi}$	0.60	VAr
$D_{s,1\phi}$	0.21	VAr

The power factor is increased to almost unity. The Czarnecki's single-phase reactive power is almost eliminated. A passive network can therefore compensate the Czarnecki single-phase reactive power, $Q_{r,1\phi}$. The *active power* and the "scattered" power are almost unchanged.

4.3.1.4 *Compensation of Czarnecki's single-phase reactive current and scattered current*

The "scattered power" requires alternative compensation and cannot be compensated for by the same passive compensating network that was implemented to compensate the Czarnecki reactive power. Czarnecki's "scattered" power results when single-phase frequency dependent conductances ($G_{h,1\phi}$) are scattered around an effective conductance $G_{e,1\phi}$ as in the case of the circuit in Figure 28.

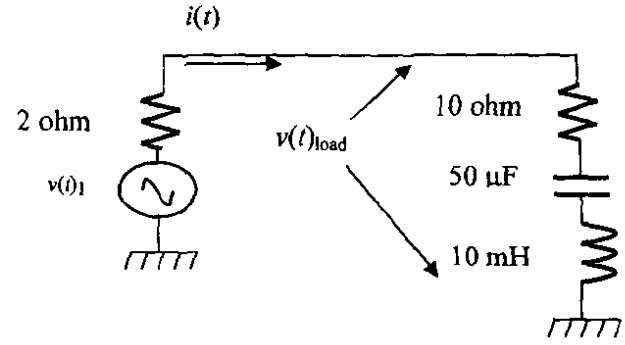

Figure 28: Circuit with frequency dependent conductances unequal at different harmonic frequencies

The load voltage and current waveform for this circuit are shown Figure 29:

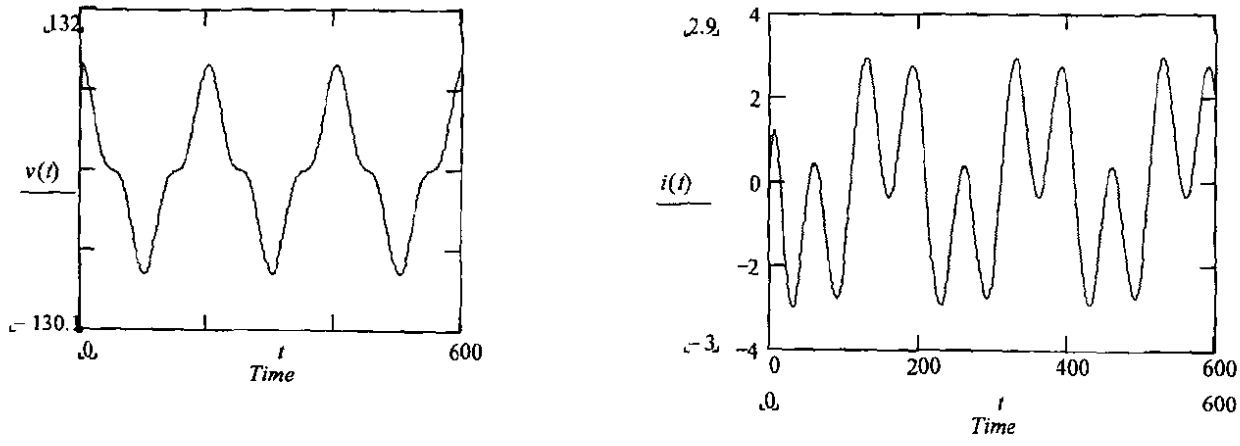

Figure 29: Load current and voltage waveforms for Figure 28

The results of applying Czarnecki's single-phase power definitions onto the waveforms in Figure 29 are listed in Table 9:

Table 9: Results of waveform analysis (Figure 29) to obtain the Czarnecki single phase powers

Symbol	Value	unit
ω_1 (= 2π50)	314.16	rad/sec
$G_{1,1\phi}$	2.66E-3	S
$B_{1,1\phi}$	0.02	S
$G_{e,1\phi}$	6.05E-3	S
ω_3 (= 3x2π50)	942.48	rad/sec
$G_{3,1\phi}$	0.04	S
$B_{3,1\phi}$	0.049	S
$P_{1\phi}$	65.51	Watt
PF	0.25	
$Q_{r,1\phi}$	228.88	VAr
$D_{s,1\phi}$	119.26	VAr

In general, load impedances are frequency dependent. Equation (106) indicate that, if $i_f(t)_{1\phi}$ is wholly compensated through a passive circuit, then, with the values tabled in Table 9, a best possible PF will be 0.48. A unity PF requires compensating for the "scattered" power with an active compensator which could be costly and complicated.

4.3.2 Czarnecki's Three Phase Power Theory

Most authors of new distortion power theories began by developing concepts for single-phase power systems and extending it to three-phase or multi-phase applications by assuming orthogonality between the phases. Czarnecki has also done this, but it appears from a study of the literature that in this he has limited his investigations only to hypothetical conditions. Such an approach results in the development of a sound mathematical formulation, but may introduce major deficiencies when it comes to practical systems.

Czarnecki's definitions appear to conform to electrical network laws for nonlinear and asymmetrically loaded three-phase systems that are fed by a non-sinusoidal voltage source and through a supply impedance, which is almost zero. When the voltage source becomes asymmetrical and/or the supply impedance becomes nonzero, in other words, as soon as the power system becomes a closer representation of the physical world, summation of the different power and current components fails to yield consistent results.

Implementation of the Czarnecki definitions and measurements in three-phase power systems generally do not require more sophisticated instrumentation than do other rival frequency-domain power theories. Even so, the Czarnecki theory so far still only enjoys limited acceptance. The Czarnecki theory requires of the practising engineer to become used to formulations and new concepts like "scattered" and "unbalanced" power. The concept of "generated" power was shown to be questionable [31] in practical power systems. It makes minimum use of those concepts from the "classical" theory that has already been

universally accepted.

A number of the new rival distortion power theories to the Czarnecki power theory appear to be more attractive to the practising engineer, and will require less of a paradigm shift in adopting them. Nevertheless, the extra effort to implement a practical theory such as Czarnecki's may be well worth the effort, if this theory is capable of correctly analysing every possible practical situation. There seems to be a problem with the Czarnecki formulations when practical power systems are studied and this matter is investigated in this chapter.

Czarnecki's three-phase power definitions are based on decomposition of the three-phase load current into five orthogonal components. In the previous section on his single-phase power theory, three of the load current components were investigated, namely the *active current*, the *reactive current* and the *scattered current*. These three components are redefined in the next section for three-phase power systems. A fourth component that could also exist in the single-phase power system, is defined and formulated only for a three-phase power system, namely the *generated current*. The fifth load current component describes the effect of unbalance in the load, namely the *unbalance current*.

4.3.2.1 Assumptions

Czarnecki made the following assumptions concerning a reference three-phase power system like the one shown in Figure 30. It is important to note that these assumptions are not always valid in a practical power system.

1. The voltage source is a non-sinusoidal but symmetrical time-dependent periodic three-phase voltage vector $v(t)_{3\phi}$ with the fundamental components having a positive phase sequence (*abc*).

2. The time-dependent periodic 3-element three-phase current vector $i(t)_{3\phi}$ is drawn by a non-linear/time-variant and unbalanced load, containing frequency-dependent elements.

The voltage and current vectors are defined as follows:

$$v(t)_{3\phi} = \begin{bmatrix} v_a(t) \\ v_b(t) \\ v_c(t) \end{bmatrix}; i(t)_{3\phi} = \begin{bmatrix} i_a(t) \\ i_b(t) \\ i_c(t) \end{bmatrix} \quad \text{with } v_b(t) = v_a(t - \frac{T}{3}); v_c(t) = v_a(t - 2\frac{T}{3}) \tag{112}$$

A schematic representation of the reference power system is shown below:

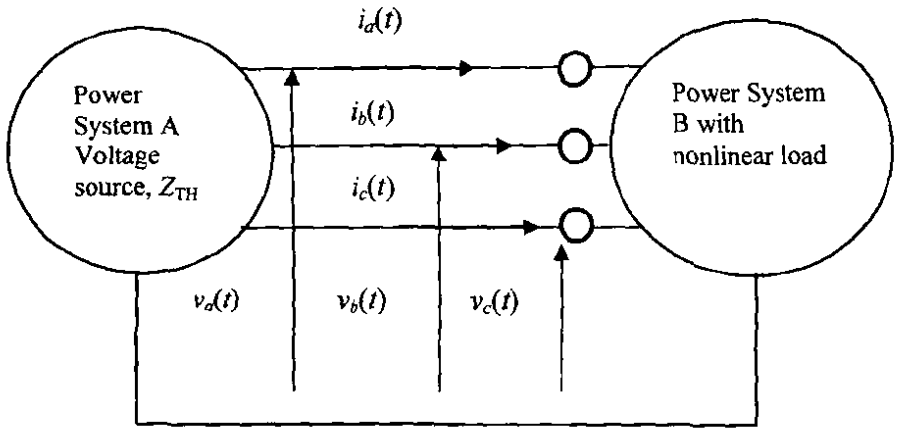

Figure 30: Reference power system for the formulation of Czarnecki's three-phase power theory

The period T of the voltage and current waveform is time-invariant and the following standard Fourier transformation for voltage and current (only shown for phase a) exists:

$$\begin{aligned} v_a(t) &= \mathrm{Re}\sqrt{2}\sum_{h=1}^{N} V_{ah} e^{jh\omega_1 t} \\ v_{ah}(t) &= \mathrm{Re}\sqrt{2} V_{ah} e^{jh\omega_1 t} \\ V_{ah} &= V_{ah} e^{j\alpha h} = \frac{\sqrt{2}}{T}\int_0^T v_a(t) e^{-jh\omega_1 t} \end{aligned} \tag{113}$$

$$\begin{aligned} i_a(t) &= \mathrm{Re}\sqrt{2}\sum_{h=1}^{N} \boldsymbol{I}_{ah} e^{jh\omega_1 t} \\ i_{ah}(t) &= \mathrm{Re}\sqrt{2}\boldsymbol{I}_{ah} e^{jh\omega_1 t} \\ \boldsymbol{I}_{ah} &= I_{ah} e^{j\alpha h} = \frac{\sqrt{2}}{T}\int_0^T i_a(t) e^{-jh\omega_1 t} \end{aligned} \tag{114}$$

A time-dependent three-phase voltage vector $v_h(t)_{3\phi}$ is defined below to refer to the time-dependent harmonic frequency components in a nonsinusoidal three-phase time-dependent voltage $v(t)_{3\phi}$. The subscript h is the harmonic number whilst a, b and c refer to the different phases. The similar notation is used for the harmonic frequency components in the three-phase current vector $\boldsymbol{i}(t)_{3\phi}$.

$$v_h(t)_{3\phi} = \begin{bmatrix} v_{ah}(t) \\ v_{bh}(t) \\ v_{ch}(t) \end{bmatrix} \tag{115}$$

The norm of the three-phase voltage vector $v(t)_{3\phi}$ (or generalised RMS value) is found through the scalar

product (similar for current):

$$\left\|v(t)_{3\phi}\right\| = \sqrt{\left(v(t)_{3\phi}, v(t)_{3\phi}\right)} \tag{116}$$

The generalised RMS values of the voltage and current vectors, written both in terms of harmonic phasors and in terms of the time-dependent phase voltages are respectively:

$$V_{3\phi} = \sqrt{\frac{1}{T}\int_0^T [v_a^2(t) + v_b^2(t) + v_c^2(t)]dt} = \sqrt{\sum_{h=1}^{N}\left(V_{ah}^2 + V_{bh}^2 + V_{ch}^2\right)} \tag{117}$$

$$I_{3\phi} = \sqrt{\frac{1}{T}\int_0^T [i_a^2(t) + i_b^2(t) + i_c^2(t)]dt} = \sqrt{\sum_{h=1}^{N}\left(I_{ah}^2 + I_{bh}^2 + I_{ch}^2\right)} \tag{118}$$

The three-phase *active* and *reactive* power is defined as:

$$\begin{aligned} P_{3\phi} &= \left[v(t)_{3\phi}, i(t)_{3\phi}\right] = \mathrm{Re}\sum_{h=1}^{N}\left(V_{ah}I_{ah}^* + V_{bh}I_{bh}^* + V_{ch}I_{ch}^*\right) = \mathrm{Re}\sum_{h=1}^{N} P_{h,3\phi} \\ Q_{h3\phi} &= \mathrm{Im}\left(V_{ah}I_{ah}^* + V_{bh}I_{bh}^* + V_{ch}I_{ch}^*\right) \end{aligned} \tag{119}$$

The (*total*) *active power* is a summation of the *active power* in each phase for each harmonic *h*. The *reactive power* is definable for a harmonic number only.

3. The apparent power definition used by Czarnecki ($S_{3\phi}$) is different to that of the IEEE *equivalent apparent power* [20] termed the *system apparent power* (S_e) or *equivalent apparent power*:

$$S_{3\phi} = V_{3\phi}I_{3\phi} = \left\|v(t)_{3\phi}\right\|\left\|i(t)_{3\phi}\right\| \tag{120}$$

Note that the definition of $V_{3\phi}$, $I_{3\phi}$ and V_e, I_e is numerically different[26].

4.3.2.2 Formulation of the Czarnecki current components

The equivalent conductance ($G_{e3\phi}$) for an asymmetric three-phase load is defined as:

---

[26] Section 4.6 discuss the formulation of the IEEE power definitions.

$$G_{e3\phi} = \frac{P_{3\phi}}{\left\| v(t)_{3\phi} \right\|^2} \tag{121}$$

The three-phase equivalent conductance $G_{e3\phi}$ defines a conductance of a symmetrical load to consume the equivalent in active power of a three-phase asymmetrical load. The three-phase *active current* vector is defined similarly to the single-phase active current [14]:

$$i_a(t)_{3\phi} = G_{e3\phi} v(t)_{3\phi} = \sqrt{2}\mathrm{Re}\begin{bmatrix} G_e V_a \\ G_e V_b \\ G_e V_c \end{bmatrix}\left(e^{j\omega_1 t}\right) \tag{122}$$

The three-phase Czarnecki reactive current makes use of a three-phase equivalent susceptance ($B_{eh,3\phi}$) that is harmonic frequency dependent. It represents an equivalent to the frequency dependent reactive element of a symmetrical load, which cause the same three-phase reactive power $Q_{h,3\phi}$ at a harmonic frequency $h\omega_1$ as drawn by the asymmetrical load at harmonic frequency $h\omega_1$:

$$B_{eh,3\phi} = \frac{-Q_{h,3\phi}}{\left\| v(t)_{3\phi} \right\|} \tag{123}$$

The Czarnecki three-phase reactive current vector per harmonic is then defined as:

$$i_{rh}(t)_{3\phi} = B_{eh,3\phi} \frac{dv_h(t)_{3\phi}}{d(h\omega_1 t)} = \sqrt{2}\mathrm{Re} B_{eh,3\phi}\begin{bmatrix} V_{ah} \\ V_{bh} \\ V_{ch} \end{bmatrix}\left(e^{jh\omega_1 t}\right) \tag{124}$$

The total three-phase reactive current defined by Czarnecki is:

$$i_r(t)_{3\phi} = \sum_{h \in N_v} i_{rh}(t)_{3\phi} \tag{125}$$

The three-phase reactive current $i_r(t)_{3\phi}$ is fundamentally different to, for example, a three-phase reactive current that makes use of the Budeanu reactive power definition which was shown to have no physical significance.

The number set N_v specifies a summation range associated with harmonic components contributed by the voltage source. A nonlinear load will yield a load current that contains harmonic components not caused by the harmonic voltage components. Two different sets of harmonic numbers are defined for the voltage

and current frequency spectra. The harmonic number set for the current, N_i, is typically a larger set than the harmonic number set for the voltage, N_v. This simply implies that N_i contains "extra" harmonic numbers due to "generated" current components caused by non-linear load action.

With N_g the "generated" harmonic numbers, the harmonic number sets are related by:

$$N_g \equiv N_i \varnothing N_v \tag{126}$$

Symbol $\varnothing$ denotes the elements in N_i that are not subsets of N_v. The mathematical formulation of the "generated" current is:

$$\boldsymbol{i}_g(t)_{3\phi} = \sum_{h \in N_g} \boldsymbol{i}_h(t)_{3\phi} \tag{127}$$

Note that the symbol of *generated current* the equation above is printed in **bold** as it represents a vector for the three-phase *generated currents.*

An asymmetrical three-phase load (assumed linear here) will bring about unbalance between the phase currents. If the load is asymmetrical, another current component can be isolated that is responsible for the increase in the RMS value of the load current:

$$\boldsymbol{i}_u(t)_{3\phi} = \boldsymbol{i}(t)_{3\phi} - \boldsymbol{i}_a(t)_{3\phi} - \boldsymbol{i}_r(t)_{3\phi} \tag{128}$$

The vector $\boldsymbol{i}_u(t)_{3\phi}$ represents the "*unbalance*" part of the three-phase load current $\boldsymbol{i}(t)_{3\phi}$ in the Czarnecki theory.

The scalar products of the three-phase vectors of current, $\boldsymbol{i}_a(t)_{3\phi}$, $\boldsymbol{i}_r(t)_{3\phi}$ and $\boldsymbol{i}_u(t)_{3\phi}$ were shown by Czarnecki [5] to be mutually orthogonal:

$$\left\|\boldsymbol{i}(t)_{3\phi}\right\|^2 = \left\|\boldsymbol{i}_a(t)_{3\phi}\right\|^2 + \left\|\boldsymbol{i}_r(t)_{3\phi}\right\|^2 + \left\|\boldsymbol{i}_u(t)_{3\phi}\right\|^2 \tag{129}$$

Three components of the three-phase load current components defined above have been assigned a physical significance [6]:

1. The three-phase *active current* $\boldsymbol{i}_a(t)_{3\phi}$: It is the load current component that enables three-phase active power transfer between the source and the load.

2. The three-phase *reactive current* $i_r(t)_{3\phi}$: It is the load current component that sustains the oscillatory exchange of energy between the reactive elements in the three-phase source and the load. It increases the RMS value of the three-phase load current.

3. The *unbalance current* $i_u(t)_{3\phi}$: It is the load current component associated to the increase in the RMS value of the three-phase load current due to unbalanced loading. This component is a unique contribution of Czarnecki in explaining the physical reason for the increase in the RMS value of the three-phase load current when the loading of phases are not perfectly balanced.

4. The *generated current* $i_g(t)_{3\phi}$: No clear physical explanation could be found to support the mathematical formulation thereof.

If the three-phase load contains frequency dependent conductances, then it can be regarded as containing harmonic conductances (symbol $G_{eh,3\phi}$) scattered around an effective value of three-phase load conductance $G_{e,3\phi}$. The three-phase harmonic conductances is a mathematical concept with symbol $G_{eh,3\phi}$ which represent the equivalent three-phase conductance of a symmetrical load at a harmonic number which will consume the same amount of three-phase harmonic active power as the asymmetrical load does at that harmonic number:

$$G_{eh,3\phi} = \frac{P_{h,3\phi}}{\left\| v_h(t)_{3\phi} \right\|^2} \tag{130}$$

A three-phase active current at a harmonic number is isolated to transfer active power at that harmonic number:

$$i_{ah}(t)_{3\phi} = G_{eh,3\phi} v_h(t)_{3\phi} \tag{131}$$

The summation of the harmonic active currents does not fully explain the total active current. The following mathematical difference was defined by Czarnecki to be the three-phase *scattered current* $i_s(t)_{3\phi}$:

$$i_s(t)_{3\phi} = \sum_{h \in N_v} i_{ah}(t)_{3\phi} - i_a(t)_{3\phi} \tag{132}$$

The *scattered current* is the fifth three-phase load current component defined by Czarnecki. No clear physical explanation is found to sustain the mathematical formulation thereof. The complete list of three-

phase current components defined by Czarnecki is:

1. The active current, $i_a(t)_{3\phi}$
2. The reactive current $i_r(t)_{3\phi}$
3. The unbalance current, $i_u(t)_{3\phi}$
4. The generated current, $i_g(t)_{3\phi}$
5. The scattered current, $i_s(t)_{3\phi}$

It is important to note that only four of the five current components are associated with the voltage source. Consider a general situation of any two interconnected power system areas (as in Figure 30) where the one area contains the primary voltage source at the fundamental frequency and the second area contains the load elements. The total three-phase load current $i(t)_{3\phi}$ at the measuring terminals between the two areas can be considered [16], [19] as containing two different components:

- Current $i_A(t)_{3\phi}$ attributed to power system area A.
- Current component $i_B(t)_{3\phi}$ attributed to power system area B.

$$i(t)_{3\phi} = i_A(t)_{3\phi} + i_B(t)_{3\phi} \tag{133}$$

The four current components current component in $i_A(t)_{3\phi}$ are the *active current*, the *reactive current*, the *scattered current* and the *unbalance current* and ascociated to subsystem A

The current component $i_B(t)_{3\phi}$ is the *load-generated current* defined in equation (126). The Czarnecki total three-phase current [5] at the measuring terminal in Figure 30 is:

$$i(t)_{3\phi} = i_a(t)_{3\phi} + i_r(t)_{3\phi} + i_s(t)_{3\phi} + i_u(t)_{3\phi} + i_g(t)_{3\phi} \tag{134}$$

The formulas for the calculation thereof are summarised in the following table:

Table 10: RMS values of the Czarnecki three-phase load current components

Name of current	Formula
Active current	$\left\|i_a(t)_{3\phi}\right\| = G_{e,3\phi}\left\|v(t)_{3\phi}\right\|$
Reactive current	$\left\|i_r(t)_{3\phi}\right\| = \sqrt{\sum_{h\in N_v} \frac{Q_{h,3\phi}^2}{\left\|v_h(t)_{3\phi}\right\|^2}}$
Unbalance current	$\left\|i_u(t)_{3\phi}\right\| = \sqrt{\sum_{h\in N_v}\left[\left\|i_h(t)_{3\phi}\right\|^2 - \left(G_{eh,3\phi}^2 + B_{eh,3\phi}^2\right)\left\|v_h(t)_{3\phi}\right\|^2\right]}$
Scattered current	$\left\|i_s(t)_{3\phi}\right\| = \sqrt{\sum_{h\in N_v}\left(G_{eh,3\phi} - G_{e,3\phi}\right)^2\left\|v_h(t)_{3\phi}\right\|^2}$
Generated current	$\left\|i_g(t)_{3\phi}\right\| = \sqrt{\sum_{h\in N_g}\left\|i_h(t)_{3\phi}\right\|^2}$
Total three-phase load current	$\left\|i(t)_{3\phi}\right\|^2 = \left\|i_a(t)_{3\phi}\right\|^2 + \left\|i_r(t)_{3\phi}\right\|^2 + \left\|i_s(t)_{3\phi}\right\|^2 + \left\|i_u(t)_{3\phi}\right\|^2 + \left\|i_g(t)_{3\phi}\right\|^2$

The RMS values of the five different three-phase Czarnecki load current components are easily obtainable from a frequency domain analysis of measured three-phase voltages and currents at a measuring terminal.

4.3.2.3 The three-phase Czarnecki power components

The five Czarnecki three-phase current components are the basis for the Czarnecki three-phase power definitions:

$$\begin{aligned} S_{3\phi}^2 &= \left\|i(t)_{3\phi}\right\|^2\left\|v(t)_{3\phi}\right\|^2 = \left(\left\|i_a(t)_{3\phi}\right\|^2 + \left\|i_r(t)_{3\phi}\right\|^2 + \left\|i_s(t)_{3\phi}\right\|^2 + \left\|i_u(t)_{3\phi}\right\|^2 + \left\|i_g(t)_{3\phi}\right\|^2\right)\left\|v(t)_{3\phi}\right\|^2 \\ &= P_{3\phi}^2 + Q_{r,3\phi}^2 + D_u^2 + D_{s,3\phi}^2 + D_{g,3\phi}^2 \end{aligned} \tag{135}$$

The Czarnecki power components and symbols are summarised below:

Table 11: The Czarnecki three-phase power components[27]

Power component	Symbol
Active power	$P_{3\phi}$
Reactive power	$Q_{r,3\phi}$
Unbalance power	D_u
Scattered power	$D_{s,3\phi}$
Generated power	$D_{g,3\phi}$
Apparent power	$S_{3\phi}$

Czarnecki's three-phase power theory is based on the above mathematical formulation of power components. It will be tested thoroughly for application in practical power systems as it was formulated by Czarnecki with the assumption that the three-phase voltage source is symmetrical with zero Thévenin equivalent impedance although the voltage source waveforms were assumed to be non-sinusoidal and connected to a three-phase non-linear and/or time-variant asymmetrical load.

4.3.2.4 The Forced Apparent Power

Czarnecki gave additional explanation to apparent power associated to the load-generated currents [19] through mathematical manipulation of the decomposed current components. The load current, voltage and power at the interconnecting terminals of subsystem A and B in Figure 30 is decomposed and "assigned" to a subsystem:

$$\begin{aligned} i(t)_{3\phi} &= \sum_h i_h(t)_{3\phi} = i_A(t)_{3\phi} + i_B(t)_{3\phi} \\ v(t)_{3\phi} &= \sum_h v_h(t)_{3\phi} = v_A(t)_{3\phi} + v_B(t)_{3\phi} \\ P &= \sum_h P_h = P_A - P_B \end{aligned} \tag{136}$$

Subscripts A and B indicate subsystem A and B. The voltage and current components are orthogonal [19]:

$$\begin{aligned} \left\| i(t)_{3\phi} \right\|^2 &= \left\| i_A(t)_{3\phi} \right\|^2 + \left\| i_B(t)_{3\phi} \right\|^2 \\ \left\| v(t)_{3\phi} \right\|^2 &= \left\| v_A(t)_{3\phi} \right\|^2 + \left\| v_B(t)_{3\phi} \right\|^2 \end{aligned} \tag{137}$$

Calculation of the source apparent power reveals Czarnecki's *forced apparent power* $S_{F,3\phi}$:

---

[27] The subscript "3ϕ" is used to distinguish between single-phase and three-phase mathematical formulations, it is omitted for the *unbalance power* as it cannot exist in single-phase power systems.

$$S_{3\phi} = \sqrt{\left\|v(t)_{3\phi}\right\|^2}\sqrt{\left\|i(t)_{3\phi}\right\|^2} = \sqrt{\left\|v_A(t)_{3\phi}\right\|^2 + \left\|v_B(t)_{3\phi}\right\|^2}\sqrt{\left\|i_A(t)_{3\phi}\right\|^2 + \left\|i_B(t)_{3\phi}\right\|^2}$$
$$= \sqrt{S_{A,3\phi}^2 + S_{B,3\phi}^2 + S_{F,3\phi}^2} \tag{138}$$

Apparent power $S_{A,3\phi}$ was defined in principle in equation (134) and is reformulated below:

$$S_{A,3\phi} = \left\|v_A(t)_{3\phi}\right\|\left\|i_A(t)_{3\phi}\right\| = \sqrt{P_{A,3\phi}^2 + Q_{rA,3\phi}^2 + D_{uA}^2 + D_{sA,3\phi}^2} \tag{139}$$

Czarnecki isolated the *load-generated* apparent power as S_B:

$$S_{B,3\phi} = \left\|v_B(t)_{3\phi}\right\|\left\|i_B(t)_{3\phi}\right\| \tag{140}$$

The *forced apparent* power $S_{F,3\phi}$ is explained [19] as "extorted[28]" apparent power and formulated as:

$$S_{F,3\phi} = \sqrt{\left\|v_A(t)_{3\phi}\right\|^2\left\|i_B(t)_{3\phi}\right\|^2 + \left\|v_B(t)_{3\phi}\right\|^2\left\|i_A(t)_{3\phi}\right\|^2} \tag{141}$$

Czarnecki state [19] that there is no power phenomenon to be assigned to the "extorted" apparent power. It renders the value contributed by the above power decomposition to practical power definitions questionable.

4.3.2.5 Physical significance of the Czarnecki current and power components

The concept of power factor quantifies the effectiveness of energy utilisation in a power system. Ideally, *active power* should be equal to *apparent power* as it is the useful power component. The increase in *apparent power* when:

- the voltage source waveform is non-sinusoidal,
- and/or the load is asymmetrical,
- and/or the load is nonlinear and/or time-variant,
- and/or the load contain frequency dependent conductances,

can be studied in terms of Czarnecki power [5] components:

---

[28] Synonoms of "extorted" can be "wring" or "force from", it is difficult to assign a physical explanation to this apparent power.

$$PF = \frac{P_{3\phi}}{S_{3\phi}} = \frac{P_{3\phi}}{\sqrt{P_{3\phi}^2 + Q_{r,3\phi}^2 + D_u^2 + D_{s,3\phi}^2 + D_{g,3\phi}^2}} \tag{142}$$

The power factor formulation in terms of the Czarnecki current components is:

$$PF = \frac{\left\| i(t)_{3\phi} \right\|}{\sqrt{\left\| i_a(t)_{3\phi} \right\|^2 + \left\| i_r(t)_{3\phi} \right\|^2 + \left\| i_s(t)_{3\phi} \right\|^2 + \left\| i_u(t)_{3\phi} \right\|^2 + \left\| i_g(t)_{3\phi} \right\|^2}} \tag{143}$$

Czarnecki explains ([9], [10], [16], [19]) how the five load current components in three-phase circuits can impact the power factor of a load as follows:

1. *Active power* and *active current*: These are the only components necessary for useful work in a three-phase electrical system. The *active current* transmits *active power* between source and load. A power system that only contains these components will have a unity power factor and no other power and current components need to be considered. This is in agreement with the physical significance of *active power* as defined in the classical power theory for sinusoidal power systems and supported by the field theory.

2. *Reactive power* and *reactive current*: The Czarnecki formulation of reactive power (compared to the Budeanu formulation thereof) and of *reactive current* describes the alternating component that brings about an interchange of power between reactive elements in the load and the source. This is in agreement with the physical significance of *reactive power* as defined in the classic power theory for sinusoidal power systems and supported by the field theory.

3. *Unbalance power* and *unbalance current*: If a three-phase load is not perfectly balanced, an increase is brought about in the RMS load current. The contribution of unbalance to the increase in RMS load current and to the increase in apparent power was mathematically isolated by Czarnecki as *unbalance current* and *unbalances power* respectively. He does not offer a clear physical explanation.

4. *Scattered power* and *scattered current*: A non-sinusoidal voltage source applied to a load with frequency dependent conductances will elicit an increase in the RMS value of the load current. Czarnecki attributed the increase in RMS load current to the "scattering" of conductances around an effective value. The *scattered current* and *scattered power* was defined and mathematically isolated. His physical explanation given is based on the "scattering" of conductances around an effective value which is difficult to explain with field theory. The concept of *scattered power* is questionable in any attempt to explain the physical significance thereof.

5. *Generated power* and *generated current:* Nonlinear and/or time-variant loads cause current harmonics that are not present in the voltage source waveform. The interaction between load-generated harmonics and voltage harmonics cause an increase in the RMS value of the source current. Czarnecki isolated this phenomenon and mathematically formulated it as *generated current* and *generated power*. No acceptable physical explanation exists. Emanuel [31] questions the physical significance thereof. If the voltage source is connected through a non-zero impedance to a load, harmonic numbers will result in the load voltage waveform at the load terminals caused by the current harmonics. Czarnecki has assumed the voltage source to be connected to the load through a perfectly zero ohm impedance. To determine from measurements obtained in a practical situation which harmonics in the voltage are due to "source only" harmonics and which are load generated, is difficult if not impossible.

The next section tests the Czarnecki power theory under practical situations.

4.3.3 The validity of the Czarnecki Three Phase Power Theory

The findings reported in this section are based on both the extensive ATP time-domain simulations of controlled practical networks and physical measurements. A measurement system was designed to measure the rather small components, e.g. "generated" power. Various representative three-phase non-sinusoidal power system scenarios were simulated in hardware in the 380 V 5 kVA base values three-phase power system. A 16 bit high speed A/D card, anti-aliasing filters and sensitive voltage and current transducers attempted an experimental setup to be as accurate as practicably possible. Application of closed loop Hall-effect sensors near maximum ratings results in less than 1% inaccuracy.

The Czarnecki power definitions were tested for conformity with accepted electrical network laws using both the measured and simulated data sets. Results indicate that, if careful consideration is not given to the assumptions made by Czarnecki in developing his power theory, erroneous results will be obtained. In order for a power theory to be universally accepted, it must be valid under every conceivable situation in a nonlinear power network, but beginning, at the least, with those conditions that are unconditionally present in all practical power networks.

4.3.4 A deficiency of the Czarnecki three-phase power definitions

In the following, the circuits shown are structured in ATPDRAW, simulated in ATP and then analysed in a MATHCAD™ program.

Example 1: A three-phase symmetrical non-sinusoidal voltage source with *zero* Thévenin impedance in the source feeding an asymmetrical nonlinear load

The voltage source $v(t)_{3\phi}$ in Figure 31 simulates an ideal voltage source with no internal impedance. It is

non-sinusoidal as it contains a 5th and a 7th harmonic component:

$$v(t)_{3\phi} = \begin{bmatrix} v_a(t) \\ v_b(t) \\ v_c(t) \end{bmatrix} = \begin{bmatrix} \sum_{h=1,5,7} v_{ah}(t) \\ \sum_{h=1,5,7} v_{ch}(t) \\ \sum_{h=1,5,7} v_{ch}(t) \end{bmatrix} = \begin{bmatrix} \sqrt{2} \sum_{h=1,5,7} V_{ah} \sin(h\omega_1 t + \alpha_{ah}) \\ \sqrt{2} \sum_{h=1,5,7} V_{bh} \sin(h\omega_1 t + \alpha_{bh}) \\ \sqrt{2} \sum_{h=1,5,7} V_{ch} \sin(h\omega_1 t + \alpha_{bh}) \end{bmatrix} \quad (144)$$

The fundamental and harmonic voltage components are symmetrical.

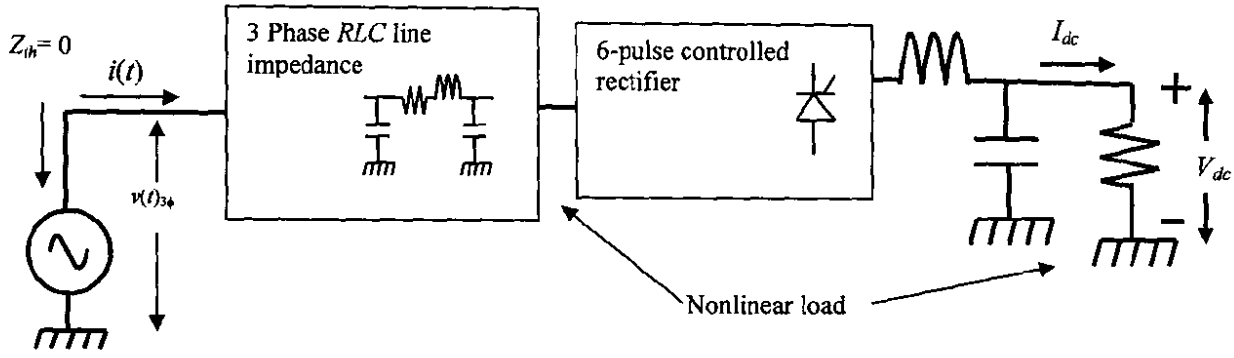

Figure 31: Single line diagram of three-phase controlled rectifier connected to a three-phase non-sinusoidal voltage source with a zero ohm Thévenin impedance in the source

The peak values of the fundamental and harmonic components in the voltage source (symmetrical between phases) and the values of the line impedances connecting the source and the load are listed below:

Table 12: Per unit voltages and line impedance values in Figure 2

	Peak value of voltages (p.u.)	*RLC* unbalanced 3ϕ line element (p.u.)
$V_{1\text{ p.u.}}$	1.0, 50 Hz	Phase *a*: $\lvert Z_a \rvert = 0.01$; *angle* = 17.4^0
$V_{5\text{ p.u.}}$	0.2, 250 Hz	Phase *b*: $\lvert Z_b \rvert = 0.05$; *angle* = 3.6^0
$V_{7\text{ p.u.}}$	0.1, 350 Hz	Phase *c*: $\lvert Z_c \rvert = 0.09$; *angle* = 2^0

The phase *a* voltage and phase *a* current at the measuring cross-section are shown in Figure 32:

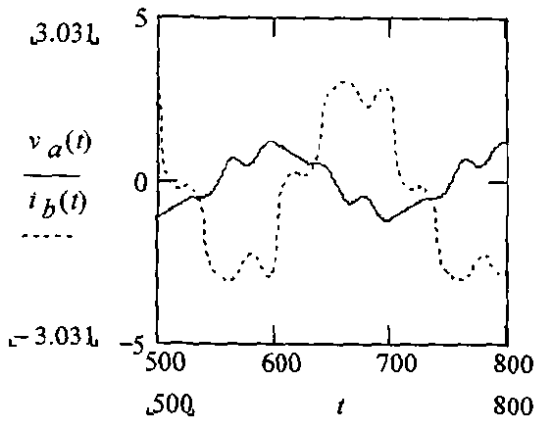

Figure 32: Voltage and current for phase a at the measuring cross-section in Figure 31

The three-phase line current is decomposed into the five Czarnecki current components and tested against network laws. A current balance and a power check are formulated below to verify the validity of the current decomposition. Tellegen's theorem requires that the summation of the Czarnecki power components has to be equal to the total apparent power at the measuring section:

$$\begin{aligned} &\left\|i(t)_{3\phi}\right\|^2 - \left(\left\|i_a(t)_{3\phi}\right\|^2 + \left\|i_r(t)_{3\phi}\right\|^2 + \left\|i_s(t)_{3\phi}\right\|^2 + \left\|i_u(t)_{3\phi}\right\|^2 + \left\|i_g(t)_{3\phi}\right\|^2\right) = 0 \\ &S_{3\phi}^2 - \left(P_{3\phi}^2 + Q_{r,3\phi}^2 + D_u^2 + D_{s,3\phi}^2 + D_{g,3\phi}^2\right) = 0 \end{aligned} \tag{145}$$

Application of the Czarnecki three-phase power and current definitions into that shown in Figure 31 results in:

Table 13 Czarnecki three-phase power theory applied on Figure 31

Description	**p.u.**
$V_{3\phi}$	1.775
$i_a(t)_{3\phi}$	4.874
$i_s(t)_{3\phi}$	0.100
$i_r(t)_{3\phi}$	0.427
$i_u(t)_{3\phi}$	0.516
$i_g(t)_{3\phi}$	0.432
Current balance	**0.0002 %**
Power balance	**0.0002 %**

From the current and energy balance in Table 13 it is clear that the Czarnecki definitions conform to

accepted electrical network laws in this example as both the current and power balance is satisfied.

Example 2: A three-phase symmetrical non-sinusoidal voltage source with a *non-zero* and asymmetrical Thévenin impedance in the source feeding an asymmetrical nonlinear load

The supply impedance in this example presents a more practical situation. The Czarnecki definitions are now applied in a system with non-zero Thévenin value for the asymmetrical impedance in the voltage source supply system. The circuit in Figure 33 is nearly identical to the previous circuit in Figure 31, differing only in the non-zero Thévenin equivalent of the source impedance, specified in Table 14 added between the source and the line that supplies the load.

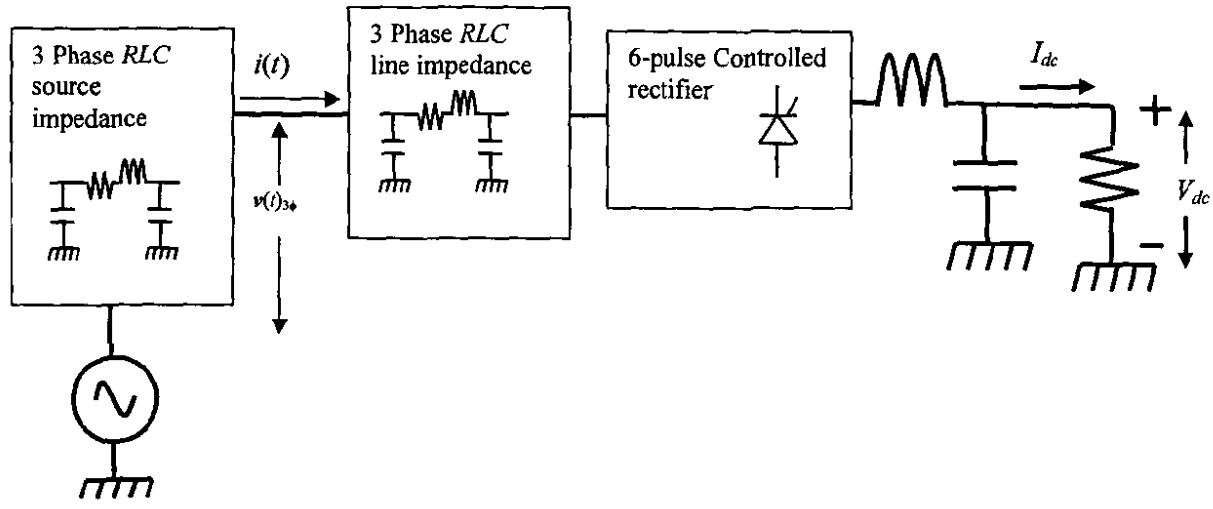

Figure 33: Single line diagram of three-phase controlled rectifier connected to a three-phase non-sinusoidal voltage source with a non-zero Thévenin impedance in the source

Table 14: Per unit source impedance Thévenin values of Figure 33

***RLC* unbalanced 3 Φ source impedance, p.u.**
Phase *a*: $\lvert Z_a \rvert = 0.033$; *angle* = 72.4^0
Phase *b*: $\lvert Z_b \rvert = 0.08$; *angle* = 51.5^0
Phase *c*: $\lvert Z_c \rvert = 0.09$; *angle* = 19.2^0

The mathematical requirement of the Czarnecki definitions creates a practical issue, namely that the summation ranges requires knowledge of which harmonics in the voltage can be blamed on the source and which are due to the harmonic load currents flowing through the now non-zero supply impedances. To demonstrate this, in the phase *b* voltage spectrum below, the "extra" harmonics are clear:

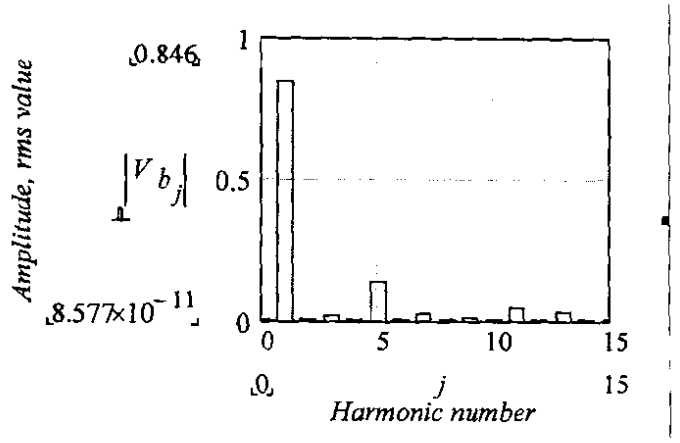

Figure 34: Additional harmonics caused by the nonzero supply impedance

Czarnecki proposed a sorting procedure based on the sign of the individual harmonic active powers [17] which becomes a complex problem in practice. Voltage harmonic components are caused by the interaction of the impedance elements between the measuring terminal and the harmonic currents generated by the nonlinear action of the load. These voltage harmonics are relatively small in magnitude compared to the harmonic components of the voltage source. Application of the Czarnecki current and power definitions requires knowledge on the number sets N_i, N_g and N_v defined in section 4.3.2.2. In the analysis presented in this document, an alternative MathCAD sorting procedure was devised that delivered satisfactory results as indicated below.

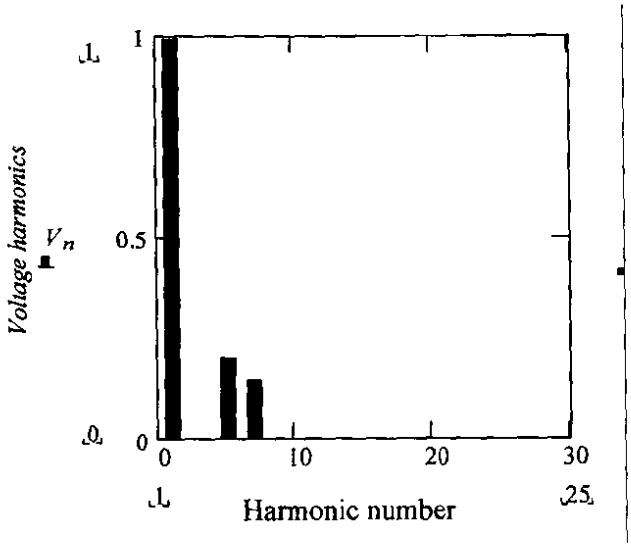

Figure 35: Voltage source "only" harmonics separated from the "generated" current harmonics by a MathCAD program. Amplitudes are relative, only the harmonic orders are relevant

Note that knowledge on the voltage source harmonics (number set N_v) is *a priori* knowledge as simulation parameters are fully controllable and it is possible to validate the results in Figure 35. The requirements of

the Czarnecki power definitions are therefore satisfied verbatim over the different harmonic number ranges as required for the purpose of this exercise. The results are tabled:

Table 15: Czarnecki three-phase power theory applied to Figure 33

Description	**p.u.**
$V_{3\phi}$	1.520
$i_a(t)_{3\phi}$	4.131
$i_s(t)_{3\phi}$	0.059
$i_r(t)_{3\phi}$	0.414
$i_u(t)_{3\phi}$	0.423
$i_g(t)_{3\phi}$	0.226
Current balance	**7.07 %**
Power Check	**7.07 %**

In Table 15 the current and power do not balance as in example 1. In both examples, the same circuit conditions are used, except for the introduction of the impedance in the source as shown in Figure 33.

Example 3: Using practical data: Three-wire measurements taken in a 380 V power system containing an asymmetrical non-linear load with a very small source impedance

Measurements were acquired at the highest possible precision[29]. The no-load three-phase voltage signal contained 'background" harmonics (*THVD* = 3.6%) as neighbouring loads such as computer laboratories are connected to the PCC (Point of Common Coupling). The no-load voltage source harmonic content has to be known in order to apply the Czarnecki three-phase power definitions correctly (the different summation ranges must be separated because the unloaded voltage source is non-sinusoidal in nature and causes corresponding harmonic load currents). The three-phase RMS values of the harmonic components in the unloaded voltage source were determined. The values are listed below up to the 13th harmonic as a percentage of the RMS value of the fundamental component:

[29] The details of the instrumentation are described in Chapter 3.

Table 16: Relative size of harmonic components in the voltage source of Example 3

$\frac{\|v(t)_3\|}{\|v(t)_1\|}\times 100$	1 %	$\frac{\|v(t)_5\|}{\|v(t)_1\|}\times 100$	3 %
$\frac{\|v(t)_7\|}{\|v(t)_1\|}\times 100$	1.4 %	$\frac{\|v(t)_9\|}{\|v(t)_1\|}\times 100$	0.4%
$\frac{\|v(t)_{11}\|}{\|v(t)_1\|}\times 100$	0.4%	$\frac{\|v(t)_{13}\|}{\|v(t)_1\|}\times 100$	0.4%

The summation ranges N_i, N_v and N_g are now defined and application of the Czarnecki three-phase power theory on example 3 results in:

Table 17: Czarnecki power theory applied on Example 3

Description	**Value**
$V_{3\phi}$	0 396 V
$i_a(t)_{3\phi}$	21.317 A
$i_s(t)_{3\phi}$	4.234 A
$i_r(t)_{3\phi}$	1.275 A
$i_u(t)_{3\phi}$	3.082 A
$i_g(t)_{3\phi}$	2.417 A
Current balance	0.95%
Power Check	0.95%

From the current and energy balance in Table 17 it is concluded that the Czarnecki power and current definitions conform to accepted electrical network laws. Note that the conditions in this example are similar to those simulated in Example 1.

Example 4: Three-wire measurements taken in a 380 V power system containing an asymmetrical non-linear load. The source impedance is purposely made to be $0.12\angle 74^0$ p.u. per phase.

Application of the Czarnecki power theory to these practical measurements yields the values listed in Table 18.

Table 18: Czarnecki power theory applied on Example 4

Description	Value
$V_{3\phi}$	373
$i_a(t)_{3\phi}$	16.812
$i_s(t)_{3\phi}$	3.388
$i_r(t)_{3\phi}$	12.812
$i_u(t)_{3\phi}$	1.794
$i_g(t)_{3\phi}$	0.703
Current balance	4.8%
Power Check	4.8%

In this example the current and power do not balance as in Example 3.

The MathCAD sorting procedure that was used is listed in Appendix B. The sorting procedure performed satisfactorily in the controlled environment used to study a power system similar to Figure 33, both for the simulated and the practical power system. The *a priori* information on the pure voltage harmonics may not be readily available in practice. A similar sorting procedure could deliver satisfactorily results in practice with an intelligent choice of the "*factor*" value. Supply impedances are typically very low and voltage induced harmonics due to "local" linear loads are relatively small when compared to the fundamental component. The Czarnecki suggestion [19] of negative harmonic active power flow as indicator of "generated" harmonics and with regarded to "where" the source is located, is not valid [57], [58]. This will be proved later.

4.3.4.1 Conclusion: A deficiency of the Czarnecki three phase power definitions

Czarnecki contributed to knowledge on non-sinusoidal power definitions when he recommended the discontinuation of the Budeanu definitions for distortion power on the ground of their erroneous numerical interpretations under certain conditions. Czarnecki endeavoured to overcome these difficulties by presenting definitions that furnish physically meaningful quantities for all measurement conditions. The examination carried out in the examples above, appears to indicate however that the Czarnecki definitions themselves furnish erroneous interpretations in practical power systems when the inevitable source impedance is present.

The implication is simple: Czarnecki's power definitions will work for theoretical power systems where ideal assumptions are allowed but not in the practical case. That assigns his own theory much of the same flavour of the Budeanu theory which he has so cryptically labelled in a special publication [2]. His theory can not be used with confidence in practice therefore because of the illustrated shortcoming.

Czarnecki's power definitions are based on current decomposition and the non-active powers are found through the product of RMS values of the voltage and the decomposed current components. This yields powers that are intrinsically apparent powers. These powers do not have a sign and their algebraic addition implies that they do not satisfy the energy conservation principle, which has to be an integral property of an electrical system.

Furthermore, Czarnecki's three-phase power theory is an extension of single-phase power definitions. This is not a sound approach when studying modern power systems. The phases of an unbalanced nonsinusoidal three-phase power system are not independent.

Czarnecki's power components are not easy to measure. Emanuel and Ferrero proposed more practical power definitions [20], [26], [41], [68], [70]. Emanuel emphasised that a non-sinusoidal power theory has to describe practical situations. For example, a finite commutation interval will result if the Thévenin impedance of the source is not perfectly zero and cause non-characteristic harmonics on the supply side of single-phase rectifiers such as even-numbered harmonic components.

Imbalance can generally exist between phase voltages in practical voltage sources and can bring about unexpected triplen harmonics (3, 6, ...) in frequency spectra. Voltage drops over the source-impedances in the supply system will have the same order than the harmonic currents drawn (the "generated currents") by a nonlinear load.

To use the direction of harmonic active power flow as suggested by Czarnecki [5], [19] to determine the existence of "generated" current, is fundamentally flawed. The harmonic active power of order h as observed at a node where a non-linear load is connected can be either positive or negative because of the influence of other neighbouring non-linear loads, the impedance of the surrounding network and the topology thereof. It was shown in [56] and in [58] how phase-controlled rectifiers exchange harmonic active power between them. The question Emanuel therefore raised in [31] towards the validity of "generated" power supports the finding of this thesis that Czarnecki's three-phase power theory can not be applied in practical three-phase power systems.

4.4 THREE-PHASE POWER THEORY FORMULATIONS IN A TRANSFORMED DOMAIN: APPLICATION OF THE PARK TRANSFORM

A number of three-phase power theories are based on single-phase formulations that are extended to include three-phase power systems. It is important that a three-phase power system is acknowledged as a unique domain in which electrical quantities have to be defined and referenced specifically to this domain.

The classical single-phase power theory can be used to analyse three-phase power systems under certain conditions. The simplifications required to do that, are valid under most circumstances. A perfectly

balanced and perfectly sinusoidal three-phase power system with only linear components, for example, permits rather simple but valid "single-phase equivalent" analysis. A three-phase unbalanced power system with non-linear and/or time variant loading, asymmetrical and/or non-sinusoidal voltage sources, cannot be analysed by means of such "single-phase equivalent" networks. One reason for the deficiency in the Czarnecki three-phase power theory, for example, is his extension of single-phase power theory formulations to three-phase power systems.

The Park transform is a mathematical tool that transforms three-phase quantities to quadrature co-ordinates (p-q) which can completely describe a three-wire three-phase power system in an equivalent synthetic domain. In the case of an unbalanced four-wire three-phase power system, a third set of zero sequence quantities results that require separate consideration.

The Park voltage and current vectors can be studied in the frequency domain and classical power definitions can be applied to these quantities. The formal properties of the original and physical three-phase power system (three-wire) in which these quantities originate are not lost. Ferrero and Superti-Furga [26] used this approach and their power theory formulations present the first approach studied as an alternative nonsinusoidal three-phase power theory.

4.4.1 Application of the Park transform: Ferrero and Superti-Furga's power definitions

The application of the Park transform in power systems was demonstrated in principle when Ferrero and Superti-Furga [26] derived power definitions based on the Park voltage and current vector. It achieved practical status when Akagi and Nabae [22] developed a novel compensator design methodology using it.

The Park transform is a special case of the Clarke transform. The d-q axis is stationary, it also known as the p-q theory. Energy analysis in the Park (or only termed p-q) domain makes use of conventional single-phase power definitions. The advantage is that all the resulting power components in the p-q domain have been assigned a physical significance. Ferrero *et al* [26], [27] explained the Park real/active power whilst the Park imaginary power was explained through application of the Poynting vector [28].

4.4.1.1 Power Definitions in the Park domain

The mathematical formulation of the Park transform was presented in section 2.3. Time-dependent power $p(t)_{\text{Park}}$ can be defined based on the Park vectors of voltages and currents, $\boldsymbol{v}(t)_{\text{Park}}$ and $\boldsymbol{i}(t)_{\text{Park}}$, respectively. This power is numerically the exact same quantity as the three-phase time-dependent power $p(t)_{3\phi}$ because the Park transform is a linear orthogonal transform:

$$
\begin{aligned}
p(t)_{\text{Park}} &= v(t)_{\text{Park}}\, i(t)_{\text{Park}} = [v_d(t) \quad v_q(t) \quad v_0(t)] \begin{bmatrix} i_d(t) \\ i_q(t) \\ i_0(t) \end{bmatrix} \\
&= v(t)_{3\phi}\, i(t)_{3\phi} \\
&= [v_a(t) \quad v_b(t) \quad v_c(t)] \begin{bmatrix} i_a(t) \\ i_b(t) \\ i_c(t) \end{bmatrix} \\
&= p(t)_{3\phi}
\end{aligned}
\tag{146}
$$

The Park time-dependent complex power $a(t)_{\text{Park}}$ is defined from the product of the Park time-dependent complex voltage and current:

$$
a(t)_{\text{Park}} = v(t)_{\text{Park}} * i(t)^{*}_{\text{Park}} \tag{147}
$$

The Park time-dependent real power $p(t)_{\text{Park}}$ and the Park time-dependent non-active/imaginary power $q(t)_{\text{Park}}$ is defined as:

$$
\begin{aligned}
a(t)_{\text{Park}} &= p(t)_{\text{Park}} + \mathrm{j}q(t)_{\text{Park}} \\
&= \mathrm{Re}[a(t)_{\text{Park}}] + \mathrm{j}[\mathrm{Im}\, a(t)_{\text{Park}}] \\
&= \left[v(t)_d\, i(t)_d + v(t)_q\, i(t)_q \right] + \mathrm{j}\left[v_q(t) i(t)_d - v(t)_d\, i(t)_q \right]
\end{aligned}
\tag{148}
$$

The three-phase time-dependent power $p(t)_{3\phi}$ relates to the Park time-dependent real power $p(t)_{\text{Park}}$ and the zero-sequence power $p_0(t)$:

$$
\begin{aligned}
p_{3\phi}(t) &= p(t)_{\text{Park}} + p_0(t) \\
p_0(t) &= v_0(t) i_0(t)
\end{aligned}
\tag{149}
$$

Akagi and Nabae [23] showed that the Park imaginary power $q(t)_{\text{Park}}$ does not involve time-dependent three-phase power. The Park imaginary power is a characteristic quantity of three phase systems and is a result of a ratio between time-dependent line voltages and line currents that are not the same for each phase [26].

The physical significance of the Park imaginary power is to be found in the field theory. Magnetic and electric fields are associated with the Park vectors of time-dependent voltage and current respectively. The magnetic and electric fields were calculated in [28]. A three-phase symmetrical resistor was used to find the conduction fields and a three-phase symmetrical inductor equivalent was used to find the pure

magnetic field. From that the Poynting vector and flux based on the Park quantities were calculated. The following interesting conclusions emerged [28]:

- The conduction field presents similar results to the single-phase Poynting vector studied for a conductor in section 2.6. The flux of the Poynting-Park vector is associated with a real quantity (the quantity $-p(t)_{3\phi}$ presents a "negative time dependent active power). It is equal to the energy (joule) that flows out of the bounded surface around the three-phase conductor.

- The electric displacement field and the magnetic field represent the capacitive and the inductive effect of the three-phase conductors. The nature of these fluxes is that the Park imaginary/non-active power is directly related to the energy exchange between phases. That is also the energy needed to compensate for the variation in energy in the different phases. The physical explanation centres on the fact that energy is removed from one phase and then supplied to another. (The compensation methodology devised by Akagi and Nabae [22] is based on this principle.) The energy exchange between phases occurs in the dielectric and magnetic fields and this energy exchange is at a rate dictated by the imaginary part of the flux of the Poynting-Park vector.

Table 19 was compiled by Ferrero *et al* [28] to summarise the calculation of the conduction, electric displacement and magnetic fields:

Table 19: The conduction field, the electric displacement field, the magnetic field and the flux as found by the Poynting-Park vector and summarised by Ferrero *et al* [28].

$$\oint_{\Sigma} \vec{e}_{dq} \times \vec{h}^{*}_{dq} \bullet \vec{n} d\Sigma = \begin{cases} \oint_{\Sigma} u \vec{j}^{*}_{dq} \bullet \vec{n} d\Sigma & \text{conduction field only} \\ \oint_{\Sigma} u \dot{\vec{d}}^{*}_{dq} \bullet \vec{n} d\Sigma & \text{electric displacement field only} \\ \oint_{\Sigma} \vec{h}^{*}_{dq} \times \dot{\vec{w}}_{dq} \bullet \vec{n} d\Sigma & \text{magnetic field only} \end{cases}$$

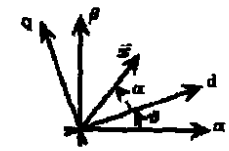

Field	Conduction	Electric displacement	Magnetic
Electric field	$\vec{e}_{dq} = \frac{\dot{j}_{dq}}{\sigma} \vec{v}_z = \frac{u}{\ell} \vec{v}_z$	$\vec{e}_{dq} = -\frac{u}{\ell} \vec{v}_z$	$\vec{e}_{dq} = -\mu \frac{N}{2\ell} r \dot{i} \vec{v}_\vartheta$
Magnetic field	$\vec{h}_{dq} = \frac{\dot{j}_{dq}}{2} r \vec{v}_\vartheta = \frac{\dot{i}}{2\pi r} \vec{v}_\vartheta$	$\dot{\vec{d}}_{dq} = -\frac{\varepsilon}{\ell} \dot{u} \vec{v}_z$ $\vec{h}_{dq} = -\frac{\varepsilon}{2\ell} r \dot{u} \vec{v}_\vartheta$	$\vec{h}_{dq} = \frac{N}{\ell} \dot{i} \vec{v}_z$
Poynting vector	$\vec{\wp}_{dq} = -\frac{u\dot{i}^*}{2\pi r \ell} \vec{v}_r$	$\vec{\wp}_{dq} = -\frac{\varepsilon r}{2\ell^2} u \dot{u}^* \vec{v}_r$	$\vec{\wp}_{dq} = -\mu \frac{N^2}{2\ell^2} r \dot{i} \dot{i}^* \vec{v}_r$
Flux of $\vec{\wp}_{dq}$	$\oint_{\Sigma} \vec{\wp}_{dq} \bullet \vec{v}_r d\Sigma = \int_0^{\ell} \int_0^{2\pi} -\frac{j^2}{2\sigma} r^2 d\vartheta dz =$ $= -R \dot{i} \dot{i}^* = -u u^* G = -p$	$\oint_{\Sigma} \vec{\wp}_{dq} \bullet \vec{v}_r d\Sigma = -\frac{\varepsilon A}{\ell} u \dot{u}^* =$ $= -C u \dot{u}^* = -\left[\dot{E}_e - j2(\dot{\alpha} + \dot{\vartheta}) E_e\right] =$ $= -(p - jq)$	$\oint_{\Sigma} \vec{\wp}_{dq} \bullet \vec{v}_r d\Sigma = -\mu \frac{N^2}{\ell} \pi R^2 \dot{i} \dot{i}^* =$ $= -L \dot{i} \dot{i}^* = -\left[\dot{E}_\mu + j2(\dot{\alpha} + \dot{\vartheta}) E_\mu\right] =$ $= -(p + jq)$

The average values of the Park time-dependent complex power are:

$$A_{\text{Park}} = P_{\text{Park}} + jQ_{\text{Park}} = \frac{1}{T} \int_T v(t)_{\text{Park}} * i(t)^*_{\text{Park}} dt \tag{150}$$

P_{Park} is equal to the average value of the Park *active power* when the zero-sequence time-dependent power $p_0(t)$ is zero. Q_{Park} is the average value of the Park imaginary power.

Because these power definitions are formulated in a single synthetic domain, accepted power theory principles can be applied. This is contrary to previous approaches (for example of Czarnecki) that extended single-phase domain power definitions to the three-phase domain. The following characteristics of the Park power quantities $a(t)_{\text{Park}}$, $p(t)_{\text{Park}}$, P_{Park}, $q(t)_{\text{Park}}$, Q_{Park} and $p_0(t)$ are important:

- The Park power definitions are quantities that can be regarded as actual powers and not apparent powers because their sign depends on the reference directions chosen for the voltages and currents.

- These powers satisfy the energy conservation principle, namely that the algebraic sum of powers associated with each element of an isolated network will sum to zero.

The Park real and imaginary powers are by definition the three-phase positive sequence active and reactive powers when the three phase system is sinusoidal, symmetrical, balanced and of positive phase rotation. The Park voltage and current vectors are then [26]:

$$\begin{aligned} v(t)_{\text{Park}} &= \sqrt{3}V_e e^{j\omega t} \\ i(t)_{\text{Park}} &= \sqrt{3}I_e e^{j\omega t-\phi} \end{aligned} \tag{151}$$

The Park real and imaginary powers are equal to the three-phase real/active power and the reactive power:

$$\begin{aligned} p(t)_{\text{Park}} &= P_{\text{Park}} = P_{3\phi} = 3V_e I_e \cos\phi \\ q(t)_{\text{Park}} &= Q_{\text{Park}} = Q_{3\phi} = 3V_e I_e \sin\phi \end{aligned} \tag{152}$$

When the balanced three-phase system is of negative phase sequence, only negative sequence voltages and currents result. Again in terms of the effective three-phase voltage values, the Park vectors of voltage and current are [26]:

$$\begin{aligned} v(t)_{Park} &= \sqrt{3}V_e e^{-j\omega t} \\ i(t)_{Park} &= \sqrt{3}I_e e^{-j(\omega t-\varphi)} \end{aligned} \tag{153}$$

The *real* and *imaginary* Park powers are [26]:

$$\begin{aligned} p(t)_{\text{Park}} &= P_{\text{Park}} = P_{3\phi} = 3V_e I_e \cos\phi \\ q(t)_{\text{Park}} &= Q_{\text{Park}} = -Q_{3\phi} = -3V_e I_e \sin\phi \end{aligned} \tag{154}$$

Application of the Park power definitions to non-sinusoidal and unbalanced but periodical three-phase systems requires the Fourier series components of the Park voltage and current vectors. This application is valid because the Park vectors are periodical too and the Park transform is a linear transform. The Park time-dependent complex power is then defined in terms of Park harmonic phasors [26]:

$$a(t)_{\text{Park}} = \sum_{h=-\infty}^{+\infty} V_{\text{Park},h} I^{*}_{\text{Park},h} + \sum_{-\infty}^{+\infty}{}_{k\neq h} V_{\text{Park},h}\ I^{*}_{\text{Park},h} e^{j(h-k)\omega t} \tag{155}$$

The Park *real* and *imaginary* powers follow from the average value of the Park time-dependent complex

power:

$$\begin{aligned} A_{\text{Park}} &= P_{\text{Park}} + jQ_{\text{Park}} \\ &= \sum_{h=-\infty}^{+\infty} V_{\text{Park},h} I^{*}_{\text{Park},h} \\ &= \text{Re}\left[\sum_{h=-\infty}^{+\infty} V_{\text{Park},h} I^{*}_{\text{Park},h}\right] + \text{j}\left[\text{Im}\left(\sum_{h=-\infty}^{+\infty} V_{\text{Park},h} I^{*}_{\text{Park},h}\right)\right] \\ &= \sum_{h=-\infty}^{+\infty} P_{\text{Park},h} + \text{j}\left[\sum_{h=-\infty}^{+\infty} Q_{\text{Park},h}\right] \end{aligned} \tag{156}$$

The Park power components apply only to a three-phase power system and not to a single-phase system. The *Park real power* (P_{Park}) is an expression of all the active powers found in each of the harmonic components and its symmetrical components ($h>0$ for the positive sequence harmonic components and $h<0$ for the negative sequence harmonic components). It implies a summation of the real powers for the positive and negative sequence components.

The Park imaginary power has a different meaning and definition [26] than the Budeanu reactive power although at a first glance the mathematical formulation appears to be similar. The Park imaginary power is based on a summation of the reactive powers in the positive sequence harmonic components ($Q_{1,h}$) with the summation of the reactive powers in the negative sequence harmonic components ($Q_{2,h}$), subtracted:

$$Q_{\text{Park}} = \sum_{h=1}^{\infty} Q_{1,h} - \sum_{h=1}^{\infty} Q_{2,h} + Q_{\text{Park},0} \tag{157}$$

The component ($h=0$) is shown separately in Equation (157) as the DC component of current can be spatially shifted with respect to voltage in the Park vectors. Note that Budeanu adds the reactive power in both the positive and negative sequence harmonic components as shown below (the Budeanu reactive power rewritten in terms of sequence components):

$$Q_B = \sum_{h=1}^{\infty} Q_{1,h} + \sum_{h=1}^{\infty} Q_{2,h} \tag{158}$$

There are important characteristics of the Park imaginary power (Q_{Park}) that must be noted [26]:

- The Park imaginary power (Q_{Park}) does not exist in a single-phase power system
- It does not yield information on possible time-dependent energy exchange between reactive elements in the load and the source.

- Q_{Park} is defined in the time-domain, but Q_B is not.
- The physical meaning of Q_{Park} is therefore completely different from the reactive power definitions of Budeanu, Czarnecki and other.
- It can be used to successfully improve the power factor of the load [26].
- It can be measured easily whereas Budeanu's reactive power cannot be easily measured [18].
- If the three-phase load is passive, linear and time-invariant, Q_{Park} is associated only with the susceptance of the load.

4.4.1.2 The Park "distortion" power, D_{Park}.

The average value of complex power (A_{Park}) is:

$$A_{\text{Park}} = \sqrt{P_{\text{Park}}^2 + Q_{\text{Park}}^2} \tag{159}$$

If the three phase apparent power, ($S_{3\phi}$), based on generalised rms values of three-phase voltage and current as in (120) is used, then the relation between $S_{3\phi}$ and the Park power components are [26]:

$$\begin{aligned} S_{3\phi}^2 &= P_{\text{Park}}^2 + Q_{\text{Park}}^2 + D_{\text{Park}}^2 \\ D_{\text{Park}}^2 &= S_{3\phi}^2 - A_{\text{Park}}^2 \end{aligned} \tag{160}$$

It is important to recognise at this point that the three-phase apparent power, $S_{3\phi}$ is not based on an algebraic quantity and does not satisfy the energy conservation principle whereas A_{Park} is an average value of an algebraic quantity and does satisfy the energy conservation principle.

Because $S_{3\phi} \geq 0$, the "difference quantity" is isolated [26] with symbol D_{Park} (160). D_{Park} is not the Budeanu distortion power D_B because the imaginary power in (157) is not the Budeanu reactive power Q_B. A physical explanation for D_{Park} is given in [26] where the Czarnecki current decomposition methodology of [5] is used. The Park current vector is substituted for the three-phase current vector (the components in the Park current vector are orthogonal, like the Czarnecki current components) and not the decomposed three-phase Czarnecki current vector. This is an attempt to overcome one of the deficiencies of the Czarnecki power theory, namely to also include asymmetry in the supply voltage signal. An alternative decomposition of the three-phase load current results:

$$I_e^2 = I_{Park,a}^2 + I_{Park,s}^2 + I_{Park,q}^2 + I_{Park,rs}^2 + I_{Park,f}^2 \tag{161}$$

The RMS value of the Park current vector, I_{Park}, is found by $\left\|i(t)_{\text{Park}}\right\|$ or from the harmonic components in $i(t)_{\text{Park}}$; namely $I_{\text{Park}} = \sqrt{\sum_{h=-\infty}^{+\infty} I_h^2}$. The RMS value of the Park active current vector ($I_{Park,a}$) is derived from the Park transform of the Czarnecki/Fryze three-phase active current vector $i_a(t)_{3\phi}$ in (122) with a similar physical meaning. The RMS value of the Park "scattered" current vector ($I_{Park,s}$) results from a Park transform of the Czarnecki three-phase "scattered" current vector $i_s(t)_{3\phi}$ in (132) and has a similar physical meaning. The RMS value of the Park "reactive "current vector ($I_{Park,r}$) results from the Park transform of the Czarnecki three-phase reactive current $i_r(t)_{3\phi}$ in(125) and has a similar physical meaning. $I_{Park,rs}$ is the RMS value of the Park current vector $i_{rs}(t)_{\text{Park}}$ which is an additional current definition in the Park domain [26] termed the "scattered reactive" current. It is calculated in the time-domain as the difference between the Park reactive current vector $i_r(t)_{\text{Park}}$ and the Park imaginary current vector $i_q(t)_{\text{Park}}$:

$$i_{rs}(t)_{Park} = i_r(t)_{Park} - i_q(t)_{Park}$$
with:
$$i_q(t)_{Park} = -jB_{e,Park}v(t)_{\text{Park}} \text{ and } B_{e,Park} = \frac{Q_{\text{Park}}}{V_{\text{Park}}^2} \tag{162}$$

$I_{Park,f}$ is the RMS value of the Park current vector $i_f(t)_{\text{Park}}$ derived from the Park transform of the "generated" current vector of Czarnecki, $i_g(t)$ (127) and which has a similar physical meaning. The components of $i_f(t)_{\text{Park}}$ is the Park current harmonics of harmonic orders that do not appear in the "true" Park voltage harmonics.

The decomposition of three-phase load current based on Park quantities in (161) enables definition of the Park *distortion power*, D_{Park}:

$$D_{\text{Park}}^2 = V_{Park}^2 I_{Park,s}^2 + V_{Park}^2 I_{Park,rs}^2 + V_{Park}^2 I_{Park,f}^2 \tag{163}$$

The following "unwanted" effects in the three-phase power system are described in equation (163):

- Non-linear loading causing harmonic numbers in the load current other than the harmonic numbers in the supply voltage
- Asymmetrical supply voltages
- Non-sinusoidal supply voltages
- Unbalanced loading

4.4.1.3 *The Park Power Factor*

Power factor of a load, based on Park power components, is defined as:

$$PF = \frac{P_{Park}}{S_{3\phi}} = \frac{P_{Park}}{\sqrt{P_{Park}^2 + Q_{Park}^2 + D_{Park}^2}} \tag{164}$$

4.4.1.4 *Compensation with Park power components*

Power factor correction, based on the Park power definitions, requires complete compensation of the time-dependent values of $q(t)_{\text{Park}}$. It was first shown by Akagi *et al* [22] that it is not sufficient to only compensate for $q(t)_{\text{Park}}$. Without energy storage elements, compensation of $q(t)_{\text{Park}}$ will represent the maximum power factor correction that is possible. Unity power factor requires a holistic consideration of the Park time-dependent power $p(t)_{\text{Park}}$. It was demonstrated by Ferrero and Superti-Furga [26] how the current decomposition of Fryze in the time domain could be re-interpreted in terms of Park components. This aspect is discussed in the next section.

4.4.1.5 *Fryze's active current and the Kusters and Moore residual current in terms of Park components*

The *active current* defined by Fryze [75] was shown to be responsible for active power transfer. In terms of the Park components, it is redefined in [26] as:

$$i_a(t)_{3\phi} = \frac{P_{\text{Park}}}{V_{\text{Park}}} v(t)_{\text{Park}} \tag{165}$$

The "unnecessary" current is the difference between the *total load current* and the *active current*:

$$i_x(t) = i(t)_{\text{Park}} - i_a(t)_{3\phi} \tag{166}$$

The RMS values of the *Park current vector*, the *active current* and the "extra" current above, is related as follows:

$$I_{\text{Park}}^2 = I_a^2 + I_x^2 \tag{167}$$

The average value of Park active power P_{Park} is related to the Fryze active current by:

$$P_{\text{Park}} = V_{\text{Park}} I_a \tag{168}$$

Equation (166) illustrates the compensation requirement, that $i_x(t)$ has to be completely eliminated for $S_{3\phi}$ to be equal to P_{Park}, which will result in a unity power factor.

4.4.1.6 Application of the Park Power components on simulated power system data

Consider the same nonsinusoidal three-phase circuit in Figure 31 used to investigate the Czarnecki's three-phase power definitions (zero Thévenin impedance between the source and the load).

Park transformation of the time-dependent three-phase load voltages and load currents results in a time-dependent Park voltage and current vector. Additional zero-sequence voltage and current result as it is an unbalanced three-phase power system. These waveforms are shown Figure 36:

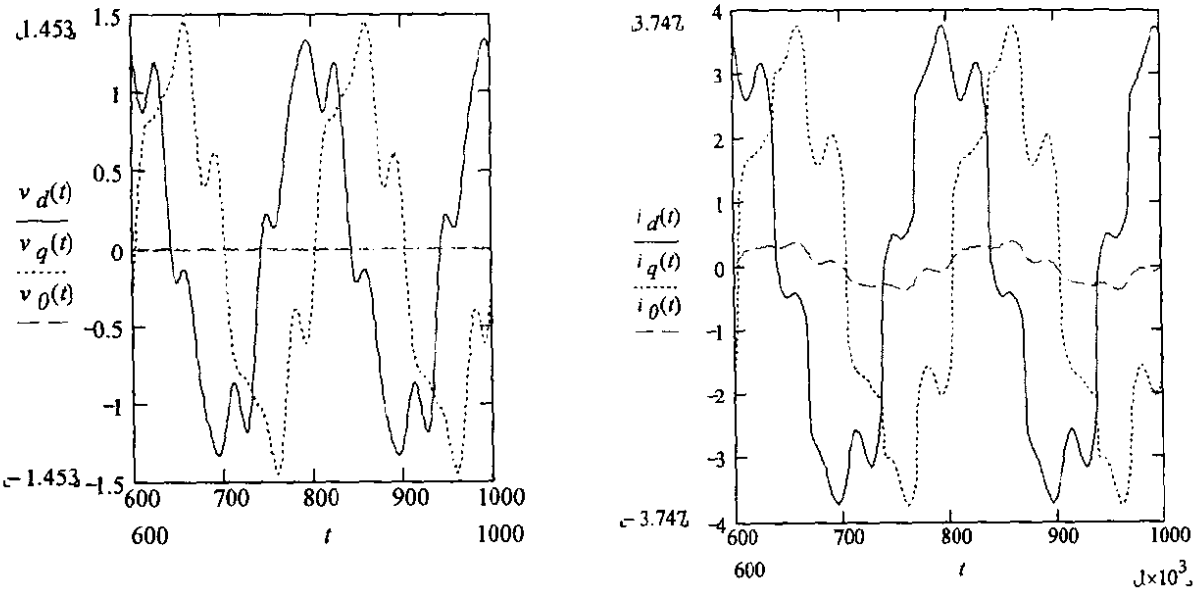

Figure 36: Park time dependent voltages at the load terminals in Figure 31

Analysis of the waveforms in Figure 36 in the frequency-domain results in:

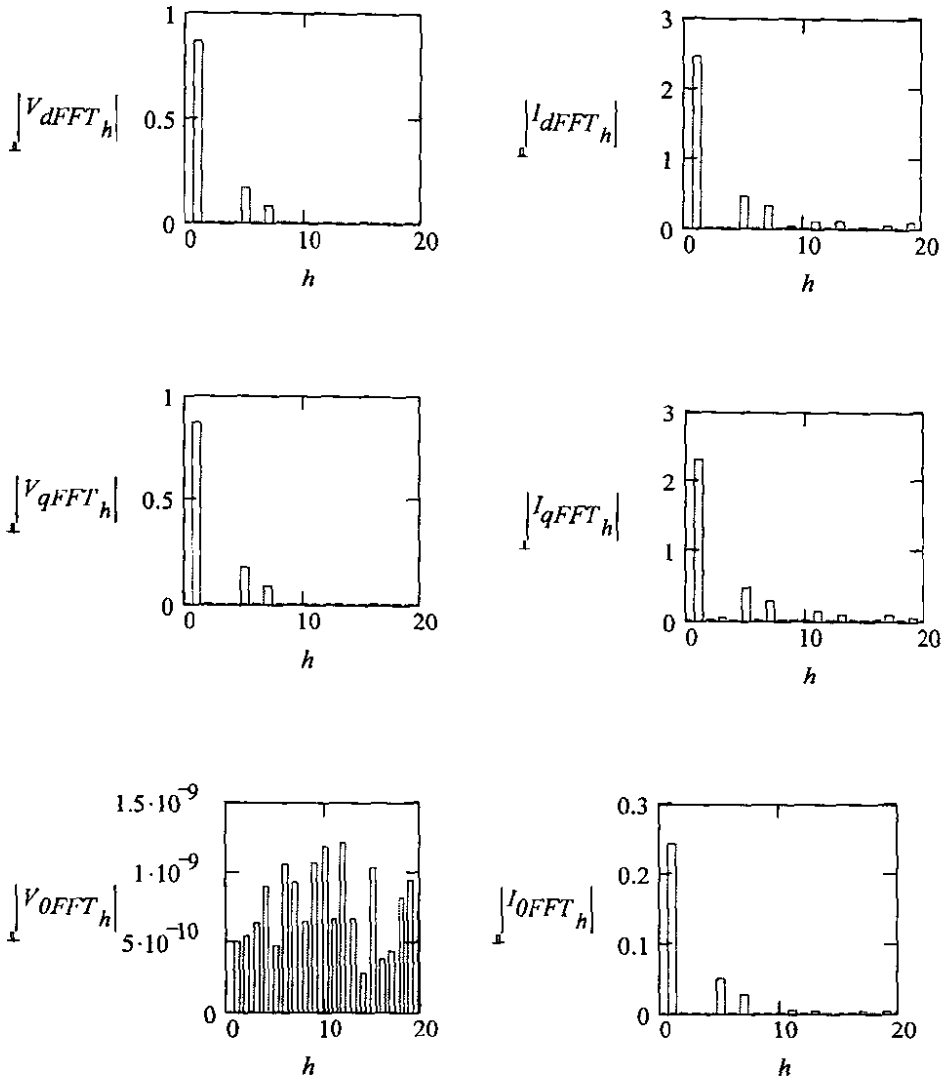

Figure 37: Frequency spectra of Park voltages and currents from Figure 36

The Park powers, at the load terminals of Figure 31 are listed in Table 20:

Table 20: Park power components calculated for the circuit in Figure 31

A_{Park}	3.143 VA
P_{Park}	3.133 Watt
Q_{Park}	0.252 VAr
PF_{Park}	0.997
$S_{3\phi}$	3.184 VA
D_{Park}	0.508
I_{check}	0 A
S_{check}	0.041 VA

The energy and current checks above prove that the Park currents and powers satisfy electrical network

laws. If tested on the circuit in Figure 33 where there is a non-zero Thévenin impedance between the source and the load, it results in the Park power values listed in Table 21:

Table 21: Park power components calculated for the measurements obtained for Figure 33

A_{Park}	4.335 VA
P_{Park}	4.325 Watt
Q_{Park}	0.303 VAR
PF_{Park}	0.998
$S_{3\phi}$	4.382 VA
D_{Park}	0.635
I_{check}	0
S_{check}	0.046

The results in Table 21 prove that no currents or powers disappear when the circuit in Figure 33 is studied by means of the Park power definitions. The Park current and power definitions still satisfy electrical network laws.

In general, power definitions that are valid under all possible circumstances are required for possible application in compensation circuits. Application of the Park power definitions in designing compensation circuits is investigated next.

4.4.1.7 Compensation with the Park power components

Important features of the Park power components [26] are:

- Measurement thereof is easy.
- The Park active power P_{Park} describes the real power associated with "useful" energy in a three-phase power system. In the case of a balanced sinusoidal three-phase power system it is equal to the three-phase active power $P_{3\phi}$.
- In the non-sinusoidal unbalanced three-phase power system the Park active power, P_{Park} represents the physical phenomenon (through field theory) of the energy that flows into a surface and that has to balance the energy that flows out of the surface by joule loss.
- The Park three-phase imaginary power is a power only applicable to a three-phase power system. It is not an extension of the concept of single-phase imaginary/reactive power.
- The Park three-phase imaginary power is not the erroneous concept of the Budeanu reactive power.

- The Park three-phase imaginary power has a physical meaning explained by field theory as it represents the variation in the ratio of energy exchange between the dielectric and magnetic energy of different phases.

- Compensation equipment can successfully be designed based on the Park voltage and current vectors as proved by Akagi *et al* [22].

Application of the Park transform on unbalanced four-wire three-phase power system quantities, results in both the Park vectors and the additional zero sequence components. This problem was overcome with the new transform of Ferrero, Giuliani and Willems [29]. This new space-vector transformation transforms four-conductor three-phase quantities into three linearly independent voltages and three linearly independent currents defined in a three-dimensional space. The transformation matrix developed, enabled a linear transformation and is orthogonal.

In the case of either balanced four-wire three-phase systems or three-wire three-phase systems, the transformed quantities are the two-dimensional Park vectors of current and voltage. Only in the case of four-wire three-phase quantities, the resultant voltage and current vectors are three-dimensional.

The mathematical principles of this new three-dimensional transform were presented in section 2.4. The next section investigates the formulation of power definitions and the application thereof in the analysis of power phenomena of four-wire three-phase unbalanced non-sinusoidal power systems.

4.5 THE FGW SPACE-VECTOR TRANSFORMATION OF FOUR-CONDUCTOR THREE PHASE POWER SYSTEMS: POWER DEFINITIONS AND APPLICATION

4.5.1 Introduction

It was demonstrated in section 4.4 that the application of the Park transform of Ferrero and Superti-Furga [26] is in perfect agreement with electrical network laws when non-sinusoidal three-wire three-phase power systems are analysed in terms of power definitions. A three-wire three-phase power system can be fully represented by the Park voltage and current quantities.

The solution to the "extra" zero sequence voltage and current quantities (and power definitions) when a four-wire three-phase system is studied, was solved by the introduction of a new transformation principle devised by Ferrero; Giuliani and Willems. A space-vector transformation was formulated based on a transformation matrix, which transforms both three-wire and four-wire systems three-phase quantities.

The resulting transformed quantities enabled the definition of power components that satisfies all the requirements of a power theory (section 1.4.7). The mathematical principles of this power theory are presented in section 2.4. It is applied in section 4.5.2 on both the simulated power system and practical

data used to analyse the preceding power theories.

4.5.2 Power definitions of transformed space-vector components

Time-dependent hypercomplex power is based on the accepted complex power definition but mathematically written here in terms of hypercomplex algebra:

$$\begin{aligned}\bar{a}(t) &= \bar{v}(t)_{dqz} \cdot \bar{i}(t)^{*}_{dqz} \\ &= a_s(t) + a_x(t)\bar{v}_x + a_y(t)\bar{v}_y + a_z(t)\bar{v}_z\end{aligned} \tag{169}$$

The components of the voltage space vector $\bar{v}(t)_{dqz}$ and current space vector $\bar{i}(t)^{*}_{dqz}$ was defined in section 2.4. The power components in the hypercomplex power $\bar{a}(t)$ results from application of hypercomplex algebraic rules:

$$a_s(t) = v_d(t)i_d(t) + v_q(t)i_q(t) + v_z(t)i_z(t) \tag{170}$$

$$a_d(t) = v_z(t)i_q(t) - v_q(t)i_z(t) \tag{171}$$

$$a_q(t) = v_d(t)i_z(t) - v_z(t)i_d(t) \tag{172}$$

$$a_z(t) = v_q(t)i_d(t) - v_d(t)i_q(t) \tag{173}$$

Power component $a_s(t)$ is a scalar equivalent to the time-dependent power transferred through a cross-section [29]. Compensation of the hypercomplex power component $\bar{a}_i(t) = \bar{a}(t) - a_s(t)$ will maximise time-dependent power transfer, further in the case of a three-conductor power system the $a_z(t)$ component is the Park imaginary power component defined in section 4.4.1.

Application of the above power definitions on different three-phase four-wire power systems is carried out in the following section.

4.5.3 Evaluation of the FGW power definitions

Four different three-phase four-wire power system circuits were simulated in ATP to evaluate both the FGW power definitions and the power definitions of the IEEE Working Group on Nonsinusoidal Power Systems: (presented in section 4.6):

1) A *Linear* circuit with increasing *balanced* loading (resistive load elements in Figure 38 is balanced in magnitude between phases and increased in discrete steps)
2) A *Linear* circuit with increasing *unbalanced* loading (resistive load elements in Figure 38 is

unbalanced in magnitude between phases and increased in discrete steps)

A generic linear circuit in which the resistive loading per phase can be adjusted to be balanced or unbalanced is shown below. The three-phase source voltage vector $v_s(t)_{3\phi}$ is perfectly symmetrical. The voltage and current vectors, $v(t)_{3\phi}$ and $i(t)_{3\phi}$ are voltage and current vectors respectively that contain the three-wire measurements referenced to earth at the measuring terminal whilst $v_n(t)$ is the voltage drop over the neutral conductor when neutral current $i_n(t)$ flows through it.

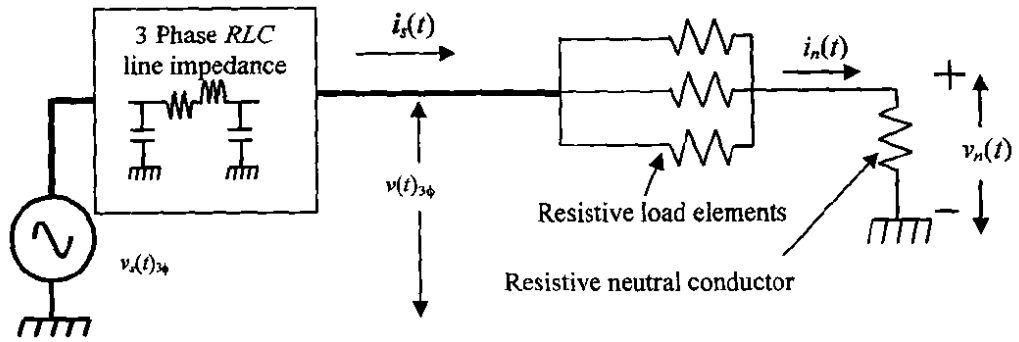

Figure 38: Linear circuit used to study four-wire three-phase power phenomena

3) A *nonlinear* circuit with increasing *balanced* but *nonlinear* loading (the resistive load element component of Figure 39 is balanced between phases and and increased in discrete steps).

4) A *nonlinear* circuit with increasing *unbalanced* and *nonlinear* loading (the resistive load element component of Figure 39 is unbalanced between phases and increased in discrete steps)

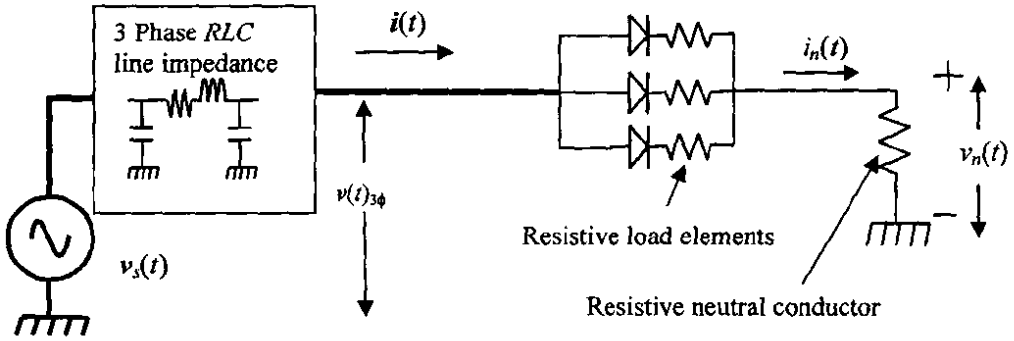

Figure 39: A nonlinear four wire three-phase power system

4.5.3.1 A four-wire three-phase power system, linear and balanced

The first case to be investigated is of a four wire three-phase power system containing pure sinusoidally shaped and balanced voltage and current waveforms. Application of the space-vector transformation on the four element phase domain voltage and current vectors $v(t)_{3\phi}$ and $i(t)_{3\phi}$ results in space voltage vector $v_{dqz}(t)$ and space current vector $i_{dqz}(t)$ with typical three-dimensional behaviour as depicted in Figure 40.

The space trajectory forms a perfect circle. Values are in p.u.:

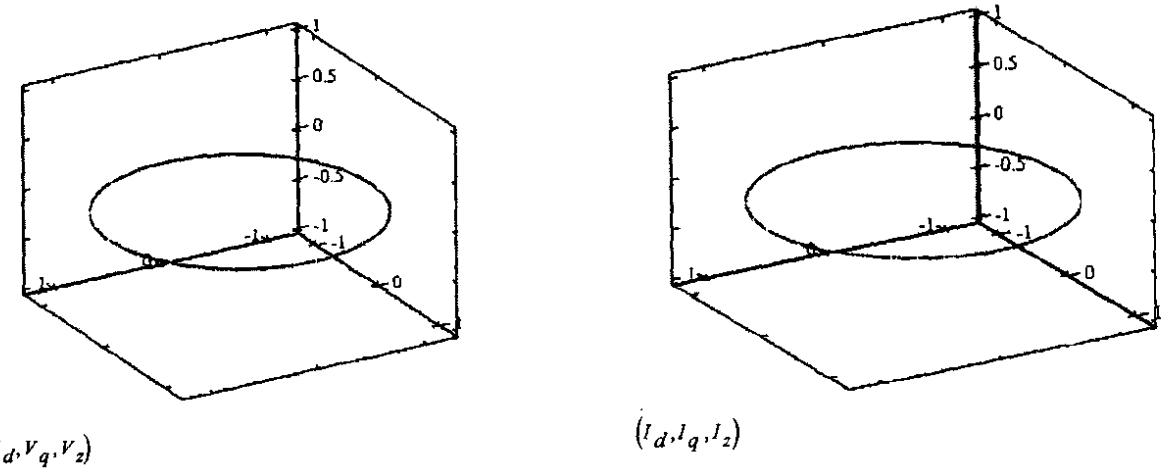

(V_d, V_q, V_z) (I_d, I_q, I_z)

Figure 40: Respective trajectories of voltage and current space vector for Figure 38 with balanced loading between phases

A two dimensional plot of the same voltage and current space vector in Figure 40 is shown below. It is clear that the results are similar to the Park transform applied to a similar three-wire power system as there is no unbalance and thus no z components.

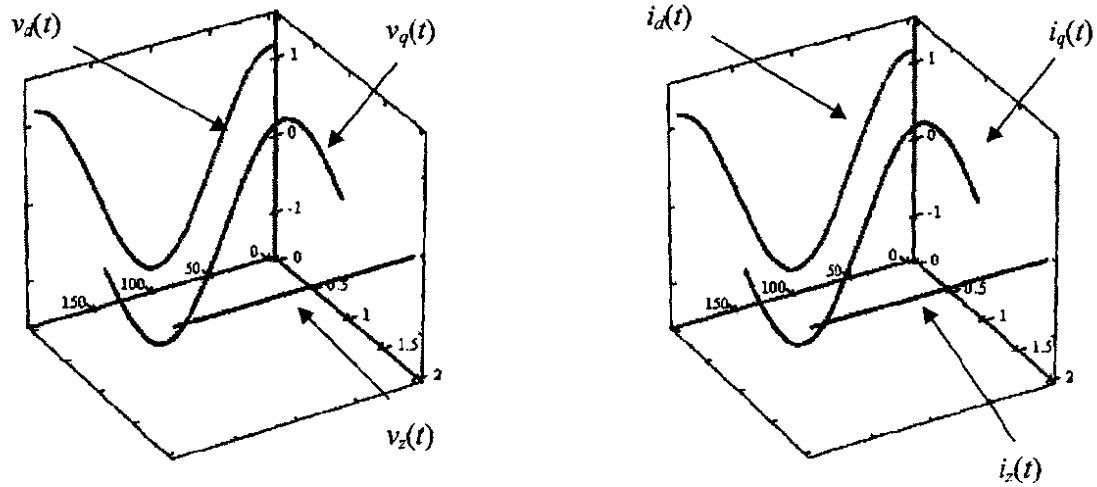

V_{FGW} I_{FGW}

Figure 41: Three-dimensional plot of $v_{dqz}(t)$ and $i_{dqz}(t)$

The hypercomplex time-dependent powers sustain the expectation that under balanced conditions in Figure 38, maximum power transfer takes place between source and load and that this power is time-independent:

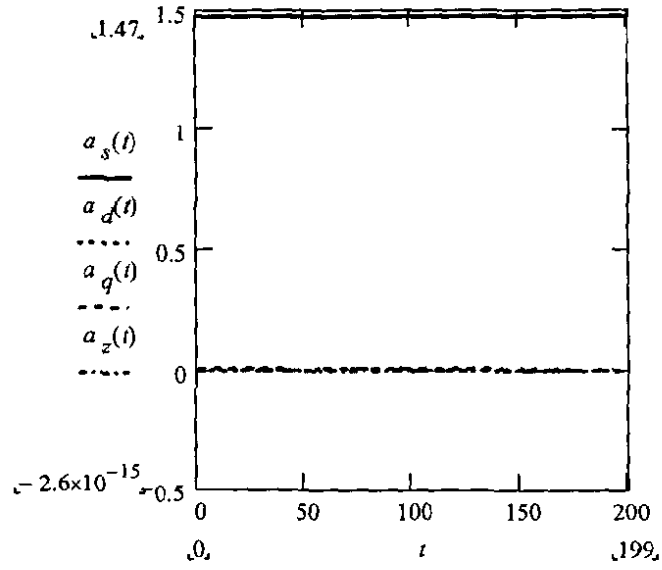

Figure 42: Time-dependent hyper-complex power delivered to the balanced load in Figure 38

4.5.3.2 Four-wire three-phase power system, linear and unbalanced

Assume that the load in Figure 38 is unbalanced between phases but fed with a symmetrical set of sinusoidal three-phase voltages. The space vector trajectory of voltage and current are respectively shown in the two figures of Figure 43.

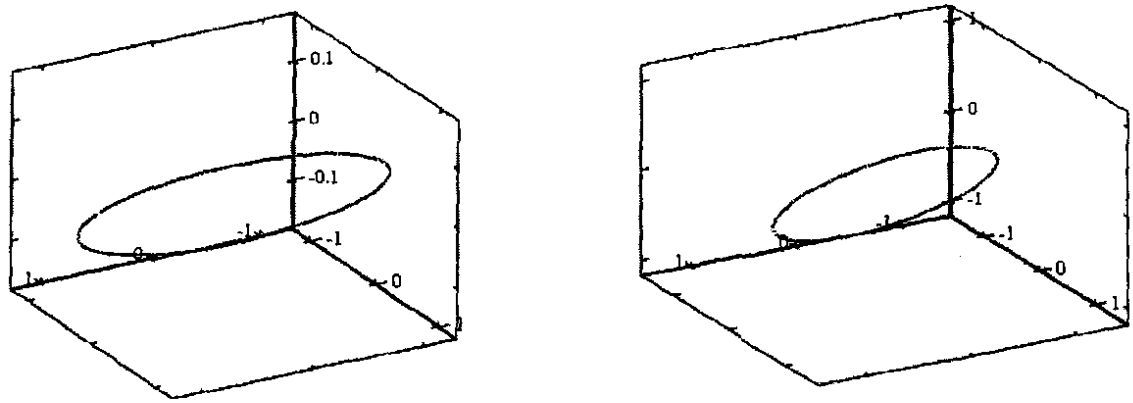

Figure 43: Trajectory of voltage and current space vector for Figure 38 with unbalanced loading between phases

The trajectory in Figure 43 significantly differs from the trajectory in Figure 40 because of the influence of unbalance results in a nonzero *z*-component. A two-dimensional plot of the voltage and current space vectors below indicates that the unbalance in the power system of Figure 38 is uniquely characterised by

the z-components of the space vectors. The advantage of the space vector transform in comparison to similar results if the Park transform was used is that the z component, in the case of the space vector transform, is an integrated part of the transformed domain and does not require separate consideration.

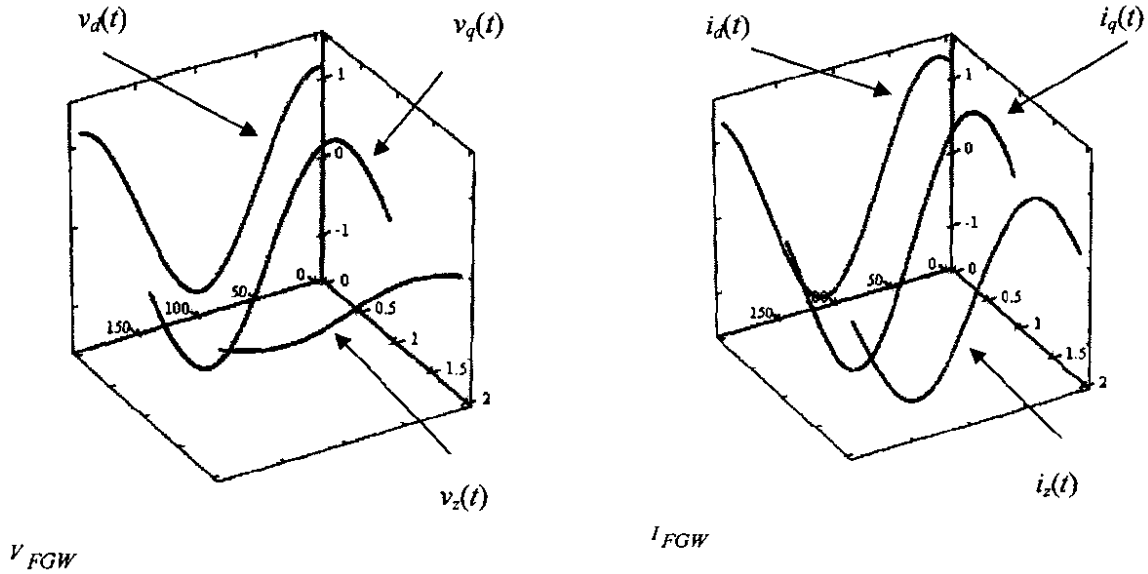

Figure 44: Two-dimensional plot of the voltage and current space vectors in Figure 43

The impact of unbalanced loading in a three-phase four wire power system is further illustrated in the time-dependent hyper-complex powers depicted in Figure 45.

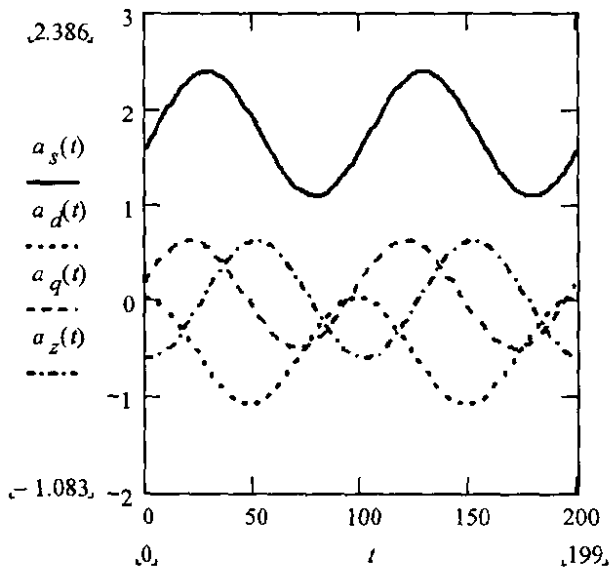

Figure 45: Time-dependent hypercomplex power components delivered for the unbalanced load in Figure 38

Comparison of Figure 45 and Figure 42 indicate that $a_s(t)$ is now time-dependent and all other hyper-complex power components influence the effectiveness of energy transfer to the three-phase load. The average values are tabled below:

Table 22: Average values of the hypercomplex powers in Figure 42 and Figure 45

Hyper complex powers, p.u. (Symmetrical Voltage source)	Balanced load	Unbalanced load
A_s	1.49	1.729
A_d	0	-0.532
A_q	0	0.057
A_z	0	3.26E-3

The $a_z(t)$ component has a near zero average value and the time-dependency in Figure 45 has similar characteristics to the reactive power in the phase domain. The most significant average value is A_d which indicates energy that is not consumed in the resistive part of the load if it is assumed that a positive average value of A_s correlates to the consumption of energy in the load.

4.5.3.3 Four-wire three-phase power system, balanced and nonlinear

The voltage source in Figure 39 is symmetrical and the loading per phase is nonlinear but balanced. The impact of nonlinearity on the voltage and current space vectors are shown by their respective trajectories in Figure 46.

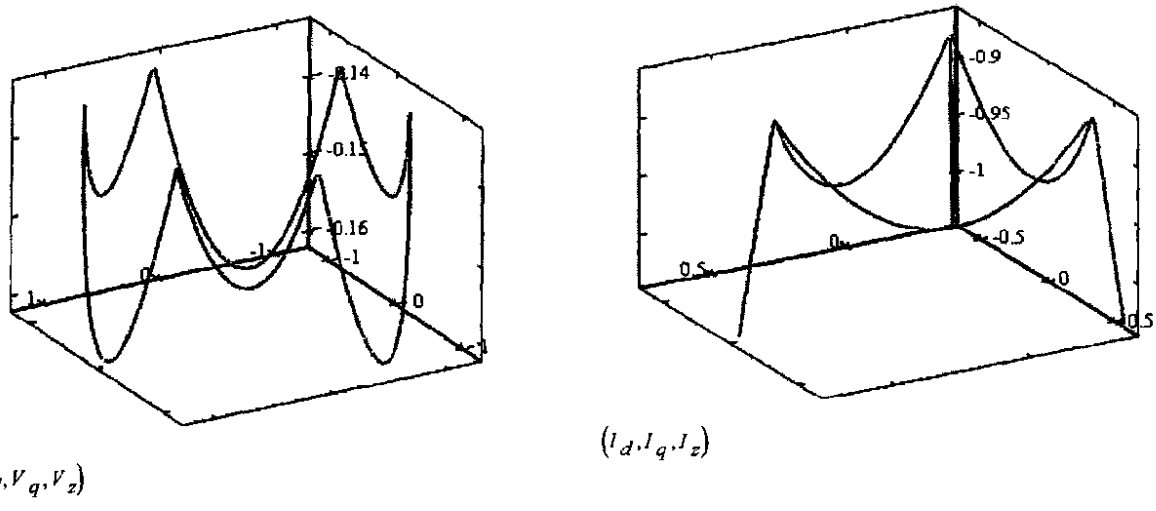

Figure 46: Trajectory of the voltage and current space vector of Figure 39 with balanced loading between phases

The impact of nonlinearity is demonstrated by a two-dimensional plot of the *d*, *q* and *z* components of the voltage and current space vectors:

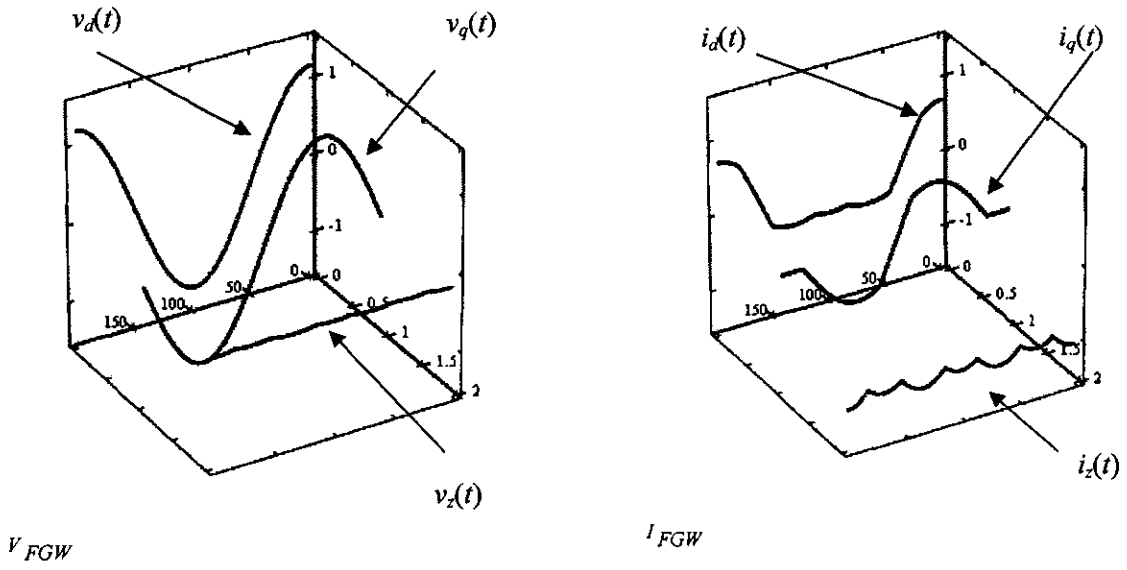

Figure 47: Two-dimensional plot of the *d*, *q*, and *z* components of the voltage and current space vectors of Figure 46

The resulting hypercomplex powers are shown in Figure 48:

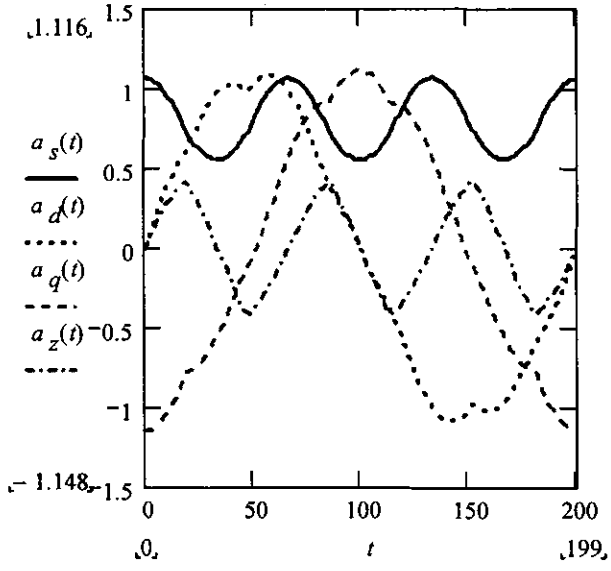

Figure 48: Time-dependent hypercomplex powers delivered to the balanced load in Figure 39

4.5.3.4 Four-wire three-phase power system, unbalanced and nonlinear

The same power system configuration of Figure 39 is used, but the loading between phases is not

balanced. The trajectory of the resulting voltage and current space vector is shown in Figure 49.

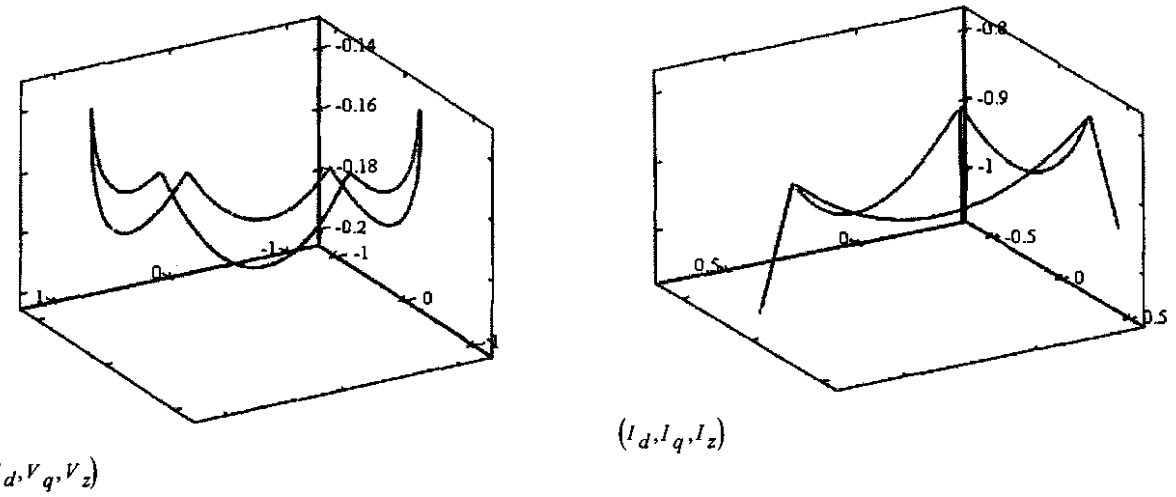

Figure 49: Trajectory of voltage and current space vectors for Figure 39 with unbalanced loading between phases

Comparison of the trajectories of Figure 49 with that of Figure 46 indicates that they are similar in shape. As in the comparison of the linear balanced load with the linear unbalanced load, the "influence" of the unbalance is to "offset" the trajectory.

The two-dimensional plot of the *d*, *q* and *z* components of the voltage and current space vectors present additional insight to the impact of unbalanced loading:

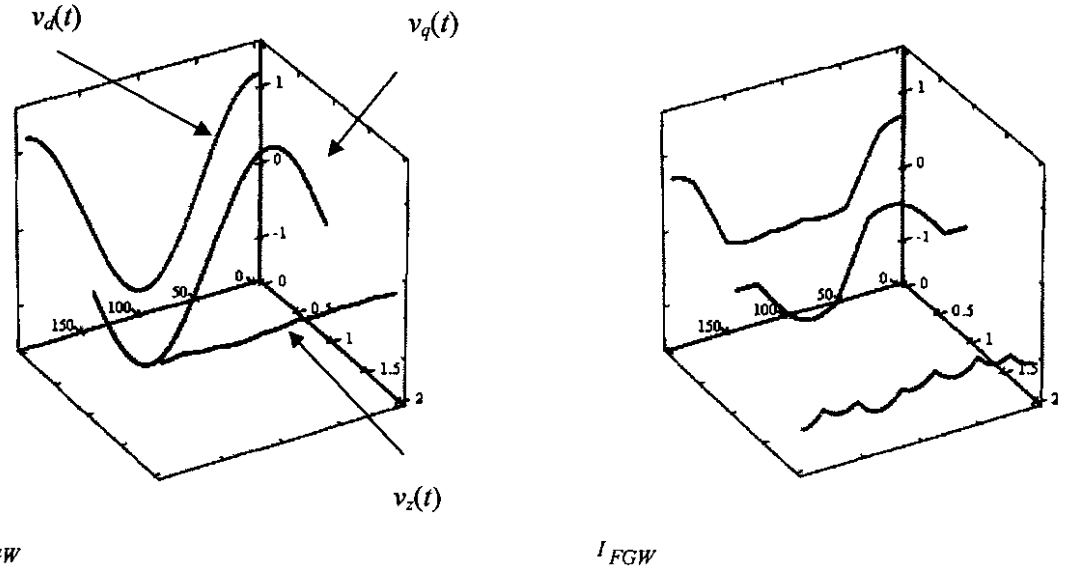

Figure 50: Two dimensional plot of voltage and current space vectors inFigure 49

The resulting hypercomplex powers are shown in Figure 51.

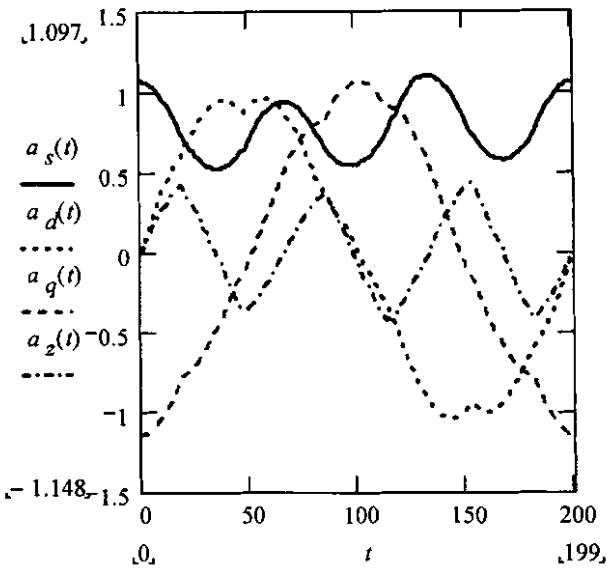

Figure 51: Time-dependent hypercomplex power delivered to an unbalanced load in Figure 39

The time-dependent hypercomplex powers in Figure 51 and Figure 48 are quite similar in shape. A comparison of the average power values and the RMS values of the components of the voltage and current space vectors reveals additional information:

Table 23: Average values of hypercomplex powers in Figure 48 in Figure 51

Hyper complex powers, p.u. (Symmetrical Voltage source)	Balanced load	Unbalanced load
A_s	0.79	0.77
A_d	-1.19E-6	-0.015
A_q	5.76E-3	-0.018
A_z	-1.12E-4	-7.16E-5

Table 23 indicates that in the case of balanced nonlinear loading (the load being a resistive load) the scalar hypercomplex power $a_s(t)$ transmits the larger part of total energy whilst unbalance and nonlinear loading cause the $a_d(t)$ and $a_q(t)$ components of total hypercomplex power $a(t)$ to decrease the effectiveness of energy on average that is transferred to the load by exporting it.

4.6 PRACTICAL DEFINITIONS FOR POWERS IN NONSINUSOIDAL ELECTRICAL POWER SYSTEMS

4.6.1 Background

The electrical engineer requires practical power definitions to analyse a power system. Some mathematical considerations have first to be agreed on when a nonsinusoidal three-phase power system is studied. The previous sections highlighted that recently, significant progress was made (for example with field theory) on certain power phenomena in non-sinusoidal power systems such as defining the imaginary power and quantifying the effect of unbalance and nonlinear loading.

The IEEE published guidelines for the practical definition of electrical quantities and power definitions in nonsinusoidal power systems in 1995 [20]. These definitions were compiled by an IEEE Working group on Non-sinusoidal Situations chaired by Alexander Emanuel of Worcester Polytechnic. Investigative application on these definitions carried out by Pretorius, van Wyk and Swart [38] proved these definitions to be practical.

These guidelines were later taken up in the IEEE Standard 1459-2000 [94]. It expanded on a number of principles and for example suggested the positive sequence fundamental apparent power S_1^+; the positive sequence fundamental reactive power Q_1^+, and the positive sequence fundamental active power P_1^+ as the most important quantities when describing the conversion and utilisation of three-phase electrical energy.

Section 4.6 presents a summarised overview and an evaluation on the application of IEEE standard 1459-2000 [94].

4.6.2 Voltage and current quantities under nonsinusoidal unbalanced conditions

Customers expect utilities to generate and distribute perfectly sinusoidal voltage waveforms at the fundamental frequency. The power definitions that are proposed in [20] separate the ideal situation of only fundamental frequency components from the "polluting components". Only three-phase power systems with nonsinusoidal waveforms with unbalance conditions (either because the supply voltage is asymmetrical or because the load elements are not balanced) are considered below. Single-phase, sinusoidal and balanced conditions are easily introduced with these definitions as a simplification of nonsinusoidal unbalanced three-phase power system.

Assume the nonsinusoidal line-neutral voltages and line currents are defined as follows[30]:

---

[30] Formulas listed in section 4.6 are a summary of reference [20] and each fromulation are not specifically referenced.

$$
\begin{aligned}
v_a(t) &= \sqrt{2}\sum_{h\neq 0}^{\infty} V_{a,h}\sin(h\omega t + \alpha_{a,h}) \\
v_b(t) &= \sqrt{2}\sum_{h\neq 0}^{\infty} V_{b,h}\sin(h\omega t + \alpha_{a,h} - 120^0 h) \\
v_c(t) &= \sqrt{2}\sum_{h\neq 0}^{\infty} V_{c,h}\sin(h\omega t + \alpha_{c,h} + 120^0 h)
\end{aligned}
\tag{174}
$$

$$
\begin{aligned}
i_a(t) &= I_{a0} + \sqrt{2}\sum_{h\neq 0}^{\infty} I_{a,h}\sin(h\omega t + \beta_{a,h}) \\
i_b(t) &= I_{b0} + \sqrt{2}\sum_{h\neq 0}^{\infty} I_{b,h}\sin(h\omega t + \beta_{a,h} - 120^0 h) \\
i_c(t) &= I_{c0} + \sqrt{2}\sum_{h\neq 0}^{\infty} I_{c,h}\sin(h\omega t + \beta_{c,h} + 120^0 h)
\end{aligned}
\tag{175}
$$

The DC components in the voltage, V_{a0}, V_{b0} and V_{c0} should always be zero. The DC values in the line currents I_{a0}, I_{b0} and I_{c0} could be nonzero depending on the nature of the load.

The *RMS line-neutral voltage* V_a and RMS line current I_a (similarly for phase b and c) are related to the harmonic components by:

$$
V_a^2 = V_{a,1}^2 + \sum_{h\neq 2}^{\infty} V_{a,h}^2 = V_{a,1}^2 + V_{aH}^2 \quad (V_{aH}^2 = \sum_{h\neq 2}^{\infty} V_{a,h}^2)
\tag{176}
$$

$$
I_a^2 = I_{a,1}^2 + \sum_{h\neq 2}^{\infty} I_{a,h}^2 = I_{a,1}^2 + I_{aH}^2 \quad (I_{aH}^2 = \sum_{h\neq 2}^{\infty} I_{a,h}^2)
\tag{177}
$$

The above formulation of voltage and current distinguish clearly between the fundamental frequency and the nonfundamental frequency (harmonic frequencies grouped) components. The *effective three phase voltage* and *current*, is written as:

$$
V_e^2 = V_{e1}^2 + V_{eH}^2
\tag{178}
$$

$$
I_e^2 = I_{e1}^2 + I_{eH}^2
\tag{179}
$$

Because there is no neutral current in a three wire power system, the expression for *effective three phase voltage* and *current* is calculated as:

$$V_e = \sqrt{\frac{V_a^2 + V_b^2 + V_c^2}{3}} \tag{180}$$

$$I_e = \sqrt{\frac{I_a^2 + I_b^2 + I_c^2}{3}} \tag{181}$$

If an artificial neutral point in a three conductor three-phase system is not used to find the line-neutral voltage values, the *effective three-phase voltage* can be calculated from the RMS phase-phase voltage values as:

$$V_e = \sqrt{\frac{V_{ab}^2 + V_{bc}^2 + V_{ca}^2}{9}} \tag{182}$$

The fundamental frequency and nonfundamental frequency components of the *effective voltage* and *current* in a three wire three-phase power system is defined as:

$$V_{e,1} = \sqrt{\frac{V_{ab,1}^2 + V_{bc,1}^2 + V_{ca,1}^2}{9}} \tag{183}$$

$$V_{eH} = \sqrt{\frac{V_{abH}^2 + V_{bcH}^2 + V_{caH}^2}{9}} \tag{184}$$

$$I_{e,1} = \sqrt{\frac{I_{a,1}^2 + I_{b,1}^2 + I_{c,1}^2}{3}} \tag{185}$$

$$I_{eH} = \sqrt{\frac{I_{aH}^2 + I_{bH}^2 + I_{cH}^2}{3}} \tag{186}$$

The *effective three phase nonfundamental voltage* and *current* value is defined as:

$$V_{eH} = \sqrt{\frac{\sum_{h\neq 1}^{\infty}\left(V_{a,h}^2 + V_{b,h}^2 + V_{c,h}^2\right)}{3}} \tag{187}$$

$$I_{eH} = \sqrt{\frac{\sum_{h\neq 1}^{\infty}\left(I_{a,h}^2 + I_{b,h}^2 + I_{c,h}^2\right)}{3}} \tag{188}$$

Unbalanced conditions in a four wire three-phase power system requires the definition of the *effective voltage* and *current* to be:

$$V_e = \sqrt{\frac{1}{18}\left[3\left(V_a^2 + V_b^2 + V_c^2\right) + V_{ab}^2 + V_{bc}^2 + V_{ca}^2\right]} \tag{189}$$

$$I_e = \sqrt{\frac{I_a^2 + I_b^2 + I_c^2 + I_n^2}{3}} \tag{190}$$

Where:

$$V_{e,1} = \sqrt{\frac{1}{18}\left[3\left(V_{a,1}^2 + V_{b,1}^2 + V_{c,1}^2\right) + V_{ab,1}^2 + V_{bc,1}^2 + V_{ca,1}^2\right]} \tag{191}$$

$$V_{eH} = \sqrt{\frac{1}{18}\left[3\left(V_{aH}^2 + V_{bH}^2 + V_{cH}^2\right) + V_{abH}^2 + V_{bcH}^2 + V_{caH}^2\right]} \tag{192}$$

$$I_{e,1} = \sqrt{\frac{I_{a,1}^2 + I_{b,1}^2 + I_{c,1}^2 + I_{n,1}^2}{3}} \tag{193}$$

$$I_{eH} = \sqrt{\frac{I_{aH}^2 + I_{bH}^2 + I_{cH}^2 + I_{nH}^2}{3}} \tag{194}$$

4.6.3 Apparent power definitions

Apparent power definitions widely used can be recognised to be either the arithmetic or vector apparent power approach. The IEEE 1459-2000 [94] formulates and then demonstrates that the concept of *effective* (or *system*) *apparent power* is the preferred approach. Power definitions used in industrial metering equipment do not in general recognise the importance of the latter definition. Most metering equipment wrongfully use the Budeanu definition of reactive power and some even report the existence of a "distortion power". The different apparent approaches are briefly formulated:

1. Arithmetic apparent power

The Budeanu power definition for single-phase power systems are applied on a per phase basis:

$$\begin{aligned} S_a &= \sqrt{P_a^2 + Q_{Ba}^2 + D_{Ba}^2} \\ S_b &= \sqrt{P_b^2 + Q_{Bb}^2 + D_{Bb}^2} \\ S_c &= \sqrt{P_c^2 + Q_{Bc}^2 + D_{Bc}^2} \end{aligned} \tag{195}$$

The arithmetic apparent power (S_A) follows:

$$S_A = S_a + S_b + S_c \tag{196}$$

2. The vector apparent power

The active, Budeanu's reactive and distortion power over all three phases can be calculated[31]:

$$\begin{aligned} P_{\Sigma,3\phi} &= P_a + P_b + P_c \\ Q_B &= Q_{Ba} + Q_{Bb} + Q_{Bc} \\ D_B &= D_{Ba} + D_{Bb} + D_{Bc} \end{aligned} \tag{197}$$

The vector apparent power (S_V) follows:

$$S_V = \sqrt{P_{\Sigma,3\phi}^2 + Q_B^2 + D_B^2} \tag{198}$$

3. The effective apparent power

The *three-phase* or *system effective apparent power* S_e can be written in terms of the contribution of the fundamental and nonfundamental frequency voltage and current components:

$$S_e^2 = (V_e I_e)^2 = (V_{e,1} I_{e,1})^2 + (V_{e,1} I_{eH})^2 + (V_{eH} I_{e,1})^2 + (V_{eH} I_{eH})^2 \tag{199}$$

---

[31] The active power per phase (P_a P_b P_c) includes the harmonic components, the three-phase joint active power is in this thesis listed as $P_{\Sigma,3\phi}$ but is similar to the P used in IEEE 1459 for three-phase definitions (same symbol is used for single-phase and three-phase).

The *three phase effective apparent power* contains a *fundamental frequency apparent power* $S_{e,1}$ and a *non-fundamental frequency apparent power* S_{eN}:

$$S_e^2 = S_{e,1}^2 + S_{eN}^2 \tag{200}$$

4. The "distortion" components in the three-phase apparent power of a nonsinusoidal unbalanced power system:

The *non-fundamental frequency apparent power* is defined as to consist of three components[32]:

$$\begin{aligned} S_{eN}^2 &= \left(V_{e,1} I_{eH}\right)^2 + \left(V_{eH} I_{e,1}\right)^2 + \left(V_{eH} I_{eH}\right)^2 \\ &= D_{eI}^2 + D_{eV}^2 + D_{eH}^2 \end{aligned} \tag{201}$$

The three components above are termed:

- $V_{e,1}I_{eH}$: The *current distortion power*, D_{eI}
- $V_{eH}I_{e,1}$: The *voltage distortion power*, D_{eV}
- $V_{eH}I_{eH}$: The *harmonic distortion power*, D_{eH}

The *effective harmonic apparent power* S_{eH} relates to the *harmonic distortion power* D_{eH} and the *effective* (or *joint*) *harmonic active power* $P_{H,3\phi}$:

$$S_{eH}^2 = P_{H,3\phi}^2 + D_{eH}^2 \tag{202}$$

The level of distortion in a three-phase power system is respectively defined by the *voltage total harmonic distortion* factor $VTHD^{33}{}_e$ and the *current total harmonic distortion* factor $ITHD_e$:

$$VTHD_e = \frac{V_{eH}}{V_{e,1}} \tag{203}$$

---

[32] The IEEE 1459-2000 used the symbol "*e*" to indicate that these distortion powers are based on "effective" three-phase values.

[33] The IEEE 1459-2000 write these symbols as THD_{eV} and THD_{eI} respectively.

$$ITHD_e = \frac{I_{e,H}}{I_{e,1}} \tag{204}$$

The equivalent total harmonic distortion factors can be used to find S_{eN}, D_{eI}, D_{eV}, D_{eH}:

$$S_{eN} = S_{e1}\sqrt{VTHD_e + ITHD_e + \left(VTHD_e ITHD_e\right)^2} \tag{205}$$

$$D_{eI} = S_{e1} ITHD_e \tag{206}$$

$$D_{eV} = S_{e1} VTHD_e \tag{207}$$

$$D_{eH} = S_{e1} ITHD_e VTHD_e \tag{208}$$

5. Harmonic pollution and unbalance:

The normalised *non-fundamental apparent power* S_{eN}/S_{eI} relates to the *total harmonic distortion factors*:

$$\left(\frac{S_{eN}}{S_{e1}}\right)^2 = \left(ITHD_e\right)^2 + \left(VTHD_e\right)^2 + \left(ITHD_e VTHD_e\right)^2 \tag{209}$$

The ratio S_{eN}/S_{eI} is an indicator of the level of harmonic distortion.

Unbalanced loading can cause the three-phase fundamental frequency apparent power to increase without an increase in the transfer of fundamental frequency active power. The IEEE 1459-2000 [94] suggested the following separation:

$$S_{u1} = \sqrt{S_{e1}^2 - \left(S_1^+\right)^2} \tag{210}$$

$$S_1^+ = 3V_1^+ I_1^+ \tag{211}$$

The component S_1^+ is the *positive sequence fundamental apparent power* calculated from the RMS values of the *fundamental positive sequence voltage* (V_1^+) and *fundamental positive sequence current* (I_1^+). The term S_{u1} is the contribution of unbalance termed the *unbalance fundamental apparent power*.

- A quantitative measure of the "level" of harmonic pollution is contained in (210). A zero value

indicates that no harmonic pollution is present. The ratio S_{eN}/S_{e1} progressively relates to the level of harmonic pollution.

- Similarly, the ratio S_{u1}/S_{e1} furnishes a progressive measure of the level of unbalance (it includes both the effect of voltage asymmetry and unbalance in loading).

6. Fundamental frequency active- and reactive power:

The *fundamental active power* and the *fundamental reactive power* for a three-phase nonsinusoidal unbalanced power system should be based on positive sequence quantities [94]:

$$\begin{aligned} \left(S_1^+\right)^2 &= \left(P_1^+\right)^2 + \left(Q_1^+\right)^2 \\ P_1^+ &= 3V_1^+ I_1^+ \cos\theta_1^+ \\ Q_1^+ &= 3V_1^+ I_1^+ \sin\theta_1^+ \end{aligned} \tag{212}$$

7. Power factor definitions:

The *power factor*[34] to be used is defined as:

$$PF_e = \frac{P_{\Sigma,3\phi}}{S_e} = \frac{P_{1,3\phi} + P_{H,3\phi}}{S_e} \tag{213}$$

The fundamental frequency power factor is defined as:

$$PF^+ = \frac{P_1^+}{S_1^+} \tag{214}$$

The *three-phase total* (or *joint*) *active power*[35] $P_{\Sigma,3\phi}$ contains both the *three-phase fundamental active power* $P_{1,3\phi}$ and the *three-phase total harmonic active power* $P_{H,3\phi}$:

$$P_{3\phi} = \sum_{h=0}^{\infty} P_{3\phi,h} = P_{3\phi,1} + \sum_{h\neq 1}^{\infty} P_{3\phi,h} = P_{3\phi,1} + P_{3\phi,H} \tag{215}$$

---

[34] The subscript "*e*" is used to indicate that this power factor formulation make use of effective apparent power.

[35] The three-phase *Joint Active Power* is the three-phase *Joint Real Power*.

The arithmetic or vector apparent power should not be used in the power factor formulation when the three-phase power system is nonsinusoidal and unbalanced:

$$PF_A = \frac{P}{S_A} \text{ (arithmetic power factor)} \tag{216}$$

$$PF_V = \frac{P}{S_V} \text{ (vector power factor)} \tag{217}$$

When the power system is balanced and sinusoidal, $PF_A=PF_V=PF_e$. The IEEE 1459-2000 demonstrate that if the power system is unbalanced and nonsinusoidal, $PF_e< PF_A< PF_V$ and therefore propose the *effective* power factor formulation to be used.

The above formulations are easy to implement when waveform data is available. The next section evaluates these definitions.

4.6.4 Application of the IEEE power definitions

Similarly to section 4.5, four different three-phase circuits are used to evaluate the validity of the IEEE Working Group definitions:

- A *Linear* circuit with increasing *balanced* loading (resistive load elements in Figure 38 is balanced in magnitude between phases and increased in discrete steps, indicated as FGW21, FGW22, FGW23 and FGW24 in Figure 52),
- A *Linear* circuit with increasing *unbalanced* loading (resistive load elements in Figure 38 is unbalanced in magnitude between phases and increased in discrete steps indicated as FGW31, FGW32, FGW33 and FGW34 in Figure 52),
- A *nonlinear* circuit with increasing *balanced* but *nonlinear* loading (the resistive load element component of Figure 39 is balanced between phases and increased in discrete steps indicated as FGW41, FGW42, FGW43 and FGW44 in Figure 52),
- A *nonlinear* circuit with increasing *unbalanced* and *nonlinear* loading (the resistive load element component of Figure 39 is unbalanced between phases and increased in discrete steps indicated as FGW51, FGW52, FGW53 and FGW54 in Figure 52).

The following quantities were evaluated:

- V_e the effective voltage,
- I_e the effective current,

- PF_e the effective power factor,
- PF^+ the fundamental frequency power factor,
- S_{en}/S_{e1} the distortion index,
- S_{u1}/S_{e1} the unbalance index

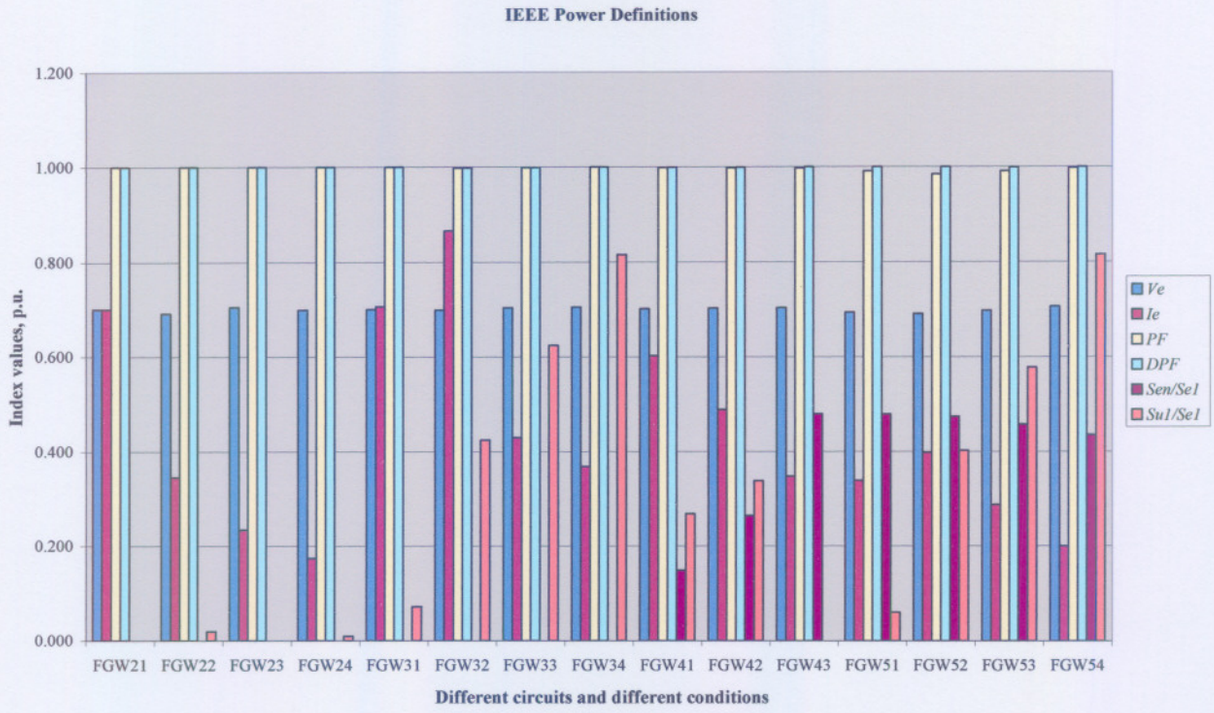

Figure 52: Evaluation of the IEEE Power definitions for nonsinusoidal conditions

The impact of distortion on the PF_e can be seen in the values calculated for circuits FGW51–FGW54. It is not significant as the loading used in the circuits studied was resistive. The PF^+ remained at unity.

The ratio S_{u1}/S_{e1} is indeed a good measure of the degree of unbalance in the power system. Values calculated for circuits FGW31-34 and circuits FGW51–54 demonstrate that regardless of linear or nonlinear loading, the "degree of unbalance" is quantified and isolated by S_{u1}/S_{e1}.

The ratio S_{eN}/S_{e1} is shown by the values plotted for circuits FGW41-43 and FGW51-54 as an effective indicator of the "degree of distortion". The distortion is quantified and isolated.

In conclusion, the IEEE 1459-2000 power definitions for nonsinusoidal conditions are indeed a solution to practical power definition formulation. A detailed investigation by Pretorius, van Wyk and Swart [38] into the formulation and application thereof in an industrial power system, confirmed the latter.

4.7 SUMMARY

The modern three-phase power system has to be considered as a self-contained entity when studying power phenomena. Formulations have to be carried out in this domain or in an equivalent transformed domain. Power definitions based on quantities formulated in a single phase domain are only valid for three-phase systems under perfectly balanced three-phase conditions.

Czarnecki's power definitions were shown to be inadequate when applied to practical power systems. Single-phase quantities were mathematically extended by him to cope with three-phase power systems. Three-phase power phenomena not described by his single-phase power definitions were then included by additional mathematical manipulation. It is important for a three-phase power theory to assign a sound physical explanation to power phenomena as found in practical three-phase power systems. This matter was shown to be lacking in Czarnecki's power definitions.

Transformation of three-phase quantities to a synthetic domain enables power definitions which can be based on classical power definitions. The space-vector transform [29] is an example of a transformation that enables power definitions that can describe power phenomena in both three wire and four wire three-phase power systems. The physical significance and application of these power components deserves research as it seems to have further exciting potential in the design of compensating equipment and tariff systems.

5 THE LOCALISATION OF DISTORTION SOURCES IN ELECTRIC POWER NETWORKS

5.1 INTRODUCTION

Various contributions to measurement techniques that are aimed at localising a specific source of distortion in a power system are found in the literature. As stated earlier, Swart *et al* [57] showed that it was not possible to localise distortion sources in a network in which more than one distortion source is present. This work was solely based on frequency-domain modelling and the models of power sources and line-commutated loads were all formulated in the frequency domain. Although the approach appeared to be mathematically sound, two further studies are still considered necessary to furnish conclusive proof of the validity of the last finding. They are respectively that of time-domain modelling and physical measurements carried out on a real power system. Chapter 5 furnishes the additional study results achieved with respect to these two methods.

Customers of electrical utilities that experience high ambient levels of voltage harmonics at their Points of Common Coupling (PCC) invariably have to contend with a range of detrimental effects in their equipment that range from lightning equipment malfunctioning to overheating and the necessity for derating rotating equipment and transformers. The utilities themselves are seldomly responsible for generating the distortion but their networks are responsible for transmitting it from other "guilty" consumers to them. These "innocent" customers look upon the utility for the low power quality, and not on the guilty parties, as the primary source of their problems. It is therefore in the interest of the utility, to dissuade active and potential harmonic producing customers through proper management and tariff penalisation.

Network analysis in the frequency domain shows that harmonic producing sources can be modelled reasonably accurately by current sources at the relevant discrete frequencies and that these currents produce voltages across the system immittances with phase angles corresponding to the angles of these immittances. In frequency domain analysis, networks and their elements allow harmonic superposition to be carried out and individual frequencies may be modelled separately. A logical consequence of the interaction of these voltages with the given immittances then is that the power angles at those harmonic frequencies will also correspond to the immittances angles. It follows, therefore, that the harmonic current sources will export real power only to the network immittances with real components and that these harmonic real power component magnitudes will be commensurate with the aggregate magnitude of the system real immittances.

When harmonic power measurements are carried out at the PCC of a given consumer, an outflow of harmonic real power furnishes proof that the harmonics originate behind the PCC and that it is caused by

that consumer [56]. Unfortunately in practical systems, the direction of harmonic power can be sunk and generated also in line commutated actively switched circuits and the simple principle of looking upon passive network real immittances as sinks is violated. In their presence, phase controlled line commutated AC/DC multiphase converters exhibit the ability of exporting and importing harmonic real powers at the individual harmonic frequencies. In addition, these magnitudes and angles change with relative changes in the firing angles of the converters, rendering a set of observed data relating to one operating condition of the network unsuitable when one of these conditions change.

This phenomenon, of course, put the lid on any scheme by means of which continuous single-point measurements, at the consumer PCC will be able to tell if it is a consumer or a producer of harmonic distortion is exporting or importing harmonic real power. It would, therefore, not be possible to show by this method whether customers were generating or consuming real harmonic power and whether they deserved to be penalised or compensated [57] in terms of a tariff system. Because the two sets of findings were in conflict, it was important that their outcomes be validated one way or another.

Because of the possibility that the frequency-domain models used were in error, the modelling was repeated in the time-domain. The results of [57] are tested in chapter 5 by time-domain modelling. In a time domain model that makes use of numerical integration, the model structures are different and it would be very unlikely that the same possible modelling errors of the frequency domain would be repeated.

The results obtained and reported in chapter 5 has now nipped any attempt in the bud that attempts to localise a distortion producing source by means of single-point measurements in an interconnected power system with more than one distortion source. The implication of this statement is simply that it is not possible to use single point measurements to establish the level of harmonic distortion contributed to a PCC by a specific customer.

5.2 HARMONIC REAL POWER, HARMONIC REACTIVE POWER AND HARMONIC COMPLEX POWER AS A CHARACTERISTIC OF A DISTORTION SOURCE

Swart [56] suggested that a systematic approach to manage the supply voltage distortion in the power system should entail the following steps:

- Find some universally agreed-upon theory for power under distorted conditions in networks;
- Find some universally agreed-upon method of evaluating distortion in networks;
- Find some universally agreed-upon method of locating sources of distortion;
- Devise appropriate measuring equipment;

- Define tariff structures that take distortion into account and

- Measure distortion and recover a charge, which would generate sufficient revenue to either pay for the alleviation of the problems or encourage the customer to take appropriate steps to reduce distortion charges.

Section 5.2.1 and 5.2.2 investigates the principle of applying harmonic real power as a distortion source localising agent.

5.2.1 The nature of a distorting load

Frequency domain modelling of a distorting load in a power system reveals important characteristics thereof. Nonlinear loads can be represented as discrete current sources at each harmonic frequency in parallel with linear Norton equivalent impedances.

The resulting harmonic power flow[36] can be studied to determine the behaviour of the harmonic real and reactive power with respect to the application of each in the localisation of a single distorting load in an electrical network.

Frequency domain modelling entails the superponated solution of the voltages and currents resulting from equivalent Norton circuits solved at each discrete harmonic frequency. For example, the source branch will only contain a current source at the fundamental harmonic order, whilst the load branches could also contain a number of parallel Norton equivalent circuits representing the harmonic orders found in the distorting Norton current source. Such an analysis approach is explained in detail in [56]. Important matters considered are:

- The phase angle and the amplitude of the distorting current do not influence the direction of the real and reactive power flow.

- The argument and amplitude of the residual admittance into which the distortion current is delivered, does not influence the direction of the real and reactive power.

- The real power will always be flowing away from the distorting branch and into the PCC towards dissipative load components.

---

[36] Admitting that the term '*power flow*' is actually a misnomer, it has been hallowed through long use and is universally employed [99]. Energy 'flows'. Power is the rate of transfer of energy and the concept of 'flow' cannot be made to stick to it. It will therefore be used here as well. The question of power flow is settled quite satisfactorily at an elementary level in standard textbooks [97], [99].

- The harmonic real power can be termed the harmonic active power, as it conforms to the accepted concept of active power.

- The flow of reactive power is in a direction that depends on the reactance of the residual susceptance, if the residual susceptance is pre-dominantly capacitive, that branch will absorb reactive power. Reactive power will be flowing into the branch.

- If the residual susceptance of a branch is pre-dominantly inductive, then that branch will deliver reactive power to the PCC.

- For a single current source considered, the residual conductance of that branch can only be positive and hence active power is always flowing out of that branch.

- As reactive power is a function of the operation of a network (such as power factor correction capacitors or distribution of power by cables), residual admittances can be found that are positive although expected to be mostly negative. The interpretation of reactive power therefore requires knowledge on the susceptance of a branch.

5.2.2 Harmonic Active Power as a localisation agent

The following matters support the use of harmonic active power as localising agent:

- If all the harmonic orders are considered, it requires a summation of real powers and/or reactive powers over all harmonic orders. Harmonic reactive power will be larger than harmonic active power in magnitude as equivalent Norton susceptances are typically much larger than the equivalent Norton conductances.

- The summation of harmonic reactive power is prone to erroneous interpretation for the reasons stated directly above.

- It is unpractical to consider complex power per harmonic order as the nature of the reactance per harmonic frequency must be known to fully interpret the measured complex power. Distortion sources that generate only a single harmonic frequency are also hypothetical. Distortion sources are "distorting" sources because of nonlinearity and as such "generate" a spectrum of harmonic real and reactive powers. Summation of reactive power will then be required, which by concept, is wrong as discussed and demonstrated in section 4.2.

- The summation of harmonic real power (in the case of a single distorting source) indicate the direction of a single nonlinear load generating it is as harmonic real power is "flowing" away from a single distorting load.

5.2.3 Conclusion

Managing the overall power system distortion is the major objective of localising different sources of distortion distributed all over the power system. If a tariff system can reflect the contribution of a certain load to the Total Harmonic Voltage Distortion (*THVD*) observed at a PCC, it will be a powerful self-regulating mechanism in power quality management. A tariff system requires continuous measurement of a load for which the tariff account has to be issued. The real power is a "usable" quantity to be measured to aid in the localisation of the distortion source and can be reflected in a tariff account. As the sign of the real power can indicate the absorption of "distortion", a customer can be compensated or penalised. In a practical power system however, these distortion sources are located all over the power system and hence the impact of interaction between these distortion sources will be studied in the next section.

5.3 ON TECHNIQUES FOR LOCALISATION OF MULTIPLE SOURCES PRODUCING DISTORTION IN ELECTRIC POWER NETWORKS

5.3.1 Frequency domain modelling: Swart *et al* [57]

Network analysis in the frequency domain shows that harmonic producing sources can be modelled by harmonic current sources at the relevant discrete frequencies. The harmonic currents produce harmonic voltages across the system harmonic immittances with phase angles corresponding to the angles of these immittances. Application of harmonic superposition enables individual frequencies to be modelled separately.

Frequency domain modelling entails frequency dependent models to be solved at each harmonic frequency. Superposition is then used to reconstruct the waveforms in the time domain. This was the principle used in [57]. A frequency domain model was developed of two 11 kV 25 MVA DC arc furnaces fed from a known source impedance. The two furnaces represented two non-linear loads/branches with the third branch the source branch. The frequency domain model was proved to accurately reproduce the actual measured time-domain waveforms. Circuit parameters of the practical network were used.

Important results were obtained:

- When the firing angles are equal in both the distorting loads (being the arc furnaces), the *Joint Harmonic Real Power* generated in each load branch is negative and summate to flow out of the PCC into the third branch which connects the PCC with the fundamental frequency energy source.

- When the firing angles are different relatively to each other in the two load branches, a situation resulted where the *Joint Harmonic Real Power* in the source branch can be nearly zero. The absolute value of the *Joint Harmonic Real Power* generated in each branch do not have to change

significantly, but it is then an almost exact match in magnitude although opposite in direction. Harmonic real power is now exchanged between the two non-linear loads. One load could therefore be classified as "distortion generating" based on the sign of the harmonic real power obtained through a single-point measurement at that load terminal whilst the other load could be classified as a "non-distorting" load as it is absorbing harmonic real power based on a single-point measurement.

Harmonic real power flow can therefore also take place between harmonic producing sources. The direction of harmonic real power is a function of the operating conditions of the electric network, such as the relative firing angles between converters. The operating characteristics of a non-linear load are determined by matters specific to the process it is used in. This matter represents a stochastic nature to the operation of distributed distortion generating loads.

All modern electric power networks contain harmonic producing sources, which are distributed all over the interconnected electric power system. Therefore:

- It is not possible to localise a specific distortion-producing source in a practical three-phase power system through single point measurements.
- It is only possible to localise distortion-producing sources in a practical power system by measuring harmonic active power flow in all the terminals of all the consumers simultaneously and synchronously.

The importance of these findings in [57] namely that localisation of distortion producing sources in modern networks is flawed if the direction for the harmonic active power is a function of the non-linear loads, require validation. The frequency domain modelling carried out originally will now be extended both to a time-domain simulation as well as practical measurements in the sections following.

5.3.2 Time domain modelling

A power system similar to Figure 53 was configured in ATPDRAW™. A purely sinusoidal three-phase voltage source supplies energy to two 6-pulse AC/DC phase controlled line commutated converters. The PCC houses a measuring cross section in each of its three branches. Measuring point A is in the line from the source to the PCC. Measuring-points B and C are in the two lines connecting the PCC with the converters.

Complex power levels at the three measuring points are calculated from three common voltage and current data sets. The *RLC* circuits shown in each leg enables the asymmetrical adjustment of the self- and mutual inductances in each leg to furnish artificial unbalance in the three lines. All parameters are computed in per-unit values derived from base values of 5 kVA and 380 V. The system fundamental

power frequency is 50 Hz.

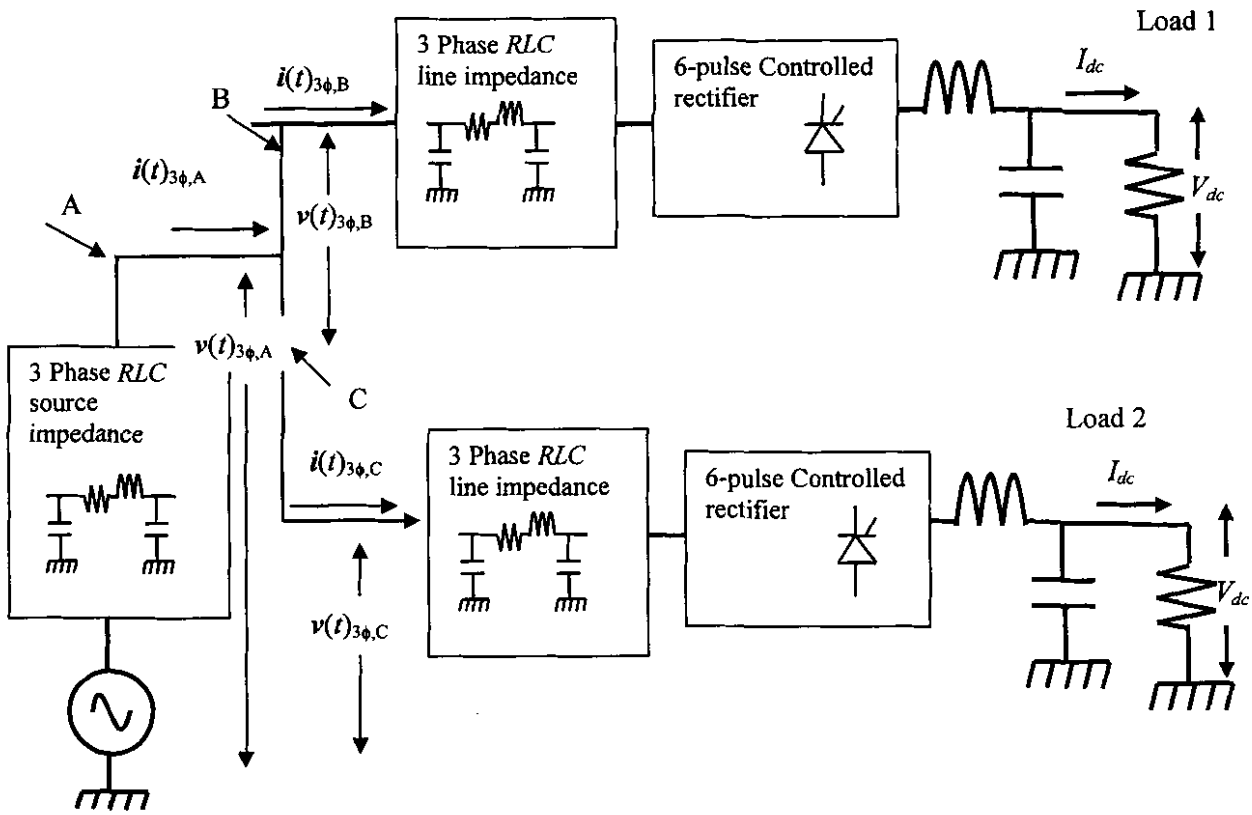

Figure 53: Simulated power system

This power system in Figure 53 was simulated in ATP. Time-domain waveform values were saved to file for each simulation run and then analysed in MathCAD. The analysis attempted to prove that a change of relative firing angle between the AC/DC line-commutated converters induces an interchange of harmonic real power between the converters as reported in [57].

The firing angle (ξ_2) for the converter fed by the lower branch was fixed at 45° throughout whilst the firing angle (ξ_1) of the converter that is fed by the upper branch is successively altered in steps for each simulation run of 5° to a total of 85°. Synchronised voltage and current measurements were recorded at points A, B and C for each of these settings and for each simulation run.

5.3.2.1 Simulation results

A total of 17 different ATP simulation runs were carried out, each with a progressive increment of 5° in the firing angle of converter 1, starting at 5° and ending at 85°. The firing angle of converter 2 was maintained constant at 45°. Typical voltage and current waveforms are shown below for one of the converters:

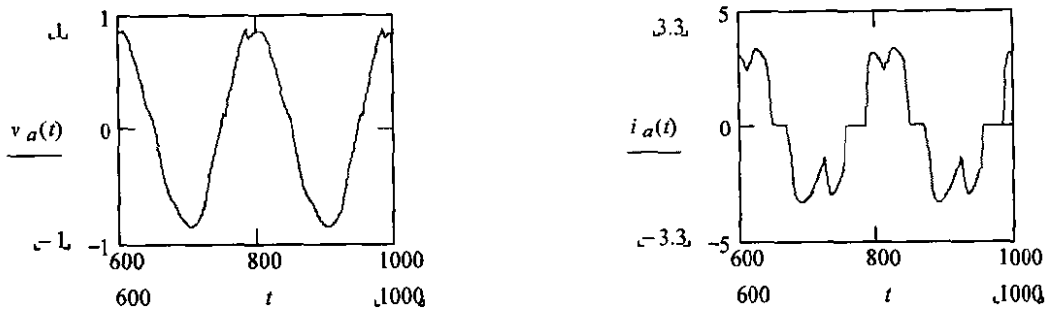

Figure 54: Typical converter voltage and current

The phase *a* voltage in Figure 54 is nonsinusoidal because of the voltage drop over the source impedance due to the non-sinusoidal load current. The frequency content of the three measuring branches was then used to calculate the *Joint Harmonic Real Power* at each measuring branch and plotted for each firing angle in Figure 55.

When the firing angles of both converters are equal (45 degrees in this case with relative firing angle ξ_2-ξ_1=0); then the *Joint Harmonic Real Power* in the two converter branches sums to the *Joint Harmonic Real Power* in the source-branch. This is a typical situation as *Joint Harmonic Real Power* is propagated towards the source and dissipated in the equivalent source imittance real component.

When the firing angle of a converter is different to the other (relative firing angle ξ_2-$\xi_1 \neq 0$); then the levels of *Joint Harmonic Real Power* in the two converter branches is seen to take on opposite signs and to roughly balance each other. As the relative firing angle (ξ_2-ξ_1) is progressively increased, the magnitude of the two powers are seen to increase to a maximum first and then to decline again, roughly returning to the same situation that was observed when both were adjusted to 45°. The same situation is seen to take place when the firing angles are again made unequal in the opposite direction.

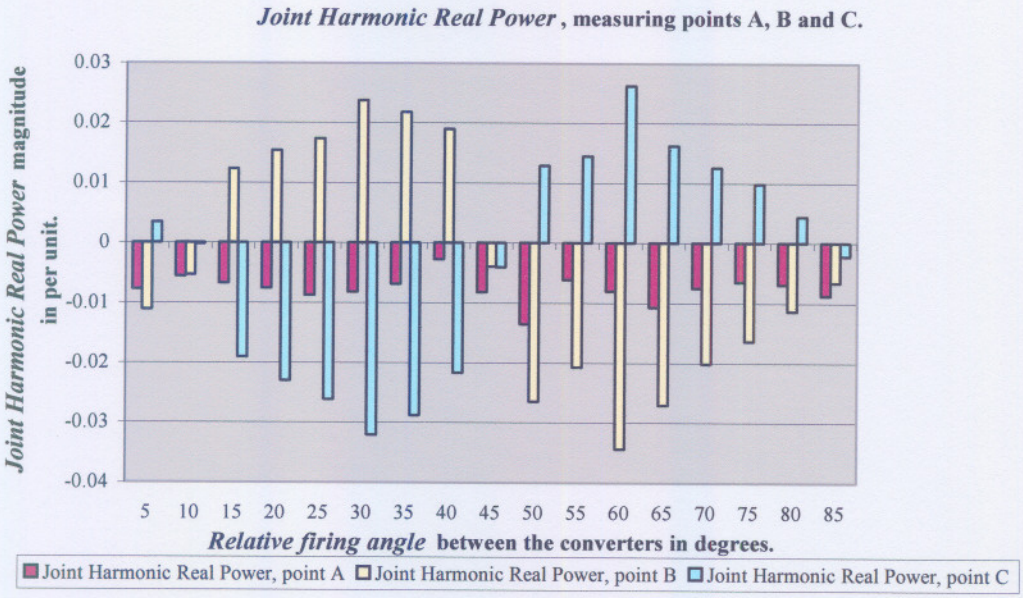

Figure 55: *Joint Harmonic Real Power* plotted against relative firing angles in the converters

The level of the *Joint Harmonic Real Power* is seen to change slightly for each firing angle (ξ_2-ξ_1) change but to remain in the direction of the source. In each case, the sum of the three joint harmonic powers in the three branches is observed to be zero as expected from circuit theory.

The reason for the sinusoidal-like change of the magnitude of the harmonic real powers in Figure 55 has not been analysed. These levels are brought about by the aggregate complex power contributions of all the harmonic levels. The corresponding change of the complex power angle in each phase will be related to the harmonic number on each converter. A change in 5° in firing angle, for example will bring about a change of 25° in the power angle in the 5^{th} harmonic, of 35° in the 7^{th}, of 55° in the eleventh harmonic and so on. Studying the behaviour of the *Joint Harmonic Real Power* in terms of sequence components is another possibility to separate the effect of unbalance for example and is subsequently presented.

5.3.2.2 Joint Harmonic Real Power: Sequence Components

Unbalance between the phases can be either due to an asymmetrical voltage source or due to an unbalanced load. The Fortesque transform can be applied to isolate the unbalance component.

Definition of the *Joint Harmonic Real Power* in the sequence components is similar to the *Joint Harmonic Real Power* in the phase components. The analysis of section 5.3.2.1 is repeated in terms of sequence components and the results are presented below.

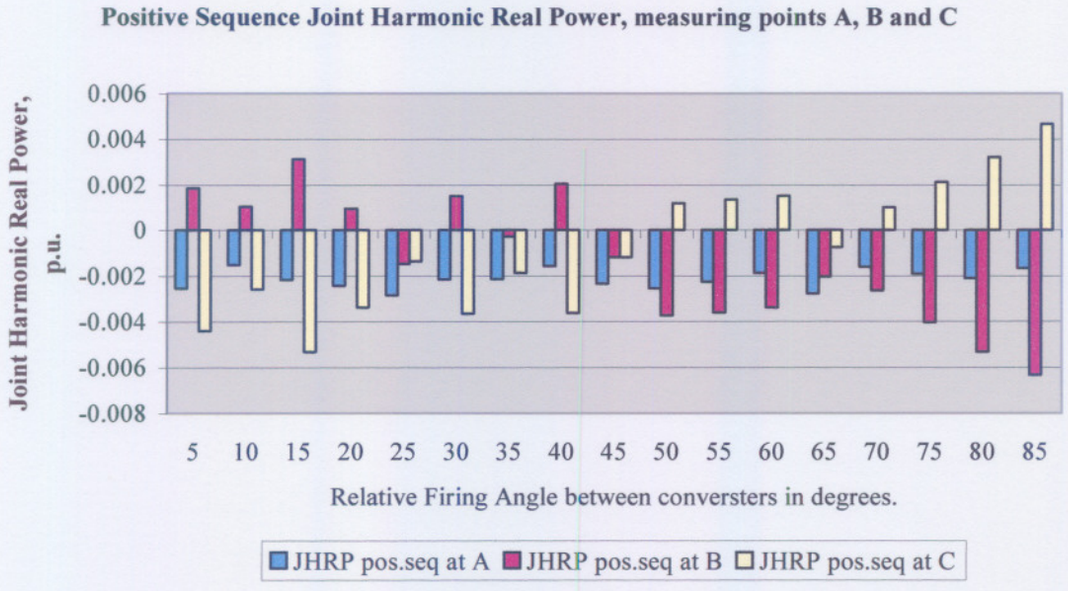

Figure 56: Positive Sequence *Joint Harmonic Real Power* levels plotted against relative firing (ξ_2-ξ_1) angles in the converters

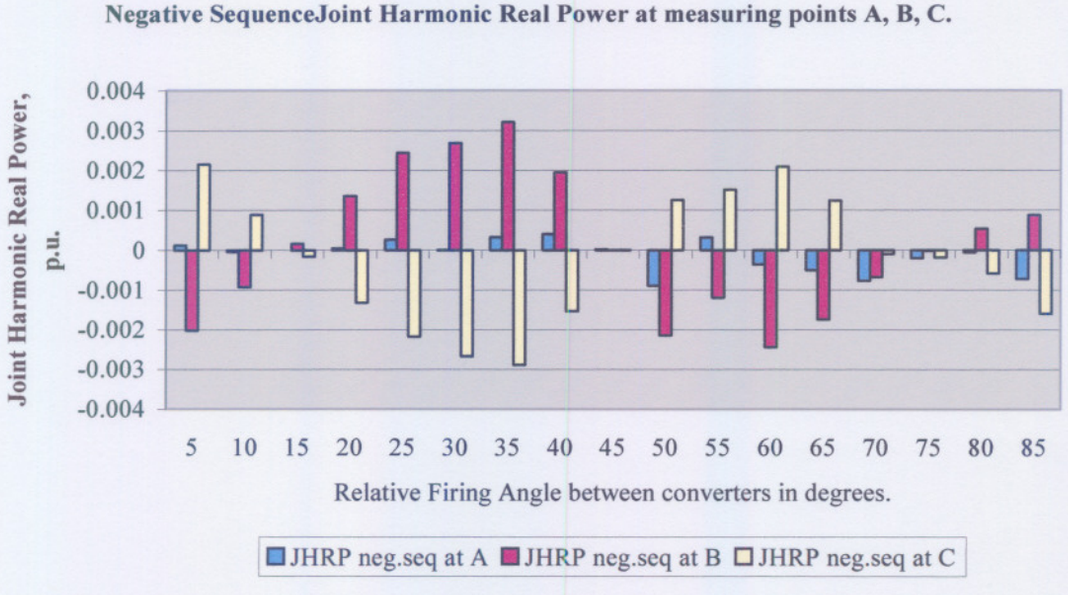

Figure 57: Negative Sequence *Joint Harmonic Real Power* levels plotted against relative firing (ξ_2-ξ_1) angles in the converters

Figure 56 indicates that *Joint Harmonic Real Power* in the positive sequence components at A at each firing-angle difference (ξ_2-ξ_1) is equal to the sum of the *Joint Harmonic Real Power* at B and C and does not change sign (direction).

An examination of the behaviour of the *Joint Harmonic Real Power* in the negative sequence components in Figure 57 shows that when the converter firing angles are identical, virtually no *Joint Harmonic Real Power* cross the measuring cross-sections A, B or C. At all other points, the *Joint Harmonic Real Power* value at A is again seen to correspond to the difference in *Joint Harmonic Real Power* values at B and C. There is an interchange of negative sequence harmonic real power between the converters and the source. The magnitude and direction of *Joint Harmonic Real Powers* in the negative sequence component is dominated by the unbalance, rather than by the absolute magnitudes of the powers.

5.3.2.3 Discussion

The results obtained through studying the *Joint Harmonic Real Power* in the phase and in the sequence components as function of firing angle show that:

- A difference in the firing angles of the converters brings about an interchange of harmonic real power between the converters and the source, rendering single-point measurements of this parameter ineffective for localising the source of the harmonic disturbance.

- Neither *positive-sequence* or *negative sequence harmonic real power* measurements will be able to assist in determining whether the harmonic producing sources are located to the left or to the right of measuring cross-sections at the PCC's of consumers.

- Measurement at the source terminals confirms that the magnitude of the *positive sequence harmonic real power* will always be propagated toward the linear harmonic source. When negative *sequence harmonic real power* is propagated away from, or into the source, it is of very little significance as to who is generating the harmonics. It does, however, contribute to show the presence of unbalance through this power quantity.

5.3.3 Real life measurements

5.3.3.1 Introduction

Verification of the computer simulation results now prove the findings in the frequency-domain and in the time domain, namely that single-point measurements in a three-phase electrical network with nonlinear distributed loads can not be used to localise sources of distortion. This now proves once-for-all that single-point measurements can not be used to localise or quantify distortion sources in a practical electrical power system.

The requirements that were met in the measurements that were carried out on a scaled-down island electrical distribution network to obtain this final proof required the following approach:

- The configuring of the scaled down power system that were set up to match the systems that were

studied in the frequency-domain and in the time-domain.

- Using instrumentation to capture waveform data synchronously in time to a very high accuracy and at all the nodes in the power system.
- Avoiding the skewing between adjacent channels when digitising waveforms.
- Digitising at as high a resolution as possible and using verifiable high accuracy voltage and current transducers.

5.3.3.2 Measurements obtained

The physical power system on which the measurements were carried out[37], are rated at base values of 5 kVA and 380 V and was set up to match the power system that was studied through frequency- and time-domain modelling in sections 5.3.1and 5.3.2. Synchronised measurements were obtained at all the three-phase nodes in the power system. It is shown in Figure 10, which is the real-life modelling of Figure 53. The instrumentation setup and specifications thereof are presented in section 3.5. To enhance readibility of this section, Figure 10 is inserted again below:

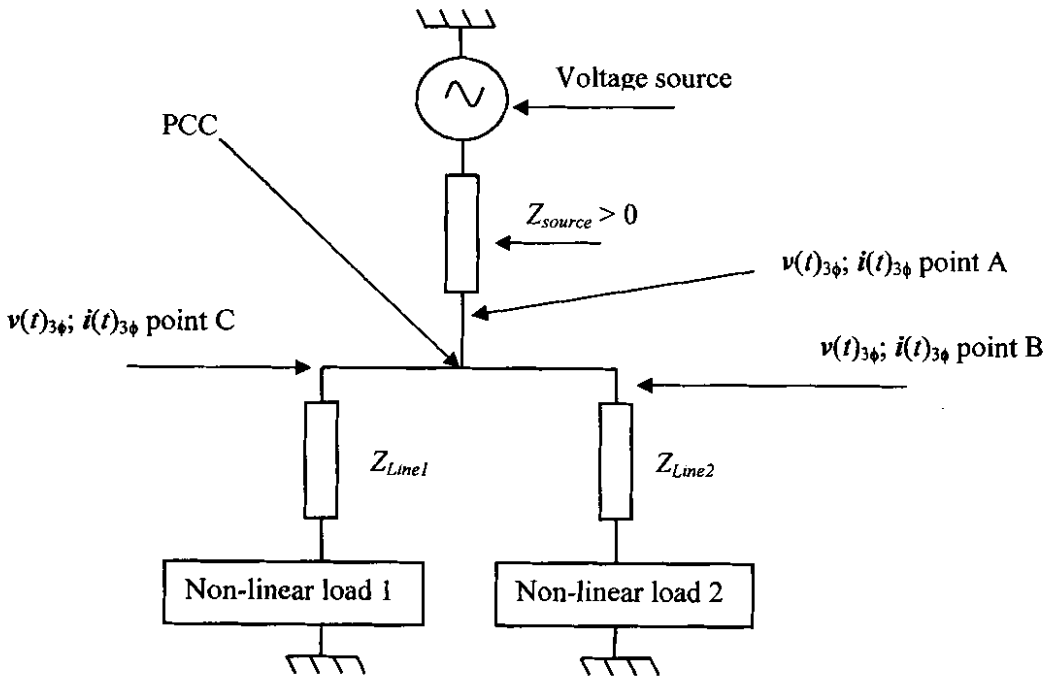

Figure 58: Measurement configuration as used with 3 Impedograph™ meters each installed at points A, B and C

[37] Appendix 3 list the specifications of the Impedograph™ instruments used to obtain measurements in Figure 58.

Two 6-pulse phase-controlled rectifiers, similar to the nonlinear loads used in the time-domain simulation of section 5.3.2 were used to set up the nonlinear loads. The firing angle of one of the two 6-pulse rectifiers was maintained constant while the other was varied. The three-phase voltages and currents at each measuring cross-section were then recorded for each setting of firing angle. Adjustment of the firing angle of one rectifier at a time, represent a difference in the relative firing angle similar to the change in relative firing angle (ξ_2 - ξ_1) as used in the frequency- and time-domain simulations as described in section 5.3.2.

Typical voltage and current waveforms that were measured for each of the three measuring points in Figure 58 and is shown below (the voltage waveforms shown reflect those at the PCC). Please note that the voltages shown in the graphs are measured between line and neutral. The supply voltage amplitude was chosen to be variable (as described for the laboratory power system in chapter 3) to adjust current amplitudes within the range that the current transducers can detect accurately.

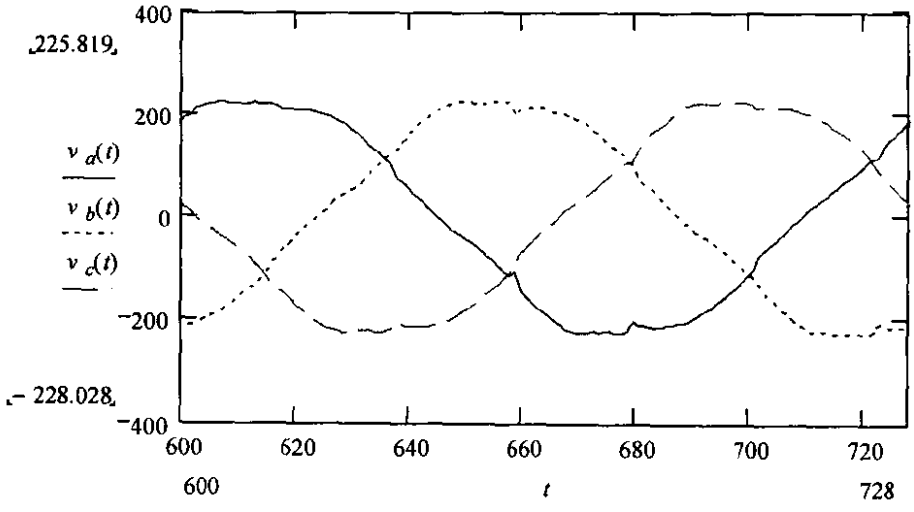

Figure 59: Typical three-phase voltage waveform at the PCC in Figure 10

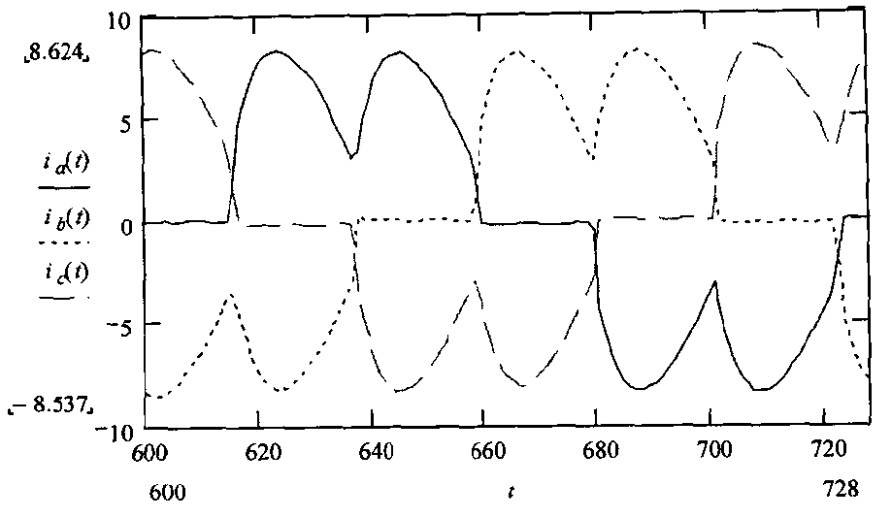

Figure 60: Typical three-phase supply line current waveform (measuring point A in Figure 58)

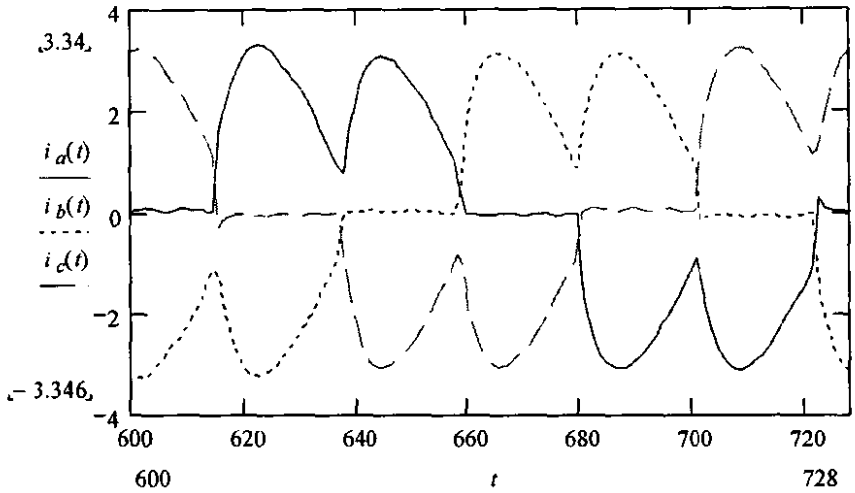

Figure 61: Typical three-phase load current waveform withdrawn by load 1 in Figure 58

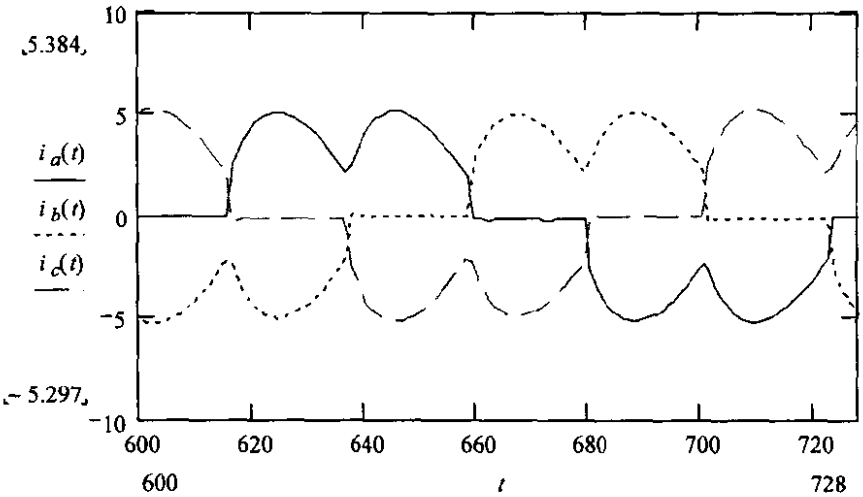

Figure 62: Typical three-phase load current waveform withdrawn by load 2 in Figure 58

Analysis of the waveforms depicted in Figure 59, Figure 60, Figure 61 and Figure 62 in the frequency domain, results in the graphs presented below (shown only for phase *b*):

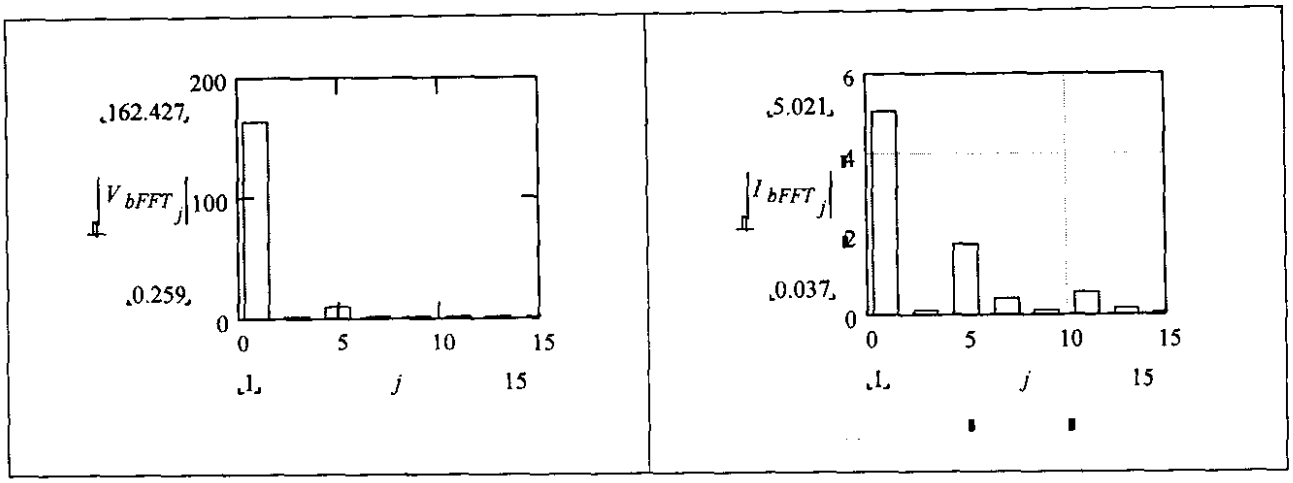

Figure 63: Harmonic content of voltage in phase *b* at PCC and total current in phase *b* drawn from the fundamental frequency energy source

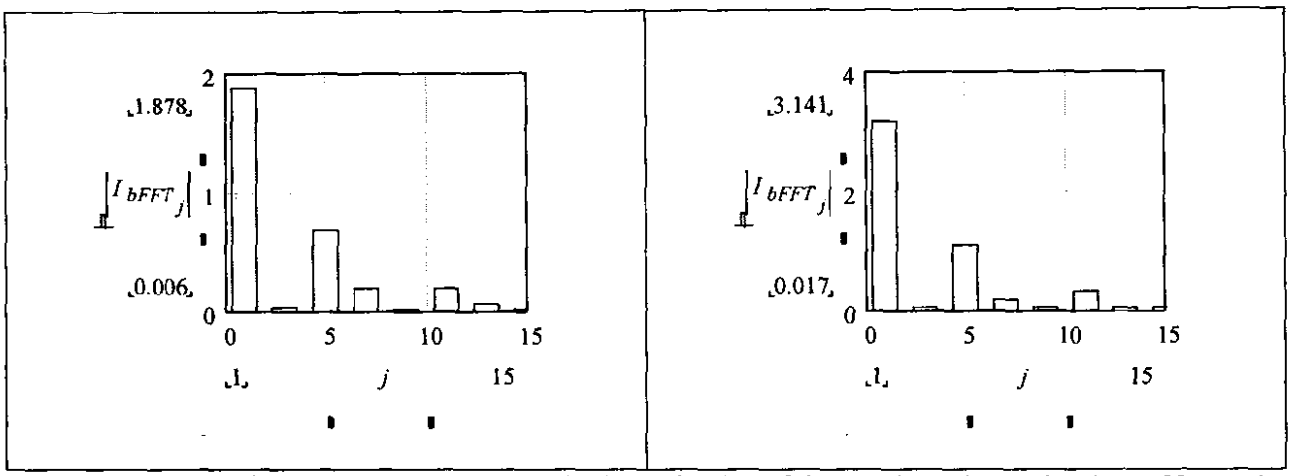

Figure 64: Harmonic content of the current withdrawn in phase *b* by nonlinear load 1 in Figure 58 (graph on the left hand side above) and nonlinear load 2 in Figure 58 (graph on the right hand side above)

5.3.3.3 Data analysis

The *Joint Harmonic Real Power* at each measuring node was calculated for each instance of firing angle. Care was taken in the data analysis carried out in MathCAD to ensure that energy conservation principles were respected. Measurement errors, for example, could be detected when the total energy flowing into the PCC did not match the total energy flowing out of the PCC into the two loads.

The firing angle of one rectifier was maintained constant while that of the other were varied to obtain a range of firing angle differences between the two rectifiers. The magnitude of the resistive load, fed by each rectifier, remained the same. Two such investigations were repeated; the first investigation used a fixed firing angle of 100^0 for the one rectifier whilst the firing angle of the second rectifier was varied.

The second investigation used a fixed firing angle of 30^0 for the one rectifier whilst the firing angle of the second rectifier was varied.

The graph below depicts the exchange of *Joint Harmonic Real Power* between the three measuring points for the first investigation. The load current of load 1 in Figure 58 was kept relatively small through a fixed firing angle of 100^0:

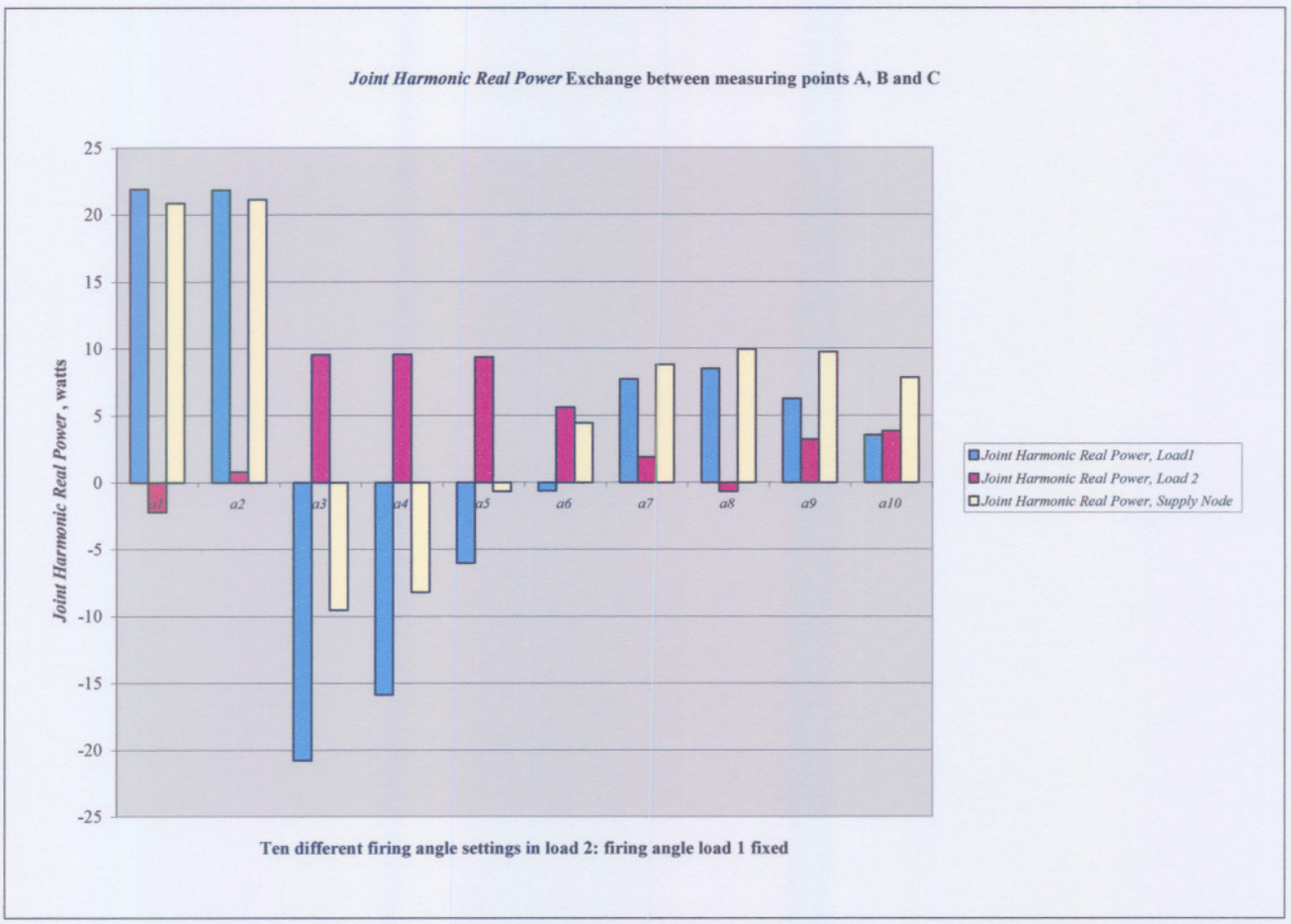

Figure 65: *Joint Harmonic Real Power* Exchange between measuring points A, B and C in Figure 53 obtained in a similar real life power system: investigation no 1

The *Joint Harmonic Real Power* in Figure 65 summates to zero for each instance of firing angle. Because the firing angle was not directly measurable, it had to be estimated from the waveform data and is therefore not indicated in exact degrees in these two investigations.

A second investigation was carried out with a fixed firing angle for load 1 in Figure 58 of 30^0:

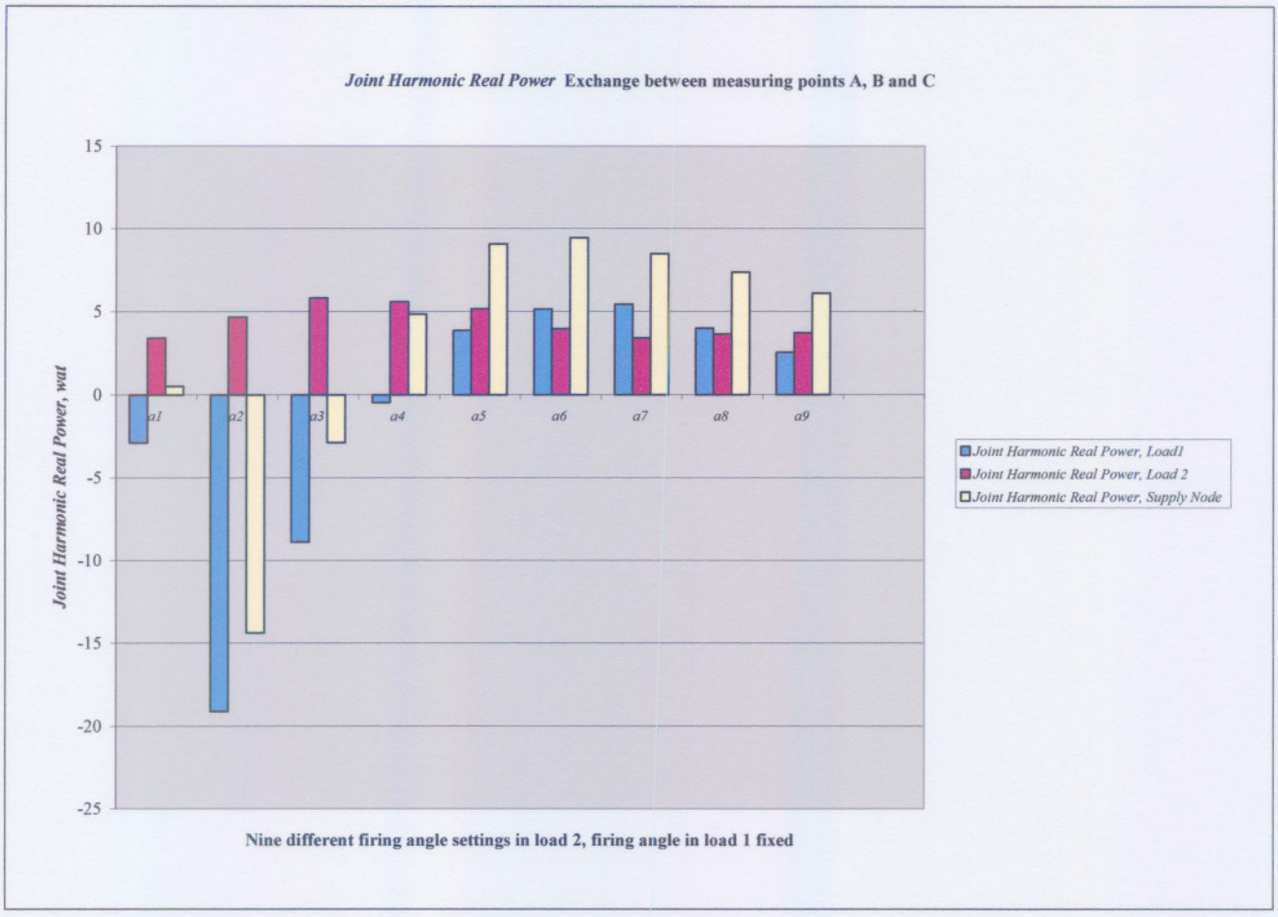

Figure 66: *Joint Harmonic Real Power* Exchange between measuring points A, B and C in Figure 53 obtained in a similar real life power system: investigation no 2

The *Joint Harmonic Real Power* in Figure 66 again summates to zero for each instance of firing angle.

5.3.4 Conclusion

The results of the time-domain simulation confirm the findings of the frequency-domain modelling presented in [57]. A final confirmation of the results of these simulation studies is furthered by the results of section 5.3.2. It was obtained through measurements in a real life power system similar to the power system used in the computer simulations.

The results reported in [58], section 5.3.2 and section 5.3.3 of this thesis presents final proof of the findings put forward in [57]. It was formulated as a research problem in chapter 1, namely that it is impossible to geographically localise a single source of distortion in a power system with distributed sources of distortion through single-point measurements.

When a network contains more than one non-linear load such as phase-controlled converters in which fundamental phase angle changes take place, there will be an interchange of harmonic real power between these loads. That makes it impossible to localise a source of distortion in a power system with more than

one distortion source through single-point measurements. It is only possible to localise distortion-producing sources in a practical power system by measuring harmonic active power flow in all the terminals of all the consumers simultaneously and synchronously.

Using the level and direction of harmonic real power in single point measurements for tariff calculation in endeavours to dissuade consumers from generating distortion is also an invalid approach. Unless ways can be found around this problem, all research and development that wishes to utilise this principle should be reconsidered.

5.4 LOCALISATION TECHNIQUES DESCRIBED IN THE LITERATURE

5.4.1 Introduction

A number of approaches have been used in literature to localise and characterise sources of steady state distortion in an interconnected power system through single-point measurement. Several indexes and approaches to quantify the contribution to *THVD* at the PCC has been formulated and reported in literature. The most important of these contributions are considered in this section.

Cristaldi [44], [45], [46] uses the Park transform to distinguish between the negative harmonic real powers generated by the load non-linearity and those that are generated by the load unbalance. The zero sequence components are discarded and the Park voltage and current vectors are decomposed into their Fourier components. The real power for the different frequency components are calculated and used in the definition [44] of two indices, an "unbalance" index C_u and a "nonlinearity" index C_{nl}. The level of the unbalance is commensurate with the magnitude of C_u. The level of the distortion is commensurate with the value of C_{nl}.

Muscas [53] contributed by formulating a *"Harmonic Global Index"* (*HGI*) and a *"Harmonic Phase Index"* (*HPI*). It is claimed that these indices can be used to localise a source of distortion by quantifying its relative distortion contribution. The indices are based on the sign of the different harmonic active powers at each frequency and relate the quadratic ratio of the polluting currents produced by the load to those produced by the supply.

Both methods above are dependent upon the direction of propagation of the real harmonic power and will not work if loads on either side of the measurement cross-section interchange harmonic real power.

A novel combination of three different indices has been combined subsequently into a "global quality index" by Cristaldi [55]. This approach is reported to achieve success in localisation of distortion source within a network with multiple distortion sources distributed over the electric power network. The three indices used in the "combined global quality index" have been proposed previously to aid in localisation of distortion sources.

1. The ratio of *global harmonic current distortion* to the *global harmonic voltage distortion* in terms of positive sequence quantities.

2. The *supply loading index*.

3. The *harmonic global index*.

The formulation of the *global quality index* is evaluated in section 5.4.4. In order to do it, it requires reporting the original power quality index formulations of Cristaldi [44] and Muscas [53] in section 5.4.3.

A different approach to the localisation of distortion sources is to use invasive methods [52], [59]. The system is purposely disturbed and the analysis is based on the resulting system response. This approach has practical drawbacks because of the difficulty of continuously injecting disturbances of sufficient magnitude into the network. The injection of disturbances in the form of momentary currents or voltages cannot be carried out continuously and continuous measurement will therefore not be possible. This method may not be affected by the presence of multiple distortion sources. It is not suitable for tariff and compensation purposes. The detail of this approach is not analysed in this document.

The use of state estimators is another approach. Farach [47], [48] described a procedure in which state estimation techniques are employed to identify the best connection localities for harmonic sensors when searching for distortion producing sources. The "underdetermined harmonic state estimator" [47] performs better with *a priori* information, but there is a limit to the general practical application of the method. The performance of the state estimator is only evaluated in the presence of a single distortion source and it still has to be proven whether it will also be able to achieve its goal in the presence of multiple distortion sources.

Another state estimation application on the localisation of distortion sources is that of Heydt [49] who suggested a least squares state estimator. As the interpretation of the results of this method depends on the direction of the real harmonic power, it will not be practicable in the presence of multiple distortion sources.

Hong and Chen [63] investigated artificial intelligence to localise sources of distortion. Fuzzy theory and artificial neural networks (ANN) is combined to localise sources of distortion without *a priori* knowledge on the localisation of these distortion sources. The validity of their claims is uncertain as they assume certain harmonic voltages to be "caused" by certain "injected' harmonic currents at busbars. Such assumptions are constrained by the principles set out in sections 5.3. Their application of fuzzy theory, ANN and the devised methodology seems novel. If parameters such as the combined global quality index v_k could be incorporated, this could be an avenue to be pursued.

Emanuel [60], [61], [62] investigated the possibility of a harmonic tariff system that make use of single

point measurements and other relevant technical issues pertaining to harmonic pollution and the localisation of the sources contributing. It is valuable reference material because of the important practical aspects that are considered, given that the synchronous measurement of all nodes in a network is not readily available.

Srinivasan [43] make use of the direction of harmonic active power to separate the load current into the "distorting" current and the "non-distorting" current. Srinivasan has only reported single-phase evaluations and results. It is not possible to use his suggestion by extending this distortion source localisation technique based on single-phase formulations to three phase networks. It will not work in a three-phase system with more than one distortion producing source.

In an analysis of the existing literature on the subject of localisation of distortion sources, the non-invasive methods using single-point measurement are based on the direction of propagation of the harmonic real powers. These methods will therefore not work in power transmission networks generally where the presence of multiple distortion sources is a practical reality. Only the approach of Cristaldi, Ferrero and Salicone [55] deserves further discussion because they employ a distributed measurement system.

5.4.2 Cristaldi: The localisation of distortion sources.

Cristaldi [44], [45] applied the Park[38] transform to separate load unbalance and non-linear loading because both can generate negative harmonic real powers. As the Park transform is a linear transform, the Park voltage and current vector will also reflect the nonsinusoidal conditions of the phase domain and a Fourier series can be used to study the frequency-domain components of the Park voltage and current vector (periodic conditions assumed):

$$v(t)_{Park} = \sum_{h=-\infty}^{+\infty} V_{Park,h} e^{jh\omega t}$$
$$i(t)_{Park} = \sum_{h=-\infty}^{+\infty} I_{Park,h} e^{jh\omega t} \qquad (218)$$

The Fourier series of the Park voltage and current vector are related to the Fortesque positive and negative sequence components. The positive harmonic orders $h > 0$, are the positive sequence components and the harmonic orders $h < 0$, are the negative sequence numbers at frequencies $|h|\omega_1$. This is shown below for the Park voltage phasors, similar to the Park current phasors:

---

[38] Detail of the Park transform applied in nonsinusoidal power systems, can be found in section 4.4.

$$V_{1h} = V_{Park,h} \quad if \quad h > 0$$
$$V_{2h}^{*} = V_{Park,h} \quad if \quad h < 0 \tag{219}$$

As the Park voltage and current phasors describe the "three phase only" components of the power system, the harmonic active power that flow through a three-phase measuring cross-section can be described accordingly [44]:

$$P_{Park,h} = P_{3\phi,h} = \mathrm{Re}\left(V_{Park,h} I_{Park,h}^{*}\right) \text{ if } h \geq 0;$$
$$P_{Park,h} = P_{3\phi,h} = \mathrm{Re}\left(V_{Park,h}^{*} I_{Park,h}\right) \text{ if } h < 0 \tag{220}$$

Both a nonlinear load and unbalance in the load when the supply voltage waveform is nonsinusoidal can cause negative harmonic active powers (fundamental frequency active power assumed positive).

Cristaldi [44] defined number sets K_l, K_u, and K_{nl} in terms of harmonic orders:

$$K_l = \left\{h \middle| \left(P_{Park,h} > 0\right) \wedge \left(P_{Park,-h} > 0\right)\right\}$$
$$K_u = \left\{h \middle| \left(P_{Park,h} < 0\right) \wedge \left(P_{Park,-h} > 0\right)\right\} \tag{221}$$
$$K_{nl} = \left\{h \middle| \left(P_{Park,h} < 0\right) \wedge \left(P_{Park,-h} < 0\right)\right\}$$

Subscript "*l*", "*u*" and "*nl*" refers to "linear", "unbalance" and "nonlinear" respectively. Based on the harmonic number sets above, the following coefficients [44] are then defined:

The *unbalance index*, C_u:

$$C_u = \frac{\sum_{h \in K_u, P_{Park,h} < 0} P_{Park,h}}{P_{Park}} \tag{222}$$

The *nonlinearity index* C_{nl}:

$$C_{nl} = \frac{\sum_{h \in K_{nl}, P_h < 0} P_{Park,h}}{P_{Park}} \tag{223}$$

P_{Park} is the total Park active power found at the measuring cross-section and is obtained by summing over all the positive and negative sequence harmonic real powers, including the fundamental.

- The indices in equation (192) are defined such that both C_u and $C_{nl} \leq 0$.
- If the effect of load unbalance is neglible at all harmonic frequencies, then $C_u = 0$.
- $C_u \neq 0$ indicates that the load is the cause of the unbalance.
- $|C_u|$ represents the level of unbalance caused by the load.
- If the effect of load non-linearity is negligible at all harmonic frequencies then $C_{nl} = 0$.
- Cristaldi [44] interpreted $C_{nl} = 0$ as that the load cannot be considered to be the source of distortion.
- $C_{nl} \neq 0$ indicate that the load is causing distortion.
- $|C_{nl}|$ represents the level of distortion caused by the nonlinear load.

The above method seems to offer a novel way to separate the load non-linearity from the load unbalance. It could have been a very exciting approach to disseminate these effects and implement it in a tariff system. These definitions are however limited to the principles furthered in sections 5.3 and in [58]. It will be valid in the presence of one distorting load in the network only is considered.

5.4.3 Muscas: The "Harmonic Phase Index" *HPI* and the "Harmonic Global Index", *HGI.*

Muscas [53] defined the harmonic phase index *HPI* and the harmonic global index *HGI* based on currents, not powers. It aims to distinguish between the quality of power delivered and the power withdrawn independent of the network conditions. These indices increase in relation to the increase in distortion and in unbalance as caused by the load. It is also claimed to be measurable with sufficient accuracy with practical instrumentation.

5.4.3.1 The Harmonic Phase Index: HPI

On a per phase basis, the three wire current flowing through a measuring cross-section is arranged into a matrix containing the phase current vectors where the rows are the harmonic current phasors arranged in three columns for each phase:

$$\boldsymbol{I}_{3\phi,h} = \begin{bmatrix} \boldsymbol{I}_{a1} & \boldsymbol{I}_{b1} & \boldsymbol{I}_{c1} \\ \downarrow & \downarrow & \downarrow \\ \boldsymbol{I}_{ah} & \boldsymbol{I}_{bh} & \boldsymbol{I}_{ch} \\ \downarrow & \downarrow & \downarrow \\ \boldsymbol{I}_{aN} & \boldsymbol{I}_{bN} & \boldsymbol{I}_{cN} \end{bmatrix} \tag{224}$$

In the above equation, $\boldsymbol{I}_{3\phi,h}$ is a matrix to group the three-phase harmonic current phasors which are arranged per phase in each of the three columns and per harmonic order h in each row. Number N is the highest harmonic order considered in equation (224).

Two current vectors are distinguished in $\boldsymbol{I}_{3\phi,h}$ as defined in equation (224):

1. Current vector $\boldsymbol{I}_{S3\phi,h}$ represents the three-phase harmonic current phasors caused by the voltage source:

$$\boldsymbol{I}_{S3\phi,h} = \begin{cases} 0 & if \quad P_{3\phi,h} \le 0 \\ \boldsymbol{I}_{3\phi,h} & if \quad P_{3\phi,h} > 0 \end{cases} \tag{225}$$

2. Current vector $\boldsymbol{I}_{L3\phi,h}$ represents the harmonic current phasors caused by the load non-linearity/time-variance and/or unbalance:

$$\boldsymbol{I}_{L3\phi,h} = \begin{cases} 0 & if \quad P_{3\phi,h} \ge 0 \\ \boldsymbol{I}_{3\phi,h} & if \quad P_{3\phi,h} < 0 \end{cases} \tag{226}$$

If the above methodology is applied to a four-wire power system, it will require special considerations as the homopolar voltage components can cause misinterpretation of the phase power [53].

The *Harmonic Phase Index* (*HPI*) is then defined based on (225) and (226):

$$HPI = \frac{k_2 I_{2,1}^2 + \left\| \boldsymbol{I}_{L3\phi,h} \right\|^2}{\left\| \boldsymbol{I}_{S3\phi,h} \right\|^2} \tag{227}$$

The index[39] k_2 is defined as either a 0 or a 1 depending on the sign of the negative sequence power at the fundamental frequency:

$$k_2 = \begin{cases} 0 & if \quad P_{2,1} \ge 0 \\ 1 & if \quad P_{2,1} < 0 \end{cases} \tag{228}$$

[39] The list of symbols contains a comprehensive explanation of symbols used, on this case, for example, take note that subscript "2" refers to negative sequence quantities.

The definition of the index *HPI* is therefore based on the ratio of quadratic distorting currents to the currents that are dominated by the supply characteristics. The index k_2 relies on the sign of the harmonic real power and will be influenced by the principles in section 5.3 if more than one distorting source is present.

5.4.3.2 Harmonic Global Index: HGI

Muscas [53] grouped the harmonic active powers derived from the Park voltage and current vector as follow:

$$\begin{aligned} P_{\text{Park},h} &= \text{Re}\left(V_{\text{Park},h} I^{*}_{\text{Park},h}\right) \quad for \quad h \geq 0 \\ P_{\text{Park},h} &= \text{Re}\left(V^{*}_{\text{Park},h} I_{\text{Park},h}\right) \quad for \quad h < 0 \\ P_{0,h} &= \text{Re}\left(V_0(h) I^{*}_0(h)\right) \end{aligned} \tag{229}$$

A matrix containing the Park current phasors is then constructed; again the "source" and the "load" Park current harmonic phasors are separated as either $I_{\text{SPark},h}$ or $I_{\text{LPark},h}$ respectively (note that this are Park harmonic current harmonic phasors whilst in section 5.4.3.1 the phase-domain current harmonic phasors were grouped).

The dimension of this matrix is (3*N*+2) with *N* the highest harmonic order considered. The complex Fourier expansion of the Park current vectors contributes (2*N*+1) elements as the harmonic index is over the range -*N* to +*N*. The remaining (*N*+1) components are the zero sequence current harmonic components, which, as it is a real Fourier series, only extend over the harmonic index range of 0 to +*N*. The construction of this matrix of current phasors is through the following methodology:

Step 1: The Park current harmonic phasors in $I_{\text{SPark},h}$ and $I_{\text{LPark},h}$ are grouped into a "source" Park current vector $I_{\text{SPark},(h+N)}$ and $I_{\text{LPark},(h+N)}$:

$$\begin{aligned} I_{\text{SPark},(h+N)} &= \begin{cases} 0 & if \quad P_{\text{Park},h} \leq 0 \\ I_{\text{Park},h} & if \quad P_{\text{Park},h} > 0 \end{cases} \\ I_{\text{LPark},(h+N)} &= \begin{cases} 0 & if \quad P_{Park,h} \geq 0 \\ I_{\text{Park},h} & if \quad P_{\text{Park},h} < 0 \end{cases} \end{aligned} \tag{230}$$

The harmonic index *h* is over the range –*N* tot +*N*.

Step 2: The zero sequence current harmonics are grouped into the "source" ($I_{\text{Spark},(h+2N+1)}$) and the "load" ($I_{\text{Lpark},(h+2N+1)}$) zero sequence current vectors:

$$I_{\text{SPark},(h+2N+1)} = \begin{cases} 0 & if \quad P_{0,h} \le 0 \\ I_0(h) & if \quad P_{0,h} > 0 \end{cases}$$
$$I_{\text{LPark},(h+2N+1)} = \begin{cases} 0 & if \quad P_{0,h} \ge 0 \\ I_0(h) & if \quad P_{0,h} < 0 \end{cases} \tag{231}$$

The "*Harmonic Global Index*" is defined as:

$$HGI = \frac{\|I_{\text{LPark}}\|^2}{\|I_{\text{SPark}}\|^2} \tag{232}$$

The Park transform enables a "global" power quality index (*HGI*) by the ratio of quadratic distorting currents to the currents dominated by the supply characteristics. The index *HGI* also use the sign of the harmonic active power which will not be valid if more than one distorting source is present in the network under consideration. Muscas [53] reports in [53] that the *HPI* and *HGI* indices correctly identify the non-linear loads as sources of distortion by single point measurements in networks with more than one distorting source in the network under consideration. This is an invalid claim as the principles of section 5.3 have demonstrated.

5.4.4 Cristaldi, Ferrero and Salicone: a Distributed Measurement approach; the Combined Global index, v_k.

A distributed measurement system that acquires non-synchronous data is described in [55] to monitor a number of power quality indices on every load connected to the PCC. A master unit then interpret these indices in order to localise and quantifies the contribution of a distortion source to unbalance and/or harmonic distortion. This power quality index is a combination of three other power quality indices. An analysis of this technique is presented.

5.4.4.1 Power Quality indices calculated at each measuring point

The *Global Harmonic Total Distortion in Voltage* and *Global Harmonic Total Distortion in Current* in a balanced three-phase power system are defined in terms of phase quantities [55]:

$$GHTD_v = \sqrt{\frac{V_e^2}{V_{e1}^2} - 1}$$
$$GHTD_i = \sqrt{\frac{I_e^2}{I_{e1}^2} - 1} \tag{233}$$

A similar nonconformity index based on the fundamental frequency positive sequence values is defined [55] for a nonsinusoidal unbalanced three-phase system for voltages and currents with respect to a balanced three-phase system:

$$GHTD_{v+} = \sqrt{\frac{V_e^2}{V_1(1)^2} - 1}$$
$$GHTD_{i+} = \sqrt{\frac{I_e^2}{I_1(1)^2} - 1} \tag{234}$$

Two ratios of current and voltage distortion are then defined; the first ratio, η, is based on phase quantities and the second ratio, η^+ is based on positive sequence quantities:

$$\eta = \frac{GHTD_i}{GHTD_v} \tag{235}$$

$$\eta^+ = \frac{GHTD_{i+}}{GHTD_{v+}} \tag{236}$$

A supply and loading quality index are defined [54] as follows:

$$\xi_{slq} = \frac{P_{3\phi}}{P_1(1)} \tag{237}$$

Symbol $P_1(1)$ refer to the active power in the fundamental frequency of the positive sequence components of voltage and current. The idea is that the supply and *loading quality index*, $\xi_{slq} > 1$ when the source is causing the distortion and that $\xi_{slq} < 1$ when the load is the prevailing source of distortion.

5.4.4.2 Rationale for the combined global index

The different indices in the previous section 5.4.4.1 have different limitations discussed in literature, such as [53], [57] and [58] and thus a combination of indices is proposed in [55]. The expectation [55] is for the previous reason thus that a combination of indices in one global index should provide "more" correct information on the localisation of the distortion source.

These indices are determined on all supply and loading lines connected to the PCC and not only at a single measuring point which was indicated to be a major limitation in the localisation of distortion sources in section 5.3.

5.4.4.3 *The Combined Global index, v_k*

The proposed combined global index is formulated as:

$$v_k = \frac{1}{3}\left(\frac{\xi_{slq_k}^{-1}}{\xi_{slq_S}^{-1}} + \frac{HGI_k}{HGI_S} + \frac{\eta_k^+}{\eta_S^+}\right) \tag{238}$$

The subscript k refers to the line number out of the PCC and S refers to the supply line feeding the PCC. Note that the index v_k is defined with the aim that the following three conditions can be distinguished:

- $v_k = 1$: The power system experience perfect sinusoidal and balanced conditions.
- $v_k > 1$: The load connected to line number k is producing distortion.
- $v_k < 1$: The voltage source connected to line number k is producing distortion (PCC injecting distortion).

5.5 CONCLUSION

The results reported in [55] are indeed promising. Application of the combined global index v_k was done by plotting the trend of the v_k for every line going out of a PCC. The results [55] clearly indicated that the three indices (η^+; ξ_{slq}; *HGI*) could not conclusively identify any of the loads as a disturbing load. Careful consideration of these results, show that these three indices in fact confirm the results obtained in sections 5.3.

Most important of [55] are the study of the trend of v_k plotted as function of time for each of the lines going out of the PCC. The combined global index clearly characterised a specific load as either contributing to distortion or absorbing distortion. A valuable contribution is in the standard uncertainty evaluation of the measured indices. Application of a 12 bit A/D card with voltage and current transducers that have a measurement uncertainty of 0.01% caused a 0.1% uncertainty in the active power calculations. The index v_k, has been calculated with an uncertainty of less than 0.06.

The determination of v_k is practical due to the sufficient certainty by which it could be measured in a low-voltage network (380V network in which the experiments were carried out.). Of all the localisation procedures currently known to the author, this methodology therefore mostly deserve further investigation.

6 CONCLUSIONS AND RECOMMENDATIONS

The modern electrical power system continues to present technological challenges to be addressed in order to effectively manage electrical energy. Solid-state technology presents exciting new opportunities and the advances therein bring about ever-increasing growth in the numbers and magnitudes of non linear loads. Nonsinusoidal conditions have not only come to stay in modern power systems, but its ferocity is also expected to increase. In order to quantify and qualify relevant nonsinusoidal phenomena, the one goal of this thesis was to evaluate alternative power theories that have been developed over the latter part of the last century. The second goal was to investigate techniques which can determine the relative contribution to the degradation of the overall power quality in an interconnected power system.

Electrical power quality is gaining recognition as an ultimately important feature of power systems. The reasons for the generation of low power quality and how it is brought about, as well as what its impacts are on power systems were discussed in chapter 1. International power quality standards were discussed to examine different approaches made in efforts to deliver acceptable electrical power quality to clients. These standards are dynamic because new knowledge enables redefinitions of distortion power and analysis through it of distorted power system operation that will enable better tariff structures to be devised.

The analysis of nonsinusoidal power systems requires special consideration, for example mathematical techniques such as the Fortesque and Park transform requires reformulation as was demonstrated in chapter 2. Unbalance between phase conductors necessitates a four-wire approach as the role of the neutral conductor can not be ignored. An alternative transform that enable three-dimensional space-vector formulation of four-wire three-phase quantities, was proposed as a mathematically and physically sound approach.

A comprehensive analysis of specifically the Czarnecki power theory resulted in a demonstration of a deficiency thereof. It is a well known power theory as it was published in numerous scientific journals. Application thereof with modern instrumentation seems to be simple. Further, the isolation of "unwanted" effects in the power system by means of the Czarnecki power components could be a powerful tool in the management of electrical power quality. It is shown to be an invalid approach to the definition of electrical power in practical three-phase power systems in chapter 4, however, rendering it less suitable for global use. The results of chapter 4 verify the concerns expressed with regard to the Czarnecki power theory by Emanuel in [31].

The deficiency of the Czarnecki power theory was shown in chapter 4. One reason is the definition of power components in the phase-domain when the waveforms in the three-phase power system are distorted and unbalanced.

Chapter 4 propose alternative approaches in defining power. To formulate power in a transformed domain, such as by application of the Park voltage and current vector is shown in chapter 4 to be valid if it is applied to a three-wire power system. Ferrero [26] advanced the analysis of three-wire three-phase power systems significantly by the latter contribution. Practical application of the Park transform in compensation of unwanted effects was successfully demonstrated by Akagi [22].

Electrical quantities relating to a four-wire power system can be transformed to a three-dimensional space vector representation of voltage and current, as formulated by Ferrero, Giuliani and Willems [29]. Chapter 4 reported it as the preferred approach in analysis of four-wire nonsinusoidal power systems and proposes further investigation as to application in compensation techniques and the devising of tariff systems.

Mathematical formulations to analyse a power system, have to be tested for validity against physical laws which require consideration of electro dynamical principles. Emanuel has advanced insight into the physical phenomena in a nonsinusoidal three-phase power system by demonstrating application of the Poynting vector [30].

Chapter 5 proved that single-point measurements in a power system with nonlinear loads distributed all over can not be used to quantify the relative contribution to overall degradation in electrical power quality. This is a validation of the results of Swart [57] and in this thesis, proved by the results of both a time-domain simulation approach and real-life measurements.

It is however impractical to measure all nodes synchronously to be able to quantify the contribution of every nonlinear load. If it was possible, then the electrical utility and all customers could be made responsible for the power quality at every node through a creative tariff formulation. This could be an important tool in managing power quality.

Harmonic pollution of the power system degrades the most important energy commodity of modern times. Important technical considerations thereto have been contributed, for example by Emanuel [60], [61], [62]. If the localisation and the contribution of a certain distortion source are known, compensation can be forced upon the responsible consumer through tariff imposition.

Localisation techniques to isolate a specific source of waveform distortion in the power system are described in the literature. Chapter 5 evaluates a few examples such as [44], [47], [49], [53] and [63]. It is then proposed that the novel combination of a new power quality index and a distributed measurement system that does not require perfectly synchronised measurements as described in [55] should be further investigated towards implementation in practical power distribution systems.

Power quality management in power systems should adopt a holistic approach to performance objectives as not only "circuit-specific" matters are influencing modern power quality management. Legislation and

regulations has to be implemented which requires not only appropriate instrumentation but also effective management models. The recommendations made in Chapter 6 on further investigations could be valuable in support of such efforts.

1 APPENDIX A: PUBLICATIONS

1.1 INTRODUCTION

Publications which are based on research work carried out in this thesis are listed in this appendix. There are other contributions made to conferences (national and international) but only the publications published in accredited journals, are used. These publications are listed in chronological order.

1.1 PAPER 1

1.1.1 Reference detail

APJ Rens, PH Swart; "On Techniques for the Localisation of multiple distortion sources in three-phase networks: time domain verification", *European Transactions on Electrical Power*, Vol. 11, No. 5, September/October 2001, pp. 317 – 322

1.1.2 Background

This paper was first delivered as a conference contribution to the *Fifth International Workshop on Power Definition and Measurements under Nonsinusoidal Conditions* held in Milan, Italy during October 2000. Thereafter, the paper was recompiled to include comments from other specialists that attended the workshop and than submitted to the ETEP journal.

1.2 PAPER 2

1.2.1 Reference detail

Rens APJ, Swart PH; "Investigating the validity of the Czarnecki three-phase power definitions", *The Transactions of the SAIEE*, March 2005, Vol. 96 No. 1, pp 35-39

1.2.2 Background

This paper was first delivered as a conference contribution to the *IEEE Africon 2000* conference held in George, South Africa during October 2002 and published in the proceedings (Vol. 2, pp 815-821). Thereafter, the paper was recompiled to include comments from the referees and than submitted to the SAIEE Transactions, an accredited journal.

1.3 PAPER 3

1.3.1 Reference detail

SL Bezuidenhout, APJ Rens, "Considerations on tariff strategies for nonsinusoidal conditions" *The Transactions of the SAIEE*, September 2004, Vol. 94 No. 3, pp 143 - 148

1.3.2 Background

This paper was first delivered as a conference contribution to the *Africon 2000* conference held in George, South Africa during October 2002 and published in the proceedings (Vol. 2, pp 823-827). Thereafter, the paper was recompiled to include comments from the referees and than published in the SAIEE Transactions, an accredited journal.

1.4 PAPER 4

1.4.1 Reference detail

C. R. van Niekerk, A P J Rens, A J Hoffman, "Identification of types of distortion sources in power systems by applying neural networks", *The Transactions of the SAIEE*, March 2004, Vol. 95 No. 1, pp 42– 46

Background

This paper was first delivered as a conference contribution to the *Africon 2000* conference held in George, South Africa during October 2002 and published in the proceedings (Vol. 2, pp 829-834). Thereafter, the paper was recompiled to include comments from the referees and than submitted to the SAIEE Transactions, an accredited journal.

1.5 PAPER 5

1.5.1 Reference detail

Rens APJ, Swart PH, "Validation of popular three phase nonsinusoidal power definitions", *Sixth International Workshop on Power Definitions and Measurements under Non-Sinusoidal Conditions*, Milan, pp. 33 – 40, October 13-15, 2003

1.5.2 Background

This paper was delivered as a conference contribution to the *Sixth International Workshop on Power Definition and Measurements under Nonsinusoidal Conditions* held in Milan, Italy during October 2003. Thereafter, the paper was published 2004 Web Journal of the Italian Electrical Engineering Society,

L'Energia Elettrica, http://www.aei.it

1.6 PAPER 6

1.6.1 Reference detail

Bezuidenhout SL, Rens APJ, "An Evaluation of Non-sinusoidal Tariff Schemes towards a Regulatory Tariff System for Non-sinusoidal Power System Conditions", *IEEE Africon 2004,* Gaberone, Botswana, pp. 637-644.

1.6.2 Background

This paper was delivered as a conference contribution to the IEEE Africon conference held in Gaberone, Botswana during October 2004.

1.7 PAPER 7

1.7.1 Reference detail

Cronje WST, Rens APJ, "Investigating the Validity of Applying Artificial Neural Networks to Localise Harmonic Distortion Sources", *IEEE Africon 2004,* Gaberone, Botswana, pp. 645-650

1.7.2 Background

This paper was delivered as a conference contribution to the *IEEE Africon* conference held in Gaberone, Botswana during October 2004.

2 APPENDIX B: HARMONIC LIMITS NRS048 (SA) AND IEEE

Table 24: NRS 048: Indicative values of planning levels for harmonic voltage (expressed as a percentage of the rated voltage of HV and EHV power systems)

1	2	3	4	5	6
Odd harmonics non-multiple of 3		**Odd harmonics multiple of 3**		**Even harmonics**	
Order	**Harmonic voltage HV-EHV**	**Order**	**Harmonic voltage HV-EHV**	**Order**	**Harmonic voltage HV-EHV**
h	%	h	%	h	%
5	2	3	2	2	1,5
7	2	9	1	4	1
11	1,5	15	0,3	6	0,5
13	1,5	21	0,2	8	0,4
17	1	>21	0,2	10	0,4
19	1			12	0,2
23	0,7			>12	0,2
25	0,7				
>25	0,2 + 0,5 × 25/h				

Total harmonic distortion (THD) ≤ 3 % in HV networks

The limits in Table 24 are for high-voltage (HV: 44 – 220 kV) and extra high-voltage (EHV: 220 – 400 kV) networks. For low voltage (LV: < 1000 V) and medium voltage networks (MV: 1 – 44 kV), different limits apply as shown in Table 25.

Table 25: Compatibility levels for harmonic voltages (expressed as a percentage of the declared voltage of LV and MV power systems).

Odd harmonics non-multiple of 3		**Odd harmonics multiple of 3**		**Even harmonics**	
Order h	**Harmonic voltage (%)**	**Order** h	**Harmonic voltage** %	**Order** h	**Harmonic voltage** %
5	6	3	5	2	2
7	5	9	1,5	4	1
11	3,5	15	0,3	6	0,5
13	3	21	0,2	8	0,5
17	2	>21	0,2	10	0,5
19	1,5			12	0,2
23	1,5			>12	0,2
25	1,5				
>25	0,2 + 1,3 × 25/h				
Total harmonic distortion (THD) ≤ 8 %					
NOTE — For each harmonic, the harmonic voltage distortion compatibility level is given as a percentage of the magnitude of the declared (fundamental frequency) voltage					

Table 26: IEEE 519 519-1992: Current distortion limits for general distribution systems (120 V to 69 000 V)

Maximum *Harmonic Current Distortion* in Percentage of I_L						
INDIVIDUAL HARMONIC ORDER (ODD HARMONICS)						
I_{SC}/I_L	< 11	11 ≤ *h* < 17	17 ≤ *h* < 23	23 ≤ *h* < 35	35 ≤ *h*	*TDD*
< 20*	4.0	2.0	1.5	0.6	0.3	5.0
20 < 50	7.0	3.5	2.5	1.0	0.5	8.0
50 < 100	10.0	4.5	4.0	1.5	0.7	12.0
100 < 1000	12.0	5.5	5.0	2.0	1.0	15.0
> 1000	15.0	7.0	6.0	2.5	1.4	20.0
Even harmonics are limited to 25% of the odd harmonic limits above.						
Current distortion limits that results in a dc offset, e.g. half-wave converters, are not allowed.						
*All power-generation equipment is limited to these values of current distortion, regardless of actual I_{SC}/I_L.						
I_{SC} = Maximum short-circuit current at PCC. I_L = Maximum demand load current (fundamental frequency component) at PCC.						

2.1 MATHCAD SORTING PROCEDURE

$Vharmonics = 0..last(V_{ah})$ {*Index of all voltage harmonics*}

$Iharmonics = 0..last(I_{ah})$ {*Index of all current harmonics*}

$$N_{V_i} := \begin{cases} Vharmonics_i & \text{if } \left(\frac{V_{ah_i}}{V_{ah_1}} \geq factor\right) \\ 0 & \text{otherwise} \end{cases}$$

$\{N_{V_i} \equiv source\ harmonics\}$

$$N_{I_i} := \begin{cases} Iharmonics_i & \text{if } \left(Iharmonics_i - N_{V_i}\right) \neq 0 \\ 0 & \text{otherwise} \end{cases}$$

$\{N_{I_i} \equiv Generated\ harmonics\}$

$\{N_V \cup N_I \triangleq N_g\}$

3 APPENDIX C: INSTRUMENTATION

3.1 PCI 6031E

Full-Featured E Series Multifunction DAQ
12 or 16-Bit, up to 1.25 MS/s, up to 64 Analog Inputs

E Series – Full-Featured

- 16 or 64 analog inputs at up to 1.25 MS/s, 12 or 16-bit resolution
- 2 analog outputs at up to 1 MS/s, 12 or 16-bit resolution
- 8 digital I/O lines (TTL/CMOS); two 24-bit counter/timers
- Analog and digital triggering
- 14 or 15 analog input signal ranges
- NI-DAQ driver simplifies configuration and measurements

Families
- NI 6071E
- NI 6070E
- NI 6062E
- NI 6052E
- NI 6040E
- NI 6033E
- NI 6032E
- NI 6031E
- NI 6030E
- NI 6020E (only digital triggering)

Operating Systems
- Windows 2000/NT/XP
- Real-time performance with LabVIEW (page 134)
- Others such as Linux and Mac OS X (page 187)

Recommended Software
- LabVIEW
- LabWindows/CVI
- Measurement Studio
- VI Logger

Other Compatible Software
- Visual Basic, C/C++, and C#

Driver Software (included)
- NI-DAQ 7

Calibration Certificate Included
See page 21.

Family	Bus	Analog Inputs	Input Resolution	Max Sampling Rate	Input Range	Analog Outputs	Output Resolution	Output Rate	Output Range	Digital I/O	Counter/Timers	Triggers
NI 6071E	PCI, PXI	64 SE/32 DI	12 bits	1.25 MS/s	±0.05 to ±10 V	2	12 bits	1 MS/s	±10 V	8	2, 24-bit	Analog, digital
NI 6070E	PCI, PXI, FireWire	16 SE/8 DI	12 bits	1.25 MS/s	±0.05 to ±10 V	2	12 bits	1 MS/s	±10 V	8	2, 24-bit	Analog, digital
NI 6062E	PCMCIA	16 SE/8 DI	12 bits	500 kS/s	±0.05 to ±10 V	2	12 bits	850 kS/s	±10 V	8	2, 24-bit	Analog, digital
NI 6052E	PCI, PXI, FireWire	16 SE/8 DI	16 bits	333 kS/s	±0.05 to ±10 V	2	16 bits	333 kS/s	±10 V	8	2, 24-bit	Analog, digital
NI 6040E	PCI, PXI	16 SE/8 DI	12 bits	500 kS/s	±0.05 to ±10 V	2	12 bits	1 MS/s	±10 V	8	2, 24-bit	Analog, digital
NI 6033E	PCI	64 SE/32 DI	16 bits	100 kS/s	±0.1 to ±10 V	0	-	-	-	8	2, 24-bit	Analog, digital
NI 6032E	PCI	16 SE/8 DI	16 bits	100 kS/s	±0.1 to ±10 V	0	-	-	-	8	2, 24-bit	Analog, digital
NI 6031E	PCI, PXI	64 SE/32 DI	16 bits	100 kS/s	±0.1 to ±10 V	2	16 bits	100 kS/s	±10 V	8	2, 24-bit	Analog, digital
NI 6030E	PCI, PXI	16 SE/8 DI	16 bits	100 kS/s	±0.1 to ±10 V	2	16 bits	100 kS/s	±10 V	8	2, 24-bit	Analog, digital
NI 6020E	NI USB	16 SE/8 DI	12 bits	100 kS/s	±0.05 to ±10 V	2	12 bits	20 S/s	±10 V	8	2, 24-bit	Digital

Table 1. NI Full-Featured E Series Model Guide (See page 228 for detailed specifications.)

Overview and Applications

NI Full-Featured E Series devices are the fastest and the most accurate multiplexed data acquisition devices available. They are ideal for applications ranging from continuous high-speed data logging to control applications to high voltage signal or sensor measurements when used with NI signal conditioning. Synchronize the operations of multiple devices using the RTSI bus or PXI trigger bus and easily integrate other hardware such as motion control and machine vision to create an entire measurement and control system.

Visit ni.com/oem for information on our quantity discounts for OEM customers.

Highly Accurate Hardware Design

NI Full-Featured E Series DAQ devices includethe following features and technologies:

Temperature Drift Protection Circuitry – Designed with components that minimize the effect of temperature changes on measurements to less than 0.0006% of reading per °C.

Resolution-Improvement Technologies – Carefully designed noise floor maximizes resolution.

Onboard Self-Calibration – Precise voltage reference included for calibration and measurement accuracy. Self-calibration is completely software controlled, with no potentiometers to adjust.

NI DAQ-STC – Timing and control ASIC designed to provide more flexibility, lower power consumption, and a higher immunity to noise and jitter than off-the-shelf counter/timer chips.

Full-Featured E Series Multifunction DAQ
12 or 16-Bit, up to 1.25 MS/s, up to 64 Analog Inputs

		Full-Featured E Series				Low-Cost E Series		Basic
Models		NI 6030E, NI 6031E, NI 6032E, NI 6033E	NI 6052E	NI 6070E, NI 6071E	NI 6040E	NI 6034E, NI 6036E	NI 6023E, NI 6024E, NI 6025E	PCI-6013, PCI-6014
Measurement Sensitivity* (mV)		0.0023	0.0025	0.009	0.008	0.0035	0.008	0.004
Nominal Range (V)								
Positive FS	**Negative FS**	**Absolute Accuracy (mV)**						
10	-10	1.147	4.747	14.369	15.373	7.58	16.504	6.904
5	-5	2.077	0.876	5.193	5.697	1.79	5.263	2.003
2.5	-2.5	–	1.190	3.605	3.859	–	–	–
2	-2	0.836	–	–	–	–	–	–
1	-1	0.422	0.479	1.452	1.556	–	–	–
0.5	-0.5	0.215	0.243	0.735	0.789	0.399	0.846	0.471
0.25	-0.25	–	0.137	0.379	0.405	–	–	–
0.2	-0.2	0.102	–	–	–	–	–	–
0.1	-0.1	0.061	0.064	0.163	0.176	–	–	–
0.05	-0.05	–	0.035	0.091	0.100	0.0611	0.106	0.069
10	0	0.976	1.232	6.765	7.269	–	–	–
5	0	1.992	2.119	5.391	5.845	–	–	–
2	0	0.802	0.850	2.157	2.271	–	–	–
1	0	0.405	0.428	1.092	1.146	–	–	–
0.5	0	0.207	0.242	0.558	0.583	–	–	–
0.2	0	0.098	0.111	0.235	0.247	–	–	–
0.1	0	0.059	0.059	0.127	0.135	–	–	–

Note: Accuracies are valid for measurements following an internal calibration. Measurement accuracies are listed for operational temperatures within ±1 °C of internal calibration temperature and ±10 °C of external or factory-calibration temperature. One-year calibration interval recommended. The Absolute Accuracy at Full Scale calculations were performed for a maximum range input voltage (for example, 10 V for the ±10 V range) after one year, assuming 100 pt averaging of data. *Smallest detectable voltage change in the input signal at the smallest input range.

Table 2. E Series Analog Input Absolute Accuracy Specifications

		Full-Featured E Series				Low-Cost E Series		Basic
Models		NI 6030E, NI 6031E, NI 6032E, NI 6033E	NI 6052E	NI 6070E, NI 6071E	NI 6040E	PCI-6036E	PCI-6024E, NI 6025E	NI 6013, NI 6014
Nominal Range (V)								
Positive FS	**Negative FS**	**Absolute Accuracy (mV)**						
10	-10	1.43	1.405	8.127	8.127	2.417	8.127	3.835
10	0	1.201	1.176	5.685	5.685	–	–	–

Table 3. E Series Analog Output Absolute Accuracy Specifications

Recommended Accessories

Signal conditioning is required for sensor measurements or voltage inputs greater than 10 V. National Instruments SCXI is a versatile, high-performance signal conditioning platform, intended for high-channel-count applications. NI SCC products provide portable, flexible signal conditioning options on a per-channel basis. Both signal conditioning platforms are designed to increase the performance and reliability of your DAQ System, and are up to 10X more accurate than terminal blocks (please visit ***ni.com/sigcon*** for more details). Refer to the table below for more information:

Sensor/Signals (>10 V)

System Description	DAQ Device	Signal Conditioning	Page
High performance	PCI-60xxE, PXI-60xxE, DAQPad-60xxE	SCXI	270
Low-cost, portable	PCI-60xxE, PXI-60xxE, DAQPad-60xxE	SCC	251

Signals (<10 V)[1]

System Description	DAQ Device	Terminal Block	Cable	Page
Shielded	PCI-60xxE/DAQPad-60xxE	SCB-68	SH6868-EP	214
Shielded	PXI-60xxE	TB-2705	SH6868-EP	214
Shielded	PCI-6071E/PCI-6033E/PCI-6031E	SCB-100	SH100100	214
Shielded	PXI-6071E/PXI-6031E	Two TBX-68s	SH1006868	214
Shielded	DAQPad-60xxE	SCB-68	SHC6868-EP	214
Low-Cost	PCI-60xxE/PXI-60xxE/DAQPad-60xxE	C8-68LP	R6868	214
Low-Cost	DAQCard-60xxE	C8-68LP	RC6868	214

[1]Terminal Blocks do not provide signal conditioning (ie. filtering, amplification, isolation, etc.), which may be necessary to increase the accuracy of your measurements.

Table 4. Recommended Accessories

Ordering Information

NI PXI-6071E 777676-01
NI PCI-6071E 777515-01
NI PXI-6070E 777060-01
NI PCI-6070E 777305-01
NI DAQPad-6070E for FireWire ..... (See page 207)
NI DAQCard-6062E ..... (See page 207)
NI PXI-6052E 777962-01
NI PCI-6052E 777745-01
NI DAQPad-6052E for FireWire ..... (See page 207)
NI PXI-6040E 777484-01
NI PCI-6040E 777383-01
NI PCI-6033E 777516-01
NI PCI-6032E 777422-01
NI PXI-6031E 777636-01
NI PCI-6031E 777514-01
NI PXI-6030E 777555-01
NI PCI-6030E 777384-01
NI DAQPad-6020E for USB ..... (See page 207)

Includes NI-DAQ driver software and calibration certificate.

For more information on warranty and value-added services, see page 20.

BUY ONLINE!
Visit ni.com/dataacquisition

16-Bit E Series Multifunction DAQ Specifications

Specifications – NI 6052E and NI 603xE

These specifications are typical for 25 °C unless otherwise noted.

Analog Input

Accuracy specifications ..... See page 228.

Input Characteristics

	Number of Channels
6052E 6030E 6032E 6034E 6036E	16 single-ended or 8 differential (software selectable per channel)
6031E 6033E	64 single-ended or 32 differential (software-selectable per channel)

Resolution ..... 16 bits, 1 in 65,536

	Maximum Sampling Rate
6052E 6034E 6036E	333 kS/s 200 kS/s
6030E 6031E 6032E 6033E	100 kS/s

Input signal ranges

Device	Range Software Selectable	Bipolar Input Range	Unipolar Input Range
6052E	20 V	±10 V	–
	10 V	±5 V	0 to 10 V
	5 V	±2.5 V	0 to 5 V
	2 V	±1 V	0 to 2 V
	1 V	±500 mV	0 to 1 V
	500 mV	±250 mV	0 to 500 mV
	200 mV	±100 mV	0 to 200 mV
	100 mV	±50 mV	0 to 100 mV
6030E	20 V	±10 V	–
6031E	10 V	±5 V	0 to 10 V
6032E	5 V	–	0 to 5 V
6033E	4 V	±2 V	–
	2 V	±1 V	0 to 2 V
	1 V	±500 mV	0 to 1 V
	500 mV	–	0 to 500 mV
	400 mV	±200 mV	–
	200 mV	±100 mV	0 to 200 mV
	100 mV	–	0 to 100 mV
6034E	20 V	±10 V	–
6036E	10 V	±5 V	–
	1 V	±500 mV	–
	100 mV	±50 mV	–

Input coupling ..... DC

Maximum working voltage

(signal + common mode) ..... Each input should remain within ±11 V of ground

Overvoltage protection

Powered on ..... ±25 V

Powered off ..... ±15 V

	Inputs Protected
6052E 6030E 6032E 6034E 6036E	AI<0..15>, AI SENSE
6031E 6033E	AI<0..63>, AI SENSE, AI SENSE2

FIFO buffer size ..... 512 samples, (1024 samples for DAQCard)

Data transfers

PCI, PXI ..... DMA, interrupts, programmed I/O

DAQCard ..... Interrupts, programmed I/O

DMA modes

PCI, PXI ..... Scatter-gather (single transfer, demand transfer)

Configuration memory size ..... 512 words

Transfer Characteristics

Relative accuracy (dithered)

Device	Typical	Maximum
6052E 6034E PCI-6036E	±1.5 LSB	±3 LSB
6030E 6031E 6032E 6033E	±0.75 LSB	±1 LSB
DAQCard-6036E	±3.0 LSB	±6 LSB

DNL

Device	Typical	Maximum
6052E 603xE (except DAQCard-6036E)	±0.5 LSB	±1 LSB
DAQCard-6036E	±1.0 LSB	+4, -2 LSB

No missing codes

DAQCard 6036E ..... 15 bits, guaranteed

Others ..... 16 bits, guaranteed

Amplifier Characteristics

Input impedance

Device	Normal Powered On	Powered Off	Overload
6052E 603xE	100 GΩ in parallel with 100 pF	820 Ω	820 Ω

Input bias and offset current

Device	Bias Current	Offset Current
6052E 6034E PCI-6036E	±200 pA	±100 pA
6030E 6031E 6032E 6033E	±1 nA	±2 nA
DAQCard-6036E	±800 pA	±100 pA

16-Bit E Series Multifunction DAQ Specifications

Specifications – NI 6052E and NI 603xE (continued)

CMRR, DC to 60 Hz

Device	Range	CMRR Bipolar (dB)	CMRR Unipolar (dB)
6052E	20 V	92	–
	10 V	97	97
	5 V	101	101
	2 V	104	104
	100 mV to 1 V	105	105
6030E	20 V	92	–
6031E	10 V	97	92
6032E	5 V	–	97
6033E	4 V	101	–
	2 V	104	101
	1 V	105	104
	100 mV to 500 mV	105	105
6034E	20 V	85	–
6036E	10 V	85	–
	1 V	96	–
	100 mV	96	–

Dynamic Characteristics

Bandwidth

Device	Range	Small Signal (-3 dB)
6052E	All ranges	480 kHz
6030E, 6031E, 6032E, 6033E	All ranges	255 kHz
6034E, 6036E	All ranges	413 kHz

System noise (LSB_{rms}, including quantization)

Device	Range	Bipolar	Unipolar
6052E	2 to 20 V	0.95	0.95
	1 V	1.1	1.1
	500 mV	1.3	1.3
	200 mV	2.7	2.7
	100 mV	5.0	5.0
6030E	2 to 20 V	0.6	0.8
6031E	1 V	0.7	0.8
6032E	400 to 500 mV	1.1	1.1
6033E	200 mV	2.0	2.0
	100 mV	–	3.8
6034E	10 to 20 V	0.8	–
PCI-6036E	1 V	1.0	–
	100 mV	6.2	–
DAQCard-6036E	10 to 20 V	1.5	–

Settling time to full-scale step

Device	Range	Accuracy ±0.00076% (±0.5 LSB)	±0.0015% (±1 LSB)	±0.0031% (±2 LSB)	±0.0061% (±4 LSB)	±0.024% (±16 LSB)
6052E	2 to 20 V	–	10 µs max	5 µs max	4 µs max	3 µs max
	1 V	–	15 µs max	5 µs max	4 µs max	3 µs max
	200 to 500 mV	–	15 µs max	10 µs max	4 µs max	3 µs max
	100 mV	–	15 µs typical	10 µs typical	4 µs max	3 µs max
6030E 6032E	All	40 µs max	20 µs max	–	10 µs max	–
6031E 6033E	All	50 µs max	25 µs max	–	10 µs max	–
6034E	1 to 20 V	–	–	5 µs max	–	–
6036E	100 mV	–	–	–	5 µs typical	–
DAQCard-6036E	10 V	–	–	5 µs max	–	–

Crosstalk

Device	Adjacent Channels	All Other Channels
6052E 603xE	-75 dB	-90 dB

Analog Output

Output Characteristics

Number of Channels	
6052E 6030E 6031E 6036E	2 voltage outputs
6032E, 6033E, 6034E	None

Resolution	
6052E 6036E 6030E 6031E	16 bits, 1 in 65,536

Maximum Update Rate	
6052E	333 kS/s
PCI-6036E	10 kS/s, system dependent
6030E 6031E	100 kS/s
DAQCard-6036	1 kS/s, system dependent

Type of DAC ..... Double buffered, multiplying

FIFO Buffer Size	
6052E, 6030E, 6031E	2,048 samples
6036E	None

Data transfers
- PCI, PXI ..... DMA, interrupts, programmed I/O
- DAQCard ..... Interrupts, programmed I/O

DMA modes
- PCI, PXI ..... Scatter-gather (single transfer, demand transfer)

Transfer Characteristics

Relative Accuracy	
6052E	±0.35 LSB typical, ±1 LSB maximum
6030E 6031E	±0.5 LSB typical, ±1 LSB maximum
6036E	±2 LSB maximum

DNL ..... ±1.0 LSB maximum

Monotonicity	
6052E 6036E 6030E 6031E	16 bits, guaranteed

Voltage Output

Ranges	
6052E	±10 V, 0 to 10 V, ±EXTREF, 0 to EXTREF; software selectable
6030E 6031E	±10 V, 0 to 10 V; software selectable
6036E	±10 V

Output coupling ..... DC
Output impedance ..... 0.1 Ω maximum
Current drive ..... ±5 mA maximum
Protection ..... Short-circuit to ground

Power-On State	
6052E 6030E 6031E	0 V (±20 mV)
PCI-6036E	0 V (±44 mV)
DAQCard-6036E	0 V (±60 mV)

16-Bit E Series Multifunction DAQ Specifications

Specifications – NI 6052E and NI 603xE (continued)

External reference input (6052E only)
- Range ..... ±11 V
- Overvoltage protection ..... ±25 V powered on, ±15 V powered off
- Input impedance ..... 10 kΩ
- Bandwidth (-3 dB) ..... 3 kHz
- Slew rate ..... 0.3 V/µs

Dynamic Characteristics

Settling time and slew rate

Device	Settling Time For Full-Scale Step	Slew Rate
6052E	3.5 µs to ±1 LSB accuracy	15 V/µs
6030E 6031E	10 µs to ±1 LSB accuracy	5 V/µs
PCI-6036E	5 µs to ±1 LSB accuracy	15 V/µs
DAQCard-6036E	5 µs to ±4.5 LSB accuracy	5 V/µs

	Noise
6052E 6030E 6031E	60 μV_{rms}, DC to 1 MHz
PCI-6036E	110 μV_{rms}, DC to 400 kHz
DAQCard-6036E	160 μV_{rms}, DC to 400 kHz

Glitch energy (at mid-scale transition)

Device	Magnitude	Duration
6052E	±10 mV	1 µs
PCI-6036E	±10 mV	1 µs

Digital I/O

- Number of channels ..... 8 input/output
- Compatibility ..... 5 V/TTL/CMOS
- Power-on state ..... Input (high impedance)
- Data transfers ..... Programmed I/O

Digital logic levels

Level	Minimum	Maximum
Input low voltage	0.0 V	0.8 V
Input high voltage	2.0 V	5.0 V
Output low voltage (I_{out} = 5 mA)	–	0.4 V
Output high voltage (I_{out} = -3.5 mA)	4.35 V	–

Timing I/O

General-Purpose Up/Down Counter/Timers

- Number of channels
  - Up/down counter/timers 2
  - Frequency Scaler 1
- Resolution
  - Up/down counter/timers ..... 24 bits
  - Frequency Scaler ..... 4 bits
- Compatibility ..... 5 VTTL/CMOS
- Digital logic levels
- Base clocks available
  - Up/down counter/timers ..... 20 MHz and 100 kHz
  - Frequency Scaler ..... 10 MHz and 100 kHz
- Base clock accuracy ..... ±0.01%
- Maximum external source frequency
  - Up/down counter/timers ..... 20 MHz
- External source selections ..... PFI <0..9>, RTSI <0..6>, analog trigger, software selectable
- External gate selections ..... PFI <0..9>, RTSI <0..6>, analog trigger, software selectable
- Minimum source pulse duration ..... 10 ns, edge-detect mode
- Minimum gate pulse duration ..... 10 ns, edge-detect mode
- Data transfers
  - PCI/PXI Up/down counter/timer ..... DMA (scatter-gather), interrupts, programmed I/O
  - DAQCard Up/down counter/timer ..... Interrupts, programmed I/O
  - Frequency Scaler ..... Programmed I/O

Triggers

Analog Triggers

	Number of Triggers
6052E 6030E 6031E 6032E 6033E	1
6034E 6036E	None

Purpose
- Analog input ..... Start and stop trigger, gate, clock
- Analog output ..... Start trigger, gate, clock
- General-purpose counter/timers ..... Source, gate

	Source
6052E 6030E 6032E	AI<0..15>, PFI 0/AI START TRIG
6031E 6033E	AI<0..63>, PFI 0/AI START TRIG

Level
- Internal source, AI<0..15/63> ..... ±full-scale
- External source, PFI 0/AI START TRIG ..... ±10 V

Slope ..... Positive or negative; software-selectable
Resolution ..... 12 bits, 1 in 4,096
Hysteresis ..... Programmable
Bandwidth (-3 dB)

Device	Internal Source AI<0..15/63>	External Source PFI 0/AI START TRIG
6052E	700 kHz	700 kHz
PCI-6030E, PCI-6031E, 6032E, 6033E	255 kHz	4 MHz
PXI-6030E, PXI-6031E	255 kHz	255 kHz

Accuracy ..... ±1% of full-scale range maximum

Digital Triggers (all devices)

Purpose
- Analog input ..... Start and stop trigger, gate, clock
- Analog output ..... Start trigger, gate, clock
- General-purpose counter/timers ..... Source, gate

Source ..... PFI <0..9>, RTSI <0..6>
Compatibility ..... 5 VTTL
Response ..... Rising or falling edge
Pulse width ..... 10 ns minimum

3.2 IMPEDOGRAPH

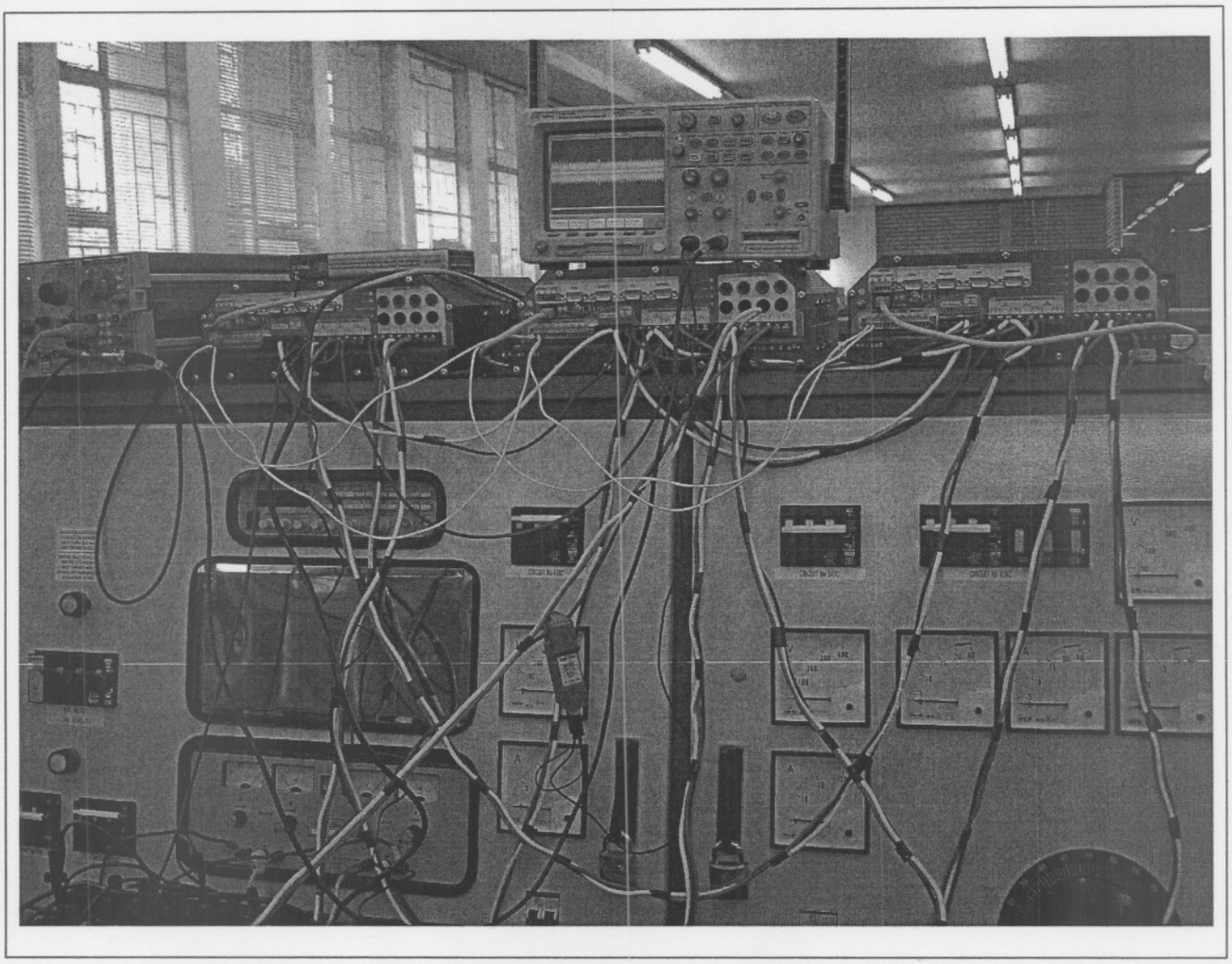

Figure 67: Three Impedographs™ measuring 9 voltage and 9 current waveforms in synchronism

Voltage Inputs:

Number of channels:	4 x differential inputs
Input range:	10 to 460 V RMS
Accuracy:	<0.1% on reading (50 to 460 V RMS)
Resolution:	15 mV RMS
VA loading:	> 1MΩ. (resistive)

Current Inputs:

Number of channels:	4 x galvanically isolated
Input range:	0 - 7.5 A RMS
Accuracy:	< 0.1% on reading (0.2 to 7.5 A RMS)
Resolution:	250 µA RMS
VA loading:	< 0.5 VA @ 7.5 A RMS

Analog to Digital Conversion:

ADC resolution:	16 bit
Maximum analog noise:	0.02% of full scale
Sampling rate:	128 samples per fundamental frequency cycle
Over-sampling:	4 times
Locking:	Frequency and Phase locked

Real Time Clock:

Synchronization source:	External GPS
Accuracy:	100 PPM (unsynchronised)

3.3 LABORATORY POWER SYSTEM

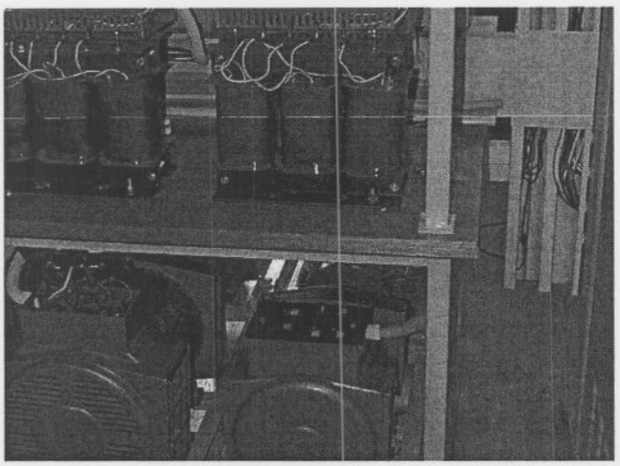

Figure 68: Synchronous generators and transformators feeding transmission line modules

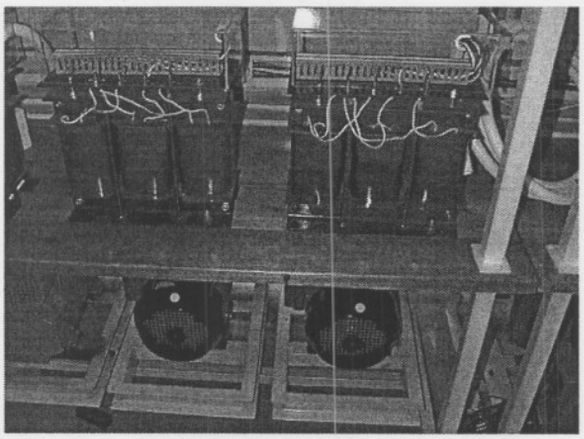

Figure 69: Induction and DC machine load simulators, transformators at receiving end of lines

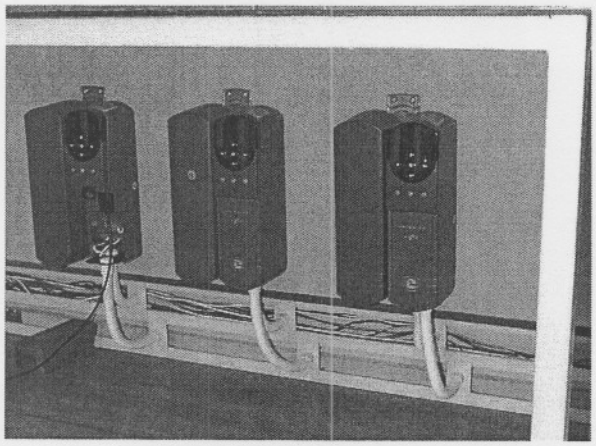

Figure 70: PWM inverters controlling induction Machines, setting control values by RS 485

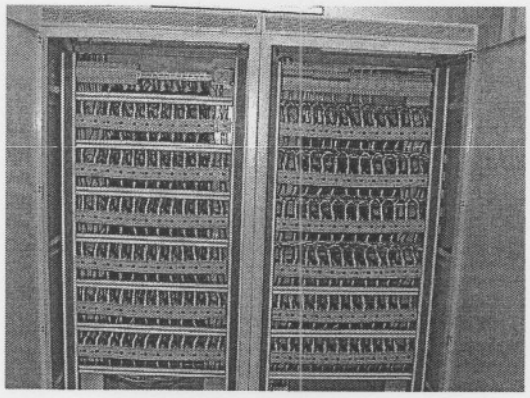

Figure 71: The matrix of contactors, note the 6 nodes (busses) are horisontally laid out

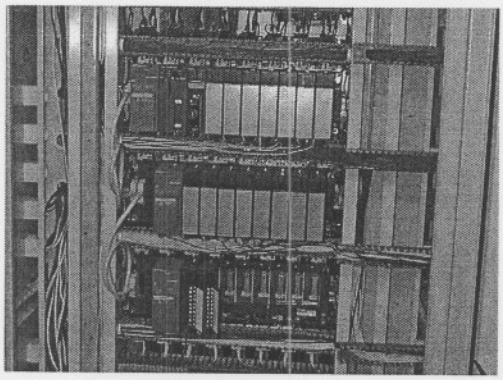

Figure 72: The Mitsibushi PLC: 1028 I/O channels possible, 248 outputs used

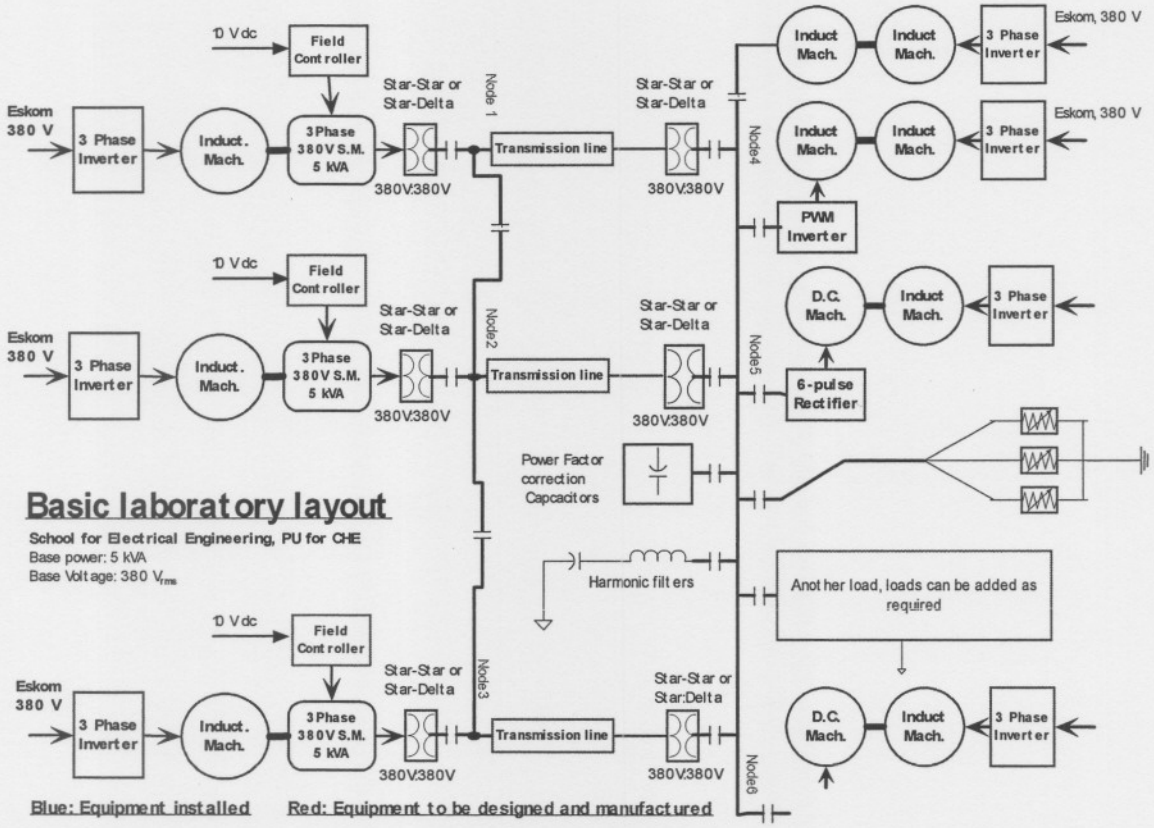

Figure 73: The laboratory layout

4 REFERENCES

[1] Budeanu G., "Reactive and Fictitious powers", *Rumanian National Institute, (Bucharest, Rumania),* 1927, *publication no* 2. Also, "The different options and conceptions regarding active power in non-sinusoidal systems", 1927, *Rumanian National Institute, publication no* 4.

[2] Czarnecki L.S., "What is wrong with the Budeanu Concept of Reactive Power and Distortion Power and why it should be Abandoned" *IEEE Transactions on Instrumentation and Measurement*; Vol. IM-36, no. 3, September 1987, pp. 834-837.

[3] Czarnecki L.S., "Distortion Power in systems with nonsinusoidal voltage", *IEE Proceedings-B*, Vol. 139, no. 3, May 1992, pp. 276-280

[4] Czarnecki L.S., "Comments on Measurement and Compensation of Fictitious Power Under Nonsinusoidal Voltage and Current Conditions", *IEEE Transactions on Instrumentation and Measurement*, vol. 38, no. 3, June 1989, pp. 839 – 841

[5] Czarnecki L.S., "Orthogonal Decomposition of the Currents in a 3-Phase Nonlinear Asymmetrical Circuit with a Nonsinusoidal Voltage Source", *IEEE Transactions on Instrumentation and Measurement*, vol. 37, no. 1, June 1989, pp. 30-34

[6] Czarnecki L.S., "Reactive and Unbalanced Currents Compensation in Three Phase Asymmetrical Circuits Under Nonsinusoidal Conditions", *IEEE Transactions on Instrumentation and Measurement*, vol. 38, no. 3, June 1989, pp. 754-759

[7] Czarnecki L.S., "Active, Reactive, and Scattered Current in Circuits with Nonperiodic Voltage of a Finite Energy", *IEEE Transactions on Instrumentation and Measurement*, vol. 37, no. 3, September 1988, pp. 398-402

[8] Czarnecki L.S., "Scattered and Reactive Current, Voltage and Power in Circuits with Nonsinusoidal Waveforms and Their Compensation", IEEE *Transactions on Instrumentation and Measurement*, vol. 40, no. 3, June 1991, pp. 563-567

[9] Czarnecki L.S., "Physical Reasons of Currents RMS Value increase in Power Systems with Nonsinusoidal Voltage", *IEEE Transactions on Power Delivery*, vol. 8, no. 1, January 1993, pp. 347-354

[10] Czarnecki L.S., "Power Related Phenomena in three-phase unbalanced systems", *IEEE Transactions on Power Delivery*, vol. 10, no. 3, July 1995, pp. 1168-1176

[11] Czarnecki L.S., "Misinterpretations of Power Properties if Electric Circuits", *IEEE*

Transactions on Power Delivery, vol. 9, no. 4, October 1994, pp. 1760-1769

[12] Czarnecki L.S., "Minimisation of Unbalanced and Reactive Currents in Three Phase Asymmetrical Circuits with Nonsinusoidal Voltage", *IEE Proceedings-B*, vol. 39, no. 4, July 1992, pp. 347-354

[13] Czarnecki L.S., "A Time Domain Approach to Reactive Current Minimization in Nonsinusoidal Situations", *IEEE Transactions on Instrumentation and Measurement*, vol. 39, no. 5, October 1990, pp. 698-703

[14] Czarnecki L.S., "Considerations on the Reactive power in Nonsinusoidal Situations", *IEEE Transactions on Instrumentation and Measurement*, vol. IM-34, no. 3, September 1985, pp. 399-404

[15] Czarnecki L.S, "Minimisation of Reactive Power under Nonsinusoidal Conditions", *IEEE Transactions on Instrumentation and Measurement*, vol. IM-36, no. 1, March 1987, pp. 18-22

[16] Czarnecki L.S., "Powers in Nonsinusoidal Networks: Their Interpretation, Analysis, and Measurement", *IEEE Transactions on Instrumentation and Measurement*, vol. 39, no. 2, April 1990, pp. 340-345

[17] Czarnecki L.S., "Currents and Power Equations at Bidirectional Flow of Harmonic Active Power in Circuits with Rotating Machines", *ETEP*, vol. 3, no. 1, January/February 1993, pp 45-52

[18] Czarnecki L.S., "Measurement principles of a reactive power meter for nonsinusoidal systems", *IEEE Transactions on instrumentation and Measurement*, vol. IM-30, 1981, pp. 209-212

[19] Webster J.G. ed, *Wiley Encyclopaedia of Electrical and Electronics Engineering*, Supplement 1, Harmonics and Power Phenomena, LS Czarnecki, 2000, pp. 195 – 217

[20] IEEE Working Group on Non-sinusoidal Situations: "Effects on Meter Performance and Definitions of Power; Practical Definitions for Power in Systems with Nonsinusoidal Waveforms and Unbalanced Loads, A Discussion", *IEEE Transactions on Power Delivery*, vol. 11, no. 1, January 1996, pp. 79-101

[21] Ferrero A.E., "Draft Document of the Working Group on Power Definitions under Nonsinusoidal Conditions", Fourth International Workshop on Power Definitions and Measurements under Nonsinusoidal Conditions, Milan, September 1997, pp. 105-109

[22] Akagi Y., Nabae. A., "Instantaneous reactive power compensator comprising switching devices without energy storage components", *IEEE Transactions on Industrial Applications*, vol. IA-20, May/June 1984, pp. 625-630

[23] Nabae A.; Tanaka T., "A New Definition of Instantaneous Active-Reactive Current and Power Based on Instantaneous Space Vectors on Polar Coordinates in Three-Phase Circuits", *IEEE Transactions on Power Delivery*, vol. 11, no. 3, July 1996, pp. 1238-1243

[24] Sharon D., "Power Factor Definitions and Power Transfer Quality in Nonsinusoidal Situations", *IEEE Transactions on Instrumentation and Measurement*, vol. 45, no. 3, June 1996,

[25] Page C.H., "Reactive Power in Nonsinusoidal Situations", *IEEE Transactions on Instrumentation and Measurement*, vol. IM-29, no. 4, December 1980, pp. 420-426

[26] Ferrero A, Superti-Furga G., "A New Approach to the Definition of Power Components in Three-Phase Systems Under Nonsinusoidal Conditions", *IEEE Transactions on Instrumentation and Measurement*, vol. 40, no. 3, June 1991, pp. 568-577

[27] Ferrero A., Morando A.P., Ottoboni R., Superti-Furga G., "On the Meaning of the Park Power Components in Three-Phase Systems under Non-Sinusoidal Conditions", *ETEP*, vol. 3, no. 1, January/February 1993, pp.

[28] Ferrero A., Leva S., Morando A.P., "An approach to the Non-Active Power Concept in terms of the Poynting-Park vector", *ETEP*, vol. 11, no. 5, September/October 2001, pp. 291-299

[29] Ferrero A., Giuliani G., Willems L., "A New Space-Vector Transformation for Four-Conductor Systems", *ETEP*, vol. 10, no. 3, May/June 2000, pp. 139-144

[30] Čakareski Ž., Emanuel A., "Poynting Vector and the Quality of Electric Energy.", *ETEP*, vol. 11, no. 6, November/December 2001, pp. 375–382

[31] Emanuel A.E., "Practical aspect of Active and generating power in Nonsinusoidal Situations: some Questions." *Fifth International Workshop on Power Definitions and Measurements under Non-sinusoidal Conditions*, Milan, October 2000, pp 51–53

[32] Ferrero A., Lazzaroni M., Salicone S., "A Calibration Procedure for a Digital Instrument for Electric Power Quality Measurement.", *IEEE Transactions on Instrumentation and Measurement*; vol. 51, no. 4, August 2002, pp. 716-722

[33] Willems J.L., "A new interpretation of the Akagi-Nabae power components for non-sinusoidal

three-phase situations", *IEEE Transactions on Instrumentation and Measurement*, vol. IM-41, , August 1992, pp. 523-527

[34] Kusters J.L., Moore W.J.M., "On the definition of Reactive power under non-sinusoidal conditions," *IEEE Transactions on Power Apparatus and Systems*, vol. PAS-99, Sept/Oct 1980, pp. 1845-1854

[35] Peng F.Z., "Generalized Instantaneous Reactive Power Theory for Three Phase Power Systems", *IEEE Transactions on Instrumentation and Measurement*; vol. 24, no. 1, February 1996, pp. 293-297

[36] Filipski P, "The Measurement of Distortion Current and Power", *IEEE Transactions on Instrumentation and Measurement*, vol. IM-33, no. 1, March 1984, pp. 36-40

[37] Enslin J.H.R., "Measurement and Compensation of Fictitious Power Under Nonsinusoidal Voltage and Current Conditions", *IEEE Transactions on Instrumentation and Measurement*, vol. 37, no. 3, September 1988, pp. 403-408

[38] Pretorius J.H.C., van Wyk J.D., Swart P.H., "An Evaluation of some Alternative Methods of Power Resolution in a Large Industrial Plant", *Proc. Of the Eight International Conference on Harmonics and Quality of Power* (ICHQP-VIII), Athens, vol. I, October 1998, pp. 331-336

[39] Arsenau, R.; "Application of a Three Phase Nonsinusoidal Calibration System for Testing Energy and Demand meters under Simulated Field Conditions", *IEEE Transactions on Power Delivery*, vol. 3, no. 3, July 1988, pp. 874 – 879

[40] Mayer D., "Power Transmission in Periodic Sinusoidal Networks an Optimization Problem", *Second International Workshop on Power Definitions and Measurements under Non-sinusoidal Conditions*, Stresa-Italy, Sept. 8 - 10, 1993, pp. 109 – 111

[41] Ferrero A.; Superti-Furga G., "A unified approach to unbalanced three-phase systems under nonsinusoidal conditions: Some definitions, Proc. 4th Int. Conf. Harmonics in Power Systems, Budapest, Hungary, Oct., 4-6, 1990, pp. 32-37.

[42] The New IEEE Standard Dictionary of Electrical and Electronic Terms, 1992, New York, IEEE

[43] Srinivasan K., "On Separating Customer and Supply side Harmonic Contributions", "IEEE Transactions on Power Delivery"; vol. 11, no. 2; April 1996, pp. 1003-1012

[44] Cristaldi L., Ferrero A., "A Digital Method for the Identification of the Source of Distortion in

Electric Power Systems", *IEEE Transactions on Instrumentation and Measurement*; vol. 44, no. 1, February 1994, pp. 14-18

[45] Cristaldi L., Ferrero A., "A Method and Related Digital Instrument for the Measurement of the Electric Power Quality", *IEEE Transactions on Power Delivery*, vol. 10, no. 3, July 1995, pp. 1183-1189

[46] Cristaldi L., Ferrero A., "Harmonic Power Flow Analysis for the Measurement of Electric Power Quality", *IEEE Transactions on Instrumentation and Measurement*; vol. 44, no. 3, June 1995, pp. 683-685

[47] Farach J.E.; Grady W.M., Araspostathis A., "An Optimal Procedure for Placing Sensors and Estimating the Locations of Harmonic Sources in Power Systems", *IEEE Transactions on Power Delivery*, vol. 8, no. 3, July 1993, pp. 1313-1310

[48] Farach J.E., Grady. W.M., Araspostathis A., "Optimal Harmonic sensor placement in fundamental network topologies", *IEE Proceedings: Generation, Transmission, Distribution*, vol. 143, no. 6, November 1996, pp. 608-612

[49] Heydt G., "Identification of Harmonic Sources by a State Estimation Technique", *IEEE Transactions on Power Delivery*, vol. 4, no. 1, January 1989, pp. 569-575

[50] Arrillaga J., Du Z.P., Watson N., "Continuous Harmonic State Estimation of Power Systems", *IEE Proc.-Gener. Trans. Distrib.*, vol. 143, no. 4, July 1996, pp. 329 – 336

[51] Tanaka T., Akagi H, "A New Method of Harmonic Power Detection Based on the Instantaneous Active Power in Three-Phase Circuits", *IEEE Transactions on Power Delivery*, vol. 10, no. 4, October 1995, pp. 1737-1742

[52] Staroszczyk Z., Mikolajuk K., "Invasive Methods for Localisation of Harmonic Distortion Sources in Power Systems", *Fourth International Workshop on Power Definitions and Measurements under Nonsinusoidal Conditions*, September 1997, Milan, pp. 77 –81

[53] Muscas C., "Assessment of Electric Power Quality: indices for identifying disturbing loads", *Fourth International Workshop on Power Definitions and Measurements under Nonsinusoidal Conditions*, Milan, September 1997, pp. 83 –87

[54] Salicone S., Ferrero A., Testa A., Castaldo D., "An Index for Assessing the Responsibility for Injecting Periodic Disturbances", *Sixth International Workshop on Power Definitions and Measurements under Non-sinusoidal Conditions*, Milan, Italy, October 13-15, 2003, pp109-118

[55] Cristaldi L., Ferrero A., Salicone S., "A distributed System for Electric Power Quality Measurement.", *IEEE Transactions on Instrumentation and Measurement*; Vol 51, No 4, August 2002, pp 776-781

[56] Swart P.H., Case M.J., van Wyk J.D., "On Techniques for Localization of Sources Producing Distortion in Electric Power Networks.", *Second International Workshop on Power Definitions and Measurements under Non-sinusoidal Conditions*, Stresa, Italy, September 8-10, 1993, pp187-190.

[57] Swart P.H., Case M.J., van Wyk J.D., "On Techniques for Localization of Sources Producing Distortion in Three Phase Networks", *ETEP*, vol. 6, no. 6, November 1996, pp. 391-396

[58] Rens A.P.J., Swart P.H., "On Techniques for the Localisation of multiple distortion sources in three-phase networks: time domain verification", *European Transactions on Electrical Power*, vol. 11, no. 5, September/October 2001, pp. 317 – 322

[59] Czarnecki L.S., Staroszczyk Z., "On-Line Measurement of Equivalent Parameters for Harmonic Frequencies of a Power Distribution System and Load", *IEEE Transactions on Instrumentation and Measurement*; vol. 45, no. 2, April 1996, pp. 467-472

[60] Davis E.J., Emanuel A., Pileggi D.J., "Harmonic Pollution Metering: Theoretical Considerations", *IEEE Transactions on Power Delivery*, vol. 15, no. 1, January 2000, pp. 19-23

[61] Davis E.J., Emanuel A., Pileggi D.J., "Evaluation of Single Point Measuring Method for Harmonic Pollution Cost Allocation", *IEEE Transactions on Power Delivery*, vol. 15, no. 1, January 2000, pp. 14-18

[62] Emanuel A.E., "On the Assessment of Harmonic Pollution", *IEEE Transactions on Power Delivery*, vol. 10, no. 3, July 1995, pp. 1693-1698

[63] Hong Y.-Y., Chen Y.-C., "Application algorithms and artificial-intelligence approach for locating multiple harmonics in distribution systems." *IEE Proc. –Gener. Transm. Distr.*, vol. 146, no. 3, May 1999, pp. 325-329

[64] Kezunovic, M. Perunicic B., "Automated Transmission Line Fault Analysis using Synchronous Sampling at two ends", *IEEE Transactions on Power Systems*, vol 11, no 1, February 1996, pp. 441-447

[65] Kezunovic M., Perunicic B., "Synchronized Sampling improves Fault Location", *IEEE Computer Applications in Power*, April 1995, pp. 30–33

[66] Nowomiejski Z., "Generalized Theory of Electric Power", *Archiv für Elektrotechnik*, vol. 63, 1981, pp. 177-182

[67] Emanuel A.E., "Energetical Factors in Power Systems with Non-Linear Loads", *Archiv für Elektrotechnik*, vol. 59, 1977, pp. 183 - 189

[68] Emanuel A.E.; "The Bucholz-Goodhue Apparent Power Definition: The Practical Approach for Nonsinusoidal and Unbalanced Systems", *IEEE Transactions on Power Delivery*, vol. 13, no. 2, April 1998, pp 344–350

[69] Emanuel A.E., "Apparent Power Definitions for Three-Phase Systems", *IEEE Transactions on Power Delivery*, vol. 14, no.3, July 1999, pp. 767-772

[70] Slonim M.A.; "Distortion Power in linear and non-linear systems", *Int. Journal on Electronics*, vol. 68, no. 5, pp. 769-778.

[71] Harashima F.; Hiroshi I.; Tsuobi K., "A Closed-Loop Control System for the Reduction of Reactive Power required by Electronic Converters", *IEEE Transactions on Industrial Electronics and Control Instrumentation*, vol. IECI-23, no. 2, May 1976, pp. 162-166

[72] Marshall D.A., van Wyk J.D., "An Evaluation of the Real-Time Compensation on Fictitious Power in Electric Energy Networks", *IEEE Transactions on Power Delivery*, vol. 6, no. 4, October 1991, pp. 1774-1780

[73] Shepherd W., Zakikhani P., "Suggested definitions of reactive power for nonsinusoidal systems", *Proc. Inst. Electr. Eng.*, no. 119(9), 1972, pp. 1361-1362

[74] Akagi H.; Kanazawa Y.; Nabae A., "Generalised, Theory of The Time-dependent Reactive Power in Three Phase Circuits", *IPEC- Tokyo*, 1983, pp. 1375-1386

[75] Fryze S., "Wirk-, Blind-, und Scheinleistung in Elektrisch Stromkreisen mit nichtsinusoidalformingen Verlauf von Strom und Spannung", *ETZ*, vol. 53, no. 25, 1932, pp. 596-599, 625-627, 700-702

[76] Heydt G., "Pitfalls of Electric Power Quality Indices", *IEEE Transactions on Power Delivery*, vol. 13, no. 2, April 1998, pp. 570 – 578

[77] Sabin D.D., Brooks D.L., Sundaram A., "Indices for Assessing Harmonic Distortion from Power Quality Measurements; Definitions and Benchmark Data", *IEEE Transactions on Power Delivery*, vol. 14, no. 2, April 1999, pp. 489-496

[78] Depenbrock M., "The FBD Method, A Generally Applicable Tool for Analyzing Power Relations", *IEEE Transactions on Power Systems*, vol. 8, no. 2, pp. 381–387, May 1993

[79] Arrilaga J., *et al.*, "The Harmonic Domain, A Frame of Reference for Power System Harmonic Analysis", *IEEE Transactions on Power Systems*, vol. 10, no. 1, February 1995, pp. 433 – 440

[80] Meyer W., Liu Tsu-Huei., "The ATP Rule Book.", 1995, Published by the Canadian/American EMTP User Group.

[81] Ferrero A., Ottoboni R., "A New Approach to the Fourier Analysis of Periodic Signals for the Minimization of the Phase Errors.", *IEEE Transactions on Instrumentation and Measurement*; vol. 40, no. 3, August 1991, pp. 694-698

[82] Andria G., Savino M., "Windows and Interpolation Algorithms to Improve Electrical Measurement Accuracy.", *IEEE Transactions on Instrumentation and Measurement*, vol. 38, no. 4, August 1989, pp. 856 – 863

[83] Hidalgo M.H., Fernandez J.G., Rivera R.R., Larrondo H.A., "A Simple Adjustable Window Algorithm to Improve FFT Measurements.", *IEEE Transactions on Instrumentation and Measurement*, vol. 51, no. 1, February 2002, pp. 31–36

[84] Ferrero A., Ottoboni R., "A Low-Cost Frequency multiplier for Synchronous Sampling of Periodic Signals.", *IEEE Transactions on Instrumentation and Measurement*, vol. 41, no. 2, April 1992, pp. 203 – 207

[85] Ferrero A., Ottoboni R., "High-Accuracy Fourier Analysis Based on Synchronous Sampling Techniques.", *IEEE Transactions on Instrumentation and Measurement*, vol. 41, no. 6, December 1992, pp. 780–785

[86] Grandke T., "Interpolation Algorithms for Discrete Fourier Transforms of Weighted Signals" *IEEE Transactions on Instrumentation and Measurement*, vol. IM-32, no. 2, June 1983, pp. 350–355

[87] George T.A., Bones D., "Harmonic power Flow Determination using the Fast Fourier Transform.", *IEEE Trans. On Power Delivery*, vol. 6, no. 2, April 1991, pp. 530–535

[88] IEEE Working Group on Power System Harmonics, "Power System Harmonics: an Overview", *IEEE Trans. On Apparatus and Systems*, vol. PAS-102, no. 8, August 1983, pp. 2455-2460

[89] Sasdelli R., Ferrero A., Menchetti A., Peretto L., "About the accuracy of some proposed procedures for revenue metering under nonsinusoidal conditions", *Third International Workshop on Power Definitions and Measurements under Non-sinusoidal Conditions*, Milano-Italy, Sept. 8 - 10, 1993, pp 89-94

[90] Czarnecki L.S., "Comments on Active Power Flow and Energy Accounts in Electrical Systems with Nonsinusoidal Waveforms and Asymmetry", *1996 IEEE/PES Winter Meeting*, Baltimore, MD, January 21-25, 1996, pp 1-7

[91] Czarnecki L., "Comments on Active power Flow and Energy Accounts in Electrical Systems with Non-Sinusoidal Waveforms and Asymmetry", *IEEE Transactions on Power Delivery*, vol. 11, no. 3, July 1996, pp. 1244-1250

[92] Domijan A., Embriz-Santander E., "Watt-hour Meter Accuracy Under Controlled Unbalanced Harmonic Voltage and Current Conditions" *IEEE Transactions on Power Delivery*, vol. 11, no. 1, January 1996, pp. 64-72

[93] Arsenau R., Filipski P.S., "Application of a Nonsinusoidal Calibration System for Calibrating Energy and Demand meters under Simulated Field Conditions.", *IEEE Transactions on Power Delivery*, vol. 3, no. 3, July 1998, pp. 874-879

[94] IEEE Std 1459-2000 "Standard Definitions for the Measurement of Electric Power Quantities under Sinusoidal, Nonsinusoidal, Balanced or Unbalanced Conditions", *The Institute of Electrical and Electronics Engineers*, Inc. New York, 2000, USA

[95] Arrillaga J., Smith B.C., Watson N.R., Woord A.R., "Power System Harmonic Analysis.", *John Wiley & Sons Ltd*, West Sussex, November 2000, England

[96] Arrillaga J., Bradley D.A., Bodger P.S., "Power System Harmonics.", *John Wiley & Sons Ltd*, 1985

[97] Glover J.D., Sarma M.S., "Power System Analysis", *Brooks/Cole*, 3rd edition, Pacific Grove, USA, 2002

[98] Kreyzig E., "Advanced Engineering Mathematics", Fifth Edition, *John Wiley & Sons Ltd*, 1983

[99] J.J. Grainger and W.D. Stevenson, Jr., "Power Systems Analysis, *McGraw-Hill*", New York, 1994

[100] Du Broff R., Marshall S., Skitek G., "Electromagnetic Concepts and Applications" *Prentice Hall*, New Jersey, 4th edition, 1996

[101] Kip A.F., "Fundamentals of Electricity and Magnetism", *McGraw-Hill*, Tokyo, 2nd edition, 1981

[102] Griffiths D.J., "Introduction to Electrodynamics", *Prentice Hall*, New Jersey, 1st edition, 1981

[103] NRS048-2 2003, South Africa.